plants

Special Issue Reprint

Advances in Plant Photobiology

Edited by
Robert Luciński

mdpi.com/journal/plants

MDPI

Advances in Plant Photobiology

Advances in Plant Photobiology

Guest Editor

Robert Luciński

MDPI

Basel • Beijing • Wuhan • Barcelona • Belgrade • Novi Sad • Cluj • Manchester

Guest Editor
Robert Luciński
Department of Plant Physiology
Adam Mickiewicz University in Poznań
Poznań
Poland

Editorial Office
MDPI AG
Grosspeteranlage 5
4052 Basel, Switzerland

This is a reprint of the Special Issue, published open access by the journal *Plants* (ISSN 2223-7747), freely accessible at: https://www.mdpi.com/journal/plants/special_issues/L2986O6H6P.

For citation purposes, cite each article independently as indicated on the article page online and as indicated below:

Lastname, A.A.; Lastname, B.B. Article Title. *Journal Name* **Year**, *Volume Number*, Page Range.

ISBN 978-3-7258-8119-2 (Hbk)
ISBN 978-3-7258-8120-8 (PDF)
https://doi.org/10.3390/books978-3-7258-8120-8

© 2026 by the authors. Articles in this reprint are Open Access and distributed under the Creative Commons Attribution (CC BY) license. The reprint as a whole is distributed by MDPI under the terms and conditions of the Creative Commons Attribution-NonCommercial-NoDerivs (CC BY-NC-ND) license (https://creativecommons.org/licenses/by-nc-nd/4.0/).

Contents

About the Editor . . . . . **vii**

Preface . . . . . **ix**

Robert Luciński
Editorial for the Special Issue on Advancements in Plant Photobiology
Reprinted from: *Plants* **2025**, *14*, 3731, https://doi.org/10.3390/plants14243731 . . . . . **1**

Sibo Chen, Siyu Yang, Wanting Liu, Kaiyuan Li, Ninghan Xue and Wenli Ji
Effects of Light–Nitrogen Interactions on Leaf Functional Traits of (*Picea neoveitchii* Mast.)
Reprinted from: *Plants* **2025**, *14*, 2550, https://doi.org/10.3390/plants14162550 . . . . . **5**

Shuiling Ji, Huijiao Yao and Bernhard Grimm
Coordinated cpSRP43 and cpSRP54 Abundance Is Essential for Tetrapyrrole Biosynthesis While cpSRP43 Is Independent of Retrograde Signaling
Reprinted from: *Plants* **2025**, *14*, 1745, https://doi.org/10.3390/plants14121745 . . . . . **23**

Qi Luo, Wei Jin, Lili Li, Kedong Xu and Yunmin Wei
Potassium-Mediated Variations in the Photosynthetic Induction Characteristics of *Phaseolus vulgaris* L.
Reprinted from: *Plants* **2025**, *14*, 1623, https://doi.org/10.3390/plants14111623 . . . . . **40**

Xiaoqian Wang, Qi Shi, Ningyu Liu, Jianxin Cao and Wei Huang
Light Intensity Dependence of CO_2 Assimilation Is More Related to Biochemical Capacity Rather than Diffusional Conductance
Reprinted from: *Plants* **2025**, *14*, 986, https://doi.org/10.3390/plants14070986 . . . . . **53**

Tri Manh Le, Yuki Sago,Yasuomi Ibaraki, Kazuhiro Harada, Kenta Arai, Yuichi Ishizaki, et al.
Effect of LED Irradiation with Different Red-to-Blue Light Ratios on Growth and Functional Compound Accumulations in Spinach (*Spinacia oleracea* L.) Accessions and Wild Relatives
Reprinted from: *Plants* **2025**, *14*, 700, https://doi.org/10.3390/plants14050700 . . . . . **67**

Scott A. Heckathorn, Clare T. Muller, Michael D. Thomas, Emily P. Vining, Samantha Bigioni, Clair Elsie, et al.
Cyanobacterial Cultures, Cell Extracts, and Individual Toxins Decrease Photosynthesis in the Terrestrial Plants *Lactuca sativa* and *Zea mays*
Reprinted from: *Plants* **2024**, *13*, 3190, https://doi.org/10.3390/plants13223190 . . . . . **86**

Ashim Kumar Das, Protik Kumar Ghosh, Sheikh Arafat Islam Nihad, Sharmin Sultana, Sanjida Sultana Keya, Md. Abiar Rahman, et al.
Salicylic Acid Priming Improves Cotton Seedling Heat Tolerance through Photosynthetic Pigment Preservation, Enhanced Antioxidant Activity, and Osmoprotectant Levels
Reprinted from: *Plants* **2024**, *13*, 1639, https://doi.org/10.3390/plants13121639 . . . . . **109**

Yun Kong and Youbin Zheng
Complex Signaling Networks Underlying Blue-Light-Mediated Floral Transition in Plants
Reprinted from: *Plants* **2025**, *14*, 1533, https://doi.org/10.3390/plants14101533 . . . . . **127**

Maria Ciesielska, Małgorzata Adamiec and Robert Luciński
The Involvement of the *S2P2* Intramembrane Protease in the Response of *Arabidopsis thaliana* Chloroplasts to High Light Stress
Reprinted from: *Plants* **2025**, *14*, 2584, https://doi.org/10.3390/plants14162584 . . . . . **169**

About the Editor

Robert Luciński

Robert Luciński is a professor at Adam Mickiewicz University in Poznań, Faculty of Biology, Department of Plant Physiology. His research interests include plant physiology, photosynthesis, chloroplast biology, plant proteolysis, chloroplast proteases, and plant responses to environmental stress. He has been actively involved as a principal investigator and key contributor in research projects investigating the physiological functions of chloroplast DEG proteases, the role of minor light-harvesting antenna complexes in excitation energy transfer, and intramembrane chloroplast proteases of the EGY family, all funded by the National Science Centre or the Polish Ministry of Science. His scientific achievements include demonstrating the intrachloroplast localization of the EGY3 and S2P2 proteins and revealing the importance of intramembrane proteases in maintaining the proper stoichiometry of Photosystem II components and in chloroplast adaptation to high light stress conditions. He is also a recipient of several Rector's Awards of Adam Mickiewicz University in Poznań.

Preface

This Special Issue Reprint is devoted to the field of plant photobiology, with a particular focus on how light acts as a key environmental signal regulating plant growth, development, and metabolic activity. The aim of this Reprint is to provide an integrated overview of current research addressing the mechanisms by which plants perceive light and convert this information into coordinated physiological and developmental responses.

The scope of this collection encompasses major areas of plant photobiology, including photoperiodism, the effects of light quality and intensity on plant morphogenesis, the processes of photosynthesis, and the molecular and physiological pathways involved in light signal transduction. It also highlights how plants adapt to changing and heterogeneous light environments through finely tuned regulatory networks.

The motivation for assembling this Special Issue Reprint stems from the rapid progress in understanding plant responses to light at multiple levels of organization, from molecular signaling pathways to whole-plant adaptation strategies. By bringing together recent research contributions, this Reprint aims to consolidate current knowledge and support further advancements in both fundamental plant science and its practical applications.

This Reprint is addressed to researchers, academics, and professionals in plant sciences, agricultural sciences, and related disciplines who are interested in the mechanisms underlying plant–environment interactions and the improvement of crop performance under variable environmental conditions.

Robert Luciński
Guest Editor

plants

MDPI

Editorial

Editorial for the Special Issue on Advancements in Plant Photobiology

Robert Luciński

Department of Plant Physiology, Institute of Experimental Biology, Faculty of Biology, Adam Mickiewicz University in Poznań, ul Uniwersytetu Poznańskiego 6, 61-614 Poznań, Poland; rtl@amu.edu.pl

Light constitutes a fundamental environmental factor that profoundly influences plant growth, development, and metabolism. Red light plays a pivotal role in light-dependent photosynthetic reactions and regulates key developmental processes, including stem elongation, leaf expansion, and flowering. In contrast, blue light is primarily involved in the regulation of phototropism, chloroplast relocation, and stomatal conductance [1].

Plant photobiology represents a scientific discipline dedicated to elucidating the mechanisms by which plants perceive and respond to light. This field encompasses investigations into a wide range of phenomena, including photoperiodism, the effects of light quality and quantity on plant growth and morphogenesis, and the mechanisms underlying photosynthesis. Furthermore, plant photobiology addresses the molecular and physiological bases of light signal transduction pathways and the adaptive responses of plants to diverse light environments.

The articles presented in this Special Issue collectively explore nearly all of these dimensions of plant photobiology, contributing novel and significant insights that deepen our understanding of plant growth, developmental regulation, and the mechanisms facilitating acclimation to fluctuating light conditions. These findings provide a robust theoretical foundation for the development of practical applications aimed at enhancing agricultural productivity while ensuring environmental sustainability.

1. Photosynthetic Activity and Adaptations of the Photosynthetic Apparatus to Changing Environmental Conditions

The photosynthetic activity of plants is directly dependent on both the intensity and the quality of light reaching the leaf surface. Plants are constantly exposed to fluctuations in light intensity, which significantly affect their growth and productivity. Potassium ions appear to play an important role in the acclimation of the photosynthetic apparatus to dynamically changing light environments [2]. Low potassium availability adversely affects the photosynthetic performance of *Phaseolus vulgaris* L. under fluctuating light conditions. Under such circumstances, the stimulation of enzymes such as Rubisco may represent an effective strategy to enhance dynamic photosynthetic performance [2].

2. Rubisco Activity and CO_2 Assimilation

Rubisco activity and CO_2 assimilation are conditioned, among other factors, by the availability of ATP and NADPH, whose efficient production depends on the proper functioning of the photosynthetic electron transport chain [3], as well as on the presence and synthesis of photosynthetic pigments, such as chlorophylls, and their incorporation into the protein complexes forming the main light-harvesting antennae of photosystems, namely LHCII and LHCI. In this context, the chloroplast signal recognition particle components,

cpSRP43 and cpSRP54, play a crucial role in directing light-harvesting chlorophyll-binding proteins to the thylakoid membranes.

A comprehensive understanding of the function of cpSRP components is therefore essential for elucidating the mechanisms regulating photosynthesis. The study by [4] demonstrated that both cpSRP43 and cpSRP54 play key roles in chloroplast pigment biosynthesis and significantly contribute to overall chloroplast functionality, although the accumulation of these proteins appears to be subject to distinct regulatory control.

3. Regulation of CO_2 Assimilation Rate

The rate of CO_2 assimilation is, as expected, closely dependent on the intensity of light reaching the leaf surface. However, the mechanisms underlying this relationship remain relatively poorly understood. Recent studies presented in this Special Issue indicate that the rate of CO_2 assimilation is largely regulated by the carboxylation capacity of Rubisco (V_{max}), which in turn depends on energy availability [3]. Characterizing these relationships provides valuable insights into the potential for improving crop performance through the manipulation of V_{max}.

4. Photoprotective Mechanisms and the Role of Chloroplast Proteases

The photosynthetic apparatus, particularly the pigment–protein complexes embedded in the thylakoid membranes that are responsible for harvesting light energy and transferring it to the reaction centers of the photosystems, is especially vulnerable to damage caused by various environmental stresses, most notably by excessive light intensity. In this context, mechanisms protecting the photosynthetic machinery against photoinhibition and photodestruction play a crucial role.

An important component of this complex network of protective and repair systems is chloroplast proteases. Some of them, referred to as intramembrane proteases, e.g., the S2P2 protease, are thought to be involved in the response of the photosynthetic apparatus already at the level of chloroplast gene expression, regulating the synthesis of key photosynthetic proteins. As demonstrated by [5], the S2P2 protease plays a significant role in shaping the stoichiometric relationships among photosystem II core proteins and influences the chloroplast's capacity to mitigate excessive levels of reactive oxygen species generated under high light stress conditions.

5. High-Temperature Stress and Its Impact on Photosynthetic Efficiency

Another major environmental factor, alongside excessive light intensity, that negatively affects photosynthetic efficiency is high temperature. This stress factor has become increasingly pronounced in recent years, coinciding with the global rise in temperature associated with climate change. Heat stress in plants adversely affects not only the process of photosynthesis itself, but also leads to disturbances in plant growth and productivity, largely by exacerbating oxidative stress within plant cells [6].

The studies presented in this Special Issue [6] indicate that the application of low concentrations of salicylic acid can effectively enhance heat tolerance in cotton (*Gossypium hirsutum*) by, among other mechanisms, protecting photosynthetic pigments from heat-induced degradation.

6. Environmental Pollution as a Stress Factor Affecting Photosynthetic Efficiency

Environmental pollution is another factor that adversely affects the efficiency of photosynthesis, which may be particularly detrimental in the case of crop species such as *Zea mays* and *Lactuca sativa*. It has been demonstrated that contamination of irrigation

water with cyanobacterial cultures and their associated toxins can lead to a reduction in net photosynthetic efficiency. Interestingly, researchers have shown that root exposure to water containing cyanobacterial toxins decreases total net photosynthesis, yet does not impair the electron transport processes within photosystem II.

Moreover, the presence of cyanobacteria in the irrigation medium also results in a decline in Rubisco activity and a reduction in total chlorophyll content in plant leaves [7].

7. Light Intensity, Nutrient Availability, and Conservation Physiology

Research on the relationship between photosynthetic efficiency, light intensity, and the availability of essential mineral nutrients such as nitrogen also provides valuable insights for developing strategies aimed at the conservation of endangered plant species. An illustrative example is the analysis of the interaction between light intensity and nitrogen supply in relation to photosynthetic performance and stress tolerance in *Picea neoveitchii* Mast. [8]. A key practical aspect of this study lies in its contribution to establishing a scientific basis for the protection and ecological restoration of endangered plant populations.

8. Light Spectral Quality and Its Impact on Plant Development

Light spectra quality is an important environmental factor determining plant growth and development. The roles of red and far-red light in the initiation of flowering are well established. However, considerably less is known about the role of blue light in this process. Nevertheless, blue light may also play an important role in the regulation of floral transition [9]. An insightful review by Kong and Zheng [9], published in this Special Issue, provides a comprehensive overview of the signaling network of blue light–mediated floral transition in plants, offering a critical analysis of the involved photoreceptors and key components of the blue-light-induced signal transduction pathway.

In turn, the practical use of combined blue and red-light spectra for supplemental lighting in spinach cultivation demonstrates that proper ratios of these wavelengths can promote favorable biomass accumulation. Moreover, the conducted studies have revealed the crucial role of phytochrome, the red-light photoreceptor, in regulating plant growth, as well as the importance of blue-light photoreceptors in mediating amino acid and sugar accumulation [1].

9. Conclusions

Light is a fundamental environmental factor influencing plant growth and developmental processes. The perception and utilization of light in plants occur at multiple levels and involve various receptors and regulatory mechanisms. Light governs not only vegetative growth but also the transition from the vegetative to the reproductive phase of development. These processes are mediated by specific red- and blue-light photoreceptors.

At the same time, blue and red light are absorbed by photosynthetic pigments within chloroplasts, driving the process of photosynthesis. This process, being directly dependent on the intensity of light reaching the leaves, is highly sensitive to fluctuations in light intensity. Consequently, over the course of evolution, plants have developed a range of mechanisms enabling them to acclimate to dynamically changing light environments.

All these aspects, along with their practical implications for crop cultivation, are addressed in the present Special Issue, which explores diverse topics within the broad field of plant photobiology.

Funding: This research received no external funding.

Data Availability Statement: All papers cited in this editorial are available in the following link: https://www.mdpi.com/journal/plants/special_issues/L2986O6H6P (accessed on 24 October 2025).

Acknowledgments: The guest editor is grateful to all authors who accepted the invitation to submit their research to this SI.

Conflicts of Interest: The author declare no conflicts of interest.

References

1. Le, T.M.; Sago, Y.; Ibaraki, Y.; Harada, K.; Arai, K.; Ishizaki, Y.; Aoki, H.; Abdelrahman, M.; Kik, C.; van Treuren, R.; et al. Effect of LED Irradiation with Different Red-to-Blue Light Ratios on Growth and Functional Compound Accumulations in Spinach (*Spinacia oleracea* L.). *Plants* **2025**, *14*, 700. [CrossRef] [PubMed]
2. Luo, Q.; Jin, W.; Li, L.; Xu, K.; Wei, Y. Potassium-Mediated Variations in the Photosynthetic Induction Characteristics of *Phaseolus vulgaris* L. *Plants* **2025**, *14*, 1623. [CrossRef]
3. Wang, X.Q.; Shi, Q.; Liu, N.Y.; Cao, J.X.; Huang, W. Light Intensity Dependence of CO_2 Assimilation is More Related to Biochemical Capacity Rather Than Diffusional Conductance. *Plants* **2025**, *14*, 986. [CrossRef] [PubMed]
4. Ji, S.; Yao, H.; Grimm, B. Coordinated cpSRP43 and cpSRP54 abundance is essential for tetrapyrrole biosynthesis while cpSRP43 is independent of retrograde signaling. *Plants* **2025**, *14*, 1745. [CrossRef] [PubMed]
5. Ciesielska, M.; Adamiec, M.; Luciński, R. The Involvement of the S2P2 Intramembrane Protease in the Response to High Light Stress of Arabidopsis thaliana chloroplasts. *Plants* **2025**, *14*, 2584. [CrossRef] [PubMed]
6. Das, A.K.; Ghosh, P.K.; Nihad, S.A.I.; Sultana, S.; Keya, S.S.; Rahman, A.; Ghosh, T.K.; Akter, M.; Hasan, M.; Salma, U.; et al. Salicylic Acid Priming Improves Cotton Seedling Heat Tolerance through Photosynthetic Pigment Preservation, Enhanced Antioxidant Activity, and Osmoprotectant Levels. *Plants* **2025**, *13*, 1639. [CrossRef] [PubMed]
7. Heckathorn, S.A.; Muller, C.T.; Thomas, M.D.; Vining, E.P.; Bigioni, S.; Elsie, C.; Franklin, J.T.; New, E.R.; Boldt, J.K. Cyanobacterial Cultures, Cell Extracts, and Individual Toxins Decrease Photosynthesis in the Terrestial Plants *Lactuca sativa* and *Zea mays*. *Plants* **2024**, *13*, 3190. [CrossRef] [PubMed]
8. Chen, S.; Yang, S.; Liu, W.; Li, K.; Xue, N.; Ji, W. Biochemical Mechanism Underlying The Effects of Light-Nitrogen Interaction on Leaf Traits and N/P Uptake in *Picea neoveitchii* Mast. *Plants* **2025**, *14*, 2550. [CrossRef]
9. Kong, Y.; Zheng, Y. Complex sygnaling Networks Underlying Blue-Light-Mediated Floral Transition in Plants. *Plants* **2025**, *14*, 1533. [CrossRef] [PubMed]

Disclaimer/Publisher's Note: The statements, opinions and data contained in all publications are solely those of the individual author(s) and contributor(s) and not of MDPI and/or the editor(s). MDPI and/or the editor(s) disclaim responsibility for any injury to people or property resulting from any ideas, methods, instructions or products referred to in the content.

plants

MDPI

Article

Effects of Light–Nitrogen Interactions on Leaf Functional Traits of (*Picea neoveitchii* Mast.)

Sibo Chen †, Siyu Yang †, Wanting Liu, Kaiyuan Li, Ninghan Xue and Wenli Ji *

College of Landscape Architecture and Arts, Northwest A&F University, Xianyang 712100, China; chensibo@nwafu.edu.cn (S.C.); byyangsiyu@163.com (S.Y.)

* Correspondence: jiwenli@nwafu.edu.cn; Tel.: +86-029-8708-0274

† These authors contributed equally to this work.

Abstract: *Picea neoveitchii* Mast., a critically endangered spruce species endemic to China, is classified as a national second-level key protected wild plant and listed as critically endangered (CR) on the International Union for Conservation of Nature (IUCN) Red List. Its habitat features complex forest light environments, and global climate change coupled with environmental pollution has increased regional nitrogen deposition, posing significant challenges to its survival. This study explores the effects of light–nitrogen interactions on the leaf functional traits of *Picea neoveitchii* Mast. seedlings by simulating combinations of light intensities (100%, 70%, and 40% full sunlight) and nitrogen application levels (0, 10, and 20 g N·m $^{-2}$·a^{-1}, where g N·m^{-2}·a^{-1} denotes grams of nitrogen applied per square meter per year). We examined changes in morphological traits, anatomical structures, photosynthetic physiology, and stress resistance traits. Results indicate that moderate shading (70% full sunlight) significantly enhances leaf morphological traits (e.g., leaf length, leaf area, and specific leaf area) and anatomical features (e.g., mesophyll tissue area and resin duct cavity area), improving light capture and stress resistance. Medium- to high-nitrogen treatments (10 or 20 g N·m^{-2}·a^{-1}) under moderate shading further increase photosynthetic efficiency, stomatal conductance, and antioxidant enzyme activity. According to the comprehensive membership function evaluation, the L2N0 (70% full sunlight, 0 g N·m^{-2}·a^{-1}) treatment exhibits the most balanced performance across both growth and stress-related traits. These findings underscore the critical role of light–nitrogen interactions in the growth and adaptability of *Picea neoveitchii* Mast. leaves, offering a scientific foundation for the conservation and ecological restoration of endangered plant populations.

Keywords: light–nitrogen interaction; leaf functional traits; photosynthesis; stress resistance; ecological adaptation

1. Introduction

Picea neoveitchii Mast., a national second-level key protected wild plant endemic to China, is listed by the National Forestry and Grassland Administration of China under the "Wild Plants with Extremely Small Population (WPESP)" directory and classified as critically endangered (CR) on the International Union for Conservation of Nature (IUCN) Red List of Threatened Species [1,2]. This species is primarily distributed in the Qinling Mountains and their subsidiary ranges, thriving in specific habitats such as valley bottoms or semi-shaded slopes within mixed coniferous–broadleaf forests, where it exhibits stringent ecological requirements [3]. In recent years, overlogging and habitat loss have precipitated a drastic population decline, garnering widespread concern for its survival.

Current research has predominantly explored endangerment mechanisms, community characteristics, genetic diversity, and seedling cultivation techniques, revealing a significant population decline driven by habitat fragmentation, weak sexual reproduction, high seed emptiness rates, and low germination success [4,5]. However, investigations into its physiological and ecological adaptation mechanisms remain nascent, particularly regarding response strategies to light–nitrogen interactions.

Light is the energy base that drives photosynthesis, and nitrogen is one of the essential nutrients that plants need most, and they coordinate the allocation strategy of plant resources [6–8]. Light fuels photosynthesis by converting solar energy into chemical energy, underpinning organic matter synthesis and energy flow within the biosphere [9]. A plant's capacity to adapt to light conditions shapes its competitive and survival potential within ecosystems, with light intensity, quality, and photoperiod influencing photosynthetic efficiency, growth morphology, and metabolic regulation [9–11]. Optimal light enhances photosynthetic rates and growth, whereas insufficient or excessive light induces photosynthetic inhibition, metabolic disruption, and growth limitation [12]. Nitrogen, an essential nutrient, forms the backbone of nucleic acids, proteins, and chlorophyll, playing a critical role in plant growth, metabolism, and reproduction [13,14]. Its availability directly impacts photosynthesis, carbon–nitrogen metabolism, and biomass accumulation, while shifts in soil nitrogen levels reflect adaptive strategies to environmental nutrient dynamics [15]. Amid global climate change and escalating environmental pollution, heightened regional nitrogen deposition profoundly alters plant community structure and species diversity, underscoring the ecological imperative of elucidating light and nitrogen effects on plants [16].

Plant functional traits underpin their adaptation to environmental conditions and life processes, spanning morphological, physiological, and ecological dimensions [17]. As the primary interface with the environment, leaves serve as hubs for photosynthesis, transpiration, and respiration, rendering their functional traits highly responsive to environmental shifts and valuable for studying adaptability [18]. These traits encompass macroscopic morphology (e.g., leaf area, specific leaf area, and dry matter content), which indicate resource acquisition and utilization efficiency and reflect growth strategies; microscopic anatomy (e.g., stomatal density and tissue structure), which governs transpiration and photosynthetic efficiency; and biochemical properties (e.g., chlorophyll content), which signal photosynthetic capacity and nutrient status [9,19–21]. Nitrogen (N) and phosphorus (P) are fundamental to plant physiology: N drives photosynthesis, metabolism, nutrient storage, and development, while P supports nucleic acids and phospholipids critical for growth and reproduction [22,23]. The N/P ratio illuminates nutrient uptake efficiency and growth rates [24]. Recent research increasingly emphasizes leaf photosynthetic traits and stress resistance, employing parameters such as net photosynthetic rate (Pn) and stomatal conductance (Gs) to assess adaptability across conditions, chlorophyll fluorescence to non-destructively probe photosystem dynamics, and metabolic regulation (e.g., protective enzymes, osmolytes, and non-structural carbohydrates) to explore stress responses [25–28].

This study targets *Picea neoveitchii* Mast. to elucidate its adaptation strategies to heterogeneous environments by examining leaf functional trait responses under varying light and nitrogen conditions. Through controlled simulation experiments, we aim to delineate the pathways by which light–nitrogen interactions influence its growth and physiological metabolism, specifically addressing how leaf traits respond to light intensity and soil nitrogen gradients. Set against the backdrop of global climate change and rising nitrogen deposition, this research seeks to unravel the effects of light–nitrogen interplay on *Picea neoveitchii* Mast.'s growth and adaptability. By enriching theoretical frameworks

for ecological adaptation in endangered plants, our findings aim to provide a scientific foundation for the conservation and restoration of this critically imperiled species.

2. Results

2.1. Effects of Light–Nitrogen Interaction on Needle Morphological and Anatomical Traits of Picea neoveitchii Mast. Seedlings

Significant differences were observed in needle length, leaf area, specific leaf area (SLA), and leaf dry matter content of *Picea neoveitchii* Mast. seedlings under varying shading and nitrogen treatments (Figure 1). Needle length was highest in the L2N2 treatment (9.66 mm), 1.45 times greater than the control group L1N0 (CK, the following have been referred to by CK, 6.67 mm). Under identical light conditions, needle length showed a non-significant variation across nitrogen levels in the L1 treatment, while in L3, only the N0 treatment resulted in a significantly longer needle length compared to N1 and N2. In contrast, needle length consistently increased with nitrogen addition under the L2 treatment. Under identical nitrogen levels, decreasing light intensity resulted in similar trends in needle length. Leaf area was greatest in the L2N2 treatment (9.64 mm^2), 2.02 times that of the control. In L1 treatments, leaf area initially increased with nitrogen application and then decreased, whereas it consistently increased in L2 and L3 treatments. SLA was highest in the L2N1 treatment (92.17 $cm^2 \cdot g^{-1}$), significantly exceeding other treatments. Leaf dry matter content showed minimal variation, with the highest values in L1N1 and L2N0 treatments (0.38 $g \cdot g^{-1}$), slightly above the control (0.37 $g \cdot g^{-1}$).

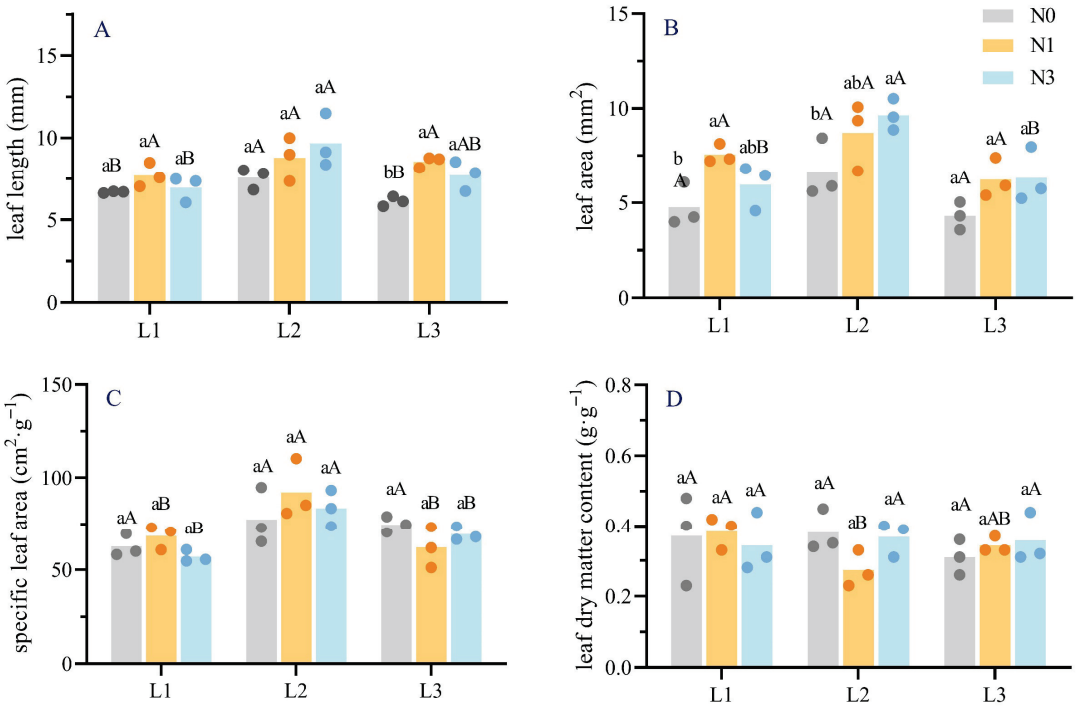


Figure 1. Effects of light and nitrogen interaction on morphological characteristics of needles of *Picea neoveitchii* Mast. seedlings. (L1: 100% full light, L2: 70% full light, and L3: 40% full light; N0: 0 g N $m^{-2} \cdot a^{-1}$, N0: 10 g N $m^{-2} \cdot a^{-1}$, and N1: 20 g N $m^{-2} \cdot a^{-1}$. Different lowercase letters indicate significant differences ($p < 0.05$) between different nitrogen application groups under the same shading treatment; different capital letters indicate significant differences ($p < 0.05$) between different shading treatment groups under the same nitrogen application treatment). (**A**) is leaf length, (**B**) is leaf area, (**C**) is specific leaf area, and (**D**) is leaf dry matter content.

Among needle traits (Table 1), needle thickness was greatest in the L2N0 treatment, 1.46 times that of L2N2. Stomatal density was highest in the CK treatment, 2.41 times that of

L2N0. Under the L2 treatment, stomatal density showed an increasing trend with nitrogen addition, and the N2 treatment exhibited a significantly higher value than N0. In contrast, under L3, no consistent or significant pattern was observed in stomatal density across nitrogen levels. Needle cross-sectional area and perimeter reached their maximum values in the L2N0 treatment, but the differences among nitrogen treatments were not statistically significant in some light conditions. Epidermal tissue area and mesophyll tissue area were greatest in the L2N0 treatment, decreasing with increasing nitrogen application. Resin duct cavity area was largest in the L3N0 treatment, 4.75 times that of CK and L2N2, with notable variation across nitrogen levels. Endodermal and central cylinder areas were greatest in the L2N0 treatment, decreasing with increasing nitrogen application. The proportions of mesophyll and resin duct cavity areas were highest in the L3N0 treatment, exhibiting distinct variation trends.

Table 1. Effects of light and nitrogen interaction on needle anatomical characteristics of *Picea neoveitchii* Mast. seedlings.

Anatomical Characteristics	N Treatment	Shading Treatment		
		L1 100% Full Light	L2 70% Full Light	L3 40% Full Light
Needle thickness (mm)	N0	0.60 ± 0.14 aA	0.79 ± 0.06 aA	0.60 ± 0.03 aA
	N1	0.62 ± 0.14 aA	0.68 ± 0.02 abA	0.55 ± 0.05 aA
	N2	0.66 ± 0.06 aA	0.54 ± 0.11 bA	0.62 ± 0.09 aA
Stomatal density (No. mm^2)	N0	56.19 ± 20.72 aA	23.32 ± 3.13 bB	31.19 ± 3.53 aB
	N1	33.19 ± 7.36 bA	23.72 ± 3.84 bA	27.95 ± 1.95 aA
	N2	35.82 ± 4.83 abA	37.81 ± 5.22 aA	32.90 ± 3.81 aA
Needle cross-sectional area (10^{-2} mm^2)	N0	40.01 ± 1.84 aB	81.07 ± 11.60 aA	54 ± 6.67 aB
	N1	49.08 ± 6.34 aA	55.72 ± 6.15 bA	47.6 ± 3.30 aA
	N2	52.33 ± 9.84 aA	50.75 ± 8.19 bA	50.2 ± 2.59 aA
Perimeter of needle section (mm)	N0	2.88 ± 0.47 aA	3.58 ± 0.43 aA	3.01 ± 0.28 aA
	N1	2.78 ± 0.19 aA	2.94 ± 0.16 bA	2.85 ± 0.01 aA
	N2	2.83 ± 0.28 aA	3.1 ± 0.20 abA	2.87 ± 0.17 aA
Epidermal tissue area (10^{-2} mm^2)	N0	6.03 ± 1.49 aA	8.85 ± 1.81 aA	6.59 ± 0.47 aA
	N1	5.93 ± 1.22 aA	6.49 ± 0.96 aA	6.85 ± 0.57 aA
	N2	7.13 ± 1.44 aA	6.83 ± 0.84 aA	6.51 ± 0.84 aA
Mesophyll tissue area (10^{-2} mm^2)	N0	30.72 ± 1.73 aB	66.81 ± 9.87 aA	42.3 ± 5.93 aB
	N1	38.12 ± 7.04 aA	45.02 ± 5.32 bA	36.38 ± 3.19 aA
	N2	40.15 ± 7.28 aA	40.25 ± 5.83 bA	39.71 ± 2.25 aA
Resin cavity area (10^{-2} mm^2)	N0	0.08 ± 0.02 bB	0.16 ± 0.09 aB	0.38 ± 0.13 aA
	N1	0.18 ± 0.04 aA	0.19 ± 0.04 aA	0.26 ± 0.06 abA
	N2	0.18 ± 0.03 aA	0.08 ± 0.02 aA	0.16 ± 0.08 bA
Endocortical area (10^{-2} mm^2)	N0	1.35 ± 0.15 aB	1.88 ± 0.2 aA	1.56 ± 0.15 aAB
	N1	1.27 ± 0.16 aA	1.49 ± 0.14 abA	1.38 ± 0.15 abA
	N2	1.41 ± 0.27 aA	1.22 ± 0.31 bA	1.20 ± 0.06 bA
Central column area (10^{-2} mm^2)	N0	2.27 ± 0.20 bB	3.36 ± 0.18 aA	3.29 ± 0.11 aA
	N1	2.53 ± 0.28 bA	2.55 ± 0.24 bA	2.73 ± 0.5 aA
	N2	3.14 ± 0.26 aA	1.88 ± 0.27 cB	2.61 ± 0.35 aA
Mesophyll tissue area ratio (%)	N0	76.76 ± 0.91 bB	82.38 ± 0.47 aA	78.23 ± 1.51 aB
	N1	79.89 ± 1.02 aA	80.76 ± 1.20 abA	76.37 ± 1.35 aB
	N2	76.79 ± 0.59 bA	79.43 ± 1.29 bA	79.11 ± 1.89 aA
Resin cavity area ratio (%)	N0	0.19 ± 0.057 bB	0.19 ± 0.077 bB	0.70 ± 0.149 aA
	N1	0.36 ± 0.10 aA	0.35 ± 0.099 aA	0.55 ± 0.10 abA
	N2	0.35 ± 0.08 aA	0.16 ± 0.017 bB	0.33 ± 0.18 bAB
Area ratio of central column (%)	N0	5.61 ± 0.28 aA	4.21 ± 0.74 aB	6.13 ± 0.59 aA
	N1	5.19 ± 0.51 aAB	4.59 ± 0.36 aB	5.69 ± 0.68 aA
	N2	6.10 ± 0.88 aA	3.71 ± 0.20 aB	5.20 ± 0.57 aA

Different lowercase letters indicate significant differences ($p < 0.05$) between different nitrogen application groups under the same shading treatment; different capital letters indicate significant differences ($p < 0.05$) between different shading treatment groups under the same nitrogen application treatment.

2.2. Effects of Light–Nitrogen Interaction on N and P Stoichiometric Characteristics of Picea neoveitchii Mast. Seedling Needles

Under varying shading and nitrogen treatments (Figure 2), nitrogen content was highest in the L1N2 treatment (23.49 mg·g^{-1}), 1.89 times that of the lowest value in the L2N0 treatment. Phosphorus content was highest in the CK treatment (2.83 mg·g^{-1}), 1.74 times that of the lowest value in the L3N2 treatment. The N/P ratio was highest in the L3N2 treatment (12.90), 2.35 times that of the control. Under identical light conditions, nitrogen content did not show statistically significant differences among nitrogen treatments in L1, L2, or L3 groups, although a slight increase was observed in L2 and L3. Phosphorus content also exhibited no significant differences among nitrogen levels, and no consistent pattern could be established across light treatments. The N/P ratio significantly increased with higher nitrogen application. Under identical nitrogen levels, nitrogen and phosphorus contents exhibited distinct patterns with changing light intensity, while the N/P ratio generally increased with decreasing light intensity across most treatments.

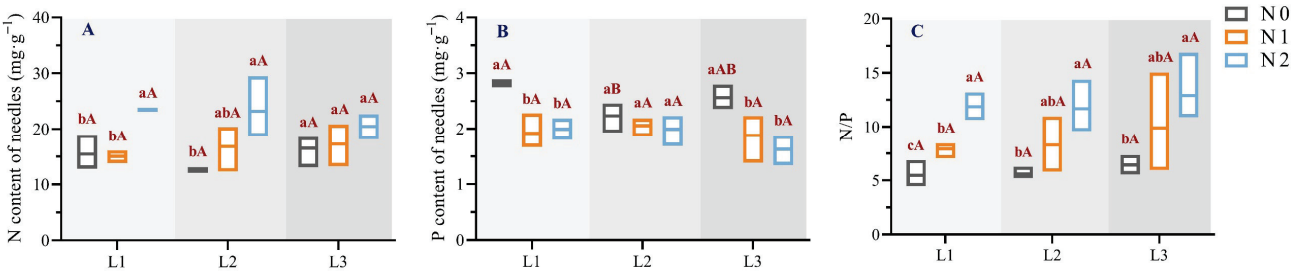


Figure 2. Effects of light–nitrogen interactions on the stoichiometric characteristics of N and P in needles of *Picea neoveitchii* Mast. seedlings. (L1: 100% full light, L2: 70% full light, and L3: 40% full light; N0: 0 g N m^{-2}·a^{-1}, N1: 10 g N m^{-2}·a^{-1}, and N2: 20 g N m^{-2}·a^{-1}. Different lowercase letters indicate significant differences ($p < 0.05$) between different nitrogen application groups under the same shading treatment; different capital letters indicate significant differences ($p < 0.05$) between different shading treatment groups under the same nitrogen application treatment). (**A**) is N content of needles, (**B**) is P content of needles, and (**C**) is N/P of needles.

2.3. Effects of Light–Nitrogen Interaction on Photosynthetic Physiological Traits of Picea neoveitchii Mast. Seedling Needles

Under varying shading and nitrogen treatments (Table 2), chlorophyll a content was highest in the L3N2 treatment (0.261 mg·g^{-1}), 2.06 times that of the L3N1 treatment. The chlorophyll content in N1 decreased compared to the control (only in L2, the decrease was insignificant), while a significant increase under the influence of nitrogen was only present in L1N2. Chlorophyll b content was highest in the L3N2 treatment (0.205 mg·g^{-1}); it decreased with increasing nitrogen in the L1 treatments, whereas in the L2 and L3 treatments, the highest values occurred in N2. Total chlorophyll content was greatest in the L3N2 treatment (0.465 mg·g^{-1}), decreasing with increasing nitrogen in the L1 treatments, but showing a decline followed by an increase in the L2 and L3 treatments. Carotenoid content showed no significant differences; in the L1 and L2 treatments, it initially decreased then increased with nitrogen application, while in the L3 treatments, it consistently decreased.

Analysis of photosynthetic and chlorophyll fluorescence parameters of *Picea neoveitchii* Mast. seedling needles (Figure 3) revealed that the net photosynthetic rate was highest in the L2N1 treatment (4.85 μmol·m^{-2}·s^{-1}), 3.13 times that of the control group. In the L1 and L2 treatments, net photosynthetic rate showed no statistically significant differences among nitrogen levels, although slight fluctuations in mean values were observed. In the L3 treatments, a modest increase in net photosynthetic rate was observed with increasing nitrogen application, but this trend was not statistically significant. Stomatal conductance was highest in the L3N2 treatment (348.92 mmol·m^{-2}·s^{-1}), 6.33 times that of the control,

with varied trends across nitrogen levels. Intercellular CO_2 concentration peaked in the L3N0 treatment (376.58 μmol·mol^{-1}), and transpiration rate was highest in the L3N2 treatment (5.84 mmol·m^{-2}·s^{-1}). Water use efficiency and transpiration rate exhibited diverse trends with changes in light and nitrogen levels. For chlorophyll fluorescence parameters, both Fv/Fm and Fv/Fo were highest in the L2N0 treatment (0.589 and 1.489, respectively), 1.96 and 3.33 times those of the control. Under identical light conditions, these parameters generally decreased then increased with increasing nitrogen application; under identical nitrogen levels, they typically increased then decreased with decreasing light intensity.

Table 2. Effects of light and nitrogen interaction on needle photosynthetic pigments of *Picea neoveitchii* Mast. seedlings.

Photosynthetic Pigment	N Treatment	Shading Treatment		
		L1 100% Full Light	L2 70% Full Light	L3 40% Full Light
Chlorophyll a content (mg·g^{-1})	N0	0.245 ± 0.058 aA	0.162 ± 0.034 aA	0.216 ± 0.03 aA
	N1	0.162 ± 0.027 bA	0.152 ± 0.046 aA	0.127 ± 0.027 bA
	N2	0.143 ± 0.018 bB	0.171 ± 0.036 aB	0.261 ± 0.025 aA
Chlorophyll b content (mg·g^{-1})	N0	0.151 ± 0.042 aA	0.086 ± 0.009 aA	0.124 ± 0.043 bA
	N1	0.093 ± 0.021 bA	0.089 ± 0.041 aA	0.046 ± 0.011 cA
	N2	0.063 ± 0.006 bB	0.092 ± 0.029 aB	0.205 ± 0.033 aA
Total chlorophyll content (mg·g^{-1})	N0	0.396 ± 0.100 aA	0.248 ± 0.043 aB	0.339 ± 0.054 bAB
	N1	0.255 ± 0.048 bA	0.240 ± 0.087 aA	0.173 ± 0.038 cA
	N2	0.206 ± 0.015 bB	0.264 ± 0.065 aB	0.465 ± 0.052 aA
Carotenoid content (mg·g^{-1})	N0	0.061 ± 0.015 aA	0.056 ± 0.005 aA	0.052 ± 0.017 aA
	N1	0.053 ± 0.010 aA	0.044 ± 0.011 aA	0.050 ± 0.010 aA
	N2	0.056 ± 0.004 aA	0.055 ± 0.010 aA	0.038 ± 0.013 aA

Different lowercase letters indicate significant differences ($p < 0.05$) between different nitrogen application groups under the same shading treatment; different capital letters indicate significant differences ($p < 0.05$) between different shading treatment groups under the same nitrogen application treatment.

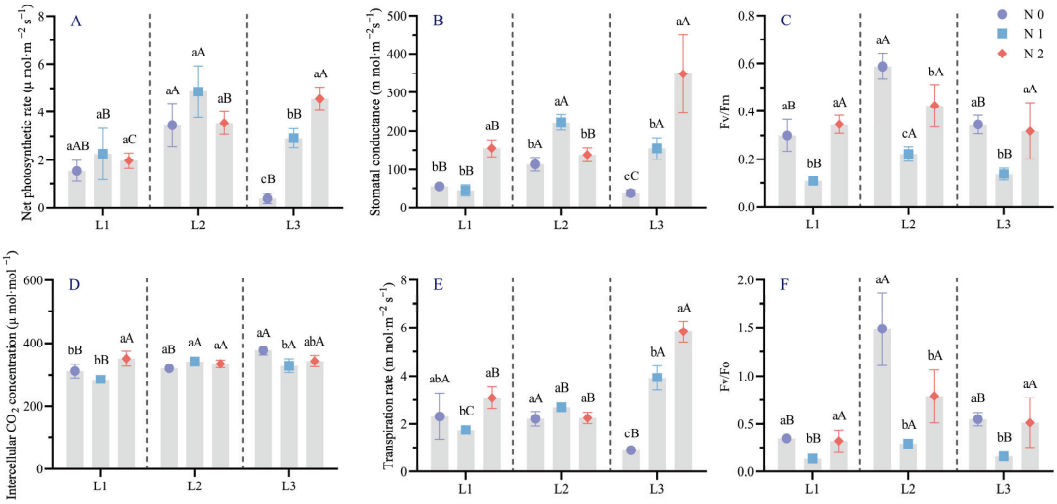


Figure 3. Effects of light and nitrogen interaction on photosynthetic parameters and chlorophyll fluorescence parameters of *Picea neoveitchii* Mast. seedlings. (L1: 100% full light, L2: 70% full light, and L3: 40% full light; N0: 0 g N m^{-2}·a^{-1}, N1: 10 g N m^{-2}·a^{-1}, and N2: 20 g N m^{-2}·a^{-1}.) (**A**) is net photosynthetic rate, (**B**) is Stomatal conductance, (**C**) is Fv/Fm, (**D**) is intercellular CO_2 concentration, (**E**) is transpiration rate, (**F**) is Fv/Fo. Different lowercase letters indicate significant differences ($p < 0.05$) between different nitrogen application groups under the same shading treatment; different capital letters indicate significant differences ($p < 0.05$) between different shading treatment groups under the same nitrogen application treatment).

2.4. Effects of Light–Nitrogen Interaction on Stress Resistance Physiological Traits of Picea neoveitchii Mast. Seedling Needles

Under varying shading and nitrogen treatments (Figure 4), superoxide dismutase (SOD) activity peaked in the L3N2 treatment at 220.03 U·g^{-1}, 1.01 times that of the control group. Under identical light conditions, SOD activity trends varied with nitrogen application, showing patterns of initial decline followed by an increase or vice versa depending on light intensity. Peroxidase (POD) activity was highest in the control group CK (30.59 U·g^{-1}·min^{-1}), four times that of the lowest value in L2N2, exhibiting complex interactions with nitrogen application and shading levels. Catalase (CAT) activity showed no significant differences, with the highest value in the L3N1 treatment (299.25 U·g^{-1}·min^{-1}), 1.06 times that of the control. CAT activity displayed varied trends across light and nitrogen levels, such as decreasing then increasing or increasing then decreasing with nitrogen application.

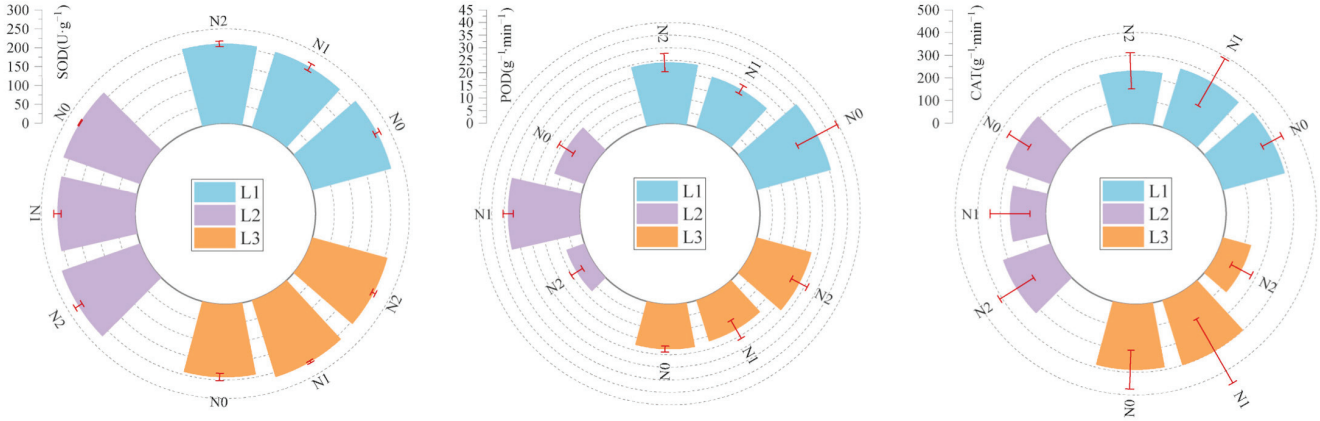


Figure 4. Effects of light and nitrogen interaction on needle protective enzyme activity of *Picea neoveitchii* Mast. seedlings. (L1: 100% full light, L2: 70% full light, and L3: 40% full light; N0: 0 g N m^{-2}·a^{-1}, N1: 10 g N m^{-2}·a^{-1}, and N2: 20 g N m^{-2}·a^{-1}. Error bars represent standard deviation. Significance was assessed at $p < 0.05$).

Under varying shading and nitrogen treatments (Table 3), the trends of multiple physiological indicators of the needles of *Picea neoveitchii* Mast. seedlings were different. The highest soluble protein content was observed in the L2N2 treatment (1.73 mg·g^{-1}), though not significantly different from the control (CK). Free proline content was highest in the L1N2 treatment (445.05 μg·g^{-1}), 1.46 times that of the control. Malondialdehyde (MDA) content was highest in the CK treatment (1.396 mmol·g^{-1}), 3.08 times that of the lowest value in L1N1. Relative conductivity reached its maximum in the CK treatment (73.42%), 1.98 times that of L3N1. Soluble sugar content was highest in the L2N0 treatment (70.50 mg·g^{-1}), while needle starch content peaked in the L1N2 treatment (13.92 mg·g^{-1}). Additionally, non-structural carbohydrate (NSC) content was highest in the L2N0 treatment (82.03 mg·g^{-1}), significantly exceeding other treatments. Overall, while some indicators like MDA and relative conductivity consistently decreased under shading and nitrogen treatments, others such as starch and NSC exhibited treatment-specific responses without a clear directional trend.

Table 3. Effects of light and nitrogen interaction on needle osmoregulation substance accumulation of *Picea neoveitchii* Mast. seedlings.

Resistance Physiological traits	N Treatment	Shading Treatment		
		L1 100% Full Light	L2 70% Full Light	L3 40% Full Light
Soluble protein content ($mg \cdot g^{-1}$)	N0	1.71 ± 0.27 aA	1.47 ± 0.39 abA	1.44 ± 0.04 aA
	N1	1.68 ± 0.03 aA	1.19 ± 0.11 bB	1.18 ± 0.14 aB
	N2	1.09 ± 0.24 bA	1.73 ± 0.08 aA	1.40 ± 0.47 aA
Free proline content ($\mu g \cdot g^{-1}$)	N0	304.95 ± 28.67 bA	287.00 ± 22.00 aA	312.84 ± 15.17 bA
	N1	314.56 ± 10.85 bAB	352.51 ± 37.09 aA	281.23 ± 12.48 bB
	N2	445.05 ± 18.41 aA	346.15 ± 55.87 aB	390.19 ± 48.11 aAB
Malondialdehyde content ($m \cdot mol\ g^{-1}$)	N0	1.3960.815 aA	0.676 ± 0.217 aAB	0.472 ± 0.098 aB
	N1	0.453 ± 0.195 bA	0.550 ± 0.097 aA	0.686 ± 0.355 aA
	N2	0.772 ± 0.337 abA	0.499 ± 0.036 aA	0.970 ± 0.432 aA
Relative electrical conductivity (%)	N0	73.42 ± 3.99 aA	60.66 ± 7.35 aA	64.77 ± 9.97 aA
	N1	63.60 ± 4.80 aA	55.22 ± 3.40 aB	37.00 ± 0.36 bC
	N2	64.60 ± 9.95 aA	38.17 ± 4.17 bB	52.07 ± 4.92 aA
Soluble sugar content ($mg \cdot g^{-1}$)	N0	58.47 ± 6.04 aB	70.50 ± 2.43 aA	48.90 ± 5.99 aB
	N1	65.95 ± 9.43 aA	51.49 ± 6.53 bB	47.19 ± 1.35 aB
	N2	59.17 ± 9.77 aA	55.61 ± 11.89 abA	50.38 ± 14.07 aA
Starch content ($mg \cdot g^{-1}$)	N0	9.99 ± 0.53 bB	11.53 ± 0.97 aAB	11.82 ± 0.76 aA
	N1	9.96 ± 1.56 bA	11.66 ± 1.35 aA	10.01 ± 0.63 bA
	N2	13.92 ± 2.27 aA	12.52 ± 2.43 aAB	9.12 ± 0.98 bB
Unstructured carbohydrates ($mg \cdot g^{-1}$)	N0	68.47 ± 6.49 aB	82.03 ± 1.76 aA	60.71 ± 6.54 aB
	N1	75.91 ± 10.88 aA	63.15 ± 6.14 bAB	57.19 ± 1.82 aB
	N2	73.08 ± 11.88 aA	68.13 ± 13.98 abA	59.5 ± 15.03 aA

Different lowercase letters indicate significant differences ($p < 0.05$) between different nitrogen application groups under the same shading treatment; different capital letters indicate significant differences ($p < 0.05$) between different shading treatment groups under the same nitrogen application treatment.

2.5. Membership Function Analysis of Leaf Functional Traits of Picea neoveitchii Mast. Seedlings

The effects of light and nitrogen on leaf functional traits of *Picea neoveitchii* Mast. seedlings are complex, resulting from multifaceted interactions. This study employed membership function analysis to comprehensively evaluate leaf functional traits under different shading and nitrogen treatments. Based on membership values (U), environmental adaptability was classified into four levels: non-resistant ($U < 0.2$), weakly resistant ($0.2 \leq U < 0.4$), moderately resistant ($0.4 \leq U < 0.6$), and highly resistant ($0.6 \leq U \leq 1$). As shown in Table 4, the mean membership values ranked as L2N0 > L2N2 > L2N1 > L1N2 > L3N0 > L3N2 > CK > L1N1 > L3N1, with L2N0 exhibiting the highest value (0.592) and L3N1 the lowest (0.362), ranging from 0.362 to 0.592. This indicates enhanced stress resistance under optimal light and nitrogen conditions. According to the principle that higher membership values correlate with greater growth promotion, treatments L2N0, L2N2, L2N1, L1N2, L3N0, and L3N2 promoted seedling growth to varying degrees compared to the control (CK). Among the treatments, L2N0 (70% full sunlight, no nitrogen) exhibited the highest comprehensive membership score (0.592), indicating a comparatively strong performance in promoting seedling growth, followed by L2N2. This suggests that, even without nitrogen application, 70% full sunlight enhanced seedling morphology, physiology, and stress resistance. Medium- to high-nitrogen treatments (N1, N2) under moderate shading (L2) further improved adaptability, particularly by increasing photosynthetic efficiency and antioxidant capacity. In contrast, low light intensity (L3) significantly reduced adaptability, likely due to limited photosynthetic carbon assimilation and energy acquisition, with high

nitrogen exacerbating carbon–nitrogen imbalances under low light. Thus, moderate shading and nitrogen application are key ecological strategies for optimizing *Picea neoveitchii* Mast. seedling growth.

Table 4. Membership function value of leaf functional traits of *Picea neoveitchii* Mast. seedlings.

Index	Subordinate Function Value								
	L1N0	**L1N1**	**L1N2**	**L2N0**	**L2N1**	**L2N2**	**L3N0**	**L3N1**	**L3N2**
Needle thickness	0.158	0.445	0.237	0.408	0.746	1.000	0.000	0.685	0.448
Leaf area	0.086	0.610	0.308	0.437	0.824	1.000	0.000	0.360	0.375
Specific leaf area	0.156	0.316	0.000	0.586	1.000	0.754	0.502	0.142	0.345
Leaf dry matter content	0.900	1.000	0.600	1.000	0.000	0.900	0.300	0.600	0.700
Needle thickness	0.260	0.309	0.488	1.000	0.569	0.000	0.248	0.049	0.341
Stomatal density	1.000	0.300	0.380	0.000	0.012	0.441	0.239	0.141	0.291
Needle cross-sectional area	0.000	0.221	0.300	1.000	0.383	0.262	0.341	0.185	0.248
Perimeter of needle section	0.125	0.000	0.063	1.000	0.200	0.400	0.288	0.088	0.113
Epidermal tissue area	0.034	0.000	0.411	1.000	0.192	0.308	0.226	0.315	0.199
Mesophyll tissue area	0.000	0.205	0.261	1.000	0.396	0.264	0.321	0.157	0.249
Resin cavity area	0.000	0.333	0.333	0.267	0.367	0.000	1.000	0.600	0.267
Endocortical area	0.221	0.103	0.309	1.000	0.426	0.029	0.529	0.265	0.000
Central column area	0.264	0.439	0.851	1.000	0.453	0.000	0.953	0.574	0.493
Mesophyll tissue area ratio	0.065	0.586	0.070	1.000	0.730	0.509	0.309	0.000	0.456
Resin cavity area ratio	0.049	0.368	0.344	0.056	0.346	0.000	1.000	0.721	0.314
Area ratio of central column	0.785	0.612	0.988	0.207	0.364	0.000	1.000	0.818	0.616
N content of needles	0.275	0.237	1.000	0.000	0.397	0.971	0.369	0.437	0.724
P content of needles	1.000	0.207	0.272	0.482	0.327	0.267	0.764	0.173	0.000
N/P	1.000	0.671	0.138	0.984	0.620	0.164	0.872	0.404	0.000
Chlorophyll a content	0.881	0.261	0.119	0.261	0.187	0.328	0.664	0.000	1.000
Chlorophyll b content	0.660	0.296	0.107	0.252	0.270	0.289	0.491	0.000	1.000
Total chlorophyll content	0.764	0.281	0.113	0.257	0.229	0.312	0.568	0.000	1.000
Carotenoid content	1.000	0.652	0.783	0.783	0.261	0.739	0.609	0.522	0.000
Net photosynthetic rate	0.260	0.419	0.354	0.574	1.000	0.623	0.000	0.567	0.933
Stomatal conductance	0.056	0.022	0.377	0.242	0.593	0.288	0.000	0.375	1.000
Intercellular CO_2 concentration	0.303	0.000	0.722	0.443	0.628	0.530	1.000	0.487	0.642
Transpiration rate	0.285	0.170	0.443	0.308	0.364	0.324	0.000	0.611	1.000
Fv/Fm	0.398	0.000	0.496	1.000	0.235	0.656	0.494	0.060	0.438
Fv/Fo	0.237	0.000	0.301	1.000	0.123	0.488	0.313	0.029	0.285
SOD activity	0.890	0.581	0.652	0.824	0.503	1.000	0.000	0.722	0.504
POD activity	1.000	0.581	0.719	0.219	0.909	0.000	0.443	0.456	0.650
CAT activity	0.908	0.832	0.603	0.475	0.168	0.547	0.939	1.000	0.000
Soluble protein content	0.969	0.922	0.000	0.594	0.156	1.000	0.547	0.141	0.484
Free proline content	0.145	0.203	1.000	0.035	0.435	0.396	0.193	0.000	0.665
Malondialdehyde content	0.000	1.000	0.661	0.763	0.897	0.951	0.980	0.752	0.452
Relative electrical conductivity	0.000	0.075	0.040	0.316	0.366	0.611	0.034	1.000	0.476
Soluble sugar content	0.484	0.805	0.514	1.000	0.184	0.361	0.073	0.000	0.137
Starch content	0.181	0.175	1.000	0.502	0.529	0.708	0.563	0.185	0.000
NSC content	0.454	0.754	0.640	1.000	0.240	0.440	0.142	0.000	0.093
Mean	0.409	0.389	0.435	0.592	0.439	0.462	0.433	0.362	0.419
Order	7	8	4	1	3	2	5	9	6

3. Discussion

3.1. Effects of Light–Nitrogen Interaction on Needle Morphological Traits of Picea neoveitchii Mast. Seedlings

Light is the energy base that drives photosynthesis, and nitrogen is one of the essential nutrients that plants need most, and they coordinate in the allocation of plant resources [29]. This study demonstrates that needle length, leaf area, and specific leaf area (SLA) of *Picea neoveitchii* Mast. seedlings peaked under moderate shading (L2), with significant increases under medium- to high-nitrogen treatments (N1, N2) (Figure 1). Given the slow growth rate of *Picea neoveitchii* Mast. and the influence of needle cohort phenology, the responses

observed here likely represent short-term acclimation mechanisms rather than long-term developmental adaptations. These changes in needle morphology reflect adaptive resource allocation strategies: under low light, increased needle length and SLA enhanced light capture to mitigate photosynthetic limitations, consistent with mechanisms proposed by Jerzy Modrzyński et al. for low-light adaptation [30,31]. However, excessive shading (L3) significantly reduced leaf area and needle length, likely due to insufficient photosynthetic products to support leaf growth [32]. Nitrogen application significantly increased needle length, indicating its role in promoting cell division and elongation [33]. Yet, excessive nitrogen (N2) led to reduced leaf area and needle length under some light conditions, possibly due to soil acidification and nutrient imbalances inhibiting growth [34]. The significant interaction between shading and nitrogen treatments indicates that moderate light–nitrogen synergy is critical for optimizing needle morphology [35]. Regarding anatomical traits, the L2N0 treatment significantly increased needle cross-sectional area, perimeter, and mesophyll tissue area, enhancing light absorption and photosynthetic capacity (Table 1). The larger resin duct cavity area and proportion observed in L2N1 suggest enhanced structural defense under moderate-light and low-nitrogen conditions. This may be associated with the stimulation of secondary metabolite synthesis, reflecting the morphological and anatomical adaptations of *Picea neoveitchii* Mast. to combined light–nitrogen variation [36,37].

Nitrogen (N) and phosphorus (P) are vital for photosynthesis, energy metabolism, and growth, with the N/P ratio serving as an indicator of nutrient limitation [38]. This study found that shading had minimal impact on needle N and P stoichiometric characteristics (Figure 2). Under low nitrogen levels (N0, N1), low light (L3) increased needle nitrogen content, likely due to its enhanced accumulation to support protein, chlorophyll, and nucleic acid synthesis for sustained growth in low-light, low-nitrogen conditions [39]. The plant growth rate hypothesis suggests that relative growth rate correlates positively with phosphorus content and P/N ratio [40]. Here, needle phosphorus content decreased with reduced light intensity, and the N/P ratio was highest under low light (L3), indicating that shading constrained seedling growth rates, consistent with prior studies [41,42]. Nitrogen application significantly increased needle nitrogen content and N/P ratio but reduced phosphorus content, suggesting that excessive nitrogen may induce nutrient imbalances, exacerbating phosphorus limitations [43]. This may be attributed to nitrogen-induced suppression of phosphorus uptake, likely caused by nutrient antagonism, microbial competition, or altered root absorption capacity under excessive nitrogen. Needle N/P ratios ranged from 5.48 to 12.90, below the threshold of 14, indicating that there was nitrogen limitation resulting from all treatments for *Picea neoveitchii* Mast. seedlings. The high background level of available nitrogen may have partially offset the response to nitrogen addition, as also reflected in the limited physiological gains with high-nitrogen treatments.

3.2. Effects of Light–Nitrogen Interaction on Photosynthetic Physiological Traits of Picea neoveitchii Mast. Seedling Needles

Photosynthetic pigments and parameters are central indicators of plant growth and productivity [22]. In this study, chlorophyll a, chlorophyll b, and total chlorophyll contents of *Picea neoveitchii* Mast. seedlings peaked under low-light and high-nitrogen conditions (L3N2) (Table 2). In low-light environments, plants typically increase photosynthetic pigment content, particularly chlorophyll b, to enhance blue–violet light absorption [44], thereby improving adaptation to low light. The lowest chlorophyll a/b ratio being in the L3N2 treatment further indicates enhanced light utilization and adaptability under low light and high nitrogen, consistent with findings in shade-tolerant *Panax notoginseng*, where high nitrogen significantly increased photosynthetic rate and stomatal conductance, boosting light-use efficiency in dynamic light conditions [45]. Moreover, ample nitrogen

supply promoted chlorophyll synthesis, further enhancing photosynthetic efficiency, which is particularly critical for plants in low-light environments [46].

Analysis of photosynthetic parameters revealed that the net photosynthetic rate (Pn) of *Picea neoveitchii* Mast. seedlings was highest under moderate shading (L2) and medium nitrogen (N1), significantly surpassing other treatments (Figure 3). Moderate shading mitigated photoinhibition from excessive light, while increased leaf area and specific leaf area enhanced photosynthetic efficiency [47]. Higher stomatal conductance (Gs) and transpiration rate (Tr) in L2 treatments further supported this, indicating that optimal light–nitrogen conditions improved needle structure, water transport, and photosynthetic capacity. However, under excessive shading (L3) or high nitrogen (N2), Pn and Gs significantly declined, likely due to damage to mesophyll cell structure and photosynthetic organelle function [48]. Higher nitrogen input (e.g., N2 treatment) may have increased needle nitrogen content and slightly altered photosynthetic pigment composition, but it did not lead to significant improvements in photosynthetic rate (Pn) or stomatal conductance (Gs). This suggests that beyond a certain threshold, additional nitrogen may not further enhance physiological function, and could potentially disrupt metabolic balance or interfere with stomatal regulation [49,50]. Chlorophyll fluorescence parameters (Fv/Fm and Fv/Fo) peaked in the L2N0 treatment, indicating that moderate shading and low nitrogen significantly enhanced PSII photochemical efficiency and light capture capacity. In contrast, these parameters decreased in the L3N2 treatment, suggesting that excessive shading and high nitrogen induced low-light stress and nutrient imbalance, impairing normal photosynthesis [51,52].

3.3. Effects of Light–Nitrogen Interaction on Stress Resistance Physiological Traits of Picea neoveitchii Mast. Seedling Needles

The stress resistance physiological traits of *Picea neoveitchii* Mast. seedling needles exhibited high sensitivity to light–nitrogen treatments, particularly in protective enzyme activity and osmoregulatory substances [53] (Figure 4). Superoxide dismutase (SOD) activity peaked in the L3N2 treatment, indicating that under low-light and high-nitrogen conditions, plants may have experienced elevated oxidative stress, which triggered enhanced antioxidant enzyme activity to mitigate reactive oxygen species (ROS) accumulation and protect cellular integrity [54]. Studies show that environmental stress induces accumulation of ROS, such as superoxide anions, hydroxyl radicals, and hydrogen peroxide, which can damage cell membranes and other components [55]. Plants counteract this by activating antioxidant enzyme systems to maintain cellular function [56]. However, peroxidase (POD) activity was highest in the control group (CK), while L2N2 significantly reduced POD activity. This response highlights a typical stress-adaptive mechanism, where reduced light may limit photosynthetic electron flow, but in combination with high nitrogen input, metabolic imbalance may still lead to ROS formation, thus requiring enhanced SOD-mediated defense. Excessive nitrogen, however, may cause metabolic imbalances, triggering oxidative stress [57,58]. Osmoregulatory substances, such as soluble protein and free proline, were significantly affected by light–nitrogen treatments [59,60]. Soluble protein content peaked in the L2N2 treatment, while free proline content was highest in L3N2, indicating enhanced stress resistance through osmoregulation under low light and high nitrogen [61]. Malondialdehyde (MDA) content and relative conductivity were highest in the control (L1N1), suggesting that moderate shading (L2) combined with low to moderate nitrogen application (particularly L2N1) effectively alleviated oxidative damage and improved membrane stability [62]. This aligns with the membership function results, where the L2N1 treatment showed the best integrated performance in terms of both growth and stress resistance. Moderate shading combined with nitrogen application activated antioxidant defense mechanisms, particularly by enhancing SOD, POD, and catalase (CAT) activities to scavenge excess ROS, protecting cell membranes, reducing lipid peroxidation,

and enhancing membrane stability [63,64]. Although L2N0 had the highest comprehensive score based on membership function, it did not outperform in all individual traits. Thus, this result suggests a balanced performance across morphology, physiology, and resistance metrics rather than superiority in specific dimensions.

4. Materials and Methods

4.1. Study Area

This experiment was conducted at a forest farm in Wudu District, Longnan City, southeastern Gansu Province, China. Wudu District (104°34′–105°38′ E, 32°47′–33°42′ N) is located in the middle reaches of the Bailong River, a tributary of the Jialing River in the Yangtze River Basin, at the intersection of Gansu, Shaanxi, and Sichuan provinces within the Qinba Mountain Range. The terrain slopes from northwest to southeast, with elevations ranging from 667 to 3600 m [65]. The climate is transitional between a north subtropical humid and a warm temperate semi-arid zone, exhibiting distinct vertical zonation with subtropical, warm temperate, and cold temperate characteristics due to its complex topography. The region experiences dry springs and winters with minimal rain or snow, rainy autumns, and frequent heavy rain or hail from June to September. The annual average temperature is 14.9 °C, with 1872 h of sunshine, a frost-free period of 210–240 days, and approximately 460 mm of annual precipitation. Vegetation primarily consists of north subtropical evergreen and deciduous broadleaf mixed forests, with additional deciduous broadleaf forests and dark coniferous forests influenced by the variable mountainous climate [66]. The soil in the experimental area is weakly acidic (pH 6.85) with moderate levels of organic matter (12.713 $g \cdot kg^{-1}$) and total nitrogen (0.993 $g \cdot kg^{-1}$), indicating fertile conditions suitable for *Picea neoveitchii* Mast. growth.

4.2. Experimental Materials

The experimental seedlings were 9-year-old *Picea neoveitchii* Mast. provided by the Forestry Research Institute of the Bailongjiang Forestry Administration, Gansu Province, sourced from a native population in Zhouqu County, Gannan, Gansu. In November 2023, seedlings were transplanted into containers (50 cm in diameter and 50 cm in height), with one seedling per container. The containers were filled with topsoil collected from the Wudu District Forest Farm, which had the following properties: pH 6.85; total nitrogen, 0.993 $g \cdot kg^{-1}$; total phosphorus, 0.737 $g \cdot kg^{-1}$; total potassium, 10.429 $g \cdot kg^{-1}$; available nitrogen, 0.469 $g \cdot kg^{-1}$ (determined using the alkali hydrolysis diffusion method); available phosphorus, 8.459 $mg \cdot kg^{-1}$; available potassium, 85.472 $mg \cdot kg^{-1}$; and organic matter, 12.713 $g \cdot kg^{-1}$. Each seedling remained in its container throughout the experimental period. After acclimation until April 2024, healthy and uniform seedlings (mean height 35.98 cm, mean basal diameter 9.09 mm) were selected as experimental materials.

Prior to the experiment, the seedlings had been cultivated under partially shaded conditions at approximately 70% of full sunlight. During the 90-day experimental period (April to June 2024), local meteorological data recorded by the Wudu District Forestry Station indicated the following monthly averages: April: mean air temperature of 13.9 °C (daily high: 20.5 °C; daily low: 8.1 °C), average relative humidity of 57%, and mean solar radiation of 15,265 $kJ \cdot m^{-2} \cdot d^{-1}$; May: mean air temperature of 19.8 °C (daily high: 26.2 °C; daily low: 14.3 °C), relative humidity of 60%, and solar radiation of 17,374 $kJ \cdot m^{-2} \cdot d^{-1}$; and June: mean air temperature of 24.7 °C (daily high: 30.6 °C; daily low: 19.4 °C), relative humidity of 64%, and solar radiation of 18,330 $kJ \cdot m^{-2} \cdot d^{-1}$. In addition, environmental conditions during photosynthetic measurements—such as external photosynthetically active radiation (PAR_e), ambient temperature, and relative humidity—are summarized in Supplementary Table S1.

4.3. Experimental Design

Shading and nitrogen application treatments were conducted from early April to early July 2024. Shading treatments included three levels: L1 (100% full sunlight), L2 (70% full sunlight), and L3 (40% full sunlight), achieved using shade nets with varying light transmittance. Nitrogen treatments comprised three levels: N0 (0 g $N \cdot m^{-2} \cdot a^{-1}$, where g $N \cdot m^{-2} \cdot a^{-1}$ denotes grams of nitrogen applied per square meter per year), N1 (10 g $N \cdot m^{-2} \cdot a^{-1}$), and N2 (20 g $N \cdot m^{-2} \cdot a^{-1}$). Nitrogen was applied as NH_4NO_3, calculated based on treatment levels, dissolved, and administered in two doses (early April and mid-May) of 200 mL per seedling per application. The experiment included eight treatment groups and one control group (L1N0, CK); each treatment group consisted of four replicates (n = 4), totaling 36 seedlings. During the treatment period, dedicated personnel managed irrigation and pest control. The treatment design is detailed in Table 5. The current year's needles from plants in different treatment groups were collected. The third round of unshaded branches facing south of a single plant from the current year were determined and the needles in the middle of the branches collected. Sampling was carried out from 10:00 to 12:00 on the 90th day of treatment (the end of the experiment).

Table 5. Double factor combination level in test design.

N Treatment	Shade Levels		
	L1 (100% Full Light)	**L2 (70% Full Light)**	**L3 (40% Full Light)**
N0 (0 g $m^{-2} \cdot a^{-1}$)	L1N0 (CK)	L2N0	L3N0
N0 (10 g $m^{-2} \cdot a^{-1}$)	L1N1	L2N1	L3N1
N1 (20 g $m^{-2} \cdot a^{-1}$)	L1N2	L2N2	L3N2

4.4. Index Measurements

4.4.1. Basic Measurements

Needle length was measured using a vernier caliper (precision: 0.01 mm) on current-year needles, which were fully developed by the end of the treatment period. The projected area of two needle fascicles (each containing two needles) was determined using an Epson V700 leaf area scanner. Their fresh weight was recorded using an analytical balance (precision: 0.1 mg). Samples were then oven-dried at 80 °C to constant weight to determine dry weight, and dry matter content was calculated as the ratio of dry weight to fresh weight ($g \cdot g^{-1}$). The specific leaf area (SLA) was calculated by dividing leaf area by dry weight ($cm^2 \cdot g^{-1}$). For anatomical observations, transverse cross-sections of needles were obtained to observe stomatal distribution using a Zeiss Axio Observer fluorescence inverted microscope. Both the adaxial (upper) and abaxial (lower) surfaces of the needles were examined to determine stomatal density, defined as the number of stomata per mm^2. Leaf width and thickness were measured from these transverse sections. The slicing method involved embedding the needle samples in paraffin, slicing them with a microtome (Leica RM2235), and staining with toluidine blue prior to microscopic imaging [67]. Leaf nitrogen and phosphorus contents were determined using a continuous flow analyzer (Skalar San++ Compact, Skalar Analytical B.V., Breda, Netherlands) after acid digestion with H_2SO_4–H_2O_2.

4.4.2. Photosynthetic and Chlorophyll Fluorescence Parameters

Measurements of gas exchange parameters were conducted under clear, cloudless skies with stable atmospheric conditions, starting at 09:00 AM local time. Current-year needles from the upper third of the canopy were selected for measurement, and the measurements were conducted immediately at the end of the treatment period. A portable CO_2/H_2O

infrared gas analyzer (Li-6400, LI-COR, Lincoln, NE, USA) was used. A buffer bottle was installed to ensure that the CO_2 concentration in the leaf chamber matched ambient levels. The photosynthetically active radiation (PAR) in the chamber was set to 1000 $\mu mol \cdot m^{-2} \cdot s^{-1}$ using a red–blue light source (6400-02B, LI-COR, Lincoln, NE, USA). Before measurements, needles were kept under ambient PAR for at least 15 min to acclimate to the chamber light conditions. The following parameters were recorded: net photosynthetic rate (Pn), stomatal conductance (Gs), intercellular CO_2 concentration (Ci), and transpiration rate (Tr). Water use efficiency (WUE) was calculated as the ratio of Pn to Tr [27]. The same current-year needles, collected from the same canopy position and at the same time, were used for in vivo chlorophyll fluorescence measurements, conducted using a handheld fluorometer (FluorPen FP110). Prior to measurement, samples were dark-adapted for 30 min using black clips. Initial fluorescence (Fo) and maximum fluorescence (Fm) were recorded to calculate the maximum photochemical efficiency of PSII (Fv/Fm) and the potential photochemical efficiency (Fv/Fo).

4.4.3. Photosynthetic Pigments and Relative Conductivity

Photosynthetic pigment content was determined using the N, N-dimethylformamide method. Current-year needles were collected immediately after the 90-day treatment period from the upper third of the seedling canopy. A 5 g fresh needle sample was fully immersed in N, N-dimethylformamide and incubated in darkness at 4 °C until completely decolorized. Absorbance was measured at 480, 647, and 664 nm using a spectrophotometer, and the contents of chlorophyll a, chlorophyll b, total chlorophyll, and carotenoids were calculated as described by Wellburn (1994) [68]. Relative conductivity was measured using a conductivity meter, following the method described by Lutts et al. (1996) [4], to assess membrane permeability and cell membrane integrity [69].

4.4.4. Protective Enzyme Activity

Fresh leaf samples (0.5 g) were flash-frozen in liquid nitrogen and stored at −80 °C. Activities of superoxide dismutase (SOD) and peroxidase (POD) were subsequently measured [27,67].

4.4.5. Osmoregulatory Substances

Soluble sugar content was determined using the anthrone–sulfuric acid method [70], proline content using the ninhydrin method [71], soluble protein content using the Coomassie Brilliant Blue G-250 staining method [72], and malondialdehyde content using the 2-thiobarbituric acid method [73].

4.5. Membership Function Calculation

To comprehensively evaluate the environmental adaptability of different treatments, a membership function method was used. The membership function value is calculated as follows:

Indicators positively correlated with seedling growth:

$$U(X_i) = (X_i - X_{min})/(X_{max} - X_{min}) \quad (1)$$

Indicators negatively correlated with seedling growth:

$$U(X_i)=1 - (X_i - X_{min})/(X_{max} - X_{min}) \quad (2)$$

where U is the membership value; i = 1, 2, 3,. . ., n; X_i is the measured value of the indicator; X_{min} is the minimum value of a certain indicator in all treatment groups; and X_{max} is the maximum value of a certain indicator in all treatment groups.

4.6. Data Analysis

Data were pre-processed using SPSS 26.0 for the normality and homogeneity of variance tests. A two-way ANOVA was conducted to assess the main and interactive effects of light and nitrogen treatments on all measured traits. Where appropriate, polynomial regression analyses were applied to evaluate quantitative trends. Statistical significance was determined at $p < 0.05$ using SPSS 26.0. Post hoc comparisons were performed using Duncan's test. Graphs were generated using GraphPad Prism 9.5 and R 4.4.2.

5. Conclusions and Prospects

This study systematically evaluated the effects of light–nitrogen interactions on the leaf functional traits of *Picea neoveitchii* Mast. seedlings. The results demonstrated that moderate shading (70% full sunlight) generally enhanced leaf morphological and physiological traits under most nitrogen conditions. In contrast, excessive nitrogen input or low light intensity exerted inhibitory effects, potentially limiting photosynthesis and disturbing metabolic balance, thereby suppressing growth. Membership function analysis identified the L2N0 treatment (70% full sunlight, 0 g $N \cdot m^{-2} \cdot a^{-1}$) as the most favorable condition, showing optimal performance in terms of both growth and stress resistance. Future research should explore the long-term effects of light–nitrogen interactions on *Picea neoveitchii* Mast. population dynamics and employ molecular biology techniques to elucidate underlying physiological and metabolic mechanisms, providing a more comprehensive theoretical basis for the conservation and restoration of this endangered species.

Supplementary Materials: The following supporting information can be downloaded at: https://www.mdpi.com/article/10.3390/plants14162550/s1, Table S1: Meteorological Data for Photosynthesis Experiments.

Author Contributions: Conceptualization, S.C. and S.Y.; methodology, S.Y.; software, S.C.; validation, S.C., W.L. and K.L.; formal analysis, S.C.; investigation, S.Y., W.L. and K.L.; resources, S.Y.; data curation, N.X.; writing—original draft preparation, S.C.; writing—review and editing, S.Y.; visualization, S.C.; supervision, W.J.; project administration, W.J.; funding acquisition, W.J. All authors have read and agreed to the published version of the manuscript.

Funding: The 2023 Provincial Forestry Reform Project of Shaanxi Province: "Conservation and Breeding of the Endangered Wild Plants '*Paeonia rockii* (S. G. Haw & Lauener) T. Hong & J. J. Li ex D. Y. Hong' and '*Picea neoveitchii* Mast.' in Shaanxi" (No. SXDY2023-01) and China's Ministry of Science and Technology's Basic Science Resources Survey Special Project (No. 2019FY101604).

Data Availability Statement: The data are not publicly available due to privacy or ethical restrictions.

Conflicts of Interest: The authors declare no conflicts of interest.

References

1. Chang, P.; Zhu, L.; Zhao, M.; Li, C.; Zhang, Y.; Li, L. The First Transcriptome Sequencing and Analysis of the Endangered Plant Species *Picea neoveitchii* Mast. and Potential EST-SSR Markers Development. *Biotechnol. Biotechnol. Equip.* **2019**, *33*, 967–973. [CrossRef]
2. Xue, N.; Li, K.; Chen, K.; Li, P.; Ji, X.; Ma, Z.; Ji, W. Predicting Climate Change Impacts on Distribution and Conservation of Critically Endangered *Picea neoveitchii* Using MaxEnt. *Front. For. Glob. Change* **2024**, *7*, 1472857. [CrossRef]
3. Ronquist, F.; Teslenko, M.; van der Mark, P.; Ayres, D.L.; Darling, A.; Hohna, S.; Larget, B.; Liu, L.; Suchard, M.A.; Huelsenbeck, J.P. MrBayes 3.2: Efficient Bayesian Phylogenetic Inference and Model Choice Across a Large Model Space. *Syst. Biol.* **2012**, *61*, 539–542. [CrossRef]

4. Bush, E.R.; Whytock, R.C.; Bahaa-El-Din, L.; Bourgeois, S.; Bunnefeld, N.; Cardoso, A.W.; Dikangadissi, J.T.; Dimbonda, P.; Dimoto, E.; Ndong, J.E.; et al. Long-Term Collapse in Fruit Availability Threatens Central African Forest Megafauna. *Science* **2020**, *370*, 1219–1221. [CrossRef]
5. Pritchard, J.K.; Stephens, M.; Donnelly, P. Inference of Population Structure Using Multilocus Genotype Data. *Genetics* **2000**, *155*, 945–959. [CrossRef]
6. Cun, Z.; Wu, H.-M.; Zhang, J.-Y.; Shuang, S.-P.; Hong, J.; An, T.-X.; Chen, J.-W. High Nitrogen Inhibits Biomass and Saponins Accumulation in a Medicinal Plant Panax Notoginseng. *PeerJ* **2023**, *11*, e14933. [CrossRef]
7. Sugiura, D.; Tateno, M. Optimal Leaf-to-Root Ratio and Leaf Nitrogen Content Determined by Light and Nitrogen Availabilities. *PLoS ONE* **2011**, *6*, e22236. [CrossRef] [PubMed]
8. Yang, C.; Huang, C.; Gou, L.; Yang, H.; Liu, G. Functional Identification and Genetic Transformation of the Ammonium Transporter PtrAMT1;6 in Populus. *Int. J. Mol. Sci.* **2023**, *24*, 8511. [CrossRef]
9. Alanazi, A.K.; Abo-Dief, H.M.; Alothman, Z.A.; Mohamed, A.T.; Pramanik, T.; Alotaibi, S.H. Effect of Plant Nanocellulose Electrolyte, Zinc Oxide Nanoparticles, and Nano-Chlorophyll Sensitiser on the Dye-Sensitised Solar Cell Performance. *Crystals* **2022**, *12*, 1771. [CrossRef]
10. Li, H.; Tang, C.; Xu, Z.; Liu, X.; Han, X. Effects of Different Light Sources on the Growth of Non-Heading Chinese Cabbage (*Brassica campestris* L.). *J. Agric. Sci.* **2012**, *4*, 262. [CrossRef]
11. Paradiso, R.; Proietti, S. Light-Quality Manipulation to Control Plant Growth and Photomorphogenesis in Greenhouse Horticulture: The State of the Art and the Opportunities of Modern LED Systems. *J. Plant Growth Regul.* **2022**, *41*, 742–780. [CrossRef]
12. Poorter, H.; Yin, X.; Alyami, N.; Gibon, Y.; Pons, T.L. MetaPhenomics: Quantifying the Many Ways Plants Respond to Their Abiotic Environment, Using Light Intensity as an Example. *Plant Soil* **2022**, *476*, 421–454. [CrossRef]
13. Monib, A.W.; Alimyar, O.; Mohammad, M.U.; Akhundzada, M.S.; Niazi, P. Macronutrients for Plants Growth and Humans Health. *J. Res. Appl. Sci. Biotechnol.* **2023**, *2*, 268–279. [CrossRef]
14. Xu, G.; Fan, X.; Miller, A.J. Plant Nitrogen Assimilation and Use Efficiency. *Annu. Rev. Plant Biol.* **2012**, *63*, 153–182. [CrossRef]
15. Zhang, R.; Nie, L.; Huang, M.; Yang, H.; Shi, C.; Wei, Y.; Song, L.; Zhu, J.; Bo, H.; Wang, J.; et al. Effects of Irrigation and Nitrogen Application on Soil Nutrients in Triploid *Populus tomentosa* Stands. *Forests* **2022**, *13*, 1046. [CrossRef]
16. Stevens, C.J.; Dise, N.B.; Gowing, D.J.G.; Mountford, J.O. Loss of Forb Diversity in Relation to Nitrogen Deposition in the UK: Regional Trends and Potential Controls. *Glob. Change Biol.* **2006**, *12*, 1823–1833. [CrossRef]
17. Joseph Wright, S.; Kitajima, K.; Kraft, N.J.B.; Reich, P.B.; Wright, I.J.; Bunker, D.E.; Condit, R.; Dalling, J.W.; Davies, S.J.; Diaz, S.; et al. Functional Traits and the Growth-Mortality Trade-off in Tropical Trees. *Ecology* **2010**, *91*, 3664–3674. [CrossRef] [PubMed]
18. Garnier, E.; Cortez, J.; Billès, G.; Navas, M.L.; Roumet, C.; Debussche, M.; Laurent, G.; Blanchard, A.; Aubry, D.; Bellmann, A.; et al. Plant Functional Markers Capture Ecosystem Properties during Secondary Succession. *Ecology* **2004**, *85*, 2630–2637. [CrossRef]
19. Li, S.; Tosens, T.; Harley, P.C.; Jiang, Y.; Kanagendran, A.; Grosberg, M.; Jaamets, K.; Niinemets, U. Glandular Trichomes as a Barrier against Atmospheric Oxidative Stress: Relationships with Ozone Uptake, Leaf Damage, and Emission of LOX Products across a Diverse Set of Species. *Plant Cell Environ.* **2018**, *41*, 1263–1277. [CrossRef]
20. Teraa, S.; Bencherif, M. From Hygrothermal Adaptation of Endemic Plants to Meteorosensitive Biomimetic Architecture: Case of Mediterranean Biodiversity Hotspot in Northeastern Algeria. *Environ Dev Sustain* **2022**, *24*, 10876–10901. [CrossRef]
21. Lv, Y.; Shao, G.; Qiu, J.; Jiao, G.; Sheng, Z.; Xie, L.; Wu, Y.; Tang, S.; Wei, X.; Hu, P. White Leaf and Panicle 2, Encoding a PEP-Associated Protein, Is Required for Chloroplast Biogenesis under Heat Stress in Rice. *J. Exp. Bot.* **2017**, *68*, 5147–5160. [CrossRef]
22. Han, W.X.; Fang, J.Y.; Guo, D.L.; Zhang, Y. Leaf Nitrogen and Phosphorus Stoichiometry across 753 Terrestrial Plant Species in China. *New Phytol.* **2005**, *168*, 377–385. [CrossRef]
23. Hua, J.; Wang, W.; Huo, J.; Wu, L.; Huang, L.; Zhong, H. Effects of Ecosystem Recovery Types on Soil Phosphorus Bioavailability, Roles of Plant and Microbial Diversity: A Meta-analysis. *Ecol. Evol.* **2025**, *15*, e71172. [CrossRef]
24. Reich, P.B.; Oleksyn, J. Global Patterns of Plant Leaf N and P in Relation to Temperature and Latitude. *Proc. Natl. Acad. Sci. USA* **2004**, *101*, 11001–11006. [CrossRef]
25. Rumyantseva, N.I.; Valieva, A.I.; Kostyukova, Y.A.; Ageeva, M.V. The Effect of Leaf Plasticity on the Isolation of Apoplastic Fluid from Leaves of Tartary Buckwheat Plants Grown In Vivo and In Vitro. *Plants* **2023**, *12*, 4048. [CrossRef]
26. Argus, R.E.; Colmer, T.D.; Grierson, P.F. Early Physiological Flood Tolerance Is Followed by Slow Post-Flooding Root Recovery in the Dryland Riparian Tree *Eucalyptus camaldulensis* Subsp Refulgens. *Plant Cell Environ.* **2015**, *38*, 1189–1199. [CrossRef]
27. Barbagallo, R.P.; Oxborough, K.; Pallett, K.E.; Baker, N.R. Rapid, Noninvasive Screening for Perturbations of Metabolism and Plant Growth Using Chlorophyll Fluorescence Imaging. *Plant Physiol.* **2003**, *132*, 485–493. [CrossRef] [PubMed]
28. Fatma, M.; Sehar, Z.; Iqbal, N.; Alvi, A.F.; Abdi, G.; Proestos, C.; Khan, N.A. Sulfur Supplementation Enhances Nitric Oxide Efficacy in Reversal of Chromium-Inhibited Calvin Cycle Enzymes, Photosynthetic Activity, and Carbohydrate Metabolism in Wheat. *Sci. Rep.* **2023**, *13*, 6858. [CrossRef]

29. Poorter, H.; Niklas, K.J.; Reich, P.B.; Oleksyn, J.; Poot, P.; Mommer, L. Biomass Allocation to Leaves, Stems and Roots: Meta-analyses of Interspecific Variation and Environmental Control. *New Phytol.* **2012**, *193*, 30–50. [CrossRef] [PubMed]
30. Huang, Z.; Liu, Q.; Tigabu, M.; Jin, S.; Ma, X.; Liu, B. Plastic Responses in Growth, Morphology, and Biomass Allocation of Five Subtropical Tree Species to Different Degrees of Shading. *Forests* **2022**, *13*, 996. [CrossRef]
31. Modrzynski, J.; Chmura, D.J.; Tjoelker, M.G. Seedling Growth and Biomass Allocation in Relation to Leaf Habit and Shade Tolerance among 10 Temperate Tree Species. *Tree Physiol.* **2015**, *35*, 879–893. [CrossRef]
32. Gong, W.; Qi, P.; Du, J.; Sun, X.; Wu, X.; Song, C.; Liu, W.; Wu, Y.; Yu, X.; Yong, T.; et al. Transcriptome Analysis of Shade-Induced Inhibition on Leaf Size in Relay Intercropped Soybean. *PLoS ONE* **2014**, *9*, e98465. [CrossRef] [PubMed]
33. Galloway, J.N.; Townsend, A.R.; Erisman, J.W.; Bekunda, M.; Cai, Z.; Freney, J.R.; Martinelli, L.A.; Seitzinger, S.P.; Sutton, M.A. Transformation of the Nitrogen Cycle: Recent Trends, Questions, and Potential Solutions. *Science* **2008**, *320*, 889–892. [CrossRef]
34. Sembiring, M.; Sabrina, T. Effectiveness of Dyella Japonica and Enterobacter Cloacae as Biofertilizers to Increase Maize (*Zea mays*) Production on Andisol Soil. *Biodiversitas J. Biol. Divers.* **2022**, *23*, 3338–3343. [CrossRef]
35. Wyka, T.P.; Oleksyn, J.; Zytkowiak, R.; Karolewski, P.; Jagodzinski, A.M.; Reich, P.B. Responses of Leaf Structure and Photosynthetic Properties to Intra-Canopy Light Gradients: A Common Garden Test with Four Broadleaf Deciduous Angiosperm and Seven Evergreen Conifer Tree Species. *Oecologia* **2012**, *170*, 11–24. [CrossRef]
36. Li, A.-M.; Wang, M.; Chen, Z.-L.; Qin, C.-X.; Liao, F.; Wu, Z.; He, W.-Z.; Lakshmanan, P.; Pan, Y.-Q.; Huang, D.-L. Integrated Transcriptome and Metabolome Analysis to Identify Sugarcane Gene Defense against Fall Armyworm (*Spodoptera frugiperda*) Herbivory. *Int. J. Mol. Sci.* **2022**, *23*, 13712. [CrossRef]
37. Van Leur, H.; Vet, L.E.M.; Van Der Putten, W.H.; Van Dam, N.M. *Barbarea vulgaris* Glucosinolate Phenotypes Differentially Affect Performance and Preference of Two Different Species of *Lepidopteran* Herbivores. *J. Chem. Ecol.* **2008**, *34*, 121–131. [CrossRef]
38. Güsewell, S. N:P Ratios in Terrestrial Plants: Variation and Functional Significance. *New Phytol.* **2004**, *164*, 243–266. [CrossRef]
39. Zhao, L.; Cai, B.; Zhang, X.; Zhang, B.; Feng, J.; Zhou, D.; Chen, Y.; Zhang, M.; Qi, D.; Wang, W.; et al. Physiological and Transcriptional Characteristics of Banana Seedlings in Response to Nitrogen Deficiency Stress. *Horticulturae* **2024**, *10*, 290. [CrossRef]
40. Perring, M.P.; Hedin, L.O.; Levin, S.A.; McGroddy, M.; De Mazancourt, C. Increased Plant Growth from Nitrogen Addition Should Conserve Phosphorus in Terrestrial Ecosystems. *Proc. Natl. Acad. Sci. USA* **2008**, *105*, 1971–1976. [CrossRef] [PubMed]
41. Bader, M.Y.; van Geloof, I.; Rietkerk, M. High Solar Radiation Hinders Tree Regeneration above the Alpine Treeline in Northern Ecuador. *Plant Ecol.* **2007**, *191*, 33–45. [CrossRef]
42. Naresh, K.S.; Kasturi Bai, K.V. Photo-Oxidative Stress in Coconut Seedlings: Early Events to Leaf Scorching and Seedling Death. *Braz. J. Plant Physiol.* **2009**, *21*, 223–232. [CrossRef]
43. Elser, J.J.; Bracken, M.E.S.; Cleland, E.E.; Gruner, D.S.; Harpole, W.S.; Hillebrand, H.; Ngai, J.T.; Seabloom, E.W.; Shurin, J.B.; Smith, J.E. Global Analysis of Nitrogen and Phosphorus Limitation of Primary Producers in Freshwater, Marine and Terrestrial Ecosystems. *Ecol. Lett.* **2007**, *10*, 1135–1142. [CrossRef]
44. Simkin, A.J.; Kapoor, L.; Doss, C.G.P.; Hofmann, T.A.; Lawson, T.; Ramamoorthy, S. The Role of Photosynthesis Related Pigments in Light Harvesting, Photoprotection and Enhancement of Photosynthetic Yield in Planta. *Photosynth. Res.* **2022**, *152*, 23–42. [CrossRef]
45. Sun, J.; Ye, M.; Peng, S.; Li, Y. Nitrogen Can Improve the Rapid Response of Photosynthesis to Changing Irradiance in Rice (*Oryza sativa* L.) Plants. *Sci. Rep.* **2016**, *6*, 31305. [CrossRef]
46. Balazadeh, S.; Schildhauer, J.; Araujo, W.L.; Munne-Bosch, S.; Fernie, A.R.; Proost, S.; Humbeck, K.; Mueller-Roeber, B. Reversal of Senescence by N Resupply to N-Starved Arabidopsis Thaliana: Transcriptomic and Metabolomic Consequences. *J. Exp. Bot.* **2014**, *65*, 3975–3992. [CrossRef]
47. Aliarab, A.; Vazifekhah, E.O.; Sadati, S.-E. Effect of Soil Moisture Content and Nitrogen Fertilizer on Survival, Growth and Some Physiological Characteristics of *Platycladus orientalis* Seedlings. *J. For. Sci.* **2020**, *66*, 511–523. [CrossRef]
48. Wang, G.; Mao, J.; Ji, M.; Wang, W.; Fu, J. A Comprehensive Assessment of Photosynthetic Acclimation to Shade in C4 Grass (*Cynodon dactylon* (L.) Pers.). *BMC Plant Biol.* **2024**, *24*, 591. [CrossRef]
49. Losacco, D.; Ancona, V.; De Paola, D.; Tumolo, M.; Massarelli, C.; Gatto, A.; Uricchio, V.F. Development of Ecological Strategies for the Recovery of the Main Nitrogen Agricultural Pollutants: A Review on Environmental Sustainability in Agroecosystems. *Sustainability* **2021**, *13*, 7163. [CrossRef]
50. Li, T.; Bi, G.; Harkess, R.L.; Denny, G.C.; Scagel, C. Nitrogen Fertilization and Irrigation Frequency Affect Hydrangea Growth and Nutrient Uptake in Two Container Types. *Hortscience* **2019**, *54*, 167–174. [CrossRef]
51. Zlobin, I.E.; Kartashov, A.V.; Pashkovskiy, P.P.; Ivanov, Y.V.; Kreslavski, V.D.; Kuznetsov, V.V. Comparative Photosynthetic Responses of Norway Spruce and Scots Pine Seedlings to Prolonged Water Deficiency. *J. Photochem. Photobiol. B-Biol.* **2019**, *201*, 111659. [CrossRef] [PubMed]
52. Gu, A.; Zhao, D.; Liu, H.; Fu, W.; Li, G.; Hao, L. Paraburkholderia Sp. GD17 Improves Tomato Plant Growth and Resistance to Botrytis Cinerea-Induced Disease. *Plant Soil* **2023**, *486*, 487–502. [CrossRef]

53. Alexieva, V.; Sergiev, I.; Mapelli, S.; Karanov, E. The Effect of Drought and Ultraviolet Radiation on Growth and Stress Markers in Pea and Wheat. *Plant Cell Environ.* **2001**, *24*, 1337–1344. [CrossRef]
54. Sharma, P.; Jha, A.B.; Dubey, R.S.; Pessarakli, M. Reactive Oxygen Species, Oxidative Damage, and Antioxidative Defense Mechanism in Plants under Stressful Conditions. *J. Bot.* **2012**, *2012*, 217037. [CrossRef]
55. Hasanuzzaman, M.; Raihan, M.R.H.; Masud, A.A.C.; Rahman, K.; Nowroz, F.; Rahman, M.; Nahar, K.; Fujita, M. Regulation of Reactive Oxygen Species and Antioxidant Defense in Plants under Salinity. *IJMS* **2021**, *22*, 9326. [CrossRef]
56. Abdulfatah, H.F. Non-Enzymatic Antioxidants in Stressed Plants: A Review. *J. Univ. Anbar Pure Sci.* **2022**, *16*, 25–37. [CrossRef]
57. Rinalducci, S.; Murgiano, L.; Zolla, L. Redox Proteomics: Basic Principles and Future Perspectives for the Detection of Protein Oxidation in Plants. *J. Exp. Bot.* **2008**, *59*, 3781–3801. [CrossRef]
58. Sachdev, S.; Ansari, S.A.; Ansari, M.I.; Fujita, M.; Hasanuzzaman, M. Abiotic Stress and Reactive Oxygen Species: Generation, Signaling, and Defense Mechanisms. *Antioxidants* **2021**, *10*, 277. [CrossRef]
59. Sikder, R.K.; Wang, X.; Zhang, H.; Gui, H.; Dong, Q.; Jin, D.; Song, M. Nitrogen Enhances Salt Tolerance by Modulating the Antioxidant Defense System and Osmoregulation Substance Content in *Gossypium hirsutum*. *Plants* **2020**, *9*, 450. [CrossRef]
60. Yemm, E.W.; Willis, A.J. The Estimation of Carbohydrates in Plant Extracts by Anthrone. *Biochem. J.* **1954**, *57*, 508–514. [CrossRef]
61. Ajmal, M.; Ullah, R.; Muhammad, Z.; Khan, M.N.; Kakar, H.A.; Kaplan, A.; Okla, M.K.; Saleh, I.A.; Kamal, A.; Abdullah, A.; et al. Kinetin Capped Zinc Oxide Nanoparticles Improve Plant Growth and Ameliorate Resistivity to Polyethylene Glycol (PEG)-Induced Drought Stress in *Vigna radiata* (L.) R. Wilczek (*Mung bean*). *Molecules* **2023**, *28*, 5059. [CrossRef]
62. Jhanzab, H.M.; Qayyum, A.; Bibi, Y.; Sher, A.; Hayat, M.T.; Iqbal, J.; Qamar, M.; Elesawy, B.H.; Ismail, K.A.; Gharib, A.F.; et al. Chemo-Blended Ag & Fe Nanoparticles Effect on Growth, Physiochemical and Yield Traits of Wheat (*Triticum aestivum*). *Agronomy* **2022**, *12*, 757. [CrossRef]
63. Addor, F.A.S. Antioxidants in Dermatology. *An. Bras. Dermatol.* **2017**, *92*, 356–362. [CrossRef]
64. Malekmohammad, K.; Sewell, R.D.E.; Rafieian-Kopaei, M. Antioxidants and Atherosclerosis: Mechanistic Aspects. *Biomolecules* **2019**, *9*, 301. [CrossRef] [PubMed]
65. He, P.; Wang, X.; Song, C.; Wang, Q.; Deng, L.; Zhong, S. Cenozoic Evolution of the Western Qinling Mt. Range Based on Thermochronologic and Sedimentary Records from the Wudu Basin, NE Tibetan Plateau. *J. Asian Earth Sci.* **2017**, *138*, 484–494. [CrossRef]
66. He, S.; Wang, D.; Li, Y.; Zhao, P. Land Use Changes and Their Driving Forces in a Debris Flow Active Area of Gansu Province, China. *Sustainability* **2018**, *10*, 2759. [CrossRef]
67. Yang, P.; Xu, L.; Xu, H.; Tang, Y.; He, G.; Cao, Y.; Feng, Y.; Yuan, S.; Ming, J. Histological and Transcriptomic Analysis during Bulbil Formation in Lilium Lancifolium. *Front. Plant Sci.* **2017**, *8*, 1508. [CrossRef]
68. Ritchie, R.J. Consistent Sets of Spectrophotometric Chlorophyll Equations for Acetone, Methanol and Ethanol Solvents. *Photosynth. Res.* **2006**, *89*, 27–41. [CrossRef] [PubMed]
69. Zhang, Y.; Zhou, X.; Yin, B.; Downing, A. Sensitivity of the Xerophytic Moss *Syntrichia caninervis* to Prolonged Simulated Nitrogen Deposition. *Ann. Bot.* **2016**, *117*, 1153–1161. [CrossRef]
70. Bebıtoglu, B.T.; Oguz, E.; Acet, N.G.; Hodzıc, A.; Temel, F.; Ada, S.; Kılıckap, A. The Neuroprotective Effect of Lamotrigine against Glutamate Excitotoxicity in SH-SY5Y Human Neuroblastoma Cells. *Marmara Med. J.* **2020**, *33*, 146–152. [CrossRef]
71. Bates, L.S.; Waldren, R.P.; Teare, I.D. Rapid Determination of Free Proline for Water-Stress Studies. *Plant Soil* **1973**, *39*, 205–207. [CrossRef]
72. Bradford, M.M. A Rapid and Sensitive Method for the Quantitation of Microgram Quantities of Protein Utilizing the Principle of Protein-Dye Binding. *Anal. Biochem.* **1976**, *72*, 248–254. [CrossRef] [PubMed]
73. Maehly, A.C.; Chance, B. The Assay of Catalases and Peroxidases. *Methods Biochem. Anal.* **1954**, *1*, 357–424. [CrossRef] [PubMed]

Disclaimer/Publisher's Note: The statements, opinions and data contained in all publications are solely those of the individual author(s) and contributor(s) and not of MDPI and/or the editor(s). MDPI and/or the editor(s) disclaim responsibility for any injury to people or property resulting from any ideas, methods, instructions or products referred to in the content.

plants

MDPI

Article

Coordinated cpSRP43 and cpSRP54 Abundance Is Essential for Tetrapyrrole Biosynthesis While cpSRP43 Is Independent of Retrograde Signaling

Shuiling Ji [1,2,*], Huijiao Yao [1] and Bernhard Grimm [2,*]

[1] Key Laboratory of Pesticide & Chemical Biology of Ministry of Education, Hubei Key Laboratory of Genetic Regulation and Integrative Biology, School of Life Sciences, Central China Normal University, Wuhan 430079, China
[2] Institute of Biology/Plant Physiology, Humboldt-Universität zu Berlin, Philippstr.13, Building 12, 10099 Berlin, Germany
* Correspondence: shuiling.ji@ccnu.edu.cn (S.J.); bernhard.grimm@rz.hu-berlin.de (B.G.)

Abstract: The chloroplast signal recognition particle (cpSRP) components cpSRP43 and cpSRP54 not only form a complex with light-harvesting chlorophyll (Chl)-binding proteins to direct them to the thylakoid membrane, but also serve other functions. cpSRP43 independently acts as a chaperone for some tetrapyrrole biosynthesis (TBS) enzymes, while cpSRP54 participates in the co-translational targeting of plastid-encoded proteins. However, it remains unclear to what extent the two cpSRP components are coregulated—despite their distinct functions—and whether both participate in genomes-uncoupled (GUN)-mediated retrograde signaling. Here, we demonstrate that cpSRP43 and cpSRP54 accumulation is strongly interdependently controlled: overexpression of one protein increases the level of the other, while a deficiency in one of the two proteins leads to a simultaneous decrease in the other component. Disruption of this balance, e.g., by combining the overexpression of one component with a knockout of the other, results in severe chlorosis, stunted growth, and reduced levels of Chl and tetrapyrrole intermediates. Moreover, cpSRP43 deficiency exacerbates the pale-green phenotype of *gun4* and *gun5* mutants, highlighting a synergistic impact on TBS; however, cpSRP43 overexpression fails to rescue these defects. Remarkably, loss of cpSRP43 does not affect the expression of nuclear-encoded photosynthetic genes under intrinsic plastid stress, clearly demonstrating that cpSRP43 is not involved in plastid-to-nucleus retrograde signaling. Overall, our findings underscore that the fine-tuned expression of cpSRP43 and cpSRP54 is crucial for proper chloroplast function and pigment biosynthesis, while cpSRP43 alone does not participate in the retrograde signaling pathway.

Keywords: chloroplast signal recognition particle (cpSRP); cpSRP43; cpSRP54; genomes-uncoupled (GUN); retrograde signaling; tetrapyrrole biosynthesis; protein abundance

1. Introduction

For many years now, the chloroplast signal recognition particle (cpSRP) pathway has been dedicated to the post-translational transfer of light-harvesting chlorophyll (Chl) a/b-binding proteins (LHCPs) from the stroma to the thylakoid membrane. Unlike canonical bacterial and cytosolic SRP pathways, which rely on an SRP RNA, the cpSRP system is uniquely composed of two protein subunits: a 54-kDa GTPase (cpSRP54) and a chloroplast-specific 43-kDa protein (cpSRP43) [1–3]. cpSRP43 plays a central role by binding directly to a conserved 18-residue hydrophobic motif (L18) within LHCP [4,5]. This interaction, that simultaneously conceals and transports LHCP, not only prevents the aggregation of LHCPs,

but also primes them for delivery to the thylakoid membrane. This is achieved, when cpSRP54 provides the essential GTP-driven targeting signal through its interaction with the SRP receptor cpFtsY, which directs the complex to the thylakoid membrane via its conserved NG (N-terminal plus GTPase) domain [6,7]. At the thylakoid, cpSRP43 interacts via its chromodomains with a linear motif in the C-terminal region of the translocase Alb3, thereby ensuring the efficient docking of the LHCP-bound complex [8,9]. The cooperative action of cpSRP43 and cpSRP54 is ultimately finely regulated: cpSRP43 undergoes conformational changes upon assembling with cpSRP54 versus Alb3, ensuring LHCP is stably bound in the stroma and efficiently released at the membrane [10]. The cpSRP pathway is thus an example of a dynamic interplay between the function of a chaperone-subunit (cpSRP43) and the GTPase-subunit (cpSRP54) to achieve precise protein targeting.

While it was originally assumed that cpSRP54 and cpSRP43 act exclusively as obligatory heterodimers, more recent studies have shown that each subunit is also involved in different functions within the chloroplast. As the majority of cpSRP54 exists in a soluble form, less than half of cpSRP54 is associated with ribosomes and mediates the co-translational insertion of several chloroplast-encoded thylakoid proteins [11,12]. Ribosome profiling has demonstrated that the conserved C-terminal tail of cpSRP54 binds directly to ribosomal protein uL4 within the exit tunnel, thereby recruiting the nascent chain to the membrane translocon [12]. In addition, cpSRP54 and FtsH2 protease coordinate the proteostasis associated at the thylakoid membrane in *Arabidopsis* [13]. This multifunctional role of cpSRP54 underscores the versatility and complexity of the cpSRP system. So far, there is no convincing indication supporting the presence of a substantial free cpSRP54 pool in the stroma. Thus, cpSRP54, which is not associated with ribosomes, could predominantly be found to be complexed with cpSRP43.

Furthermore, the sole cpSRP43 has been initially shown to interact directly with glutamyl-tRNA reductase (GluTR), the enzyme catalyzing the first committed step in tetrapyrrole biosynthesis, thereby preventing its aggregation and enhancing the production of 5-aminolevulinate (ALA), the rate-limiting step for Chl and heme synthesis [14]. Intriguingly, when cpSRP43 is associated in the heterodimeric cpSRP43/cpSRP54 complex, its ability to stabilize tetrapyrrole biosynthetic enzymes is inhibited [15]. This suggests a regulatory mechanism by which cpSRP43 switches between a "transit complex" mode (bound to cpSRP54 to target LHCP) and a "chaperone" mode (free to interact with tetrapyrrole enzymes) [15]. Supporting this model, cpSRP54 itself appears to play a more limited role in chaperoning enzymes of Chl biosynthesis—for instance, cpSRP54 was shown to promote the thylakoid membrane association of the light-dependent protochlorophyllide oxidoreductase (LPOR) enzyme, whereas cpSRP43 primarily stabilizes LPOR in green leaves and during heat stress [16]. Thus, cpSRP43 and cpSRP54 can independently assist different clients in chloroplasts, and an appropriate balanced accumulation of both cpSRP components is likely critical for maintaining both efficient LHCP transport and a robust Chl biosynthetic capacity.

Chl biosynthesis, which relies particularly on a coordinated metabolite flux to avoid the accumulation of photodynamically active tetrapyrrole intermediates, also exhibits interdependencies for retrograde signaling from the plastid to the nucleus [17–19]. Chloroplasts convey their developmental and metabolic status to the nucleus to modulate the nuclear transcriptional control of photosynthesis-associated nuclear genes (PhANGs) [20]. Perturbations in tetrapyrrole metabolism have visualized this intracellular signaling. The well-described genomes-uncoupled (*GUN*) mutants of *Arabidopsis* have shown that defects in tetrapyrrole biosynthesis (TBS)—often caused by mutations in key components, such as GUN4 (a porphyrin-binding cofactor that stimulates magnesium (Mg) chelatase) and GUN5 (the CHLH subunit of Mg chelatase)—result in abnormal PhANG expression when

chloroplast development is compromised [18,19]. The *gun4-1* allele harbors a point mutation in the GUN4 gene, causing a leucine-to-phenylalanine substitution at amino acid 88 (L88F) that destabilizes the protein and drastically reduces its abundance in the chloroplast. In contrast, the *gun4-3* allele contains a T-DNA insertion near the C-terminus of GUN4, leading to very low levels of a truncated, largely nonfunctional protein [19]. In *gun5-1*, a single nucleotide substitution (C→T) in the third exon converts an alanine to valine at position 990 (A990V) in the CHLH protein; this mutation, located in a highly conserved region, disrupts the CHLH function by weakening the Mg chelatase activity [18]. Collectively, these *GUN* mutants highlight distinct facets of how disrupted TBS in *Arabidopsis* impairs Chl production and disturbs plastid-to-nucleus signaling, underscoring the tight coupling of plastid pigment metabolism and nuclear gene expression.

Although the cpSRP pathway and plastid retrograde signaling have been separately studied in the past, recent evidence suggests a mutual interaction between these processes. cpSRP43 connects the LHCP insertion machinery with tetrapyrrole metabolism by chaperoning enzymes like GUN4 and GUN5/CHLH, raising the question of whether cpSRP43 might influence the activation of GUN-dependent signals. Moreover, from the perspective of protein homeostasis, the maintenance of an appropriate stoichiometry of cpSRP43 and cpSRP54 may be crucial. To date, the physiological consequences of deregulated cpSRP43/cpSRP54 levels in vivo remain poorly understood. Do the two genes for cpSRP43 or cpSRP54 show mutual transcriptional control and do both proteins require each other for stability and function in the chloroplast? And moreover, what happens to Chl biosynthesis, chloroplast development, and signaling when the balance of the expression of both cpSRP components is disrupted?

In this study, we address these critical questions by analyzing *Arabidopsis* lines with modified levels of cpSRP43 and cpSRP54. Our approach includes overexpression lines and single and double mutants that combine defects in the cpSRP pathway with mutations in the key components GUN4 or GUN5 of the GUN-mediated retrograde signaling pathway.

2. Results

2.1. Correlation of cpSRP43 and cpSRP54 Abundance in cpSRP54 Overexpression Lines

Although cpSRP43 and cpSRP54 form a heterodimeric cpSRP complex that facilitates the translocation of LHCPs across the chloroplast stroma to the thylakoid membrane, accumulating evidence indicates that additional pools of these proteins exist independently of the heterodimeric complex. Therefore, the question arose whether cpSRP43 and cpSRP54 abundances are strictly correlated.

To address this issue, we generated a series of cpSRP54 overexpression lines (*cpSRP54-OX*) exhibiting varying elevated cpSRP54 protein levels. The overexpression of cpSRP54 in the cpSRP54-deficient mutant (*ffc*) significantly rescued the pale-green phenotype and restored the seedling morphology to resemble wild-type plants (Col-0) (Figure 1A). While *ffc* shows trace amounts of cpSRP43, line #4 (shown in Figure 1A) displayed extremely low levels of cpSRP54 and failed to rescue the pale-green phenotype. No cpSRP54 levels were immunologically detectable in lines #7, #9, #14, #15, and #20 and, therefore, these are not real *cpSRP54-OX* lines (Figure 1A,B). Immunoblot analyses showed that cpSRP43 abundance was closely correlated with cpSRP54 levels across the *cpSRP54-OX* lines: a higher accumulation of cpSRP54 corresponded to elevated cpSRP43 levels, whereas a reduced cpSRP54 content was associated with lower cpSRP43 abundance (Figure 1B). The quantitative analysis of the immunoblot signal further clarified this correlation, showing a synchronous increase and decrease in the cpSRP43 and cpSRP54 levels in different transgenic lines (Figure 1C). These results strongly suggest a strict correlation between cpSRP43 and cpSRP54 abundances, despite the presence of their distinct functional pools.

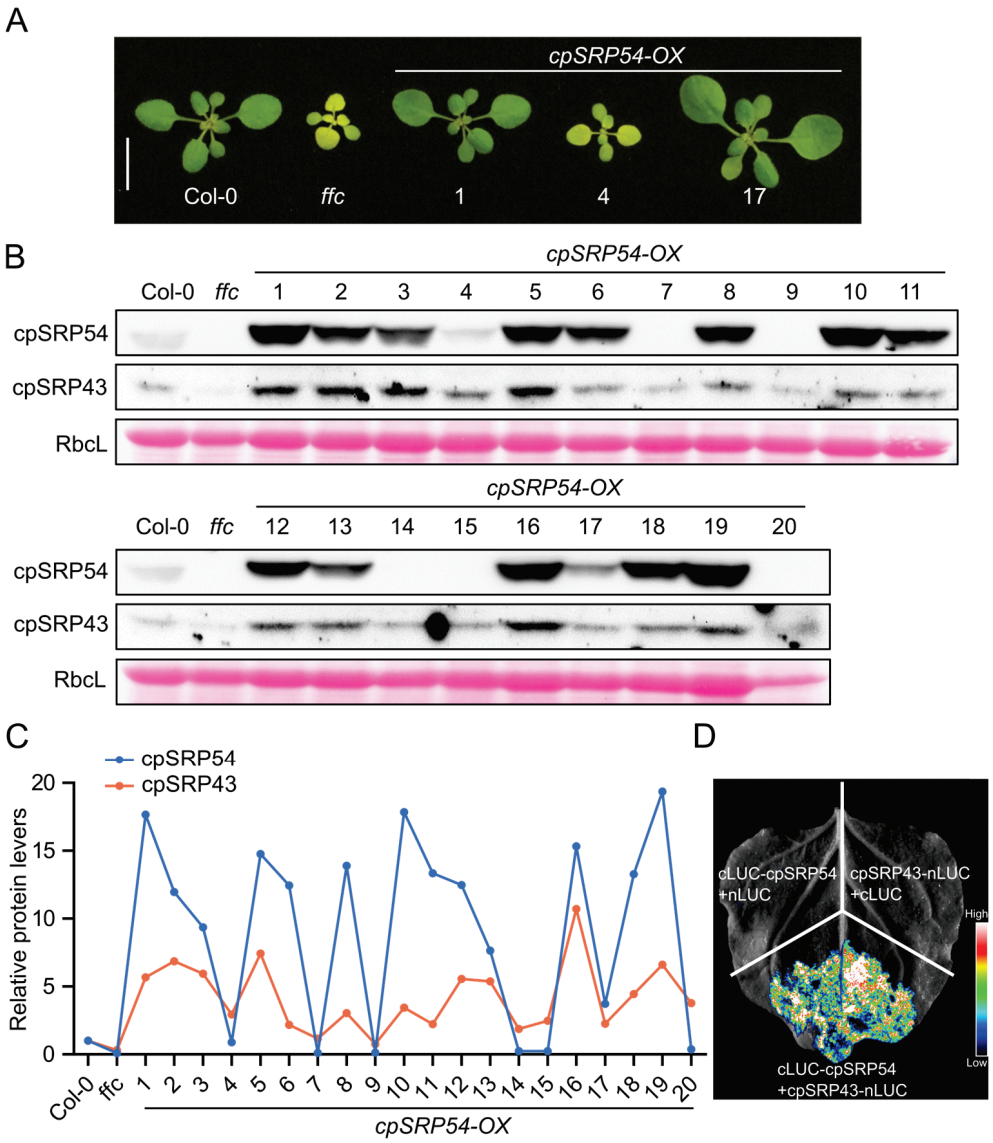


Figure 1. cpSRP43 abundance correlates with cpSRP54 abundance. (**A**) Representative images of the wild type (Col-0), the cpSRP54-deficient mutant (*ffc*), and three independent cpSRP54 overexpression lines (*cpSRP54-OX* #1, #4, and #17). Plants were grown under the standard conditions and photographs were taken at the same developmental stage. Scale bar = 1 cm. (**B**) Immunoblot analysis of cpSRP54 and cpSRP43 in Col-0, *ffc*, and a series of *cpSRP54-OX* lines (#1–20). RbcL (the large subunit of Rubisco) stained with Ponceau S serves as a loading control. (**C**) Relative protein levels of cpSRP54 and cpSRP43 in *ffc* and *cpSRP54-OX* lines compared with Col-0. The band intensities from (**B**) were quantified using ImageJ software (v1.8.0.345) and normalized to the corresponding RbcL signals. (**D**) Split Firefly Luciferase Complementation Imaging assay demonstrating the interaction between cpSRP54 and cpSRP43. *Nicotiana benthamiana* leaves were transiently co-expressed with cpSRP43 fused to the N-terminal fragment of firefly luciferase (nLUC) and cpSRP54 fused to the C-terminal fragment (cLUC). Negative controls included co-expression of cpSRP43-nLUC with cLUC alone, and cLUC-cpSRP54 with nLUC alone. Luminescence intensity is shown by the false color scale at the lower right, with higher intensity indicating stronger protein–protein interaction.

To further substantiate the physical interaction between cpSRP43 and cpSRP54, we performed a Split Firefly Luciferase Complementation Imaging (LCI) assay in *Nicotiana benthamiana* leaves. The co-expression of cpSRP43 fused to the N-terminal fragment of firefly luciferase (nLUC) and cpSRP54 fused to the C-terminal fragment (cLUC) resulted in a robust luminescence signal, confirming their direct interaction in vivo. In contrast,

negative controls—consisting of cpSRP43-nLUC with cLUC alone or cLUC-cpSRP54 with nLUC alone—displayed only background luminescence (Figure 1D). These results, together with the abundance correlation analyses, provide both quantitative and direct biochemical evidence for the functional and physical association of cpSRP43 and cpSRP54.

2.2. Disruption of the Correlation Between cpSRP43 and cpSRP54 Abundance Impairs Plant Growth

Given that cpSRP43 abundance is dependent on cpSRP54, we explored whether cpSRP54 levels are reciprocally affected by changes in cpSRP43 abundance. To this end, we used plant lines expressing wild-type levels (Ler-0), overexpressed levels (*cpSRP43-OX*), or no cpSRP43 (*chaos*). The phenotypic analysis revealed that *chaos* seedlings were pale green and exhibited growth retardation, whereas the overexpression of cpSRP43 in the wild type rescued these defects, yielding phenotypical seedlings comparable to those of Ler-0 (Figure 2A,B). Immunoblot analysis revealed that cpSRP54 levels progressively decreased from the *cpSRP43-OX* through Ler-0 to *chaos* (Figure 2C). The quantitative analysis confirmed this trend and clearly illustrates that the abundance of cpSRP54 declined in parallel with the decreasing cpSRP43 levels (Figure 2D). Conversely, in the series from the *ffc* to the *cpSRP54-OX*, cpSRP43 abundance consistently increased with elevated cpSRP54 levels (Figure 2C,D). These results indicate an interdependent correlation between the accumulation of cpSRP43 and cpSRP54.

To further investigate this relationship, we disrupted the correlation between cpSRP43 and cpSRP54 by generating double mutants: *ffc* was crossed with *cpSRP43-OX* and *chaos* was crossed with *cpSRP54-OX*, yielding the double mutants *cpSRP43-OX*/*ffc* and *cpSRP54-OX*/*chaos* (Figure 2A,B). It is noteworthy that the ecotype backgrounds differ in the lines used: *chaos* and *cpSRP43-OX* lines are Ler-0 seedlings, whereas *ffc* and *cpSRP54-OX* are Col-0 seedlings. We show the different electrophoretic mobility of GluTR of Ler-0 and Col-0 seedlings via immunoblotting to clarify the ecotype of the double mutants. Leaf extracts from both *cpSRP43-OX*/*ffc* and *cpSRP54-OX*/*chaos* showed GluTR mobility identical to those from Ler-0 (Figure 2C), confirming the genetic Ler-0 background of these double mutants.

The phenotypical analysis revealed that a genetic disruption of the abundance of cpSRP43 and cpSRP54 led to a strong impairment of seedling growth. Specifically, neither *cpSRP54-OX*/*chaos* nor *cpSRP43-OX*/*ffc* lines rescued the pale-green phenotype of the *chaos* or *ffc* mutants (Figure 2A,B). Instead, these double mutants exhibited significantly smaller and paler seedlings compared to their parental lines (Figure 2A,B), indicating that a genetic disruption of the correlative accumulation of cpSRP43 and cpSRP54 severely impairs plant growth. Despite this, the immunoblot profiles of GluTR, LHCb, and LHCa in the double mutants closely resembled those of the respective single null mutants (Figure 2C).

Consistent with these phenotypes, the HPLC analyses showed significantly lower or comparable Chl contents in the double mutants relative to parental and wild-type lines (Figure 3A). The levels of tetrapyrrole intermediates Mg-protoporphyrin (MgP), Mg-protoporphyrin monomethyl ester (MgMME), and protochlorophyllide (Pchlide) were markedly reduced compared to their parental lines (Figure 3B,C). Correspondingly, the content of the end-product heme was also significantly lower in the double mutants compared with parental lines and the wild type (Figure 3D). Collectively, these findings strongly support that the maintenance of the correlated abundance of cpSRP43 and cpSRP54 is critical for normal chloroplast function, TBS, and overall plant growth.

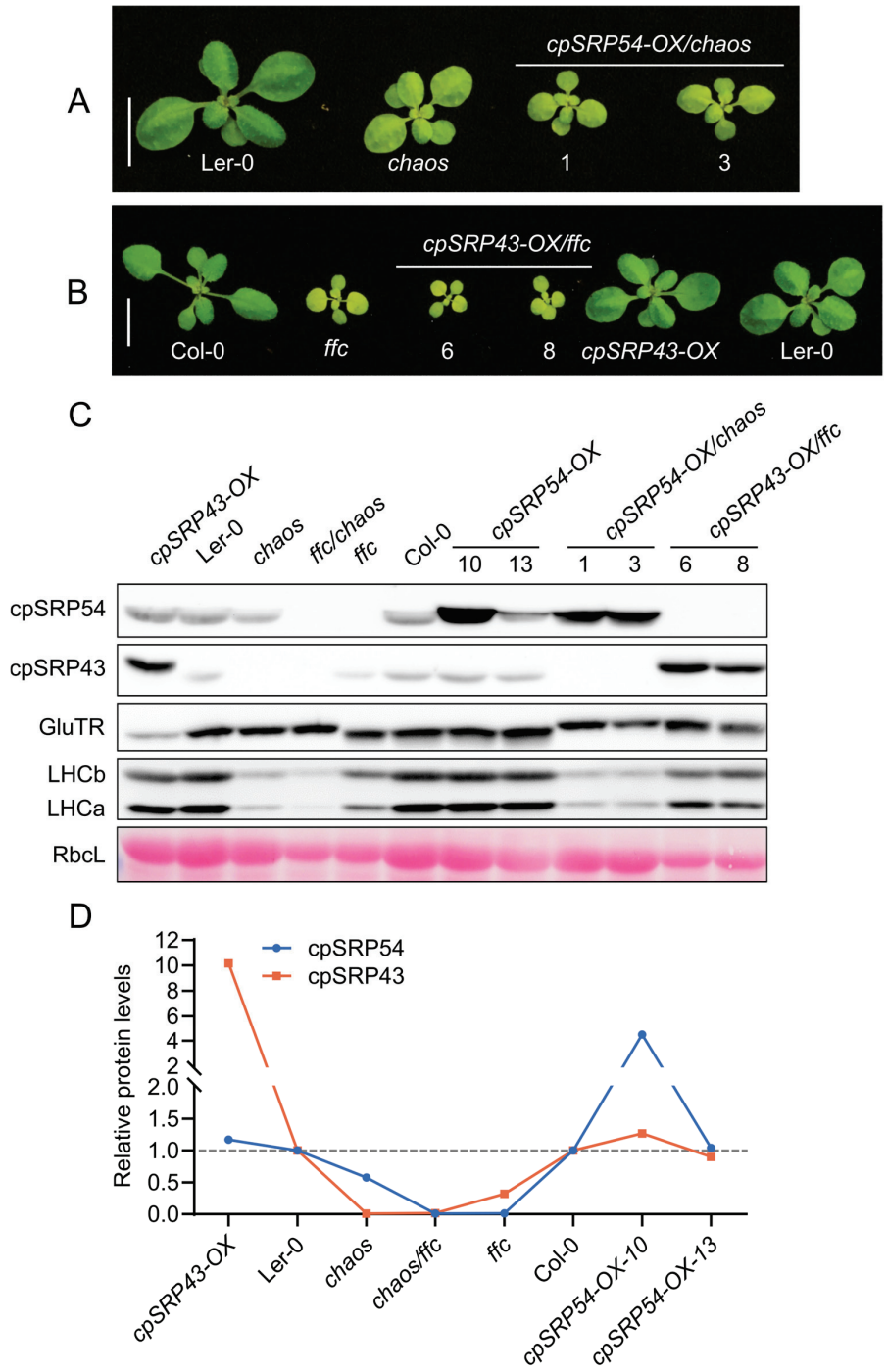


Figure 2. Disrupted cpSRP43–cpSRP54 balance impairs plant growth. (**A**) Representative images of Ler-0 (wild-type), the cpSRP43-deficient mutant *chaos*, and two independent cpSRP54 overexpression lines in the *chaos* background (*cpSRP54-OX*/*chaos* #1 and #3). Plants were grown under the same conditions and photographed at the same developmental stage. Scale bar = 1 cm. (**B**) Representative images of Col-0 (wild-type), the cpSRP54-deficient mutant *ffc*, two independent cpSRP43 overexpression lines in the *ffc* background (*cpSRP43-OX*/*ffc* #6 and #8), a *cpSRP43-OX* line in *chaos* background, and Ler-0. Scale bar = 1 cm. (**C**) Immunoblot analysis of cpSRP54, cpSRP43, GluTR (Glutamyl-tRNA reductase), LHCb (Light-harvesting chlorophyll a/b-binding protein b), and LHCa (Light-harvesting chlorophyll a/b-binding protein a) in the indicated genotypes. RbcL stained with Ponceau S serves as a loading control. (**D**) Quantification of relative cpSRP54 and cpSRP43 protein levels, normalized to their respective wild-type ecotype (Col-0 for *ffc* and *cpSRP54-OX* lines, Ler-0 for *chaos* and its derivative lines), based on the immunoblot signals from (**C**). The gray dashed line indicates the baseline levels of cpSRP54 and cpSRP43 in wild-type plants (Col-0 and Ler-0).

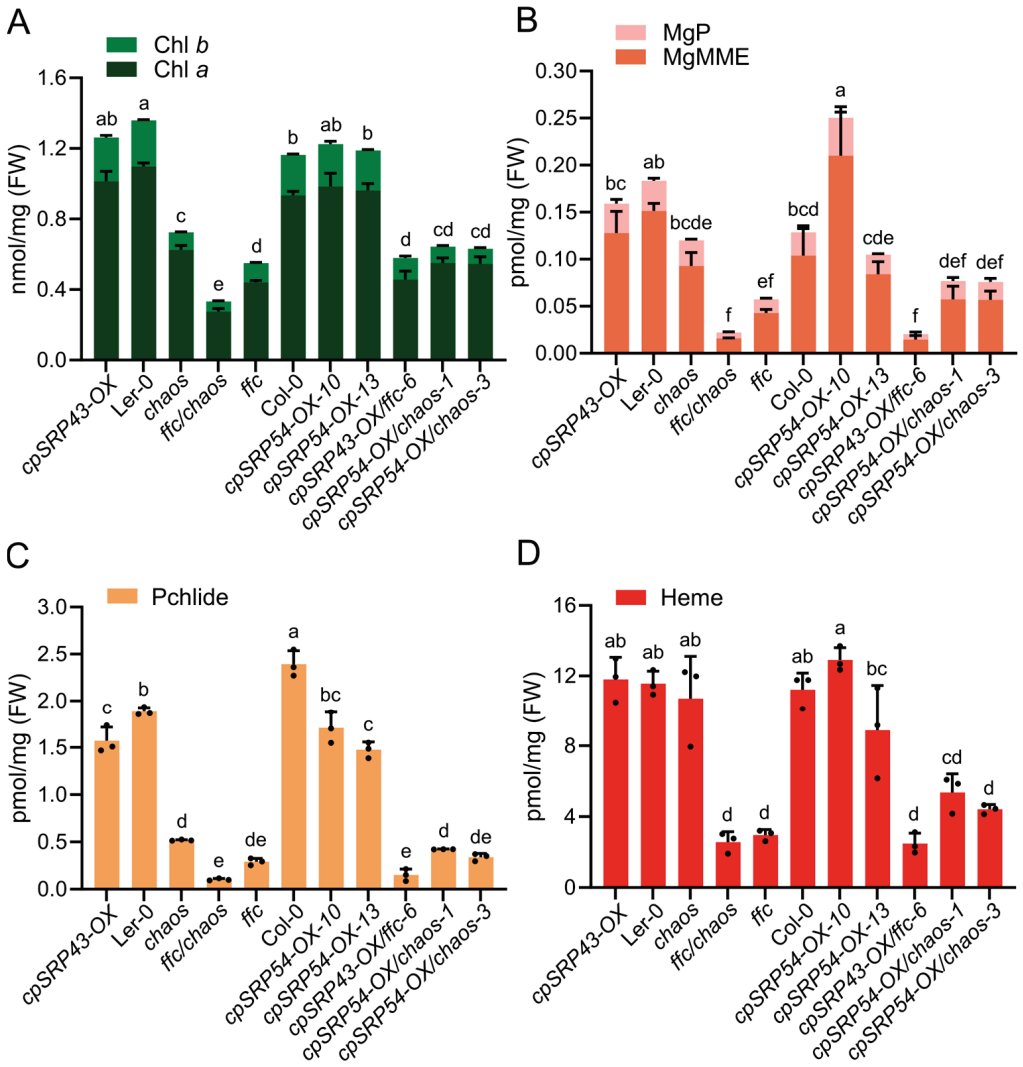


Figure 3. Disrupted cpSRP43–cpSRP54 balance impairs the tetrapyrrole biosynthesis pathway. (**A**) Quantification of chlorophyll *a* (Chl *a*) and chlorophyll *b* (Chl *b*) content in the indicated genotypes. (**B**) Analysis of tetrapyrrole intermediates, including Mg-protoporphyrin IX (MgP) and Mg-protoporphyrin IX monomethyl ester (MgMME) in the indicated genotypes. (**C**) Measurement of protochlorophyllide (Pchlide) levels across different *Arabidopsis* lines. (**D**) Heme content in the indicated genotypes. All data are presented as the mean ± SD from three biological replicates. Individual data points are represented by small black dots. Letters above the bars indicate significant differences, as determined by one-way ANOVA followed by Tukey's HSD multiple comparison test ($p < 0.05$). FW, fresh weight.

2.3. Double Mutants for cpSRP43 and GUN4/GUN5 Are Severely Growth-Retarded and Impaired in Tetrapyrrole Biosynthesis

It has previously been shown that cpSRP43 acts as a chaperone, protecting GUN4 and GUN5 (CHLH) from their own aggregation under standard and heat shock conditions and thus preserving their stability [15]. However, it remains unclear whether the genetic relationship between cpSRP43 and GUN4/GUN5 is epistatic or synergistic. To address this question and clarify their common or mutual functional roles in chloroplast development and TBS, we investigated whether the simultaneous disruption of the expression of *cpSRP43* and *GUN4/GUN5* would exacerbate the defects observed in single mutants. Therefore, we generated double mutants by crossing *chaos* with *gun4-1*, *gun4-3*, and *gun5-1*.

The phenotypic analyses showed that the resulting double mutants—*gun4-1/chaos*, *gun4-3/chaos*, and *gun5-1/chaos*—displayed severely impaired growth compared to their re-

spective parental single mutants, as evidenced by significantly smaller and paler seedlings (Figure 4A). Consistent with these phenotypes, immunoblot analyses revealed substantial reductions in the abundance of exemplary proteins essential for TBS and the assembly of the photosynthetic complexes, such as GluTR, LHCb, and LHCa, in these double mutants (Figure 4B). Biochemical quantifications using HPLC showed that levels of Chl *a*/*b* were notably diminished in the double mutants relative to parental and wild-type lines (Figure 4C). Correspondingly, TBS intermediates, including MgP, MgMME, and Pchlide, exhibited significant decreases (Figure 4D,E). These results suggest that the simultaneous inactivation of cpSRP43 and GUN proteins involved in the Mg chelation of protoporphyrin IX exacerbates defects in TBS and chloroplast development, underscoring a critical genetic interaction between cpSRP43 function and GUN-mediated signaling as well as tetrapyrrole biosynthesis pathways that are all essential for maintenance of normal plant growth.

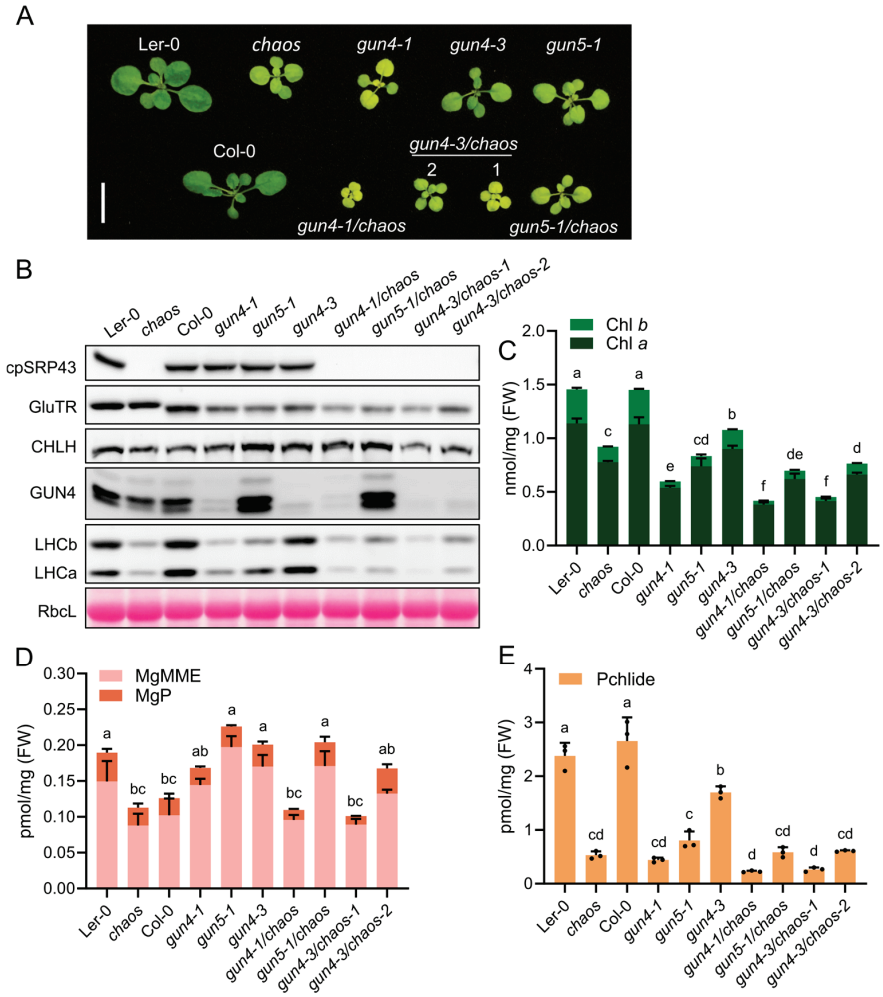


Figure 4. Combination of *chaos* and *gun* mutants exacerbates growth defects. (**A**) Representative phenotypes of wild-type (Ler-0 and Col-0), the *chaos* mutant, and *gun* mutants (*gun4-1*, *gun4-3*, and *gun5-1*), and double mutants (*gun4-1*/*chaos*, *gun5-1*/*chaos*, and *gun4-3*/*chaos* lines #1 and #2). Scale bar = 1 cm. (**B**) Immunoblot analysis of cpSRP43, GluTR, CHLH (H subunit of Mg-chelatase), GUN4 (genomes uncoupled 4), LHCb, and LHCa proteins across the indicated genotypes. RbcL stained with Ponceau S serves as a loading control. (**C**) Chl *a* and Chl *b* contents in the indicated genotypes. (**D**) Analysis of tetrapyrrole intermediates MgP and MgMME in the indicated genotypes. (**E**) Pchlide content in the indicated genotypes. All data are presented as the mean ± SD from three biological replicates. Individual data points are represented by small black dots. Letters above the bars indicate significant differences, as determined by one-way ANOVA followed by Tukey's HSD multiple comparison test ($p < 0.05$). FW, fresh weight.

2.4. cpSRP43 Overexpression Does Not Rescue Gun Mutant Phenotypes

Given that the *chaos*/*gun* double mutants exhibit a more severe phenotype and indicate a synergistic relationship between the genes involved either in the cpSRP function and the TBS/retrograde signaling, we investigated whether cpSRP43 overexpression could alleviate the growth defects in the *gun4* and *gun5* mutants. We, therefore, compared the growth and leaf pigmentation of *cpSRP43-OX* lines in *gun4* and *gun5* backgrounds to their respective parental mutants (Figure 5A). The *cpSRP43-OX*/*gun* combination plants remained small and pale (chlorotic), closely resembling the stunted, light-green appearance of the *gun* mutants, underscoring that elevated cpSRP43 expression failed to rescue the characteristic pale and growth-deficient phenotype of *gun4* and *gun5* (Figure 5A).

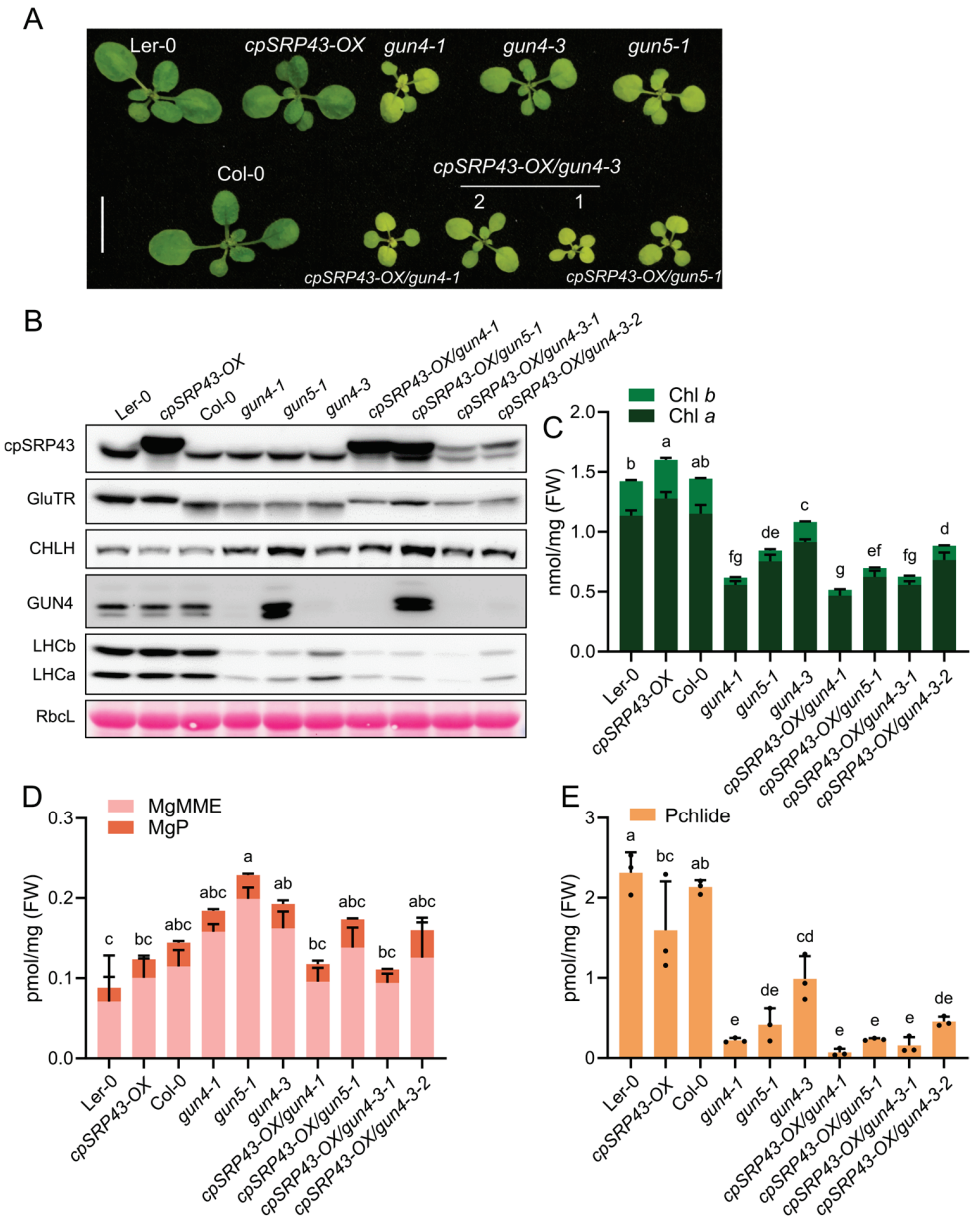


Figure 5. Overexpression of cpSRP43 cannot rescue the *gun* phenotype. (**A**) Representative phenotypes of wild-type (Ler-0 and Col-0), the *cpSRP43-OX* line, *gun* mutants (*gun4-1*, *gun4-3*, and *gun5-1*), and the corresponding double mutants (*cpSRP43-OX*/*gun4-1*, *cpSRP43-OX*/*gun4-3* lines #1 and #2, and *cpSRP43-OX*/*gun5-1*). Scale bar = 1 cm. (**B**) Immunoblot analysis of cpSRP43, GluTR, CHLH, GUN4, LHCb, and LHCa in the indicated genotypes. RbcL stained with Ponceau S serves as a loading control. (**C**) Quantification of Chl *a* and Chl *b* in the indicated genotypes. (**D**) Analysis of the tetrapyrrole

intermediates MgP and MgMME in the indicated genotypes. (**E**) Quantification of Pchlide in the indicated genotypes. All data are presented as the mean ± SD from three biological replicates. Individual data points are represented by small black dots. Different letters above the bars indicate significant differences, as determined by one-way ANOVA followed by Tukey's HSD multiple comparison test ($p < 0.05$). FW, fresh weight.

Immunoblot analysis of key chloroplast proteins revealed significant changes in their abundance associated with the *gun* mutations (Figure 5B). For example, the protein levels of GluTR, CHLH, GUN4, LHCa, and LHCb were all altered in the *gun* mutant compared to the wild type, reflecting the disruptions in Chl biosynthesis, the formation of the photosynthetic complexes, and likely, retrograde signaling (Figure 5B). Notably, the *cpSRP43-OX/gun* showed protein abundance patterns similar to their respective *gun* parental lines for each marker protein examined. These results indicate that cpSRP43 overexpression does not compensate for the defects in chloroplast protein homeostasis caused by *gun* mutations. The expression of TBS enzymes (GluTR, CHLH, and GUN4) and photosystem antenna components (LHC proteins) in *cpSRP43-OX/gun* plants is consistent with the impaired functional properties of *gun* mutants (Figure 5B).

Consequently, *cpSRP43-OX/gun* accumulated similar amounts of Chl *a* and Chl *b* as the *gun* parental lines (Figure 5C). Likewise, the levels of MgMME, MgP, and Pchlide were generally comparable between *cpSRP43-OX/gun* lines and the corresponding *gun* mutants (Figure 5D,E). These data indicate that cpSRP43 overexpression does not substantially modify the core pigment biosynthetic performance in *gun* mutant plants. One notable exception was observed in the *gun4* background: the *cpSRP43-OX/gun4-3* line showed a further reduction in the total Chl content compared to the *gun4-3* mutant (Figure 5C), consistent with its slightly more pronounced pale leaf phenotype. Nevertheless, the pigment content of cpSRP43 overexpressors was basically the same as that of the *gun* mutants, emphasizing that cpSRP43 overexpression has little effect on TBS in the *gun4* or *gun5* background when Mg chelatase activity and Chl synthesis are reduced.

2.5. cpSRP43 Is Not Involved in Plastid-to-Nucleus Retrograde Signaling

Molecular communication between plastids and the nucleus, known as retrograde signaling, plays a critical role in coordinating nuclear gene expression in response to the functional status of plastids. To explore whether cpSRP43 also contributes to plastid-localized retrograde signaling, we analyzed PhANG transcript levels in *chaos* under conditions that disrupt plastid biogenesis (e.g., NF treatment). As a positive control, the *gun4-1* mutant exhibited an elevated expression of all tested PhANGs compared to the wild type (Col-0) (Figure 6A–E). In contrast, the *chaos* mutant showed PhANG expression comparable to that of the wild type (Ler-0), suggesting that the absence of cpSRP43 does not disrupt plastid-to-nucleus retrograde signaling (Figure 6A–E).

The DMSO-treated group served as the control for the NF treatment and the results indicated that DMSO did not significantly affect PhANG expression in either *chaos* or *gun4-1* compared with the wild type (Figure S1). Collectively, these findings indicate that cpSRP43 is not involved in the plastid-to-nucleus retrograde signaling pathway, and makes it possible to distinguish its role from that of GUN4 and GUN5, which, in addition to their function in the Mg chelation of protoporphyrin, are assigned a role in retrograde signal transmission.

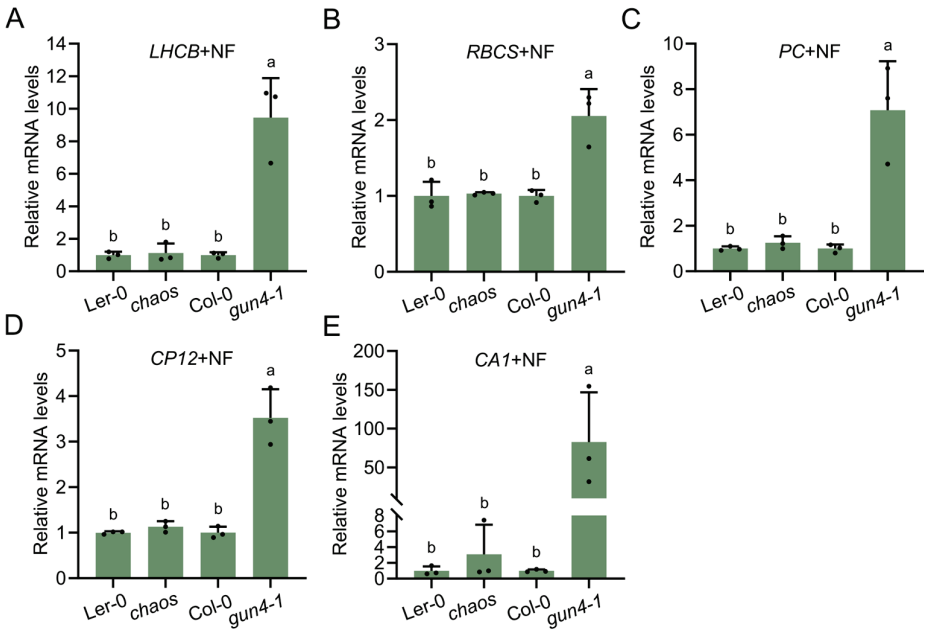


Figure 6. cpSRP43 is not involved in plastid-to-nucleus retrograde signaling pathway. (**A**–**E**) Relative mRNA levels of PhANGs, including *LIGHT HARVESTING CHLOROPHYLL-BINDING PROTEINS (LHCB)*, *RuBisCO SMALL SUBUNIT (RBCS)*, *PLASTOCYANIN (PC)*, *CHLOROPLAST PROTEIN 12 (CP12)*, and *CARBONIC ANHYDRASE1* (*CA1*). (**A**) *LHCB*, (**B**) *RBCS*, (**C**) *PC*, (**D**) *CP12*, and (**E**) *CA1* in Ler-0, the *chaos*, Col-0, and the *gun4-1* mutant treated with 5 μM norflurazon (NF). All data are presented as means ± SD from three biological replicates, with individual data points shown as small black dots. Letters above the bars indicate significant differences ($p < 0.05$) determined by one-way ANOVA followed by Tukey's HSD multiple comparison test.

3. Discussion

3.1. Interdependence of cpSRP43 and cpSRP54 Abundance

Our findings reveal a strong functional interdependence between cpSRP43 and cpSRP54 in *Arabidopsis* and emphasize that these two cpSRP components perform closely related functions. This mutual dependence of the expression of both proteins is remarkable considering that cpSRP43 and cpSRP54 have other functions in addition to the role of the heterodimeric cpSRP complex for the LHCP transfer through the stroma. cpSRP43 not only partners with cpSRP54 to target LHCPs to the thylakoid membrane [3,21], but it also acts independently as a chaperone for enzymes of the TBS pathway [14–16]. Conversely, cpSRP54 has its own role in the co-translational targeting of certain chloroplast-encoded proteins in cooperation with other auxiliary factors [12]. Despite these separate activities, our results indicate an obvious balance in cpSRP43 and cpSRP54 accumulation in plant cells. This coordination likely serves to synchronize Chl production with the availability of LHCP apoproteins, thereby linking pigment biosynthesis to thylakoid protein insertion in a highly regulated fashion.

Consistent with a model of mutual stabilization, altering the level of one cpSRP subunit had a direct impact on the abundance of the other protein. In *cpSRP54-OX*, cpSRP43 protein levels rose in parallel with cpSRP54 levels, whereas in a cpSRP43-overexpressing line, cpSRP54 levels were elevated relative to the wild type. Conversely, the absence of either subunit led to a marked decrease in the steady-state level of its partner. These observations strongly suggest that cpSRP43 and cpSRP54 post-translationally stabilize each other, likely through the formation of a cpSRP43–cpSRP54 complex.

Disrupting the cpSRP43–cpSRP54 balance had severe consequences for plant growth and chloroplast development. Neither increasing cpSRP43 in a cpSRP54-null mutant nor

increasing cpSRP54 in a cpSRP43-null background could rescue the characteristic pale, stunted phenotype of the single mutants. This outcome indicates that an excess of one subunit cannot compensate for the loss of its partner. On the contrary, such an imbalance seems to be even more harmful. One possible interpretation is that any unpaired cpSRP subunit might be nonfunctional and could even affect the role of other interacting proteins or could also affect the quality control for other functional protein groups. Meanwhile, the limiting subunit, especially cpSRP54, is insufficient to carry out the essential role of the cpSRP pathway in LHCP trafficking [3,22,23]. The pronounced growth impairment in these mutants underscores that both cpSRP43 and cpSRP54 are required in concert and that their functions in chloroplast protein targeting (and perhaps other processes) are not redundant.

3.2. Synergistic Defects in cpSRP and GUN4/GUN5 Double Mutants

A major outcome of our study is the severe phenotype observed when cpSRP mutations are combined with lesions in the *GUN4* or *GUN5* genes. Individually, *gun4* and *gun5* mutants are pale green and exhibit reduced Chl levels due to impaired Mg chelation within the biosynthetic pathway. However, when the *chaos* mutation is combined with *gun4* or *gun5*, the double mutants are dramatically smaller, more chlorotic, and accumulate even less Chl than either single mutant. This synergistic effect can be explained by considering how cpSRP and GUN4/GUN5 each contribute to the production and utilization of Chl in the photosynthetic apparatus via different mechanisms. GUN5/CHLH functions as an Mg chelatase subunit directly responsible for inserting Mg^{2+} into protoporphyrin IX, a critical step in Chl biosynthesis [18], while GUN4 acts as a cofactor that binds porphyrins, stimulates Mg-chelatase activity, and participates in sensing chloroplast tetrapyrrole levels for signaling [19,24,25]. Defects in either GUN4 or GUN5 result in less Chl availability for photosynthesis. In contrast, a cpSRP43 defect leads to Chl deficiency by preventing the proper insertion of LHCPs and by destabilizing enzymes such as CHLH and GUN4 themselves [15]. Essentially, a *cpSRP43* mutant simultaneously hampers the assembly of Chl-binding proteins and undermines the pigment biosynthesis, as evidenced by the reduced CHLH and GUN4 protein levels observed in *chaos*. The lack of pigments also destabilized the chlorophyll-binding proteins of the photosynthetic protein complexes [26,27]. The chloroplasts of double mutant *gun4/chaos* and *gun5/chaos,* therefore, experience a twofold deficit, which cannot be compensated. These deficiencies in the function of GUN4/5 and cpSRP components lead to an enhanced failure in Chl accumulation and ultimately to an arrest in chloroplast biogenesis (Figure 4). This amplified deficiency manifests itself in the extreme chlorosis and growth arrest that we have observed.

3.3. cpSRP43 Overexpression Cannot Rescue Gun Mutants

Our experiments showed that overexpressing cpSRP43 in *gun4* or *gun5* knock-down mutants failed to ameliorate their chlorotic, slow-growing phenotypes. This outcome is actually not surprising: the partial block of Mg-chelatase activity in these *gun* mutants impairs the tetrapyrrole metabolism, which apparently cannot be overcome by providing more of a cpSRP43 chaperone capacity. Regardless of how much cpSRP43 is present, it cannot directly increase the production of Mg chelatase or the synthesis of ALA, and thus the Chl precursor flow remains limited. It only chaperones existing subunits of Mg chelatase. For example, in wild-type plants, boosting cpSRP43 or cpSRP54 alone does not lead to higher Chl levels than normal, indicating that the Chl biosynthesis was already working at its maximal metabolic flow rate in the presence of normal cpSRP levels. cpSRP components are not a limiting factor for Chl synthesis, but only another supporting factor among several post-translational control mechanisms for this metabolic pathway [14,28]. In contrast, the overexpression of GUN4 can increase Chl production, as

GUN4 directly enhances enzyme activities in the pathway [29]. Our *cpSRP43-OX/gun4* experiment reinforces this understanding: without GUN4, the rate-limiting steps of the Chl synthesis cannot be accelerated. These observations highlight the specificity of cpSRP43's role—it is necessary as a chaperone for proper chloroplast biogenesis, but not sufficient to drive it when crucial biosynthetic components are missing. Any attempt to enhance the Chl content or photosystem assembly must, therefore, address the metabolic bottlenecks (like the Mg-chelation step) in addition to providing assembly factors and chaperones.

3.4. cpSRP43 and Retrograde Signaling

Despite the significant role of cpSRP43 in chloroplast development, our data clearly indicate that it does not participate in plastid-to-nucleus retrograde signaling (Figure 6). Mutations in *GUN4* or *GUN5* impair this signaling. *chaos* did not show a *gun*-type modified expression of PhANGs. When chloroplast development was chemically disrupted (by NF treatment), *chaos* seedlings repressed PhANG transcripts to wild-type levels, confirming no impact on the GUN-mediated retrograde signaling pathway. This finding allows a clear distinction between the roles of cpSRP43 and those of GUN4/GUN5; the latter influence both Chl synthesis and is involved in retrograde signaling, while cpSRP43 impacts Chl synthesis and utilization without affecting nuclear feedback signaling. The albino or pale phenotype of *chaos* mutants suggests multiple layers of the chloroplast dysfunction responses. Chloroplast assembly is compromised due to LHCP targeting failure and enzyme instability, but the mutants still produce proper retrograde signals to downregulate nuclear gene expression. Thus, cpSRP43 functions downstream of retrograde cue generation and influences the chloroplast assembly, but not the signaling mechanism itself.

3.5. Coordination of Chloroplast Biogenesis and Future Directions

Together, these results highlight how chloroplast biogenesis relies on the coordination of protein-targeting machineries with metabolic pathways. The cpSRP system and the tetrapyrrole biosynthetic pathway must work in tandem to achieve efficient Chl incorporation into photosynthetic complexes. An interruption in one activity is detrimental, but an interruption in both areas is disastrous, as we have seen. This interdependence exemplifies a broader principle of organelle development: the stoichiometry of multi-component processes (like pigment synthesis and apoprotein integration) must be tightly regulated to avoid imbalances that could lead to proteotoxic stress or metabolite accumulation. From an applied perspective, understanding this coordination could inform strategies to improve the plant vitality. For instance, balancing the expression of Chl-binding proteins with the rate of Chl production might be a key consideration in engineering crops with an enhanced photosynthetic performance. Future research directions include elucidating mechanisms maintaining cpSRP43/cpSRP54 balance, understanding adaptive regulation under stress conditions, and exploring interactions with other chloroplast assembly pathways and signaling networks. These studies could significantly enhance strategies to improve crop vitality and stress tolerance.

4. Materials and Methods

4.1. Plant Materials and Growth Conditions

Arabidopsis thaliana seedlings were grown in a 16 h light/8 h dark period on soil in a growth chamber (CLF PlantClimatics, Wertingen, Germany) at 22 °C and 100 µmol photons $m^{-2}s^{-1}$. Unless otherwise stated, the standard growth condition in this study is 16 h light/ 8 h dark, 100 µmol photons $m^{-2}s^{-1}$ at 22 °C. The information on the *Arabidopsis* lines used in this study is listed in Table S1.

4.2. Crossing of Arabidopsis Thaliana

Arabidopsis crosses were performed by emasculating unopened flower buds of designated maternal plants using fine forceps under a stereomicroscope (Olympus, Tokyo, Japan). Pollen from selected paternal plants was then applied directly onto the stigma of emasculated flowers. Crossed plants were marked and covered loosely to avoid contamination. Mature siliques were individually harvested, and resulting F1 seeds were collected, stratified at 4 °C for two days, and then germinated for subsequent analysis.

4.3. Analysis of TBS Intermediates and End-Products

Rosette leaves (40–60 mg) were harvested and their fresh weight (FW) was determined. TBS intermediates and end-products were extracted from frozen or lyophilized leaf powders in 400 µL of ice-cold pigment-extraction buffer (acetone: 0.2 M NH_4OH = 9:1, *v*/*v*) at −20 °C for at least 1 h. After centrifugation (14,000× *g*, 20 min at 4 °C), the supernatant was subjected to HPLC. The pellet was retained for extraction of non-covalently bound heme using AHD buffer (acetone: hydrochloric acid: dimethyl sulfoxide = 10:0.5:2, *v*/*v*/*v*) at room temperature. HPLC analyses were conducted using the Agilent 1100 or 1290 HPLC system equipped with a diode array and fluorescence detectors (Agilent Technologies, Santa Clara, CA, USA), essentially as described previously [30].

4.4. Norflurazon Treatment

The sterile cultivation of *Arabidopsis* plants was conducted on Petri dishes with Murashige and Skoog medium (MS, with vitamins, Duchefa Biochemie, Haarlem, The Netherlands) mixed with plant cultivation agar (4.43 g/L MS, 0.5 g/L MES, 8 g/L agar, and pH 5.7 with NaOH). About 50 µL of seeds were incubated for 10 min in 1 mL of sterilization solution (70% ethanol (*v*/*v*), 0.05% (*v*/*v*) Triton X-100). The sterilization solution was then removed and the seeds were washed in 70% ethanol (*v*/*v*) twice. Then, the seeds were washed with 100% ethanol (*v*/*v*) twice and dried. The sterilized seeds were sown either dry or mixed with sterile water. To analyze the retrograde signaling pathway [17], *Arabidopsis* seeds were grown on the sterilized MS plates in the presence of 5 µM norflurazon (NF, 5 mM in DMSO as stock). After stratification for 2 days, seedlings were grown in continuous light for 5–6 days.

4.5. RNA Extraction and qRT-PCR

Total RNA was extracted from *Arabidopsis* leaves frozen in liquid nitrogen using the citric-acid extraction method [31]. Aliquots (2 µg) of DNase-treated RNA were reverse-transcribed using oligo $(dT)_{18}$ primers and RevertAid reverse transcriptase (Thermo Fisher Scientific, Waltham, MA, USA). qPCR was carried out in the CFX96-C1000 96-well plate thermocycler (Bio-Rad, Hercules, CA, USA) by using 2×qPCR Mastermix (Bimake, Houston, TX, USA). *Actin* (At3g18780) was routinely used as the reference gene. Relative expression was calculated in Bio-Rad CFX Manager v1.6 using the $2^{-\Delta\Delta Ct}$ method. Primers for qRT-PCR are listed in Table S2.

4.6. Protein Extraction and Western Blot Analysis

Whole 14–18-day-old rosette seedlings were harvested from 3–6 individual plants of each genotype. In the case of plants grown under standard conditions, freshly harvested leaves were ground in liquid nitrogen and total leaf proteins were extracted from the powder using 2×Laemmli buffer [100 mM Tris-HCl pH 6.8, 4% (*w*/*v*) SDS, 20% (*v*/*v*) glycerol, 200 mM DTT, and 0.01% Bromophenol Blue] and incubated at 95 °C for 10 min. The protein concentration was determined and normalized to leaf fresh weight. In the case of heat shock experiments, rosette leaves were harvested before or after heat treatment

and ground in liquid nitrogen. Total leaf protein was extracted from frozen plant material in PEB buffer [2% (*w*/*v*) SDS, 56 mM Na_2CO_3, 12% (*w*/*v*) sucrose, and 2 mM EDTA] and protein concentrations were determined using the Pierce BCA Protein Assay Kit (Thermo Fisher Scientific). All samples in PEB buffer were diluted to the same protein concentration, supplemented with 56 mM DTT, and incubated at 70 °C for 20 min. Aliquots (15 μg) of protein were subjected to SDS-PAGE (sodium dodecyl sulfate–polyacrylamide gel electrophoresis), transferred to nitrocellulose membranes (GE Healthcare, Chicago, IL, USA), and probed with specific antibodies. Antibodies against GluTR (1:1000), GUN4 (1:2000) were generated in our laboratory. Antibodies against cpSRP43 (1:2500) and cpSRP54 (1:2500) were kindly donated by Prof. Danja Schünemann (Ruhr University, Bochum, Germany). Those directed against CHLH (1:1000) were kindly provided by Dr. Da-Peng Zhang (Tsinghua University, Beijing, China). Immunoblotting signals visualized by Clarity™ Western ECL (Bio-Rad) were detected with a CCD camera (Intas Science Imaging Instruments, Göttingen, Germany).

4.7. Split Firefly Luciferase Complementation Imaging Assay

The coding sequence (CDS) of cpSRP43, excluding the chloroplast transit peptide, was cloned into the JW771 vector (Bio-Vector NTCC, Beijing, China) to create a fusion with the N-terminal end of firefly luciferase (nLUC). Similarly, the CDS of cpSRP54 lacking its transit peptide was cloned into the JW772 vector (Bio-Vector NTCC, Beijing, China), resulting in a fusion with the C-terminal of firefly luciferase (cLUC). *Agrobacterium tumefaciens*-mediated infiltration was employed to co-express cpSRP43-nLUC and cLUC-cpSRP54 in *Nicotiana benthamiana* leaves, using the GV3101 strain (containing the helper plasmid pSoup-P19), following the procedure described by Gou et al. [32]. As negative controls, the empty JW771 and JW772 vectors were infiltrated individually. Luciferase activity was visualized 48–72 h after infiltration by spraying 0.8 mM D-luciferin (aladdin, Shanghai, China) and detecting chemiluminescence with a Tanon-5200 Multi imaging system (Tanon Science & Technology, Shanghai, China).

4.8. Image Processing and Graphic Evaluation

Image files (Western blots, protein gels, photographs, etc.) were processed with Photoshop CS3 (v10.0.1, Adobe, San Jose, CA, USA) and Inkscape (v1.2.1, https://inkscape.org/). Blot signals of proteins were quantified densitometrically using the ImageJ software (v1.8.0.345, NIH, Bethesda, Maryland, USA), with all quantifications performed using standardized protocols, including background subtraction, to minimize the potential subjective nature of this approach. Graphical representations were generated in GraphPad Prism 8.0 or v9.1.2 (226). Statistical analyses were performed using Excel 2016 or GraphPad Prism v.9.1.2 (226).

5. Conclusions

In summary, this study demonstrates that cpSRP43 and cpSRP54 function in a mutually dependent manner to support chloroplast development in *Arabidopsis thaliana*. A balanced abundance of these cpSRP subunits is essential for normal Chl biosynthesis and the proper assembly of light-harvesting complexes, as any disruption of their equilibrium leads to impaired growth and pale, chlorotic phenotypes. Moreover, although the cpSRP and the functions of the two proteins GUN5 and GUN4 for Chl synthesis and retrograde signaling synergistically influence TBS, our findings reveal that cpSRP43—despite its essential role in chloroplast protein and pigment homeostasis—does not participate in plastid-to-nucleus retrograde signaling. This distinction clearly sets its function apart from that of the GENOMES-UNCOUPLED regulators GUN4 and GUN5.

Supplementary Materials: The following supporting information can be downloaded at: https://www.mdpi.com/article/10.3390/plants14121745/s1, Figure S1: Expression of nuclear-encoded photosynthesis-associated genes (*PhANGs*) in *chaos* and *gun4-1* mutants under standard conditions (without NF); Table S1: Genotypes used and analyzed in this study; Table S2: List of primers used in this study and raw data.

Author Contributions: Conceptualization, S.J. and B.G.; methodology, S.J. and B.G.; software, S.J.; validation, S.J. and B.G.; formal analysis, S.J., H.Y. and B.G.; investigation, S.J. and H.Y.; resources, B.G.; data curation, S.J. and B.G.; writing—original draft preparation, S.J.; writing—review and editing, S.J. and B.G.; visualization, S.J.; supervision, B.G.; project administration, B.G.; funding acquisition, S.J. and B.G. All authors have read and agreed to the published version of the manuscript.

Funding: This work was financially supported by China Postdoctoral Science Foundation (2023M731247, 2024T170319) and by the self-determined research funds of CCNU from the colleges' basic research and operation of MOE (CCNU23XJ010).

Data Availability Statement: All raw data and Supplementary Files supporting the findings of this study will be uploaded and made available alongside the manuscript. Further information or additional datasets are available from the corresponding author upon reasonable request.

Acknowledgments: We thank Yang Li (Central China Normal University) for providing us the LCI vectors JW771 and JW772.

Conflicts of Interest: The authors declare no conflicts of interest.

References

1. Franklin, A.; Hoffman, N. Characterization of a chloroplast homologue of the 54-kDa subunit of the signal recognition particle. *J. Biol. Chem.* **1993**, *268*, 22175–22180. [PubMed]
2. Klimyuk, V.I.; Persello-Cartieaux, F.; Havaux, M.; Contard-David, P.; Schuenemann, D.; Meiherhoff, K.; Gouet, P.; Jones, J.D.; Hoffman, N.E.; Nussaume, L. A chromodomain protein encoded by the *Arabidopsis CAO* gene is a plant-specific component of the chloroplast signal recognition particle pathway that is involved in LHCP targeting. *Plant Cell* **1999**, *11*, 87–99. [CrossRef] [PubMed]
3. Schuenemann, D.; Gupta, S.; Persello-Cartieaux, F.; Klimyuk, V.I.; Jones, J.D.; Nussaume, L.; Hoffman, N.E. A novel signal recognition particle targets light-harvesting proteins to the thylakoid membranes. *Proc. Natl. Acad. Sci. USA* **1998**, *95*, 10312–10316. [PubMed]
4. Tu, C.J.; Peterson, E.C.; Henry, R.; Hoffman, N.E. The L18 domain of light-harvesting chlorophyll proteins binds to chloroplast signal recognition particle 43. *J. Biol. Chem.* **2000**, *275*, 13187–13190. [CrossRef]
5. DeLille, J.; Peterson, E.C.; Johnson, T.; Moore, M.; Kight, A.; Henry, R. A novel precursor recognition element facilitates posttranslational binding to the signal recognition particle in chloroplasts. *Proc. Natl. Acad. Sci. USA* **2000**, *97*, 1926–1931.
6. Moore, M.; Goforth, R.L.; Mori, H.; Henry, R. Functional interaction of chloroplast SRP/FtsY with the ALB3 translocase in thylakoids: Substrate not required. *J. Cell Biol.* **2003**, *162*, 1245–1254. [CrossRef]
7. Jaru-Ampornpan, P.; Chandrasekar, S.; Shan, S.O. Efficient interaction between two GTPases allows the chloroplast SRP pathway to bypass the requirement for an SRP RNA. *Mol. Biol. Cell* **2007**, *18*, 2636–2645. [CrossRef]
8. Falk, S.; Sinning, I. cpSRP43 is a novel chaperone specific for light-harvesting chlorophyll a,b-binding proteins. *J. Biol. Chem.* **2010**, *285*, 21655–21661. [CrossRef]
9. Falk, S.; Ravaud, S.; Koch, J.; Sinning, I. The C terminus of the Alb3 membrane insertase recruits cpSRP43 to the thylakoid membrane. *J. Biol. Chem.* **2010**, *285*, 5954–5962.
10. Horn, A.; Hennig, J.; Ahmed, Y.L.; Stier, G.; Wild, K.; Sattler, M.; Sinning, I. Structural basis for cpSRP43 chromodomain selectivity and dynamics in Alb3 insertase interaction. *Nat. Commun.* **2015**, *6*, 8875.
11. Nilsson, R.; Brunner, J.; Hoffman, N.E.; van Wijk, K.J. Interactions of ribosome nascent chain complexes of the chloroplast-encoded D1 thylakoid membrane protein with cpSRP54. *EMBO J.* **1999**, *18*, 733–742. [CrossRef] [PubMed]
12. Hristou, A.; Gerlach, I.; Stolle, D.S.; Neumann, J.; Bischoff, A.; Dunschede, B.; Nowaczyk, M.M.; Zoschke, R.; Schunemann, D. Ribosome-Associated Chloroplast SRP54 Enables Efficient Cotranslational Membrane Insertion of Key Photosynthetic Proteins. *Plant Cell* **2019**, *31*, 2734–2750. [CrossRef] [PubMed]
13. Lei, Y.; Li, B.; Wang, X.; Wei, J.; Wang, P.; Zhao, J.; Yu, F.; Qi, Y. Chloroplast SRP54 and FtsH protease coordinate thylakoid membrane-associated proteostasis in *Arabidopsis*. *Plant Physiol.* **2023**, *192*, 2318–2335. [CrossRef] [PubMed]

14. Wang, P.; Liang, F.C.; Wittmann, D.; Siegel, A.; Shan, S.O.; Grimm, B. Chloroplast SRP43 acts as a chaperone for glutamyl-tRNA reductase, the rate-limiting enzyme in tetrapyrrole biosynthesis. *Proc. Natl. Acad. Sci. USA* **2018**, *115*, E3588–E3596. [CrossRef]
15. Ji, S.; Siegel, A.; Shan, S.-o.; Grimm, B.; Wang, P. Chloroplast SRP43 autonomously protects chlorophyll biosynthesis proteins against heat shock. *Nat. Plants* **2021**, *7*, 1420–1432. [CrossRef]
16. Ji, S.; Grimm, B.; Wang, P. Chloroplast SRP43 and SRP54 independently promote thermostability and membrane binding of light-dependent protochlorophyllide oxidoreductases. *Plant J.* **2023**, *115*, 1583–1598. [CrossRef]
17. Susek, R.E.; Ausubel, F.M.; Chory, J. Signal transduction mutants of *Arabidopsis* uncouple nuclear *CAB* and *RBCS* gene expression from chloroplast development. *Cell* **1993**, *74*, 787–799. [CrossRef]
18. Mochizuki, N.; Brusslan, J.A.; Larkin, R.; Nagatani, A.; Chory, J. *Arabidopsis* genomes uncoupled 5 (GUN5) mutant reveals the involvement of Mg-chelatase H subunit in plastid-to-nucleus signal transduction. *Proc. Natl. Acad. Sci. USA* **2001**, *98*, 2053–2058. [CrossRef]
19. Larkin, R.M.; Alonso, J.M.; Ecker, J.R.; Chory, J. GUN4, a regulator of chlorophyll synthesis and intracellular signaling. *Science* **2003**, *299*, 902–906. [CrossRef]
20. Woodson, J.D.; Perez-Ruiz, J.M.; Chory, J. Heme synthesis by plastid ferrochelatase I regulates nuclear gene expression in plants. *Curr. Biol.* **2011**, *21*, 897–903. [CrossRef]
21. Hutin, C.; Havaux, M.; Carde, J.P.; Kloppstech, K.; Meiherhoff, K.; Hoffman, N.; Nussaume, L. Double mutation cpSRP43--/cpSRP54-- is necessary to abolish the cpSRP pathway required for thylakoid targeting of the light-harvesting chlorophyll proteins. *Plant J. Cell Mol. Biol.* **2002**, *29*, 531–543. [CrossRef] [PubMed]
22. Amin, P.; Sy, D.A.; Pilgrim, M.L.; Parry, D.H.; Nussaume, L.; Hoffman, N.E. *Arabidopsis* mutants lacking the 43-and 54-kilodalton subunits of the chloroplast signal recognition particle have distinct phenotypes. *Plant Physiol.* **1999**, *121*, 61–70. [CrossRef] [PubMed]
23. Ziehe, D.; Dünschede, B.; Schünemann, D. From bacteria to chloroplasts: Evolution of the chloroplast SRP system. *Biol. Chem.* **2017**, *398*, 653–661. [CrossRef] [PubMed]
24. Davison, P.A.; Schubert, H.L.; Reid, J.D.; Iorg, C.D.; Heroux, A.; Hill, C.P.; Hunter, C.N. Structural and biochemical characterization of Gun4 suggests a mechanism for its role in chlorophyll biosynthesis. *Biochemistry* **2005**, *44*, 7603–7612. [CrossRef]
25. Tarahi Tabrizi, S.; Sawicki, A.; Zhou, S.; Luo, M.; Willows, R.D. GUN4-Protoporphyrin IX Is a Singlet Oxygen Generator with Consequences for Plastid Retrograde Signaling. *J. Biol. Chem.* **2016**, *291*, 8978–8984. [CrossRef]
26. Espineda, C.E.; Linford, A.S.; Devine, D.; Brusslan, J.A. The *AtCAO* gene, encoding chlorophyll a oxygenase, is required for chlorophyll b synthesis in *Arabidopsis thaliana*. *Proc. Natl. Acad. Sci. USA* **1999**, *96*, 10507–10511. [CrossRef]
27. Paulsen, H.; Finkenzeller, B.; Kühlein, N. Pigments induce folding of light-harvesting chlorophyll a/b-binding protein. *Eur. J. Biochem.* **1993**, *215*, 809–816. [CrossRef]
28. Yu, B.; Gruber, M.Y.; Khachatourians, G.G.; Zhou, R.; Epp, D.J.; Hegedus, D.D.; Parkin, I.A.; Welsch, R.; Hannoufa, A. *Arabidopsis* cpSRP54 regulates carotenoid accumulation in *Arabidopsis* and *Brassica napus*. *J. Exp. Bot.* **2012**, *63*, 5189–5202. [CrossRef]
29. Peter, E.; Grimm, B. GUN4 is required for posttranslational control of plant tetrapyrrole biosynthesis. *Mol. Plant* **2009**, *2*, 1198–1210. [CrossRef]
30. Wang, P.; Richter, A.S.; Kleeberg, J.R.W.; Geimer, S.; Grimm, B. Post-translational coordination of chlorophyll biosynthesis and breakdown by BCMs maintains chlorophyll homeostasis during leaf development. *Nat. Commun.* **2020**, *11*, 1254. [CrossRef]
31. Onate-Sanchez, L.; Vicente-Carbajosa, J. DNA-free RNA isolation protocols for *Arabidopsis thaliana*, including seeds and siliques. *BMC Res. Notes* **2008**, *1*, 93. [CrossRef]
32. Gou, J.-Y.; Felippes, F.F.; Liu, C.-J.; Weigel, D.; Wang, J.-W. Negative regulation of anthocyanin biosynthesis in *Arabidopsis* by a miR156-targeted SPL transcription factor. *Plant Cell* **2011**, *23*, 1512–1522. [CrossRef]

Disclaimer/Publisher's Note: The statements, opinions and data contained in all publications are solely those of the individual author(s) and contributor(s) and not of MDPI and/or the editor(s). MDPI and/or the editor(s) disclaim responsibility for any injury to people or property resulting from any ideas, methods, instructions or products referred to in the content.

plants

MDPI

Article

Potassium-Mediated Variations in the Photosynthetic Induction Characteristics of *Phaseolus vulgaris* L.

Qi Luo [1,2], Wei Jin [2,3], Lili Li [1,3], Kedong Xu [1,2,*] and Yunmin Wei [1,2,*]

[1] Key Laboratory of Plant Genetics and Molecular Breeding, Zhoukou Normal University, Zhoukou 466001, China; luoqi@zknu.edu.cn (Q.L.); lilili@zknu.edu.cn (L.L.)
[2] Henan Plant Gene and Molecular Breeding Engineering Research Center, Zhoukou Normal University, Zhoukou 466001, China; jinw877@126.com
[3] College of Life Science and Agriculture, Zhoukou Normal University, Zhoukou 466001, China
* Correspondence: xukd1107@126.com (K.X.); weiym1024@163.com (Y.W.); Tel.: +86-159-3944-7029 (K.X.); +86-133-4021-3922 (Y.W.)

Abstract: Plants are commonly exposed to fluctuating illumination under natural light conditions, causing dynamic photosynthesis and further affecting plant growth and productivity. In this context, although the vital role of potassium (K) in steady-state photosynthesis has been well-established, knowledge of the dynamic changes in photosynthesis mediated by K remains scarce. Here, the gas-exchange and chlorophyll fluorescence parameters under steady-state and dynamic photosynthetic responses were quantified in *Phaseolus vulgaris* L. seedlings grown under K-deficient (−K, 0.02 mM K) and normal K (+K, 2 mM K) conditions. After a transition from low to high light, the time course–induction curves of the net photosynthetic rate (A), stomatal conductance (g_s), mesophyll conductance (g_m), and maximum carboxylation rate (V_{cmax}) showed an obvious decline in the −K treatment. In comparison with the +K treatment, however, there were no statistical differences in the initial A and V_{cmax} values in *P. vulgaris* supplied with deficient K, suggesting that the K-deficiency-induced decreases in A and V_{cmax} were light-dependent. Interestingly, the time to reach 90% of the maximum A, g_s, and g_m significantly decreased in the −K treatment in comparison with the +K treatment by 27.2%, 45.6%, and 52.9%, respectively, whereas the time to reach 90% of the maximum V_{cmax} was correspondingly delayed by almost two-fold. The photosynthetic limitation during the induction revealed that the biochemical limitation was the dominating factor that constrained A under the −K conditions, while, under the +K conditions, the main limiting factor changed from biochemical limitation to stomatal limitation over time. Moreover, g_m imposed the smallest limitation on A during induction in both K treatments. These results indicate that a decreased K supply decreases the photosynthetic performance under fluctuating light in *P. vulgaris* and that improving the induction responses of biochemical components (i.e., V_{cmax}) has the potential to enhance the growth and productivity of crops grown in K-poor soil.

Keywords: photosynthetic induction; potassium; photosynthetic limitation; *Phaseolus vulgaris* L.; maximum carboxylation rate

1. Introduction

Potassium (K), alongside nitrogen and phosphorus, is the most important macronutrient for plant growth. In particular, it participates in many essential physiological processes, e.g., photosynthesis, osmotic regulation, and stomata regulation [1,2]. Consequently, K deficiency is widely recognized as a major limiting factor on photosynthetic carbon assimilation and ultimately impairs plant productivity [3]. In recent years, steady-state

photosynthesis under optimal environmental conditions has become a major focus for elucidating how K deficiency limits photosynthetic carbon assimilation, as K-deficiency-induced photosynthesis stress in a leaf is a dynamically aggravated process [4]. Moreover, increasing evidence indicates that the reduction in the net photosynthetic rate (A) under K-limited conditions cannot be ascribed solely to stomatal limitations and is instead due to the integrated contribution of stomatal, mesophyll, and biochemical (carboxylation-related) factors [5–7].

Potassium plays an essential role in regulating guard cell turgor [8], and a deficiency or an inadequate supply of K results in a decrease in stomatal conductance (g_s), thereby reducing CO_2 diffusion into the leaf chloroplast [9]. However, even if g_s is partially maintained under these conditions, the photosynthetic capacity remains suboptimal [10,11], suggesting that additional resistances are involved. Mesophyll conductance (g_m) from the sub-stomatal cavities to the carboxylation sites inside the chloroplast stroma has emerged as a major constraint of A under K stress. According to Lu et al. [12], K starvation causes disadvantages in leaf structure alterations among different plant species, such as a reduced internal air space, a decreased exposed surface area of chloroplasts in intercellular airspaces, and an increased distance from the chloroplast to the cell wall, which largely impede internal CO_2 diffusion and finally reduce g_m. In addition, K is essential for the activation of enzymes in the Calvin–Benson cycle, particularly the rubisco enzyme [13]. K-starved plants often exhibit rubisco activity reduction, delayed RuBP regeneration, and disrupted stromal ion homeostasis, which ultimately contribute to declined carboxylation efficiency [14,15]. Overall, elucidating these relative contributions of limiting factors is crucial for optimizing K management strategies to sustain high crop productivity.

However, while a lot of supporting evidence has been found in the literature to explain the effect of K deficiency on the steady-state photosynthesis of plants, such as wheat [16], rice [17], oilseed rape [14], and maize [18], plants in natural or semi-natural ecosystems are rarely exposed to controlled, steady-state conditions. Instead, environmental factors, especially irradiance, change rapidly (over seconds to minutes throughout the day) due to variable solar position, cloud movement, or self-shading under canopies [19]. Plants therefore frequently encounter rapid fluctuations in light intensity, especially in seasons when the weather is changeable. Under these conditions, the capacity of photosynthetic systems to adjust, which is termed "dynamic photosynthesis", is critical for enhancing daily carbon gain by plants [20]. A previous study showed that faster stomatal opening and the activation of electron transport persevere as the most effective targets for increasing photosynthetic responses by plants under dynamic light conditions [21], which may be largely determined by K ions. However, the role of K in dynamic photosynthesis responses has not yet been fully explored. Therefore, it is essential to understand how K affects the rate and flexibility of photosynthetic responses to changeable environmental conditions.

Similar to steady-state photosynthesis, dynamic photosynthesis is also controlled by g_s, g_m, and the biochemical capacity (i.e., the maximum carboxylation rate, V_{cmax}), which are generally downregulated under K-deficient conditions [22,23]. However, the integrated mechanisms that cause the variation in dynamic photosynthesis by K deficiency are complex, and the relative contributions of stomatal, mesophyll, and biochemical limitations during light transitions have not been clearly defined. It is speculated that the increase in the relative ratios of g_s, g_m, or V_{cmax} under K deficiency reflect an excess capacity relative to photosynthetic system demands, potentially facilitating faster induction. On the contrary, these unchanged or decreased ratios may imply slower photosynthetic responses. This raises critical questions as to whether K-deficient plants exhibit delayed photosynthetic induction and, more importantly, which components (stomatal, mesophyll, or biochemical factors) exert the predominant limiting factor under such conditions.

To address these questions, we used common bean (*Phaseolus vulgaris* L.) as an experimental material to investigate the impact of potassium deficiency on both steady-state and dynamic photosynthesis. Specifically, the objectives of this study were to (1) evaluate the effects of K deficiency on steady-state photosynthetic performance; (2) characterize the dynamic variations in A, g_s, g_m, and V_{cmax} during photosynthetic induction; and (3) quantify the dominant constraint on photosynthesis during induction using a time-integrated limitation analysis.

2. Results

2.1. Photosynthetic Parameter Variations During Photosynthetic Induction

As demonstrated by the curves in Figure 1, the leaf net photosynthetic rate (A), stomatal conductance (g_s), mesophyll conductance (g_m), and, particularly, the maximum carboxylation rate (V_{cmax}) rapidly responded when *P. vulgaris* was exposed to sudden light irradiation. Specifically, the induction curves of A under both potassium-deficient (−K) and normal potassium (+K) conditions showed typical logarithmic increases, and A was markedly higher under +K than under −K throughout the induction period after the low-to-high light transition. Interestingly, *P. vulgaris* L. under the −K conditions reached steady state faster than that under the +K conditions, within almost 15 min, with this increasing to more than 20 min under the +K conditions. The induction of g_{sc}, g_m, and V_{cmax} showed almost the same responses as A. However, it is worth noting that the improvement in g_{sc} and g_m under −K was quite limited. In comparison with the initial g_{sc}, the increase in g_{sc} at the end of the induction period was 42% under −K and 211% under +K. As for photosynthetic system II (PSII), the actual phytochemical efficiency of PSII (ΦPSII) was substantially higher in the +K treatment than in the −K treatment (Figure S1).

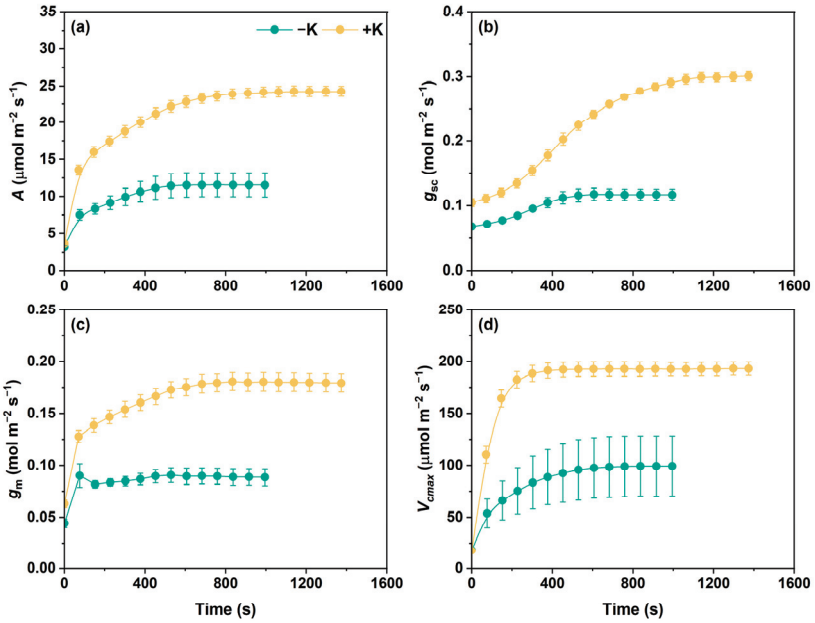


Figure 1. Dynamic photosynthetic traits of *Phaseolus vulgaris* L. during photosynthetic induction at 1000 μmol m^{-2} s^{-1} photosynthetic photon flux density (PPFD) as affected by K nutrition. Leaves were initially acclimated to a steady state under low light (100 μmol m^{-2} s^{-1} PPFD), followed by exposure to high light (1000 μmol m^{-2} s^{-1} PPFD). A, net photosynthetic rate (**a**); g_{sc}, stomatal conductance to CO_2 (**b**); g_m, mesophyll conductance to CO_2 (**c**); V_{cmax}, the maximum carboxylation rate (**d**).

2.2. Steady Changes in Photosynthetic Traits During Photosynthetic Induction

There were no statistical differences between the −K and +K treatments in terms of either A_i or V_{cmaxi} after low-light induction (100 PPFD); nevertheless, both g_{si} and g_{mi} were significantly higher under the +K conditions than under the −K conditions, increasing by approx. 54.4% and 42.3% (Figure 2). For *P. vulgaris* L. exposed to 1000 PPFD light induction, the steady-state photosynthetic parameters A_f, g_{scf}, g_{mf}, and V_{cmaxf} were significantly higher under the +K treatment than under the −K treatment, among which K had the greatest effect on g_{scf}. Compared with the −K treatment, g_{scf} increased by about 158% under the +K treatment (Figure 2).

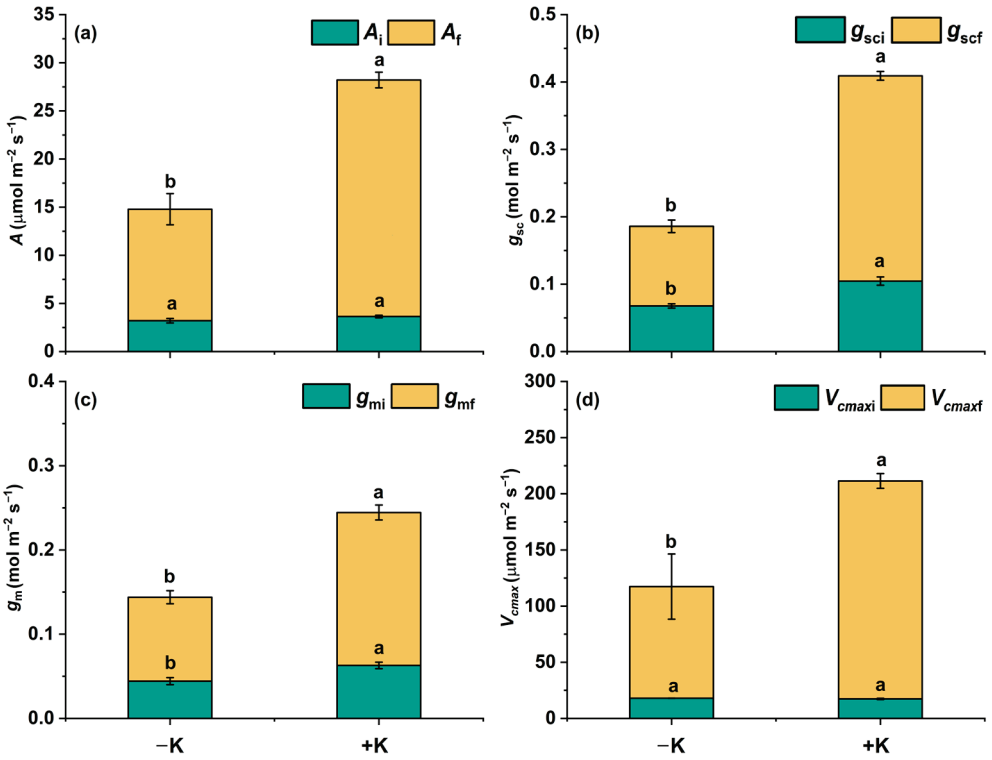


Figure 2. Steady-state photosynthetic parameters of *Phaseolus vulgaris* L. after light photosynthetic induction as affected by K nutrition. A_i (**a**), g_{sci} (**b**), g_{mi} (**c**), and V_{cmaxi} (**d**) are the steady-state A, g_{sc}, g_m, and V_{cmax} of the last 1 min of the low-light induction period (100 μmol m^{-2} s^{-1} PPFD). A_f (**a**), g_{scf} (**b**), g_{mf} (**c**), and V_{cmaxf} (**d**) are the steady-state A, g_{sc}, g_m, and V_{cmax} of the last 1 min of the high-light induction period (1000 μmol m^{-2} s^{-1} PPFD). Different letters indicate significant differences between the treatments ($p < 0.05$). Data are presented as means ± SE (n = 5).

2.3. Dynamic Changes in Photosynthetic Traits During Photosynthetic Induction

In general, during the light induction period (Figure 1), most photosynthetic parameters under the −K treatment were found to approach 90% of full induction more rapidly than under the +K treatment (Figure 3). Specifically, for A, the time to 90% maximum (t_{A90}) was approx. 363 s compared to 498 s, and, for g_{sc} and g_m, the time to 90% maximum under +K was 83.7% (t_{gsc90}) and 112.1% (t_{gm90}) longer than that under −K. On the contrary, V_{cmax} required a significantly longer time to reach the 90% maximum ($t_{vcmax90}$) under the −K treatment, being almost 2-fold longer than under the +K treatment.

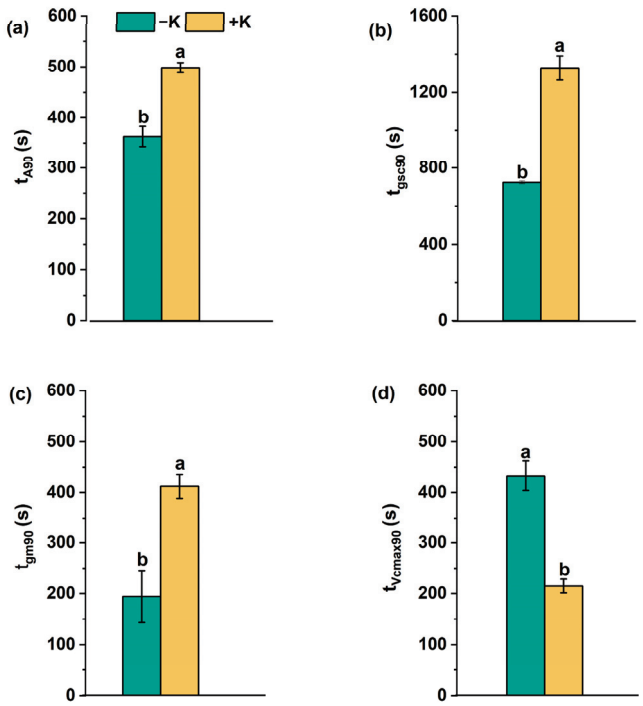


Figure 3. Dynamic photosynthetic parameters of *Phaseolus vulgaris* L. during photosynthetic induction as affected by K nutrition. t_{A90} (**a**), t_{gsc90} (**b**), t_{gm90} (**c**), and $t_{vcmax90}$ (**d**) are the times to reach 90% photosynthetic induction, full stomatal opening, mesophyll opening, and biochemical activation. Different letters indicate significant differences between the treatments ($p < 0.05$). Data are presented as means ± SE (n = 5).

2.4. Temporal Responses of Photosynthetic Limitations During Photosynthetic Induction

To further examine the contributions of g_{sc}, g_m, and V_{cmax} to A during photosynthetic induction, the deviation in A (dA) at a given time point was quantitatively partitioned into components corresponding to stomatal (dA_s), mesophyll (dA_m), and biochemical (dA_b) limitations. As shown in Figure 4, in the first 300 s of induction under the −K treatment, the dA_b values accounted for the largest proportion of the total limitation, in comparison with dA_s and dA_m. However, in *P. vulgaris* L. treated with +K, the relative biochemical limitation was initially almost 100%, then it decreased rapidly after illumination, and it gradually decreased to 0% after 300 s. On the contrary, during the induction period, dA_s increased gradually and became the main limiting factor of dA after 2 min. Moreover, the dA_m values were the lowest throughout the entire induction period in both the −K and +K treatments, despite subtle differences being observed between the treatments; i.e., in the −K treatment, mesophyll limitation occurred in the initial stages of the induction, while, in the +K treatment, it occurred in the mid-to-late stages.

When integrating the relative limitations of photosynthesis over the entire induction period, it was observed that the K supply significantly affected the main photosynthetic limiting factor of *P. vulgaris* L., despite there being no statistical differences in σ_m between the −K and +K treatments (Figure 5). Under the −K conditions, the biochemical limitation (σ_b) was the strongest limiting factor of photosynthesis, accounting for 67.2% of the total photosynthetic limitation. Meanwhile, under the +K conditions, the stomatal limitation (σ_s) was found to account for 49.4% of the total limitation, followed by the biochemical limitation (40.2%) and mesophyll limitation (10.5%).

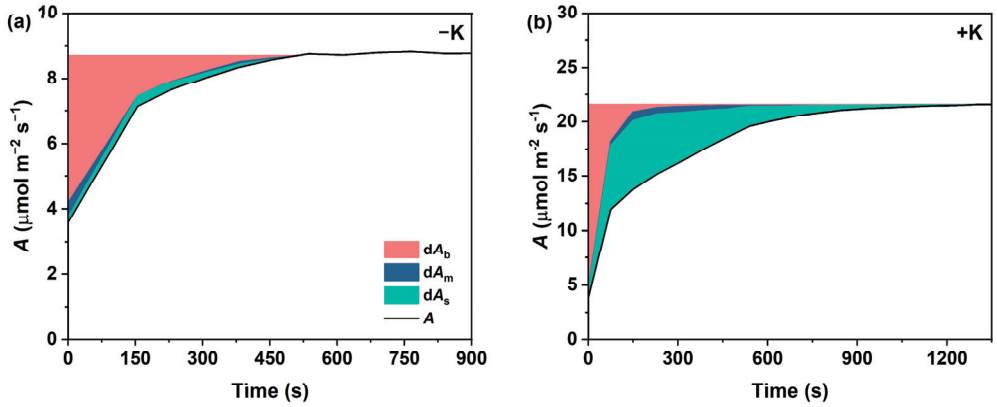


Figure 4. Dynamic variations in the biochemical limitation (dA_b), mesophyll conductance limitation (dA_m), and stomatal limitation (dA_s) of *Phaseolus vulgaris* L. during photosynthetic induction under K-deficient condition (**a**) and normal K condition (**b**).

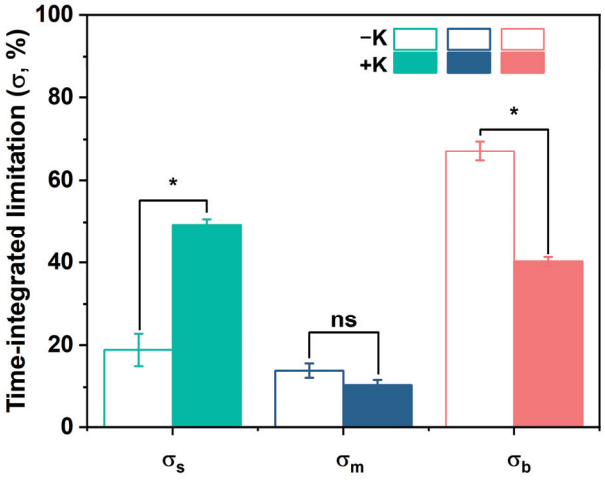


Figure 5. Impact of K nutrition on the relative time-integrated limitations involving stomatal limitation (σ_s), mesophyll conductance limitation (σ_m), and biochemical limitation (σ_b) in response to the photosynthetic induction of *Phaseolus vulgaris* L. Data are presented as means ± SE (n = 5). Asterisks indicate significant differences between the treatments (*, $p < 0.05$; ns, no significant difference).

3. Discussion

Previous studies have demonstrated the general presence of weakened photosynthetic carbon assimilation under K-deficient or inadequate conditions [12,24,25]. In the present study, the steady-state *A* (A_f as an indicator) of *P. vulgaris L.* in the −K treatment declined by 52.9% in comparison with A in normal K supply. In addition to the steady-state *A* under high light, the photosynthetic responses to changes in illumination significantly affect the carbon gain of plants [26,27]; the average *A* value under the −K conditions during the photosynthetic induction process was 10 μmol m^{-2} s^{-1}, statistically lower than that under the +K conditions (average of 20.8 μmol m^{-2} s^{-1}), with an average decline of 51.0%. It is worth noting that the time required for *A* to reach a steady state in −K was significantly shorter than that in +K, despite there being a decrease in the *A* value under the −K conditions. Similar trends were observed in the response curves for g_{sc}, g_m, and V_{cmax} during the induction.

According to Kaiser [20], the time to reach 90% *A* of the full induction (t_{A90}) is defined as the photosynthetic response rate, which is mainly influenced by nutrition, plant species, and stress factors. For instance, tomatoes supplied with high nitrogen levels showed a much faster photosynthetic induction response than those supplied with moderate

or low nitrogen levels [28]; however, in *Panax notoginseng*, a higher nitrogen content in leaves caused a slower photosynthetic induction rate [29]. Zhang et al. [30] found that tomato exposed to salt stress demonstrated a significantly reduced response rate, resulting in an increased t_{A90}. These findings indicate that plants under nutrient or other stress conditions have a prolonged photosynthetic induction time, which results in an increased t_{A90}. However, in our current results, the t_{A90} values decreased by approx. 27.2% in the K-deficient treatment compared to in the normal K treatment.

It is generally accepted that the actual t_{A90} is a comprehensive result influenced by t_{gs90}, t_{gm90}, and $t_{Vcmax90}$. As shown in Figure 3, the t_{gs90} and t_{gm90} of plants supplied with deficient K were significantly shorter than those of plants supplied with normal K nutrition. However, not all plant responses occurred within the same timescale; A and g_m responded and reached 90% of steady state within 5–8 min, whereas changes in g_s took more than 10 min (Figure 3), in accordance with previous studies [31–33]. Therefore, it was supposed that the lower t_{gsc90} under the −K conditions may be mainly responsible for the rapid t_{A90}. As g_{sci} was not higher in the −K treatment than in the +K treatment as expected, it is logical to believe that the K deficiency induced stomatal closure, thereby decreasing t_{gsc90} during the irradiation. Stomatal movement occurs with channel-mediated K^+ uptake over time [32] due to the vital role of potassium in the osmotic mechanism of stomata aperture modulation. During the photosynthetic induction, the light-dependent influx and efflux of potassium of guard cells could have been affected by the K deficiency and, thus, regulated stomatal closure [34,35]. Similar results were obtained in studies on tea [36], *Eucalyptus grandis* [37], rice [38], and olive [39]. Further studies are needed to analyze the dynamic responses of stomatal movement mediated by K supplement during photosynthetic induction. Moreover, K is essential for increasing enzyme activity in higher plants [40,41]. According to a study on *Brassica napus*, a decrease in K decreased the rubisco content and activity by 37% and 58.4%, respectively, causing a decreased carboxylation rate [42]. In the present study, although there were no statistical differences regarding the initial V_{cmax} between treatments, the final state of V_{cmax} was significantly reduced in the −K treatment compared to in the +K treatment and was accompanied by a longer $t_{Vcmax90}$ (Figures 2 and 3).

A sufficient understanding of photosynthetic limiting factors during light fluctuation is of relevance to solving the substantial decline in daily carbon accumulation in plants [21,43]. A recent study by Liu et al. [22] demonstrated the important role of g_m in limiting A during photosynthetic induction. However, another study on Arabidopsis and tobacco found opposite results, showing a transition from a stomatal-dominating limitation to a biochemical limitation during induction [28]. In the present study, in *P. vulgaris* L. plants supplied with deficient K, photosynthetic limitations due to g_s, g_m, and biochemical factors changed slightly upon the transition from low to high light, in which condition A was mainly constrained by biochemical factors, while, under the normal K conditions, the predominating photosynthetic limiting factors gradually changed from biochemical limitation to stomatal limitation during the induction process. Meanwhile, g_m consistently imposed the smallest limitation on A between the K treatments. As it turns out, the limiting factors of photosynthetic induction changed frequently, induced by external environmental conditions, plant species, or genotypes [22,44,45].

As evident in Figure 5, under both the −K and +K conditions, g_m was identified as being the least limiting of the three photosynthetic components on a time-integrated scale, while the biochemical capacity (i.e., V_{cmax}) was the most significant limiting factor of photosynthetic induction for the plants supplied with deficient K. In contrast to our findings, Lu et al. [12] found that the g_m limitation contributed to more than one-half of the A decline under K-deficient conditions. In this regard, this may reflect the adaptive

strategies of plants to −K stress at different time scales, as several processes underlying photosynthesis activate or deactivate cooperatively [46]. However, although a reduced g_{sc} was observed in the K-deficient conditions, it takes a certain amount of time for stomatal opening to occur in photosynthetic induction, whereas the activation of the rubisco enzyme usually occurs faster (several seconds to minutes) [47,48]. However, as K^+ plays a critical role in the biosynthesis and activation of rubisco, the deficient K supply resulted in an increased $t_{Vcmax90}$ and, finally, constrained *A*, especially during the short period of photosynthetic induction.

4. Materials and Methods

4.1. Plant Material

A hydroponic culture experiment was conducted in a plant culture room with an illuminated light source maintained at approx. 800 μmol m^{-2} s^{-1} photosynthetic photon flux density (PPFD). The photoperiod was set to 16 h at 25 °C per day and 18 °C per night, and the relative humidity was 50–60%. *P. vulgaris* seeds were germinated in moist filter papers at 4 °C for 12 h, which were then fixed to a transit box for germination. After 7 d, uniform seedlings were transferred to 10 L plastic containers and supplied with one-quarter-strength nutrient solution (for the composition, see below). Five days later, the seedlings were supplied with one-half-strength nutrient solution. After another 5 d, the seedlings were supplied with full-strength nutrition with K-deficient (−K, 0.02 mM K_2SO_4) or normal K treatment (+K, 2 mM K_2SO_4). The composition of the full-strength nutrition solution was as follows: 5 mM N with mixed $(NH_4)_2SO_4$ and $Ca(NO_3)_2$, 1mM $NaH_2PO_4 \cdot 2H_2O$, 2 mM K_2SO_4, 2.5 mM $CaCl_2$, 1 mM $MgSO_4$, 0.05 mM Fe-EDTA, 10 μM H_3BO_3, 10 μM $MnCl_2 \cdot 4H_2O$, 0.3 μM $CuSO_4 \cdot 5H_2O$, 0.8 μM $ZnSO_4 \cdot 7H_2O$, and 0.01 μM $Na_2MoO_4 \cdot 2H_2O$. The pH of the nutrient solution was adjusted to 7.0 ± 0.1 every day and was completely changed every 3 d.

4.2. Measurement of Gas Exchange and Fluorescence

Two weeks after the treatments started, fully expanded leaves of each plant were selected for the measurement of gas-exchange parameters from 9:00 to 11:30, using a portable gas-exchange system (Li-6400XT, Li-Cor, Lincoln, NE, USA). The PPFD was set to 1000 μmol m^{-2} s^{-1} (red light–blue light, 90%:10%), the vapor pressure deficit (VPD) was between 1.4 and 1.6 Kpa, the air flow rate was 500 μmol s^{-1}, the leaf temperature was 25 ± 0.3 °C, and the CO_2 concentration was maintained at 400 ± 10 μmol mol^{-1}. Once steady state was achieved, the steady-state fluorescence yield (F_s) and maximum fluorescence (F_m') were recorded with a light-saturating pulse (0.8 s) of 8000 μmol m^{-2} s^{-1}; in the meantime, the net photosynthetic rate (*A*), CO_2 concentration in intercellular spaces (C_i), and leaf stomatal conductance (g_s) were recorded. As g_s is the stomatal conductance to water vapor, it is expressed in terms of stomatal conductance to CO_2 (g_{sc}) in subsequent calculations, which was calculated as $g_{sc} = g_s/1.6$.

4.3. Estimation of Mesophyll Conductance (g_m)

The actual phytochemical efficiency of PSII (ΦPSII) was then calculated as follows:

$$\Phi PSII = (F_m' - F_s)/F_m' \quad (1)$$

The liner electron transfer rate (J) was given as

$$J = \Phi PSII \times PPFD \times \alpha \times \beta \quad (2)$$

where α is the leaf absorption and β is the proportion of quanta absorbed by PSII, assumed to be 0.85 and 0.5, respectively. Taken together, the variable J method was used to calculate g_m [49], given as follows:

$$g_m = \frac{A}{C_i - \frac{\Gamma^*(J+8(A+R_d))}{J-4(A+R_d)}} \quad (3)$$

$$C_c = C_i - \frac{A}{g_m} \quad (4)$$

where Γ* is the CO_2 compensation point in the absence of mitochondrial respiration and R_d is the mitochondrial respiration rate in the light. Γ* was assumed to be 40.0 μmol m^{-2} s^{-1}, and R_d was assumed to be 1.0 μmol m^{-2} s^{-1}. Using the above equation, g_m could be calculated at each time point.

4.4. Calculations of the Maximum Carboxylation Rate of Rubisco (V_{cmax})

According to Mott et al. [50], plants can maintain saturated RuBP under both low- and high-light irradiance conditions; therefore, rubisco activation was modulated to limit A for the transition from low to high irradiation. It was then assumed that the Rubisco limitation would adequately constrain A throughout photosynthetic induction. V_{cmax} was determined as follows:

$$V_{cmax} = \frac{(A + R_d)(C_i + K_m)}{(C_i - \Gamma^*)} \quad (5)$$

where R_d is the rate of respiration in the light, and K_m is the effective CO_2 Michaelis–Menten constant for rubisco. Here, K_m was set to 509.5 at 25 °C. Using the above equation, V_{cmax} could be calculated at each time point.

4.5. Determination of Photosynthetic Induction Parameters

For induction, leaves were initially acclimated to a steady state under low light (100 μmol m^{-2} s^{-1} PPFD) for 30 min, followed by exposure to high light (1000 μmol m^{-2} s^{-1} PPFD) until the photosynthetic parameters approached a steady state. Gas-exchange measurements were recorded every second for the first minute and every five seconds thereafter. Plants were randomly selected and measured from 9:00 to 11:30. Measurements were repeated 4 times on individual replicates for each treatment over a span of 2 days to reduce the time effects. For each treatment, 5 biological replicates were used, and all calculations were performed on single replicates.

Photosynthetic induction was calculated according to the following equations, where the subscripts "i" and "f" refer to the steady-state assimilation rate (A) values in the last minute of low light and high light, respectively:

$$IS = \frac{A - A_i}{A_f - A_i} \quad (6)$$

The induction of g_{sc}, g_m, and V_{cmax} over the same duration was also calculated by replacing A with g_{sc}, g_m, and V_{cmax}, respectively.

Moreover, t_{A90}, t_{gsc90}, t_{gm90}, and $t_{Vcmax90}$ were defined as the time required to obtain 90% of the difference between the initial and maximum values of photosynthetic induction, stomatal opening, mesophyll conductance, and the maximum values of V_{cmax}, respectively.

4.6. Limitation Analysis

The relative changes in light-saturated assimilation can be expressed in terms of the relative changes in stomatal, mesophyll conductance, and biochemical capacity, Hence, the A variation can be modeled using

$$\frac{\mathrm{d}A}{A} = \mathrm{d}A_{\mathrm{s}} + \mathrm{d}A_{\mathrm{m}} + \mathrm{d}A_{\mathrm{b}} \tag{7}$$

where $\mathrm{d}A_{\mathrm{stom}}$, $\mathrm{d}A_{\mathrm{mes}}$, and $\mathrm{d}A\mathrm{b}_{\mathrm{iochem}}$ are the stomatal, mesophyll conductance, and biochemical limitations on A, which can be determined using

$$\mathrm{d}A_{\mathrm{s}} = \frac{\partial A}{\partial g_{\mathrm{sc}}}\mathrm{d}g_{\mathrm{sc}} \tag{8}$$

$$\mathrm{d}A_{\mathrm{m}} = \frac{\partial A}{\partial g_{\mathrm{m}}}\mathrm{d}g_{\mathrm{m}} \tag{9}$$

$$\mathrm{d}A_{\mathrm{b}} = \frac{\partial A}{\partial V_{\mathrm{cmax}}}\mathrm{d}V_{\mathrm{cmax}} \tag{10}$$

where $\mathrm{d}g_{\mathrm{sc}}$, $\mathrm{d}g_{\mathrm{m}}$, and $\mathrm{d}V_{\mathrm{cmax}}$ are the variations between the final state and steady-state g_{sc}, g_{m}, and V_{cmax}, respectively.

Given that $A = g_{\mathrm{sc}}\,(C_{\mathrm{a}} - C_{\mathrm{i}})$, solving the partial derivatives combined with Equation (1) gives

$$\frac{\partial A}{\partial g_{\mathrm{sc}}} = \frac{\frac{A}{g_{\mathrm{sc}}^2}((V_{\mathrm{cmax}} - R_{\mathrm{d}}) - A)}{(V_{\mathrm{cmax}} - R_{\mathrm{d}})(\frac{1}{g_{\mathrm{sc}}}) + (C_{\mathrm{a}} + K_{\mathrm{m}})\Big) - 2(\frac{1}{g_{\mathrm{sc}}}\Big)A} \tag{11}$$

$$\frac{\partial A}{\partial g_{\mathrm{m}}} = \frac{\frac{A}{g_m^2}((V_{\mathrm{cmax}} - R_{\mathrm{d}}) - A)}{(V_{\mathrm{cmax}} - R_{\mathrm{d}})(\frac{1}{g_{\mathrm{sc}}}) + (C_{\mathrm{a}} + K_{\mathrm{m}})\Big) - 2(\frac{1}{g_{\mathrm{sc}}}\Big)A} \tag{12}$$

$$\frac{\partial A}{\partial V_{\mathrm{cmax}}} = \frac{(C_{\mathrm{a}} - \Gamma^*) - A\Big(\frac{1}{g_{\mathrm{sc}}}\Big)}{(V_{\mathrm{cmax}} - R_{\mathrm{d}})(\frac{1}{g_{\mathrm{sc}}}) + (C_{\mathrm{a}} + K_{\mathrm{m}})\Big) - 2(\frac{1}{g_{\mathrm{sc}}}\Big)A} \tag{13}$$

4.7. Statistical Analysis

All statistical analyses were carried out using SPSS 25.1. A one-way ANOVA was performed to evaluate the significant differences in the parameters between groups. Graphical depiction was conducted with Origin Pro 2020. Data are presented as mean ± standard error (SE).

5. Conclusions

In the current study, we examined the effects of K supplementation on photosynthetic induction after transfer from low to high light in *P. vulgaris* L., and the induction curves of A, g_{sc}, g_{m}, and V_{cmax} showed significant differences during the induction process. Regarding the time course of photosynthesis induction, t_{A90}, t_{gm90}, and t_{gsc90} were shorter under the −K conditions than under the +K conditions, while the induction time of V_{cmax} was significantly delayed, which further caused a lag in changes in t_{A90} under the K-deficient conditions. During the transition from low to high light, increasing the induction responses of V_{cmax} may have the potential to improve A in *P. vulgaris* plants, especially when they are grown under low-K conditions, whereas the photosynthetic induction of A was rarely limited by g_{m} under both the −K and +K treatments. Taken together, the present study demonstrates the important role of biochemical capacities in limiting A during photosynthetic induction. Therefore, improving biochemical-related parameters,

such as rubisco enzyme activity, is likely an effective strategy for improving dynamic photosynthetic performance in *P. vulgaris* under K-deficient conditions.

Supplementary Materials: The following supporting information can be downloaded at: https://www.mdpi.com/article/10.3390/plants14111623/s1, Figure S1: Actual phytochemical efficiency of PSII photosystem (ΦPSII) of *Phaseolus vulgaris* L. during photosynthetic induction at 1000 μmol m^{-2} s^{-1} photosynthetic photon flux density (PPFD) as affected by K nutrition.

Author Contributions: Conceptualization, Q.L. and L.L.; investigation, W.J.; data curation, W.J. and K.X.; writing—original draft preparation, Q.L. and K.X.; writing—review and editing, Y.W. and L.L.; project administration, Y.W.; funding acquisition, K.X. and Y.W. All authors have read and agreed to the published version of the manuscript.

Funding: This research was funded by the Projects of the Joint Fund of Henan Province's Science and Technology Research and Development Program (225101610054) and the Department of Science and Technology Planning Project of Henan Province (222102110057 and 242102110299).

Data Availability Statement: Data are contained within the article.

Conflicts of Interest: The authors declare no conflicts of interest.

Abbreviations

A	net photosynthetic rate
g_{sc}	stomatal conductance to CO_2
g_m	mesophyll conductance to CO_2
V_{cmax}	maximum carboxylation rate
ΦPSII	actual phytochemical efficiency of PSII
A_i	steady-state A during the last 1 min of low-light induction period
g_{si}	steady-state g_{sc} during the last 1 min of low-light induction period
g_{mi}	steady-state g_m during the last 1 min of low-light induction period
V_{cmaxi}	steady-state V_{cmax} during the last 1 min of low-light induction period
A_f	steady-state A during the last 1 min of high-light induction period
g_{sf}	steady-state g_{sc} during the last 1 min of high-light induction period
g_{mf}	steady-state g_m during the last 1 min of high-light induction period
V_{cmaxf}	steady-state V_{cmax} during the last 1 min of high-light induction period
t_{A90}	time for A to reach 90% of photosynthetic induction
t_{gs90}	time for g_{sc} to reach 90% of photosynthetic induction
t_{gm90}	time for g_m to reach 90% of photosynthetic induction
$t_{Vcmax90}$	time for V_{cmax} to reach 90% of photosynthetic induction
dA_b	transient biochemical limitation during photosynthetic induction
dA_m	transient mesophyll conductance limitation during photosynthetic induction
dA_s	transient stomatal conductance limitation during photosynthetic induction
σ_b	time-integrated biochemical limitation during photosynthetic induction
σ_m	time-integrated mesophyll conductance limitation during photosynthetic induction
σ_s	time-integrated transient stomatal conductance limitation during photosynthetic induction

References

1. Rawat, J.; Pandey, N.; Saxena, J. Role of potassium in plant photosynthesis, transport, growth and yield. In *Role of Potassium in Abiotic Stress*; Springer: Berlin/Heidelberg, Germany, 2022; pp. 1–14.
2. Tränkner, M.; Tavakol, E.; Jákli, B. Functioning of potassium and magnesium in photosynthesis, photosynthate translocation and photoprotection. *Physiol. Plant.* **2018**, *163*, 414–431. [CrossRef] [PubMed]
3. Pettigrew, W.T. Potassium influences on yield and quality production for maize, wheat, soybean and cotton. *Physiol. Plant.* **2008**, *133*, 670–681. [CrossRef]
4. Hu, W.; Lu, Z.; Gu, H.; Ye, X.; Li, X.; Cong, R.; Ren, T.; Lu, J. Potassium availability influences the mesophyll structure to coordinate the conductance of CO_2 and H_2O during leaf expansion. *Plant. Cell Environ.* **2022**, *45*, 2987–3000. [CrossRef] [PubMed]

5. Lu, Z.; Ren, T.; Pan, Y.; Li, X.; Cong, R.; Lu, J. Differences on photosynthetic limitations between leaf margins and leaf centers under potassium deficiency for *Brassica napus* L. *Sci. Rep.* **2016**, *6*, 21725. [CrossRef] [PubMed]
6. Jin, S.H.; Huang, J.Q.; Li, X.Q.; Zheng, B.S.; Wu, J.S.; Wang, Z.J.; Liu, G.H.; Chen, M. Effects of potassium supply on limitations of photosynthesis by mesophyll diffusion conductance in *Carya cathayensis*. *Tree Physiol.* **2011**, *31*, 1142–1151. [CrossRef] [PubMed]
7. Jákli, B.; Tavakol, E.; Tränkner, M.; Senbayram, M.; Dittert, K. Quantitative limitations to photosynthesis in K deficient sunflower and their implications on water-use efficiency. *J. Plant Physiol.* **2017**, *209*, 20–30. [CrossRef]
8. Sawhney, B.; Zelitch, I. Direct determination of potassium ion accumulation in guard cells in relation to stomatal opening in light. *Plant Physiol.* **1969**, *44*, 1350. [CrossRef]
9. Lu, Z.; Xie, K.; Pan, Y.; Ren, T.; Lu, J.; Wang, M.; Shen, Q.; Guo, S. Potassium mediates coordination of leaf photosynthesis and hydraulic conductance by modifications of leaf anatomy. *Plant Cell Environ.* **2019**, *42*, 2231–2244. [CrossRef]
10. Pan, Y.; Cao, Y.; Chai, Y.; Meng, X.; Wang, M.; Wang, G.; Guo, S. Identification of photosynthetic parameters for superior yield of two super hybrid rice varieties: A cross-scale study from leaf to canopy. *Front. Plant Sci.* **2023**, *14*, 1110257. [CrossRef]
11. Xiong, D.; Huang, J.; Peng, S.; Li, Y. A few enlarged chloroplasts are less efficient in photosynthesis than a large population of small chloroplasts in *Arabidopsis thaliana*. *Sci. Rep.* **2017**, *7*, 5782. [CrossRef]
12. Lu, Z.; Lu, J.; Pan, Y.; Lu, P.; Li, X.; Cong, R.; Ren, T. Anatomical variation of mesophyll conductance under potassium deficiency has a vital role in determining leaf photosynthesis. *Plant Cell Environ.* **2016**, *39*, 2428–2439. [CrossRef] [PubMed]
13. Yan, J.; Ye, X.; Song, Y.; Ren, T.; Wang, C.; Li, X.; Lu, J. Sufficient potassium improves inorganic phosphate-limited photosynthesis in *Brassica napus* by enhancing metabolic phosphorus fractions and Rubisco activity. *Plant J.* **2023**, *113*, 416–429. [CrossRef] [PubMed]
14. Lu, Z.; Pan, Y.; Hu, W.; Cong, R.; Ren, T.; Guo, S.; Lu, J. The photosynthetic and structural differences between leaves and siliques of Brassica napus exposed to potassium deficiency. *BMC Plant Biol.* **2017**, *17*, 240. [CrossRef]
15. Zhang, W.; He, X.; Chen, X.; Han, H.; Shen, B.; Diao, M.; Liu, H. Exogenous selenium promotes the growth of salt-stressed tomato seedlings by regulating ionic homeostasis, activation energy allocation and CO_2 assimilation. *Front. Plant Sci.* **2023**, *14*, 1206246. [CrossRef]
16. Wang, Y.; Zhang, Z.; Liang, Y.; Han, Y.; Han, Y.; Tan, J. High potassium application rate increased grain yield of shading-stressed winter wheat by improving photosynthesis and photosynthate translocation. *Front. Plant Sci.* **2020**, *11*, 134. [CrossRef] [PubMed]
17. Hou, W.; Tränkner, M.; Lu, J.; Yan, J.; Huang, S.; Ren, T.; Cong, R.; Li, X. Interactive effects of nitrogen and potassium on photosynthesis and photosynthetic nitrogen allocation of rice leaves. *BMC Plant Biol.* **2019**, *19*, 302. [CrossRef]
18. Qi, D.; Zhao, X.; Le, X.; Jiang, C.; Wang, X.; Yi, H.; Yu, H. Effects of potassium deficiency on photosynthesis, chloroplast ultrastructure, ROS, and antioxidant activities in maize (*Zea mays* L.). *J. Integr. Agr.* **2019**, *18*, 395–406.
19. Qi, D.U.; Zhao, X.H.; Le, X.I.A.; Jiang, C.J.; Wang, X.G.; Yi, H.A.N.; Jing, W.A.N.G.; Yu, H.Q. A canopy conundrum: Can wind-induced movement help to increase crop productivity by relieving photosynthetic limitations? *J. Exp. Bot.* **2019**, *70*, 2371–2380.
20. Kaiser, E.; Morales, A.; Harbinson, J.; Kromdijk, J.; Heuvelink, E.; Marcelis, L. Dynamic photosynthesis in different environmental conditions. *J. Exp. Bot.* **2015**, *66*, 2415–2426. [CrossRef]
21. Sakoda, K.; Yamori, W.; Groszmann, M.; Evans, J. Stomatal, mesophyll conductance, and biochemical limitations to photosynthesis during induction. *Plant Physiol.* **2021**, *185*, 146–160. [CrossRef]
22. Liu, T.; Barbour, M.; Yu, D.; Rao, S.; Song, X. Mesophyll conductance exerts a significant limitation on photosynthesis during light induction. *N. Phytol.* **2021**, *233*, 360–372. [CrossRef] [PubMed]
23. Wang, X.; Zeng, Z.; Shi, Z.; Wang, J.; Huang, W. Variation in photosynthetic efficiency under fluctuating light between rose cultivars and its potential for improving dynamic photosynthesis. *Plants* **2023**, *12*, 1186. [CrossRef]
24. Wang, X.G.; Zhao, X.H.; Jiang, C.J.; Li, C.H.; Cong, S.; Wu, D.; Chen, Y.Q.; Yu, H.Q.; Wang, C.Y. Effects of potassium deficiency on photosynthesis and photoprotection mechanisms in soybean (*Glycine max* (L.) Merr.). *J. Integr. Agric.* **2015**, *14*, 856–863. [CrossRef]
25. Zhao, D.; Oosterhuis, D.; Bednarz, C. Influence of potassium deficiency on photosynthesis, chlorophyll content, and chloroplast ultrastructure of cotton plants. *Photosynthetica* **2001**, *39*, 103–109. [CrossRef]
26. Sakoda, K.; Taniyoshi, K.; Yamori, W.; Tanaka, Y. Drought stress reduces crop carbon gain due to delayed photosynthetic induction under fluctuating light conditions. *Physiol. Plant.* **2022**, *174*, e13603. [CrossRef] [PubMed]
27. Zotz, G.; Mikona, C. Photosynthetic Induction and leaf carbon gain in the Tropical understorey Epiphyte, *Aspasia principissa*. *Ann. Bot.* **2003**, *91*, 353–359. [CrossRef]
28. Sun, H.; Zhang, Y.; Zhang, S.; Huang, W. Photosynthetic induction under fluctuating light is affected by leaf nitrogen content in tomato. *Front. Plant Sci.* **2022**, *13*, 835571. [CrossRef]
29. Chen, J.W.; Kuang, S.; Long, G.; Meng, Z.; Li, L.; Chen, Z.; Zhang, G.; Yang, S. Steady-state and dynamic photosynthetic performance and nitrogen partitioning in the shade-demanding plant *Panax notoginseng* under different levels of growth irradiance. *Acta Physiol. Plant.* **2014**, *36*, 2409–2420. [CrossRef]

30. Zhang, Y.; Kaiser, E.; Marcelis, L.; Yang, Q.; Li, T. Salt stress and fluctuating light have separate effects on photosynthetic acclimation, but interactively affect biomass. *Plant Cell Environ.* **2020**, *43*, 2192–2206. [CrossRef]
31. Lawson, T.; Vialet-Chabrand, S. Speedy stomata, photosynthesis and plant water use efficiency. *N. Phytol.* **2019**, *221*, 93–98. [CrossRef]
32. Lawson, T.; Blatt, M. Stomatal size, speed, and responsiveness impact on photosynthesis and water use efficiency. *Plant Physiol.* **2014**, *164*, 1556–1570. [CrossRef] [PubMed]
33. Liu, Q.; Jin, W.; Huang, L.; Wang, D.; Xu, K.; Wei, Y. Photosynthetic Induction Characteristics in Saplings of Four Sun-Demanding Trees and Shrubs. *Plants* **2025**, *14*, 144. [CrossRef]
34. Imtiaz, H.; Mir, A.; Corpas, F.; Hayat, S. Impact of potassium starvation on the uptake, transportation, photosynthesis, and abiotic stress tolerance. *Plant Growth Regul.* **2023**, *99*, 429–448. [CrossRef]
35. Humble, G.; Hsiao, T. Light-dependent influx and efflux of potassium of guard cells during stomatal opening and closing. *Plant Physiol.* **1970**, *46*, 483–487. [CrossRef] [PubMed]
36. Nagarajah, S. The effect of potassium deficiency on stomatal and cuticular resistance in tea (*Camellia sinensis*). *Physiol. Plant.* **1979**, *47*, 91–94. [CrossRef]
37. Christina, M.; Le Maire, G.; Battie-Laclau, P.; Nouvellon, Y.; Bouillet, J.P.; Jourdan, C.; de Moraes Gonçalves, J.L.; Laclau, J.P. Measured and modeled interactive effects of potassium deficiency and water deficit on gross primary productivity and light-use efficiency in *Eucalyptus* grandis plantations. *Global Chang. Biol.* **2015**, *21*, 2022–2039. [CrossRef]
38. Mao, X.; Zheng, Y.; Xiao, K.; Wei, Y.; Zhu, Y.; Cai, Q.; Chen, L.; Xie, H.; Zhang, J. *OsPRX2* contributes to stomatal closure and improves potassium deficiency tolerance in rice. *Biochem. Biophy. Res. Commun.* **2018**, *495*, 461–467. [CrossRef]
39. Arquero, O.; Barranco, D.; Benlloch, M. Potassium starvation increases stomatal conductance in olive trees. *HortScience* **2006**, *41*, 433–436. [CrossRef]
40. Marschner, P. *Marschner's Mineral Nutrition of Higher Plants*, 3rd ed.; Academic Press: Cambridge, MA, USA, 2012; pp. 181–188.
41. Cui, J.; Tcherkez, G. Potassium dependency of enzymes in plant primary metabolism. *Plant Physiol. Biochem.* **2021**, *166*, 522–530. [CrossRef]
42. Hu, W.; Ren, T.; Meng, F.; Cong, R.; Li, X.; White, P.; Lu, J. Leaf photosynthetic capacity is regulated by the interaction of nitrogen and potassium through coordination of CO_2 diffusion and carboxylation. *Physiol. Plant.* **2019**, *167*, 418–432. [CrossRef]
43. Deans, R.; Farquhar, G.; Busch, F. Estimating stomatal and biochemical limitations during photosynthetic induction. *Plant Cell Environ.* **2019**, *42*, 3227–3240. [CrossRef] [PubMed]
44. Huang, G.; Zhang, Q.; Wei, X.; Peng, S.; Li, Y. Nitrogen can alleviate the inhibition of photosynthesis caused by high temperature stress under both steady-state and flecked irradiance. *Front. Plant Sci.* **2017**, *8*, 945. [CrossRef]
45. Li, Y.T.; Li, Y.; Li, Y.N.; Liang, Y.; Sun, Q.; Li, G.; Liu, P.; Zhang, Z.S.; Gao, H.Y. Dynamic light caused less photosynthetic suppression, rather than more, under nitrogen deficit conditions than under sufficient nitrogen supply conditions in soybean. *BMC Plant Biol.* **2020**, *20*, 339. [CrossRef] [PubMed]
46. Zhang, N.; Berman, S.; Berg, T.; Chen, Y.; Marcelis, L.; Kaiser, E. Biochemical versus stomatal acclimation of dynamic photosynthetic gas exchange to elevated CO_2 in three horticultural species with contrasting stomatal morphology. *Plant Cell Environ.* **2024**, *47*, 4516–4529. [CrossRef] [PubMed]
47. Bernacchi, C.; Portis, A.; Nakano, H.; Von Caemmerer, S.; Long, S. Temperature response of mesophyll conductance. Implications for the determination of Rubisco enzyme kinetics and for limitations to photosynthesis in vivo. *Plant Physiol.* **2002**, *130*, 1992–1998. [CrossRef]
48. Perdomo, J.; Capó-Bauçà, S.; Carmo-Silva, E.; Galmés, J. Rubisco and rubisco activase play an important role in the biochemical limitations of photosynthesis in rice, wheat, and maize under high temperature and water deficit. *Front. Plant Sci.* **2017**, *8*, 490. [CrossRef]
49. Harley, P.; Loreto, F.; Di Marco, G.; Sharke, T. Theoretical considerations when estimating the mesophyll conductance to CO_2 flux by analysis of the response of photosynthesis to CO_2. *Plant Physiol.* **1992**, *98*, 1429–1436. [CrossRef]
50. Mott, K.; Woodrow, I. Modelling the role of Rubisco activase in limiting non-steady-state photosynthesis. *J. Exp. Bot.* **2000**, *51*, 399–406. [CrossRef]

Disclaimer/Publisher's Note: The statements, opinions and data contained in all publications are solely those of the individual author(s) and contributor(s) and not of MDPI and/or the editor(s). MDPI and/or the editor(s) disclaim responsibility for any injury to people or property resulting from any ideas, methods, instructions or products referred to in the content.

plants

MDPI

Communication

Light Intensity Dependence of CO_2 Assimilation Is More Related to Biochemical Capacity Rather than Diffusional Conductance

Xiaoqian Wang [1], Qi Shi [1], Ningyu Liu [1], Jianxin Cao [2,*] and Wei Huang [1,*]

[1] Kunming Institute of Botany, Chinese Academy of Sciences, Kunming 650201, China; wangxiaoqian@mail.kib.ac.cn (X.W.); shiqide0720@163.com (Q.S.); liuningyu@mail.kib.ac.cn (N.L.)
[2] Yunnan Academy of Forestry and Grassland, Kunming 650201, China
* Correspondence: jxcao627@163.com (J.C.); huangwei@mail.kib.ac.cn (W.H.)

Abstract: The response of CO_2 assimilation rate (A_N) to incident light intensity reflects the efficiency of light utilization. The light intensity dependence of A_N varies widely among different plant species, yet the underlying mechanisms remain poorly understood. To elucidate this issue, we measured the light intensity dependence of gas exchange and chlorophyll fluorescence in twelve tree species. The results indicated that (1) with increasing light intensity, the variation in A_N was closely related to stomatal conductance (g_s), mesophyll conductance (g_m), the maximum velocity of Rubisco carboxylation (V_{cmax}), and electron transport rate (ETR); (2) compared with A_N at sub-saturating light, the increase in A_N at saturating light was more strongly associated with V_{cmax} and ETR than with g_s and g_m; and (3) the increase in V_{cmax} and A_N from 600 to 2000 μmol photons m^{-2} s^{-1} were positively correlated with the maximum capacity of V_{cmax}. These findings suggest that V_{cmax} is an energy-dependent process that significantly regulates the light intensity dependence of A_N in plants. This provides valuable insights for crop improvement through the manipulation of V_{cmax}.

Keywords: photosynthesis; light response; Rubisco carboxylation; stomatal conductance; mesophyll conductance

1. Introduction

Plants utilize photosynthesis to convert light energy into chemical energy in the form of ATP and NADPH, which are used to assimilate CO_2 and synthesize organic matter. The maximum A_N largely varies among different plants due to changes in stomatal conductance (g_s), mesophyll conductance (g_m), and biochemical capacity [1–5]. Under field environments, natural light intensity usually fluctuates during the daytime due to changes in solar position and cloud cover [6,7]. Light intensity significantly influences the CO_2 assimilation rate (A_N) through effects on g_s, g_m, Rubisco activation state, and electron transport rate (ETR) [8–10]. The response of A_N to incident light intensity plays a significant role in determining plant growth and crop yield [11].

With the increase in light intensity, A_N usually increases gradually to reach the maximum value at saturating light. Many previous studies have measured the light response curves of A_N in plants [8,12,13], pointing out that the light saturation point (LSP) of A_N largely differs between species. For example, LSP is lower than 300 μmol photons m^{-2} s^{-1} in some low-photosynthesis plants, such as *Paphiopedilum* species and *Pleione aurita* [12,13]. By comparison, LSP is approximately 1500 μmol photons m^{-2} s^{-1} in some high-photosynthesis plants, such as tobacco and tomato [10,14]. Although such species-dependent

LSP is related to the maximum A_N under saturating light, mechanisms underlying the variation in light intensity dependence of A_N have not been well clarified.

At a given incident light intensity, the value of A_N can be limited by diffusional CO_2 conductance and/or biochemical capacities [15]. Specifically, A_N under low light is mainly limited by the availability of ATP and NADPH produced through ETR [16]. With the increase in light intensity, the major limitation of A_N gradually shifts from ETR to RuBP carboxylation/regeneration [17]. According to the photosynthesis model, ETR = PPFD × Φ_{PSII} × s, where PPFD is the photosynthetic photon flux density, Φ_{PSII} is the effective quantum yield of photosystem II (PSII) photochemistry, and s is the proportion of light energy absorbed by leaves allocated to PSII, with a typical value of 0.45. At a moderate illumination of 600 μmol photons m^{-2} s^{-1}, ETR can theoretically reach 189 μmol photons m^{-2} s^{-1} when Φ_{PSII} is assumed to be 0.7. The value of A_N can theoretically reach 23.6 μmol CO_2 m^{-2} s^{-1} based on the assumption that A_N = ETR/8. Since the saturating A_N of most species is lower than 23.6 μmol CO_2 m^{-2} s^{-1}, their LSP of A_N is theoretically lower than 600 μmol photons m^{-2} s^{-1}. However, the actual LSP is usually higher than 600 μmol photons m^{-2} s^{-1}. This discrepancy between theoretical and actual LSP is caused by the actual Φ_{PSII}, which is related to the consumption rates of ATP and NADPH required for Rubisco carboxylation. As we know, the capacity of Rubisco carboxylation is determined by V_{cmax} and chloroplast CO_2 concentration, the latter of which is tightly related to CO_2 diffusional conductance (g_s and g_m) [18–20]. Therefore, the light intensity dependence of A_N is theoretically determined by the light responses of V_{cmax}, g_s, and/or g_m. In angiosperms, V_{cmax} and g_s usually increase with increasing illumination, but g_m is maintained stable in some species and gradually increases in others [8,9,21–23]. However, it remains unclear whether the light intensity dependence of A_N is mainly related to V_{cmax} or diffusional CO_2 conductance (g_s and g_m).

In this study, we measured light response data of gas exchange and chlorophyll fluorescence in twelve tree species with the aim of systematically understanding the main factor influencing the light intensity dependence of A_N. The results indicated that the relative increase in A_N at saturating light compared with that at sub-saturating light was mainly determined by the increased kinetics of V_{cmax} rather than g_s and g_m. Therefore, optimizing the light intensity dependence of V_{cmax} has the potential to enhance crop yield.

2. Materials and Methods

2.1. Plant Materials and Growth Condition

In this study, we used the seedlings of twelve tree species with variation in the photosynthetic capacity: *Chaenomeles cathayensis* (Hemsl.) C. K. Schneid., *Cercis glabra* Pamp., *Pterocarya stenoptera* C. DC., *Idesia polycarpa* Maxim., *Idesia polycarpa* var. vestita Diels, *Melia azedarach* L., *Pistacia chinensis* Bunge, *Fraxinus retusifoliolata* Feng ex P. Y. Bai, *Hypericum monogynum* L., *Styrax grandiflorus* Griff., *Sunhangia elegans* (DC.) H. Ohashi and K. Ohashi, and *Alnus nepalensis* D. Don. All plants were cultivated in greenhouses in Kunming, Yunnan, China. The day/night temperature is 30/20 °C, relative humidity is about 60%, and the maximum light intensity to which leaves were exposed is approximately 1000 μmol photons m^{-2} s^{-1}. To avoid any water and nutrient stress, plants were cultivated using a soilless substrate and drip irrigation techniques.

2.2. Gas Exchange and Chlorophyll Fluorescence Measurements

In the morning of clear days in summer, gas exchange and chlorophyll fluorescence were measured at 25 °C using the chlorophyll fluorescence probe of the LI-6400XT portable photosynthesis system (LI-COR Inc., Lincoln, NE, USA). Mature sun leaves were initially exposed to high light (1500 μmol photons m^{-2} s^{-1}, composed of 90% red light and 10%

blue light) for at least 30 min to complete photosynthetic induction. Subsequently, we measured the light intensity dependence of photosynthesis by gradually decreasing light intensity from 2000 to 100 μmol photons m^{-2} s^{-1}. After exposure to each light intensity (2000, 1500, 1000, 600, 400, 200, and 100 μmol photons m^{-2} s^{-1}) for 3 min, the data for gas exchange and chlorophyll fluorescence were then recorded.

In our study, we utilized the multi-phase flash (MPF) protocol following standard procedures to determine the parameters of chlorophyll fluorescence [24]. The light intensity for measurement was set at 1 μmol m^{-2} s^{-1}, while the maximum flash intensity reached 8000 μmol m^{-2} s^{-1}. During the second phase of the MPF, the flash intensity was reduced by 60%, with the three flash phases lasting 0.3 s, 0.7 s, and 0.4 s, respectively. Subsequently, we calculated the effective quantum yield of photochemistry for photosystem II (Φ_{PSII}) and the total electron transport rate through photosystem II (ETR) using the following equations [25,26]:

$$\Phi_{PSII} = \frac{\left(F_m{}' - F_s\right)}{F_m{}'}$$

$$ETR = \Phi_{PSII} \times PPFD \times 0.45$$

where PPFD represents the light intensity and 0.45 represents the proportion of light energy absorbed by leaves allocated to photosystem II.

2.3. Calculation of the Mesophyll Conductance

Mesophyll conductance (g_m) was calculated by combining the gas exchange data and chlorophyll fluorescence data with the following equation [27]:

$$g_m = \frac{A_N}{C_i - \Gamma^*(ETR + 8(A_N + R_d))/(ETR - 4(A_N + R_d))}$$

where A_N represents the net photosynthetic rate, C_i represents the intercellular CO_2 concentration, Γ* represents the CO_2 compensation point in the absence of mitochondrial respiration, and a typical value of 40 μmol mol^{-1} is used [9]; R_d represents the dark respiration rate measured at night.

The chloroplast CO_2 concentration (C_c) was calculated as follows [28]:

$$C_c = C_i - \frac{A_N}{g_m}$$

The maximum carboxylation rate of Rubisco (V_{cmax}) was calculated as follows [18,29]:

$$V_{cmax} = \frac{(A_N + R_d)(C_c + K_c(1 + O/K_o))}{\left(C_c - \Gamma^*\right)}$$

where K_c (404 μmol mol^{-1}) and K_o (278 mmol mol^{-1}) are the Rubisco Michaelis–Menten constants for CO_2 and oxygen, respectively; O (210 mmol mol^{-1}) is the oxygen concentration in the chloroplasts.

2.4. Quantitative Calculation of Photosynthetic Limitation

The quantitative calculation formula for the photosynthetic limiting factor is as follows [15]:

$$L_s = \frac{g_{tot}/g_s \times \partial A_N/\partial C_c}{g_{tot} + \partial A_N/\partial C_c}$$

$$L_m = \frac{g_{tot}/g_m \times \partial A_N/\partial C_c}{g_{tot} + \partial A_N/\partial C_c}$$

$$L_b = \frac{g_{tot}}{g_{tot} + \partial A_N / \partial C_c}$$

where L_s, L_m, and L_b represent the degree of limitation of photosynthesis by g_s, g_m, and biochemical capacity, respectively, and g_{tot} represents the overall CO_2 diffusive conductance, with g_{tot} and $\partial A_N / \partial C_c$ being calculated as follows, respectively:

$$g_{tot} = \frac{g_s \times g_m}{g_s + g_m}$$

$$\partial A_N / \partial C_c = V_{cmax} \frac{\Gamma^* + K_c(1 + O/K_o)}{(C_c + K_c(1 + O/K_o))^2}$$

2.5. Calculation of Electron Flow for Photorespiration

The rate of electron flow for photorespiration (J_O) was calculated according to the following equation [30]:

$$J_O = 2/3 \times (ETR - 4 \times (A_N + R_d))$$

2.6. Statistical Analysis

Six independent leaves from six different plants were used for each species. The software SigmaPlot 10.0 was used for graphing and fitting.

3. Results

3.1. The Steady-State Photosynthesis at Saturating Light

We first measured steady-state photosynthesis at a saturating light intensity of 2000 μmol photons m^{-2} s^{-1}. As shown in Table 1, the net CO_2 assimilation rate (A_N) ranged from 10.9 ± 0.66 to 21.3 ± 0.45 μmol m^{-2} s^{-1}, stomatal conductance (g_s) ranged from 0.14 ± 0.01 to 0.62 ± 0.04 mol m^{-2} s^{-1}, mesophyll conductance (g_m) ranged from 0.09 ± 0.01 to 0.24 ± 0.04 mol m^{-2} s^{-1}, electron transport rate (ETR) ranged from 89.6 ± 2.8 to 175 ± 4.6 μmol m^{-2} s^{-1}, and the maximum velocity of Rubisco carboxylation (V_{cmax}) ranged from 91.5 ± 11 to 199 ± 15 μmol m^{-2} s^{-1}. These results indicated that photosynthetic capacity varied substantially among the studied tree species.

Table 1. Area-based photosynthetic characteristics for evergreen and deciduous angiosperm tree species. Average values ± SE (n ≥ 5) are shown for area-based maximum net photosynthetic rate (A_N), stomatal conductance (g_s), mesophyll conductance (g_m), maximum velocity of Rubisco carboxylation (V_{cmax}), and electron transport rate (ETR).

Species	A_{area} (μmol m^{-2} s^{-1})	g_s (mol m^{-2} s^{-1})	g_m (mol m^{-2} s^{-1})	V_{cmax} (μmol m^{-2} s^{-1})	ETR (μmol m^{-2} s^{-1})
Ch. cathayensis	13.1 ± 0.43	0.406 ± 0.031	0.095 ± 0.01	91.5 ± 11	89.6 ± 2.8
Ce. glabra	21.1 ± 0.85	0.615 ± 0.043	0.16 ± 0.02	111 ± 11	137 ± 8.2
Pt. stenoptera	14.7 ± 0.49	0.303 ± 0.042	0.12 ± 0.005	118 ± 14	104 ± 6.0
Id. polycarpa	16.3 ± 0.77	0.314 ± 0.037	0.16 ± 0.01	101 ± 9.1	105 ± 5.4
Id. Polycarpa var. vestita	16.0 ± 0.78	0.446 ± 0.039	0.18 ± 0.04	139 ± 25	116±8.3
Me. azedarach	16.3 ± 0.76	0.302 ± 0.05	0.12 ± 0.01	155 ± 25	126 ± 6.9
Pi. chinensis	12.5 ± 0.97	0.177 ± 0.037	0.091 ± 0.01	144 ± 24	111 ± 6.4
Fr. retusifoliolata	15.4 ± 0.23	0.285 ± 0.02	0.15 ± 0.02	108 ± 12	105 ± 3.0
Hy. monogynum	21.3 ± 0.45	0.588 ± 0.06	0.17 ± 0.02	161± 22	156 ± 7.6
St. grandiflorus	10.9 ± 0.66	0.142 ± 0.01	0.10 ± 0.01	120 ± 9.9	88.9 ± 4.3
Su. elegans	19.2 ± 0.71	0.359± 0.07	0.24 ± 0.04	162 ± 30	152 ± 12
Al. nepalensis	19.4 ± 1.6	0.428 ± 0.09	0.13 ± 0.01	200 ±15	176 ± 4.6

3.2. Light Intensity Dependence of Photosynthetic Parameters

We next measured gas exchange and chlorophyll fluorescence under light conditions ranging from 100 to 2000 μmol photons m^{-2} s^{-1}. As shown in Figure 1A, A_N increased rapidly with increasing light intensity from 100 to 400 μmol photons m^{-2} s^{-1}, but increased by an average of 18% when light intensity increased from 600 to 2000 μmol photons m^{-2} s^{-1}. At a high light intensity of 1500 μmol photons m^{-2} s^{-1}, A_N was almost saturated in all twelve tree species. Concomitantly, g_s displayed a slight increase throughout the entire light response curve in all studied species (Figure 1B), while g_m increased by an average of 32% with increasing light intensity from 600 to 2000 μmol photons m^{-2} s^{-1} (Figure 1C). For all studied species, ETR increased rapidly as light intensity increased from 100 to 600 μmol photons m^{-2} s^{-1}. During the light course from 600 to 1000 μmol photons m m^{-2} s^{-1}, ETR increased by an average of 12% (Figure 2A). In the twelve studied tree species, ETR was approximately saturated at a high light intensity of 1000 μmol photons m^{-2} s^{-1} (Figure 2A). Similar to the light response trend of ETR, V_{cmax} gradually increased with light intensity increasing from 400 to 1000 μmol photons m^{-2} s^{-1}, and was almost saturated at 1000 μmol photons m^{-2} s^{-1} in these studied species (Figure 2B). Across the light intensity range from 400 to 2000 μmol photons m^{-2} s^{-1}, the variation in A_N was tightly correlated with the variations in g_s (R^2 = 0.66, p < 0.0001, Figure 3A), g_m (R^2 = 0.47, p < 0.0001, Figure 3B), V_{cmax} (R^2 = 0.26, p < 0.0001, Figure 3C), and ETR (R^2 = 0.76, p < 0.0001, Figure 3D). These results suggest that variation in A_N among these tree species is related to variations in g_s, g_m, $V_{cmax,}$ and ETR.

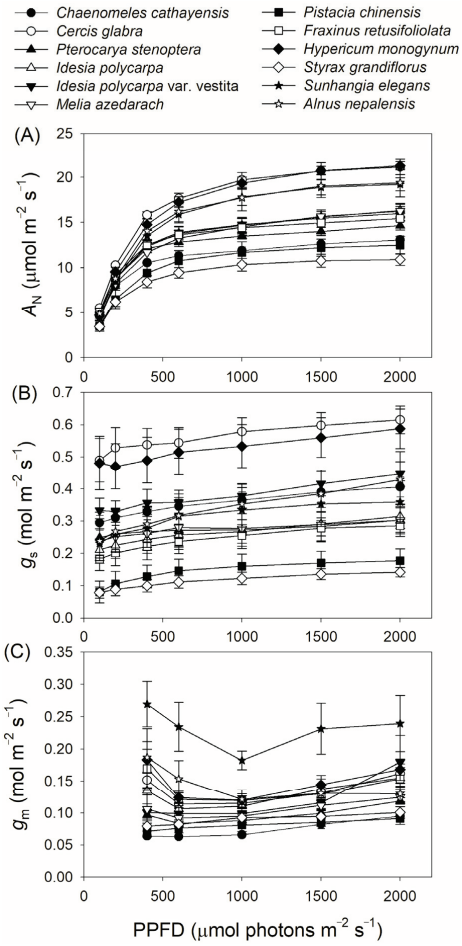


Figure 1. Light intensity dependence of net CO_2 assimilation rate (A_N) (**A**), stomatal conductance (g_s) (**B**), and mesophyll conductance (g_m) (**C**) in twelve tree species. Data are shown as means ± SE (n = 6).

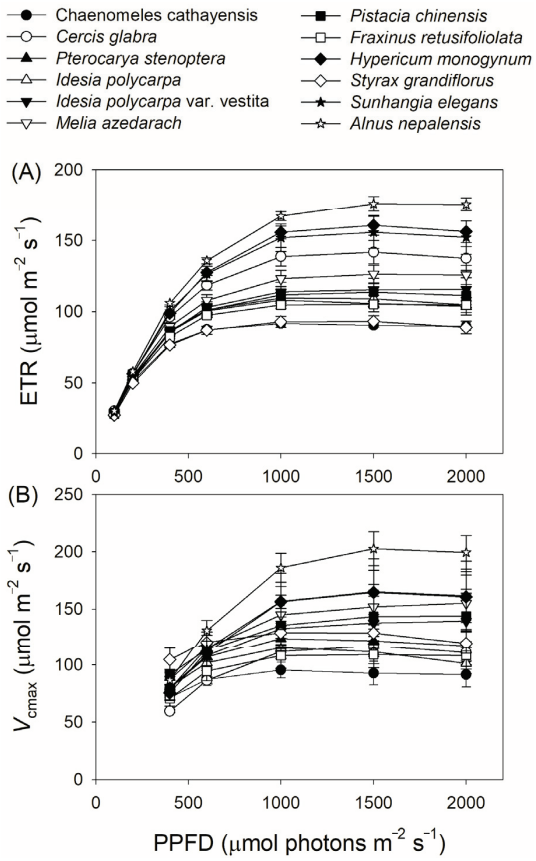


Figure 2. Light intensity dependence of electron transport rate (ETR) (**A**) and the maximum velocity of Rubisco carboxylation (V_{cmax}) (**B**) in the twelve tree species. Data are shown as means ± SE (n = 6).

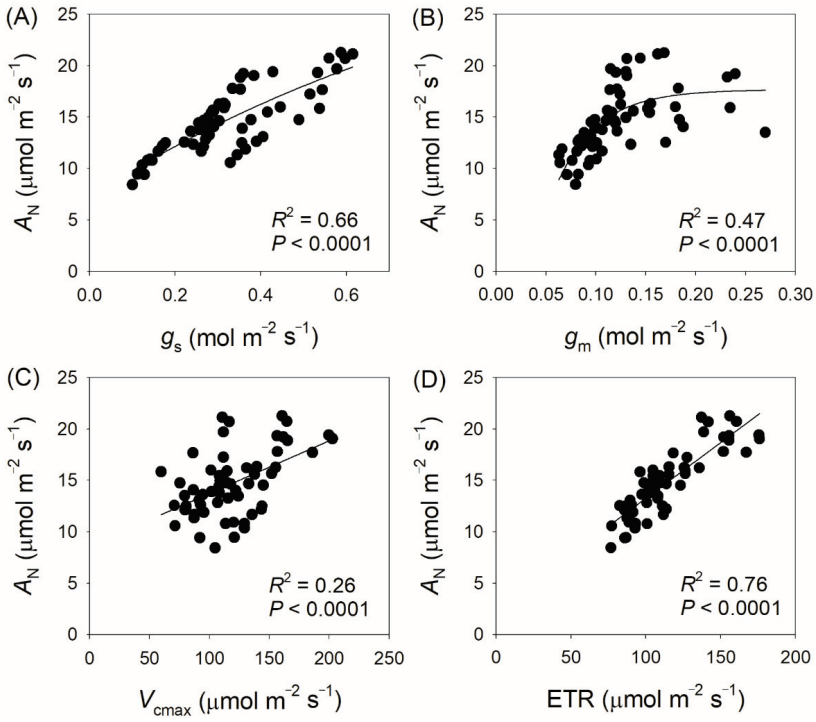


Figure 3. Relationship between A_N, g_s, g_m, V_{cmax}, and ETR across light intensities from 400 to 2000 μmol photons m^{-2} s^{-1} among the twelve tree species. A_N, net CO_2 assimilation rate; g_s, stomatal conductance; g_m, mesophyll conductance; V_{cmax}, the maximum velocity of Rubisco carboxylation; ETR, electron transport rate. (**A**) relationship between A_N and g_s; (**B**) relationship between A_N and g_m; (**C**) relationship between A_N and V_{cmax}; (**D**) relationship between A_N and ETR.

3.3. Correlation Between Physiological Parameters and CO_2 Assimilation Rate

Compared with A_N at 400 μmol photons m^{-2} s^{-1} ($A_{N\text{-}400}$), A_N at 2000 μmol photons m^{-2} s^{-1} ($A_{N\text{-}2000}$) reached 120–144% in the studied species, with g_s reaching 114–142%, g_m reaching 85–178%, V_{cmax} reaching 115–213%, and ETR reaching 116–158% (Figure 4). The variation in $A_{N\text{-}2000}/A_{N\text{-}400}$ was not significantly correlated with $g_{s\text{-}2000}/g_{s\text{-}400}$ (Figure 4A) or $g_{m\text{-}2000}/g_{m\text{-}400}$ (Figure 4B), but was significantly correlated with $V_{cmax\text{-}2000}/V_{cmax\text{-}400}$ (R^2 = 0.57, p = 0.005, Figure 4C) and ETR_{2000}/ETR_{400} (R^2 = 0.68, p = 0.001, Figure 4D). Similarly, the variation in $A_{N\text{-}2000}/A_{N\text{-}600}$ was not significantly correlated with $g_{s\text{-}2000}/g_{s\text{-}600}$ (Figure 5A) or $g_{m\text{-}2000}/g_{m\text{-}600}$ (Figure 5B), but was significantly correlated with $V_{cmax\text{-}2000}/V_{cmax\text{-}600}$ (R^2 = 0.64, p = 0.002, Figure 5C) and ETR_{2000}/ETR_{600} (R^2 = 0.66, p = 0.001, Figure 5D). Therefore, the relative increase in A_N at 2000 μmol photons m^{-2} s^{-1} compared with that at 400 and 600 μmol photons m^{-2} s^{-1} is mainly determined by the light intensity dependence of V_{cmax} and ETR rather than g_s and g_m.

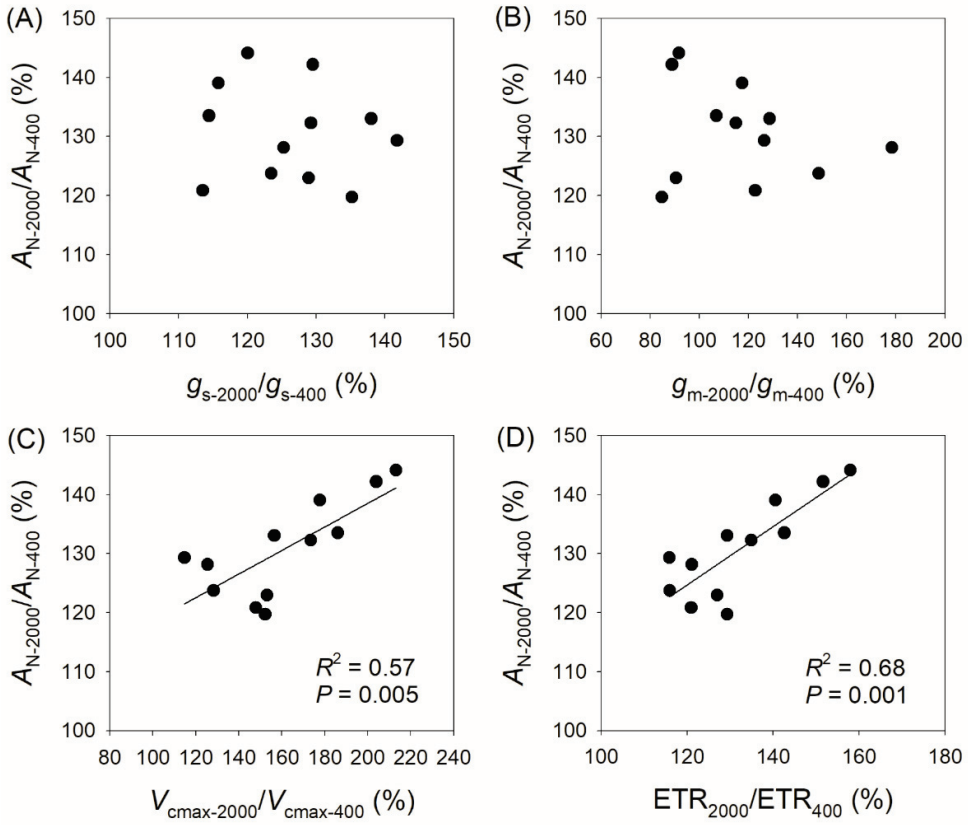


Figure 4. Relationships between $A_{N\text{-}2000}/A_{N\text{-}400}$, $g_{s\text{-}2000}/g_{s\text{-}400}$, $g_{m\text{-}2000}/g_{m\text{-}400}$, $V_{cmax\text{-}2000}/V_{cmax\text{-}400}$, and ETR_{2000}/ETR_{400} among the twelve tree species. $A_{N\text{-}2000}/A_{N\text{-}400}$, the ratio of net CO_2 assimilation rate (A_N) at 2000 μmol photons m^{-2} s^{-1} to that at 400 μmol photons m^{-2} s^{-1}; $g_{s\text{-}2000}/g_{s\text{-}400}$, the ratio of stomatal conductance (g_s) at 2000 μmol photons m^{-2} s^{-1} to that at 400 μmol photons m^{-2} s^{-1}; $g_{m\text{-}2000}/g_{m\text{-}400}$, the ratio of mesophyll conductance (g_m) at 2000 μmol photons m^{-2} s^{-1} to that at 400 μmol photons m^{-2} s^{-1}; $V_{cmax\text{-}2000}/V_{cmax\text{-}400}$, the ratio of maximum velocity of Rubisco carboxylation (V_{cmax}) at 2000 μmol photons m^{-2} s^{-1} to that at 400 μmol photons m^{-2} s^{-1}; ETR_{2000}/ETR_{400}, the ratio of electron transport rate (ETR) at 2000 μmol photons m^{-2} s^{-1} to that at 400 μmol photons m^{-2} s^{-1}. (**A**) relationship between $A_{N\text{-}2000}/A_{N\text{-}400}$ and $g_{s\text{-}2000}/g_{s\text{-}400}$; (**B**) relationship between $A_{N\text{-}2000}/A_{N\text{-}400}$ and $g_{m\text{-}2000}/g_{m\text{-}400}$; (**C**) relationship between $A_{N\text{-}2000}/A_{N\text{-}400}$ and $V_{cmax\text{-}2000}/V_{cmax\text{-}400}$; (**D**) relationship between $A_{N\text{-}2000}/A_{N\text{-}400}$ and ETR_{2000}/ETR_{400}.

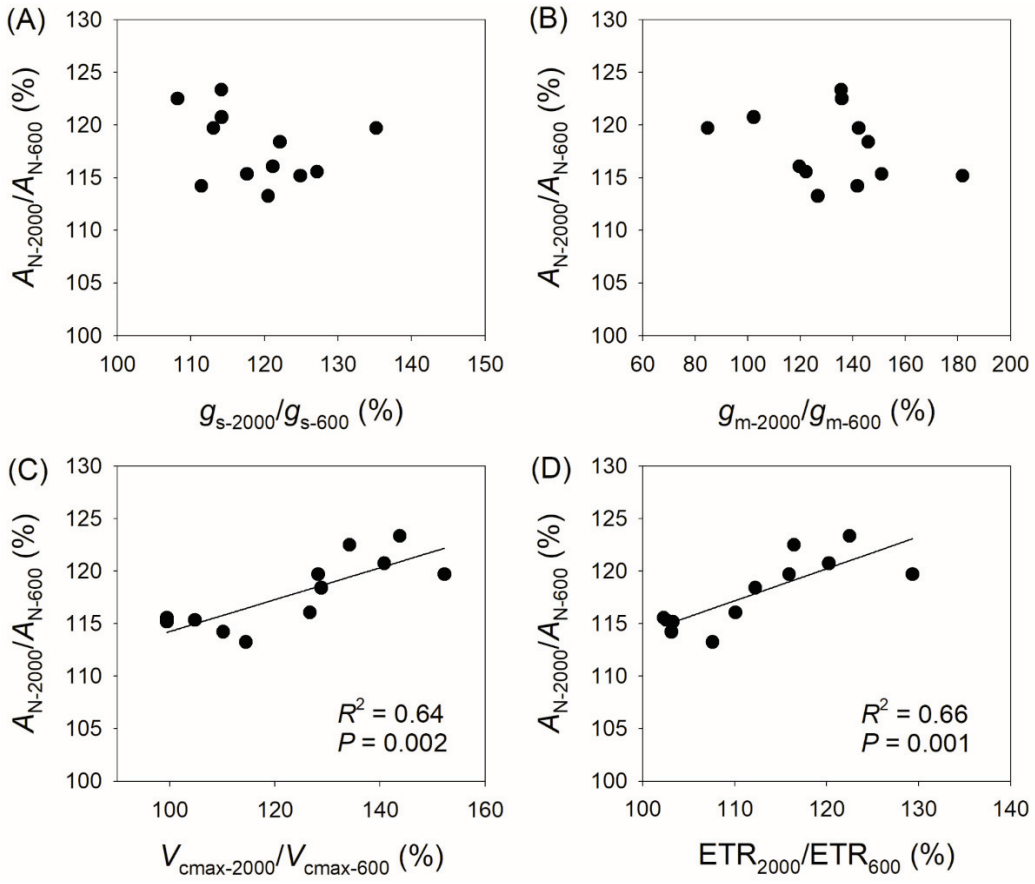


Figure 5. Relationships between $A_{N\text{-}2000}/A_{N\text{-}600}$, $g_{s\text{-}2000}/g_{s\text{-}600}$, $g_{m\text{-}2000}/g_{m\text{-}600}$, $V_{cmax\text{-}2000}/V_{cmax\text{-}600}$, and ETR$_{2000}$/ETR$_{600}$ among the twelve tree species. $A_{N\text{-}2000}/A_{N\text{-}600}$, the ratio of net CO_2 assimilation rate (A_N) at 2000 μmol photons m^{-2} s^{-1} to that at 600 μmol photons m^{-2} s^{-1}; $g_{s\text{-}2000}/g_{s\text{-}600}$, the ratio of stomatal conductance (g_s) at 2000 μmol photons m^{-2} s^{-1} to that at 600 μmol photons m^{-2} s^{-1}; $g_{m\text{-}2000}/g_{m\text{-}600}$, the ratio of mesophyll conductance (g_m) at 2000 μmol photons m^{-2} s^{-1} to that at 600 μmol photons m^{-2} s^{-1}; $V_{cmax\text{-}2000}/V_{cmax\text{-}600}$, the ratio of maximum velocity of Rubisco carboxylation (V_{cmax}) at 2000 μmol photons m^{-2} s^{-1} to that at 600 μmol photons m^{-2} s^{-1}; ETR$_{2000}$/ETR$_{600}$, the ratio of electron transport rate (ETR) at 2000 μmol photons m^{-2} s^{-1} to that at 600 μmol photons m^{-2} s^{-1}. (**A**) relationship between $A_{N\text{-}2000}/A_{N\text{-}600}$ and $g_{s\text{-}2000}/g_{s\text{-}600}$; (**B**) relationship between $A_{N\text{-}2000}/A_{N\text{-}600}$ and $g_{m\text{-}2000}/g_{m\text{-}600}$; (**C**) relationship between $A_{N\text{-}2000}/A_{N\text{-}600}$ and $V_{cmax\text{-}2000}/V_{cmax\text{-}600}$; (**D**) relationship between $A_{N\text{-}2000}/A_{N\text{-}600}$ and ETR$_{2000}$/ETR$_{600}$.

In addition, we found a positive correlation between $V_{cmax\text{-}2000}/V_{cmax\text{-}400}$ and ETR$_{2000}$/ETR$_{400}$ (R^2 = 0.95, p < 0.0001, Figure 6A), a negative correlation between $V_{cmax\text{-}2000}/V_{cmax\text{-}400}$ and $C_{c\text{-}2000}/C_{c\text{-}400}$ (R^2 = 0.75, p = 0.0003, Figure 6B), a negative correlation between $V_{cmax\text{-}2000}/V_{cmax\text{-}400}$ and $L_{b\text{-}2000}/L_{b\text{-}400}$ (R^2 = 0.67, p = 0.001, Figure 6C), and a positive correlation between $V_{cmax\text{-}2000}/V_{cmax\text{-}400}$ and $J_{O\text{-}2000}/J_{O\text{-}400}$ (R^2 = 0.95, p < 0.0001, Figure 6D). Similarly, we observed a positive correlation between $V_{cmax\text{-}2000}/V_{cmax\text{-}600}$ and ETR$_{2000}$/ETR$_{600}$ (R^2 = 0.94, p < 0.0001, Figure 7A), a negative correlation between $V_{cmax\text{-}2000}/V_{cmax\text{-}600}$ and $C_{c\text{-}2000}/C_{c\text{-}600}$ (R^2 = 0.81, p < 0.0001, Figure 7B), a negative correlation between $V_{cmax\text{-}2000}/V_{cmax\text{-}600}$ and $L_{b\text{-}2000}/L_{b\text{-}600}$ (R^2 = 0.81, p < 0.0001, Figure 7C), and a positive correlation between $V_{cmax\text{-}2000}/V_{cmax\text{-}600}$ and $J_{O\text{-}2000}/J_{O\text{-}600}$ (R^2 = 0.92, p < 0.0001, Figure 7D). These results indicate that the coordinated changes in V_{cmax} and ETR compensate for the decrease in C_c and the increase in J_O and diminish the biochemical limitation of A_N.

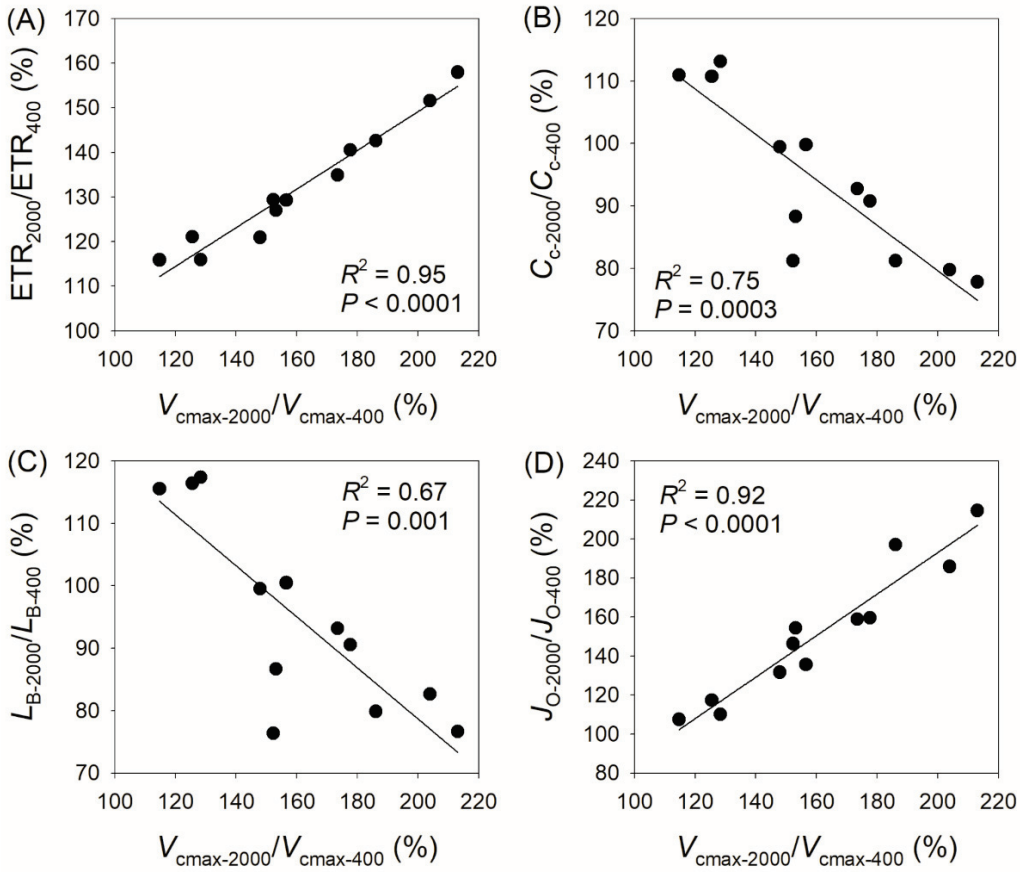


Figure 6. Relationships between $V_{cmax\text{-}2000}/V_{cmax\text{-}400}$, ETR_{2000}/ETR_{400}, $C_{c\text{-}2000}/C_{c\text{-}400}$, $L_{B\text{-}2000}/L_{B\text{-}400}$, and $J_{O\text{-}2000}/J_{O\text{-}400}$ among the twelve tree species. $V_{cmax\text{-}2000}/V_{cmax\text{-}400}$, the ratio of maximum velocity of Rubisco carboxylation (V_{cmax}) at 2000 μmol photons m^{-2} s^{-1} to that at 400 μmol photons m^{-2} s^{-1}; ETR_{2000}/ETR_{400}, the ratio of electron transport rate (ETR) at 2000 μmol photons m^{-2} s^{-1} to that at 400 μmol photons m^{-2} s^{-1}; $C_{c\text{-}2000}/C_{c\text{-}400}$, the ratio of chloroplast CO_2 concentration (C_c) at 2000 μmol photons m^{-2} s^{-1} to that at 400 μmol photons m^{-2} s^{-1}; $L_{B\text{-}2000}/L_{B\text{-}400}$, the ratio of biochemical limitation (L_B) at 2000 μmol photons m^{-2} s^{-1} to that at 400 μmol photons m^{-2} s^{-1}; $J_{O\text{-}2000}/J_{O\text{-}400}$, the ratio of photorespiration (J_O) at 2000 μmol photons m^{-2} s^{-1} to that at 400 μmol photons m^{-2} s^{-1}. (**A**), relationship between ETR_{2000}/ETR_{400} and $V_{cmax\text{-}2000}/V_{cmax\text{-}400}$; (**B**) relationship between $C_{c\text{-}2000}/C_{c\text{-}400}$ and $V_{cmax\text{-}2000}/V_{cmax\text{-}400}$; (**C**) relationship between $L_{B\text{-}2000}/L_{B\text{-}400}$ and $V_{cmax\text{-}2000}/V_{cmax\text{-}400}$; (**D**) relationship between $J_{O\text{-}2000}/J_{O\text{-}400}$ and $V_{cmax\text{-}2000}/V_{cmax\text{-}400}$.

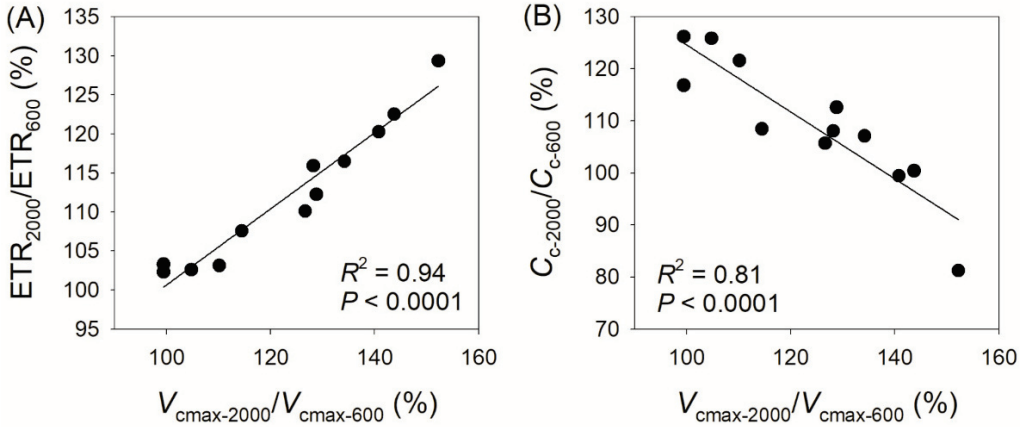


Figure 7. *Cont.*

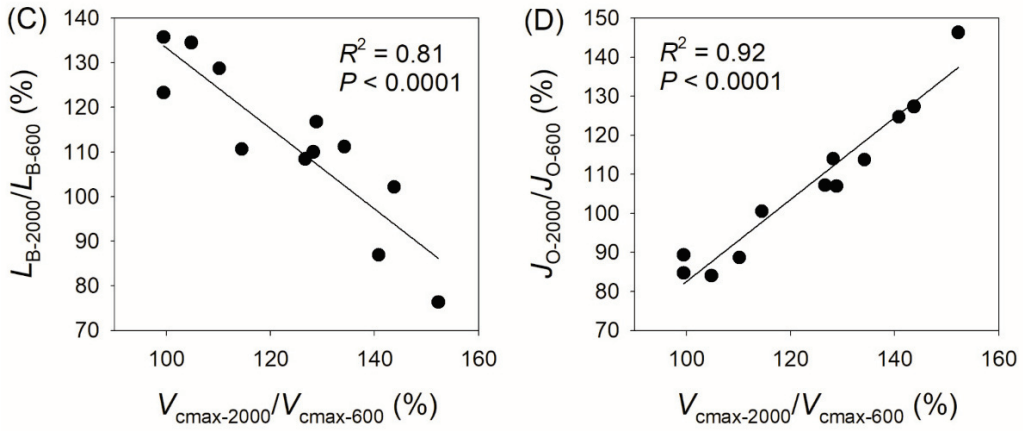


Figure 7. Relationships between $V_{cmax\text{-}2000}/V_{cmax\text{-}600}$, ETR_{2000}/ETR_{600}, $C_{c\text{-}2000}/C_{c\text{-}600}$, $L_{B\text{-}2000}/L_{B\text{-}600}$, and $J_{O\text{-}2000}/J_{O\text{-}600}$ among the twelve tree species. $V_{cmax\text{-}2000}/V_{cmax\text{-}600}$, the ratio of maximum velocity of Rubisco carboxylation (V_{cmax}) at 2000 μmol photons m^{-2} s^{-1} to that at 600 μmol photons m^{-2} s^{-1}; ETR_{2000}/ETR_{600}, the ratio of electron transport rate (ETR) at 2000 μmol photons m^{-2} s^{-1} to that at 600 μmol photons m^{-2} s^{-1}; $C_{c\text{-}2000}/C_{c\text{-}600}$, the ratio of chloroplast CO_2 concentration (C_c) at 2000 μmol photons m^{-2} s^{-1} to that at 600 μmol photons m^{-2} s^{-1}; $L_{B\text{-}2000}/L_{B\text{-}600}$, the ratio of biochemical limitation (L_B) at 2000 μmol photons m^{-2} s^{-1} to that at 600 μmol photons m^{-2} s^{-1}; $J_{O\text{-}2000}/J_{O\text{-}600}$, the ratio of photorespiration (J_O) at 2000 μmol photons m^{-2} s^{-1} to that at 600 μmol photons m^{-2} s^{-1}. (**A**) relationship between ETR_{2000}/ETR_{600} and $V_{cmax\text{-}2000}/V_{cmax\text{-}600}$; (**B**) relationship between $C_{c\text{-}2000}/C_{c\text{-}600}$ and $V_{cmax\text{-}2000}/V_{cmax\text{-}600}$; (**C**) relationship between $L_{B\text{-}2000}/L_{B\text{-}600}$ and $V_{cmax\text{-}2000}/V_{cmax\text{-}600}$; (**D**) relationship between $J_{O\text{-}2000}/J_{O\text{-}600}$ and $V_{cmax\text{-}2000}/V_{cmax\text{-}600}$.

4. Discussion

The light intensity dependence of photosynthesis varies widely among different plants and is tightly related to plant growth and crop yield [11]. According to the C_3 photosynthesis model, the CO_2 assimilation rate (A_N) at a given incident light intensity can be limited by light energy (as indicated by ETR), diffusional CO_2 conductance (g_s and g_m), and V_{cmax} [18]. With increasing illumination from sub-saturating to saturating light, angiosperms typically display gradual increases in ETR and g_s, and g_m remains stable in some species but gradually increases in others [8,9,21,22]. However, the major factor affecting the light intensity dependence of A_N remains unclear.

In this study, we found that light intensity dependence of A_N, V_{cmax}, and ETR varied among the twelve studied tree species (Figures 1 and 2). Furthermore, the increase in A_N from sub-saturating to saturating light among the twelve studied tree species was tightly related to changes in V_{cmax} and ETR, with no significant correlation to changes in g_s and g_m (Figures 4 and 5). Therefore, variation in the light intensity dependence of A_N among species is primarily determined by biochemical capacity rather than diffusional conductance. Compared with sub-saturating light, the increase in V_{cmax} under saturating light suggests an elevation in the Rubisco activation state [31], allowing for increases in Rubisco carboxylation and oxygenation. The ETR-dependent regeneration rates of ATP and NADPH are mainly determined by their consumption rates, which in turn are influenced by primary metabolism, including CO_2 assimilation and photorespiration [32–34]. When CO_2 assimilation is restricted, the inactivation of chloroplast ATP synthase results in an increase in proton gradient (ΔpH) across the thylakoid membranes, which slows down the electron flow at cytochrome b_6/f complex [32,35]. Therefore, the coordination between V_{cmax} and ETR tightly determines the light intensity dependence of A_N.

The biological significance of V_{cmax} in the light response of A_N aligns with the general understanding that V_{cmax} is an energy-dependent process. For example, V_{cmax} gradually increases upon transition from low to high light, imposing a significant on A_N [22,36]. With increasing maximum V_{cmax}, the time required to reach 95% of the maximum V_{cmax} during light induction also gradually increases [37]. In *Arabidopsis thaliana*, the value of V_{cmax} at 1200 μmol photons m^{-2} s^{-1} is 2-fold higher than that at 100 μmol photons m^{-2} s^{-1} [22]. Consistently, we found that V_{cmax} at 600 μmol photons m^{-2} s^{-1} was substantially higher than that at 400 μmol photons m^{-2} s^{-1} in the twelve tree species (Figure 2). Furthermore, as $V_{cmax\text{-}2000}/V_{cmax\text{-}400}$ and $V_{cmax\text{-}2000}/V_{cmax\text{-}600}$ increased, ETR_{2000}/ETR_{400} and ETR_{2000}/ETR_{600} also increased simultaneously (Figures 6 and 7), suggesting that ETR provides the essential energy for the increase in V_{cmax} through Rubisco activation.

Accompanying the increase in V_{cmax} under saturating light, the value of C_c decreased (Figures 6 and 7), resulting in an inevitable increase in the rate of Rubisco oxygenation (photorespiration). Photorespiration begins with the oxygenation of RuBP catalyzed by Rubisco, producing 2-phosphoglycolate (2-PG). Given that 2-PG inhibits central enzymes in the Calvin–Benson cycle and glycolysis, it must be converted into glycerate-3-P through the photorespiratory pathway. This process requires additional ATP and NADPH produced by ETR. Therefore, $J_{O\text{-}2000}/J_{O\text{-}400}$ and $J_{O\text{-}2000}/J_{O\text{-}600}$ positively increased with the increases in $V_{cmax\text{-}2000}/V_{cmax\text{-}400}$ and $V_{cmax\text{-}2000}/V_{cmax\text{-}600}$ (Figures 6 and 7). Under conditions of high V_{cmax}, the rate of RuBP oxygenation was inevitably elevated in normal air. Such enhancement of photorespiration accelerates the consumption rate of ATP and NADPH. This process not only prevents substrate limitation of chloroplast ATP synthase but also favors electron transfer from PSI to $NADP^+$ [38,39]. Therefore, photorespiration participates in the light intensity dependence of V_{cmax} and ETR.

Considering the strong effect of V_{cmax} on the light intensity dependence of A_N, it is surprising that the light intensity dependence of V_{cmax} varies among different species (Figure 2). We found that the values of $V_{cmax\text{-}2000}/V_{cmax\text{-}600}$ and $A_{N\text{-}2000}/A_{N\text{-}600}$ were positively correlated with the steady-state V_{cmax} at 2000 μmol photons m^{-2} s^{-1} (Figure 8). As a result, the light intensity dependence of V_{cmax} and A_N is largely determined by the maximum capacity of V_{cmax}. In plants with low V_{cmax} capacity, such as *Chaenomeles cathayensis*, V_{cmax} can reach its maximum value at 600 μmol photons m^{-2} s^{-1} (Figure 2). By comparison, in plants with high V_{cmax} capacity, such as *Alnus nepalensis*, V_{cmax} saturates at 1500 μmol photons m^{-2} s^{-1} (Figure 2). In wild-type plants, the maximum value of leaf V_{cmax} is tightly related to leaf Rubisco content or leaf nitrogen content [5,40,41]. Therefore, variation in the light intensity dependence of V_{cmax} and A_N among tree species may be determined by leaf Rubisco content or leaf nitrogen content.

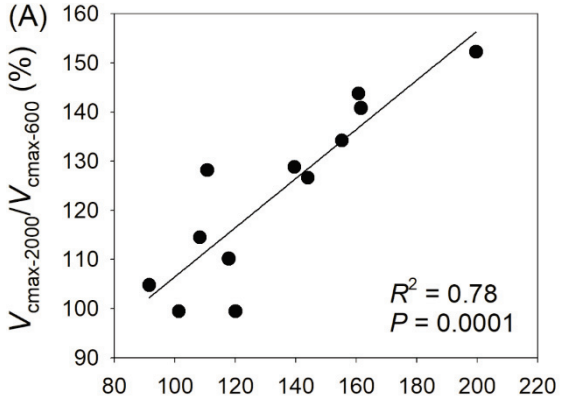


Figure 8. *Cont*.

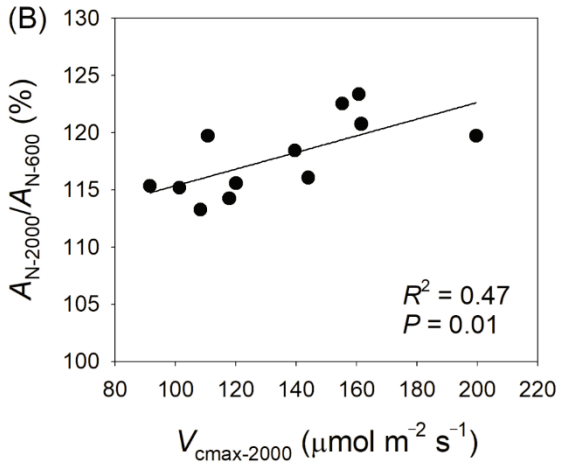


Figure 8. Relationships between $V_{cmax\text{-}2000}/V_{cmax\text{-}600}$, $A_{N\text{-}2000}/A_{N\text{-}600}$, and $V_{cmax\text{-}2000}$ among the twelve tree species. $V_{cmax\text{-}2000}/V_{cmax\text{-}600}$, the ratio of maximum velocity of Rubisco carboxylation (V_{cmax}) at 2000 μmol photons m^{-2} s^{-1} to that at 600 μmol photons m^{-2} s^{-1}; $A_{N\text{-}2000}/A_{N600}$, the ratio of net CO_2 assimilation rate (A_N) at 2000 μmol photons m^{-2} s^{-1} to that at 600 μmol photons m^{-2} s^{-1}; $V_{cmax\text{-}2000}$, the value of V_{cmax} at 2000 μmol photons m^{-2} s^{-1}. (**A**) relationship between $V_{cmax\text{-}2000}/V_{cmax\text{-}600}$ and $V_{cmax\text{-}2000}$; (**B**) relationship between $A_{N\text{-}2000}/A_{N\text{-}600}$ and $V_{cmax\text{-}2000}$.

5. Conclusions

We document that the light intensity dependence of A_N is more related to the light response of V_{cmax} rather than the light response of g_s and g_m. Furthermore, the light response of V_{cmax} is in turn influenced by its maximum capacity. Therefore, the maximum V_{cmax} plays a significant role in determining the light intensity dependence of A_N. We propose that increasing the maximum V_{cmax} or enhancing the nitrogen distribution into Rubisco has the potential to improve A_N under sub-saturating and saturating light conditions. This strategy provides insight into crop improvement.

Author Contributions: Conceptualization, W.H. and J.C.; Methodology, X.W., J.C. and W.H.; Software, X.W. and W.H.; Validation, X.W.; Formal analysis, W.H.; Investigation, X.W., Q.S. and N.L.; Resources, J.C.; Data curation, X.W.; Writing—original draft, W.H.; Project administration, W.H.; Funding acquisition, W.H. All authors have read and agreed to the published version of the manuscript.

Funding: This work was supported by the Major Science and Technology Projects in Yunnan Province (202202AE090012), by the National Natural Science Foundation of China (31971412, 32171505), and by West Light Foundation of the Chinese Academy of Sciences.

Data Availability Statement: The data presented in this study are available on request from the corresponding author. Data available on request due to privacy.

Conflicts of Interest: The authors declare no conflicts of interest.

References

1. Carriquí, M.; Cabrera, H.M.; Conesa, M.; Coopman, R.E.; Douthe, C.; Gago, J.; Gallé, A.; Galmés, J.; Ribas-Carbo, M.; Tomás, M.; et al. Diffusional Limitations Explain the Lower Photosynthetic Capacity of Ferns as Compared with Angiosperms in a Common Garden Study. *Plant Cell Environ.* **2015**, *38*, 448–460. [CrossRef] [PubMed]
2. Gago, J.; Daloso, D.; Figueroa, C.M.; Flexas, J.; Fernie, A.R.; Nikoloski, Z. Relationships of Leaf Net Photosynthesis, Stomatal Conductance, and Mesophyll Conductance to Primary Plant Metabolism: A Multi-Species Meta-Analysis Approach. *Plant Physiol.* **2016**, *171*, 265–279. [CrossRef] [PubMed]
3. Peguero-Pina, J.J.; Sisó, S.; Flexas, J.; Galmés, J.; García-Nogales, A.; Niinemets, Ü.; Sancho-Knapik, D.; Saz, M.Á.; Gil-Pelegrín, E. Cell-Level Anatomical Characteristics Explain High Mesophyll Conductance and Photosynthetic Capacity in Sclerophyllous Mediterranean Oaks. *New Phytol.* **2017**, *214*, 585–596. [CrossRef] [PubMed]

4. Sun, H.; Zhang, S.B.; Peguero-Pina, J.J.; Huang, W. Cell-Anatomical and Physiological Mechanisms Underlying the Faster Carbon Gain of Deciduous Trees Relative to Evergreen Trees. *Environ. Exp. Bot.* **2023**, *209*, 105286. [CrossRef]
5. Shi, Q.; He, B.; Knauer, J.; Peguero-Pina, J.J.; Zhang, S.-B.; Huang, W. Leaf Nutrient Basis for the Differentiation of Photosynthetic Traits between Subtropical Evergreen and Deciduous Trees. *Plant Physiol.* **2025**, *197*, kiae566. [CrossRef]
6. Pearcy, R.W. Sunflecks and Photosynthesis in Plant Canopies. *Annu. Rev. Plant Physiol. Plant Mol. Biol.* **1990**, *41*, 421–453. [CrossRef]
7. Pearcy, R.W.; Krall, J.P.; Sassenrath-Cole, G.F. Photosynthesis in Fluctuating Light Environments. In *Photosynthesis and the Environment*; Kluwer Academic Publishers: Dordrecht, The Netherlands, 1996; pp. 321–346.
8. Yang, Y.-J.; Hu, H.; Huang, W. The Light Dependence of Mesophyll Conductance and Relative Limitations on Photosynthesis in Evergreen Sclerophyllous Rhododendron Species. *Plants* **2020**, *9*, 1536. [CrossRef]
9. Xiong, D.; Douthe, C.; Flexas, J. Differential Coordination of Stomatal Conductance, Mesophyll Conductance, and Leaf Hydraulic Conductance in Response to Changing Light across Species. *Plant Cell Environ.* **2018**, *41*, 436–450. [CrossRef]
10. Yamori, W.; Evans, J.R.; Von Caemmerer, S. Effects of Growth and Measurement Light Intensities on Temperature Dependence of CO_2 Assimilation Rate in Tobacco Leaves. *Plant Cell Environ.* **2010**, *33*, 332–343. [CrossRef]
11. Long, S.P.; Taylor, S.H.; Burgess, S.J.; Carmo-Silva, E.; Lawson, T.; De Souza, A.P.; Leonelli, L.; Wang, Y. Into the Shadows and Back into Sunlight: Photosynthesis in Fluctuating Light. *Annu. Rev. Plant Biol.* **2022**, *73*, 617–648. [CrossRef]
12. Chang, W.; Zhang, S.B.; Li, S.Y.; Hu, H. Ecophysiological Significance of Leaf Traits in Cypripedium and Paphiopedilum. *Physiol. Plant.* **2011**, *141*, 30–39. [CrossRef] [PubMed]
13. Zhang, W.; Huang, W.; Zhang, S.-B. The Study of a Determinate Growth Orchid Highlights the Role of New Leaf Production in Photosynthetic Light Acclimation. *Plant Ecol.* **2017**, *218*, 997–1008. [CrossRef]
14. Zeng, Z.-L.; Wang, X.-Q.; Zhang, S.-B.; Huang, W. Mesophyll Conductance Limits Photosynthesis in Fluctuating Light under Combined Drought and Heat Stresses. *Plant Physiol.* **2024**, *194*, 1498–1511. [CrossRef] [PubMed]
15. Grassi, G.; Magnani, F. Stomatal, Mesophyll Conductance and Biochemical Limitations to Photosynthesis as Affected by Drought and Leaf Ontogeny in Ash and Oak Trees. *Plant Cell Environ.* **2005**, *28*, 834–849. [CrossRef]
16. Yamori, W.; Sakata, N.; Suzuki, Y.; Shikanai, T.; Makino, A. Cyclic Electron Flow around Photosystem I via Chloroplast NAD(P)H Dehydrogenase (NDH) Complex Performs a Significant Physiological Role during Photosynthesis and Plant Growth at Low Temperature in Rice. *Plant J.* **2011**, *68*, 966–976. [CrossRef]
17. Yamori, W.; Nagai, T.; Makino, A. The Rate-Limiting Step for CO_2 Assimilation at Different Temperatures Is Influenced by the Leaf Nitrogen Content in Several C_3 Crop Species. *Plant Cell Environ.* **2011**, *34*, 764–777. [CrossRef]
18. Farquhar, G.D.; von Caemmerer, S.; Berry, J.A. A Biochemical Model of Photosynthetic CO_2 Assimilation in Leaves of C_3 Species. *Planta* **1980**, *149*, 78–90. [CrossRef]
19. Zhu, X.-G.; Long, S.P.; Ort, D.R. Improving Photosynthetic Efficiency for Greater Yield. *Annu. Rev. Plant Biol.* **2010**, *61*, 235–261. [CrossRef]
20. Long, S.P.; Bernacchi, C.J. Gas Exchange Measurements, What Can They Tell Us about the Underlying Limitations to Photosynthesis? Procedures and Sources of Error. *J. Exp. Bot.* **2003**, *54*, 2393–2401. [CrossRef]
21. Yamori, W.; Kusumi, K.; Iba, K.; Terashima, I. Increased Stomatal Conductance Induces Rapid Changes to Photosynthetic Rate in Response to Naturally Fluctuating Light Conditions in Rice. *Plant. Cell Environ.* **2020**, *43*, 1230–1240. [CrossRef]
22. Liu, T.; Barbour, M.M.; Yu, D.; Rao, S.; Song, X. Mesophyll Conductance Exerts a Significant Limitation on Photosynthesis during Light Induction. *New Phytol.* **2022**, *233*, 360–372. [CrossRef] [PubMed]
23. Bunce, J.A. Light Dependence of Carboxylation Capacity for C_3 Photosynthesis Models. *Photosynthetica* **2016**, *54*, 484–490. [CrossRef]
24. Loriaux, S.D.; Avenson, T.J.; Welles, J.M.; Mcdermitt, D.K.; Eckles, R.D.; Riensche, B.; Genty, B. Closing in on Maximum Yield of Chlorophyll Fluorescence Using a Single Multiphase Flash of Sub-Saturating Intensity. *Plant Cell Environ.* **2013**, *36*, 1755–1770. [CrossRef] [PubMed]
25. Krall, J.P.; Edwards, G.E. Relationship between Photosystem II Activity and CO_2 Fixation in Leaves. *Physiol. Plant.* **1992**, *86*, 180–187. [CrossRef]
26. Genty, B.; Briantais, J.-M.; Baker, N.R. The Relationship between the Quantum Yield of Photosynthetic Electron Transport and Quenching of Chlorophyll Fluorescence. *Biochim. Biophys. Acta-Gen. Subj.* **1989**, *990*, 87–92. [CrossRef]
27. Harley, P.C.; Loreto, F.; Di Marco, G.; Sharkey, T.D. Theoretical Considerations When Estimating the Mesophyll Conductance to CO_2 Flux by Analysis of the Response of Photosynthesis to CO_2. *Plant Physiol.* **1992**, *98*, 1429–1436. [CrossRef]
28. Flexas, J.; Ribas-Carbó, M.; Diaz-Espejo, A.; Galmés, J.; Medrano, H. Mesophyll Conductance to CO_2: Current Knowledge and Future Prospects. *Plant. Cell Environ.* **2008**, *31*, 602–621. [CrossRef]
29. De Kauwe, M.G.; Lin, Y.S.; Wright, I.J.; Medlyn, B.E.; Crous, K.Y.; Ellsworth, D.S.; Maire, V.; Prentice, I.C.; Atkin, O.K.; Rogers, A.; et al. A Test of the "one-Point Method" for Estimating Maximum Carboxylation Capacity from Field-Measured, Light-Saturated Photosynthesis. *New Phytol.* **2016**, *210*, 1130–1144. [CrossRef]

30. Valentini, R.; Epron, D.; Angelis, P.D.E.; Matteucci, G.; Dreyer, E. In Situ Estimation of Net CO_2 Assimilation, Photosynthetic Electron Flow and Photorespiration in Turkey Oak (*Q. cerris* L.) Leaves: Diurnal Cycles under Different Levels of Water Supply. *Plant Cell Environ.* **1995**, *18*, 631–640. [CrossRef]
31. Yamori, W.; Masumoto, C.; Fukayama, H.; Makino, A. Rubisco Activase Is a Key Regulator of Non-Steady-State Photosynthesis at Any Leaf Temperature and, to a Lesser Extent, of Steady-State Photosynthesis at High Temperature. *Plant J.* **2012**, *71*, 871–880. [CrossRef]
32. Kanazawa, A.; Kramer, D.M. In Vivo Modulation of Nonphotochemical Exciton Quenching (NPQ) by Regulation of the Chloroplast ATP Synthase. *Proc. Natl. Acad. Sci. USA* **2002**, *99*, 12789–12794. [CrossRef] [PubMed]
33. Rott, M.; Martins, N.F.; Thiele, W.; Lein, W.; Bock, R.; Kramer, D.M.; Schöttler, M.A. ATP Synthase Repression in Tobacco Restricts Photosynthetic Electron Transport, CO_2 Assimilation, and Plant Growth by Overacidification of the Thylakoid Lumen. *Plant Cell* **2011**, *23*, 304–321. [CrossRef] [PubMed]
34. Murata, N.; Takahashi, S.; Nishiyama, Y.; Allakhverdiev, S.I. Photoinhibition of Photosystem II under Environmental Stress. *Biochim. Biophys. Acta-Bioenerg.* **2007**, *1767*, 414–421. [CrossRef]
35. Zivcak, M.; Kalaji, H.M.; Shao, H.B.; Olsovska, K.; Brestic, M. Photosynthetic Proton and Electron Transport in Wheat Leaves under Prolonged Moderate Drought Stress. *J. Photochem. Photobiol. B Biol.* **2014**, *137*, 107–115. [CrossRef]
36. Sakoda, K.; Yamori, W.; Groszmann, M.; Evans, J.R. Stomatal, Mesophyll Conductance, and Biochemical Limitations to Photosynthesis during Induction. *Plant Physiol.* **2021**, *185*, 146–160. [CrossRef]
37. Salter, W.T.; Merchant, A.M.; Richards, R.A.; Trethowan, R.; Buckley, T.N. Rate of Photosynthetic Induction in Fluctuating Light Varies Widely among Genotypes of Wheat. *J. Exp. Bot.* **2019**, *70*, 2787–2796. [CrossRef]
38. Smith, K.; Strand, D.D.; Kramer, D.M.; Walker, B.J. The Role of Photorespiration in Preventing Feedback Regulation via ATP Synthase in Nicotiana Tabacum. *Plant. Cell Environ.* **2024**, *47*, 416–428. [CrossRef]
39. Walker, B.J.; VanLoocke, A.; Bernacchi, C.J.; Ort, D.R. The Costs of Photorespiration to Food Production Now and in the Future. *Annu. Rev. Plant Biol.* **2016**, *67*, 107–129. [CrossRef]
40. Yamori, W.; Takahashi, S.; Makino, A.; Price, G.D.; Badger, M.R.; von Caemmerer, S. The Roles of ATP Synthase and the Cytochrome B6/f Complexes in Limiting Chloroplast Electron Transport and Determining Photosynthetic Capacity. *Plant Physiol.* **2011**, *155*, 956–962. [CrossRef]
41. Wang, X.-Q.; Sun, H.; Zeng, Z.-L.; Huang, W. Within-Branch Photosynthetic Gradients Are More Related to the Coordinated Investments of Nitrogen and Water than Leaf Mass per Area. *Plant Physiol. Biochem.* **2023**, *198*, 107681. [CrossRef]

Disclaimer/Publisher's Note: The statements, opinions and data contained in all publications are solely those of the individual author(s) and contributor(s) and not of MDPI and/or the editor(s). MDPI and/or the editor(s) disclaim responsibility for any injury to people or property resulting from any ideas, methods, instructions or products referred to in the content.

plants

MDPI

Article

Effect of LED Irradiation with Different Red-to-Blue Light Ratios on Growth and Functional Compound Accumulations in Spinach (*Spinacia oleracea* L.) Accessions and Wild Relatives

Tri Manh Le [1], Yuki Sago [1], Yasuomi Ibaraki [1], Kazuhiro Harada [2], Kenta Arai [2], Yuichi Ishizaki [2], Hitoshi Aoki [2], Mostafa Abdelrahman [3], Chris Kik [4], Rob van Treuren [4], Theo van Hintum [4] and Masayoshi Shigyo [1,*]

[1] Graduate School of Sciences and Technology for Innovation, Yamaguchi University, Yamaguchi 753-8511, Japan; e005wfv@yamaguchi-u.ac.jp
[2] Research and Development Division, Nichirei Foods Inc., Chiba 261-0002, Japan
[3] Institute of Genomics for Crop Abiotic Stress Tolerance, Department Plant and Soil Science, Texas Tech University, Lubbock, TX 79409, USA; mosabdel@ttu.edu
[4] Centre for Genetic Resources, The Netherlands, Wageningen University and Research, 6708 PB Wageningen, The Netherlands; theo.vanhintum@wur.nl
* Correspondence: shigyo@yamaguchi-u.ac.jp

Abstract: The utilization of red and blue light-emitting diode (LED) lights for cultivating leafy vegetables in closed plant factories has increased in recent years. This study examined the growth and biosynthesis of functional compounds in twelve *Spinacia* accessions, including cultivars and wild relatives, under the irradiation of fluorescent light and three different red-to-blue LED light combinations (red:blue = 1:1, 1:3, and 3:1). Results showed that, except for the three examined Japanese cultivars, the fresh weight of most spinach accessions increased when red light comprised 50–75% of the light's spectral composition. This indicated the vital role of the red-light photoreceptor phytochrome in inducing plant growth. The contribution of blue-light photoreceptors was also notable. Significant variations in the accumulation of amino acids and sugars were observed in specific accessions. The effects of spectral photons on the primary metabolite pathways were probably the leading causes of these variations. Some critical enzymes in the Gamma-aminobutyric acid (GABA) shunt cycle and the asparagine and glycolysis pathways were suggested as rate-limiting enzymes, which determined the biosynthesis of functional compounds. Among the examined *Spinacia* accessions, 'CGN09429', 'CGN09511', and the wild *S. turkestanica* 'CGN25013' were identified as potential breeding materials, while red:blue = 1:1 was determined as the optimal red-to-blue ratio for spinach growth in a closed-cultivation system.

Keywords: plant factory; plant growth; chlorophyll; carotenoid; sugar content; amino acid content

1. Introduction

The growth and development of plants are significantly influenced by red and blue light, which play critical roles in photosynthesis and photomorphogenesis [1]. Red light is particularly effective in promoting several light-dependent reactions in photosynthesis and plays a key role in processes such as stem elongation, leaf expansion, and flowering. Blue light, on the other hand, affects stomatal conductance, phototropism, and the relocation of chloroplasts under certain conditions. These two types of light are absorbed by chlorophyll and carotenoids, which have maximum absorption peaks at specific wavelengths. The emergence of light-emitting diodes (LEDs) as a promising light source for horticulture

production, offering selectable and narrow-spectrum emission, high energy-usage efficiency, and a long consumption time, opens up new possibilities for plant cultivation and nutrition research.

Spinach (*Spinacia oleracea* L.) is widely regarded as an important food crop due to its rich nutritional composition, which includes vitamins and minerals, as well as phytochemicals and bioactive compounds that promote health benefits beyond essential nutrition [2,3]. Based on their geographical origin, *S. oleracea* can be divided into two main groups: the eastern group and the western group [4]. Eastern cultivars feature narrow, hastate leaves that are smooth and often have an appetizing taste, but they are prone to bolting. In contrast, western cultivars have rounder leaves that are enlarged and exhibit a savoy texture, with a delayed tendency to bolt [5]. Additionally, the genus *Spinacia* includes two wild species, *S. turkestanica* and *S. tetrandra*, that are morphologically close to *S. oleracea* [6]. These three species are considered to form the primary gene pool for spinach [7]. The wild species interbreed with cultivated spinach, providing crucial genetic resources for introducing novel traits to enhance spinach varieties, particularly for commercial cultivars intended for growth under artificial irradiation. Numerous studies have emphasized the impact of red and blue light on the growth of spinach. However, there are still divergent viewpoints. The shoot dry weight of spinach grown under sole blue light was recorded to be much lower than those grown under white and sole red light [8]. Some studies suggest that a decrease in the red-to-blue light ratio generally decreases plant biomass, leaf length, width, and number of leaves [9,10]. Additionally, the importance of additional blue light to enhance the growth of spinach has been emphasized [11]. Even though there are some reports about the effects of different spectral compositions on the carotenoids or phenolic compounds in spinach [11–13], other functional compounds, such as amino acids or sugar content, have not been exhaustively studied. As amino acids and sugars play vital roles in plant physiology and contribute to the taste of leafy vegetables, it becomes possible to control the growth and taste of spinach for commercial production by applying suitable light conditions. Given the limited number of studies conducted and the fact that the focus of these studies on cultivated spinach has neglected the possibility that important genetic resources can be found in the two crossable wild relatives of spinach [14,15], further research on the suitable red and blue ratio for spinach cultivation is crucial. Therefore, this study aims to (1) examine how different combinations of red (R) and blue (B) LEDs impact the growth, phytopigments, amino acid content, and sugar content of various spinach accessions and wild relatives in a closed production system; and (2) determine the optimal red-to-blue ratio for each accession to guide further studies.

2. Results

2.1. Growth Features

The Japanese spinach cultivar 'Solomon' and 'CGN25120' exhibited the highest fresh weights (Figure S1). In contrast, the wild accession *S. tetrandra* 'CGN25085' showed the lowest yield. Among the CGN accessions, light conditions considerably influenced the fresh weights of spinach in both eastern and western groups (Figure 1). In general, CGN spinach achieved higher yields under RB11 and RB31 conditions. Specifically, the fresh weights of 'CGN09513' and 'CGN09643' were highest under RB31, while 'CGN09511' achieved its maximum fresh weight under RB11 (Figure 1). Other CGN accessions did not show significant differences between the two ratios. Meanwhile, a decline in fresh weight under strong blue light in RB13 was observed in eight of nine CGN accessions. The fresh weight of 'CGN09429', 'CGN09511', and 'CGN25258' under the RB13 were lower than those under the control condition. Interestingly, 'TSP515' was the only Japanese cultivar affected by changes in the red:blue ratio, with its fresh weight decreasing under both RB31 and RB11

conditions. Although trends in dry weight followed those of fresh weight (Figure 1), the dry matter ratios of certain accessions, such as 'CGN25258' and 'Solomon', significantly increased with greater blue light intensity. Concerning the leaf area indexes, leaf area was increased under the irradiation of RB31 or RB11 in all nine CGN accessions and 'Solomon' (Figure 2). 'TSP515' exhibited he largest leaf area under RB13, while there was no significant change in 'Bentenmaru'. The specific leaf area was lowest under the RB13 condition in ten accessions, including all CGN accessions and 'Solomon'. The impact of light on the specific leaf area was not significant in 'Bentenmaru' and 'TSP515'.

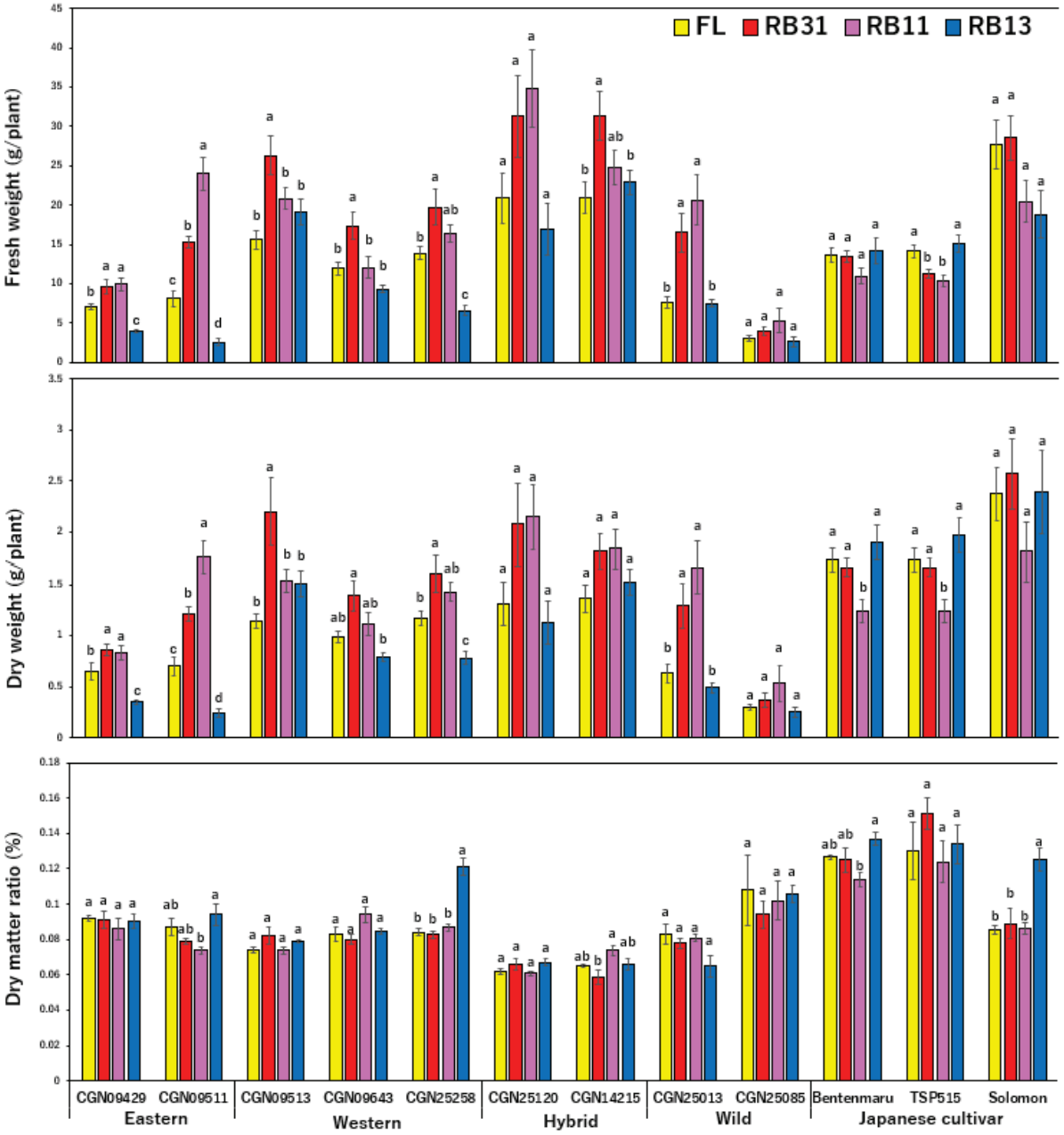


Figure 1. Effects of different light conditions on the growth features of spinach accessions and wild relatives (n = 6–10). Error bars represent the standard error (±SE). A one-way ANOVA was performed to determine significant differences in the effect of light on each accession. Different letters denote significant differences within one single accession by the post-hoc SNK test ($p < 0.05$).

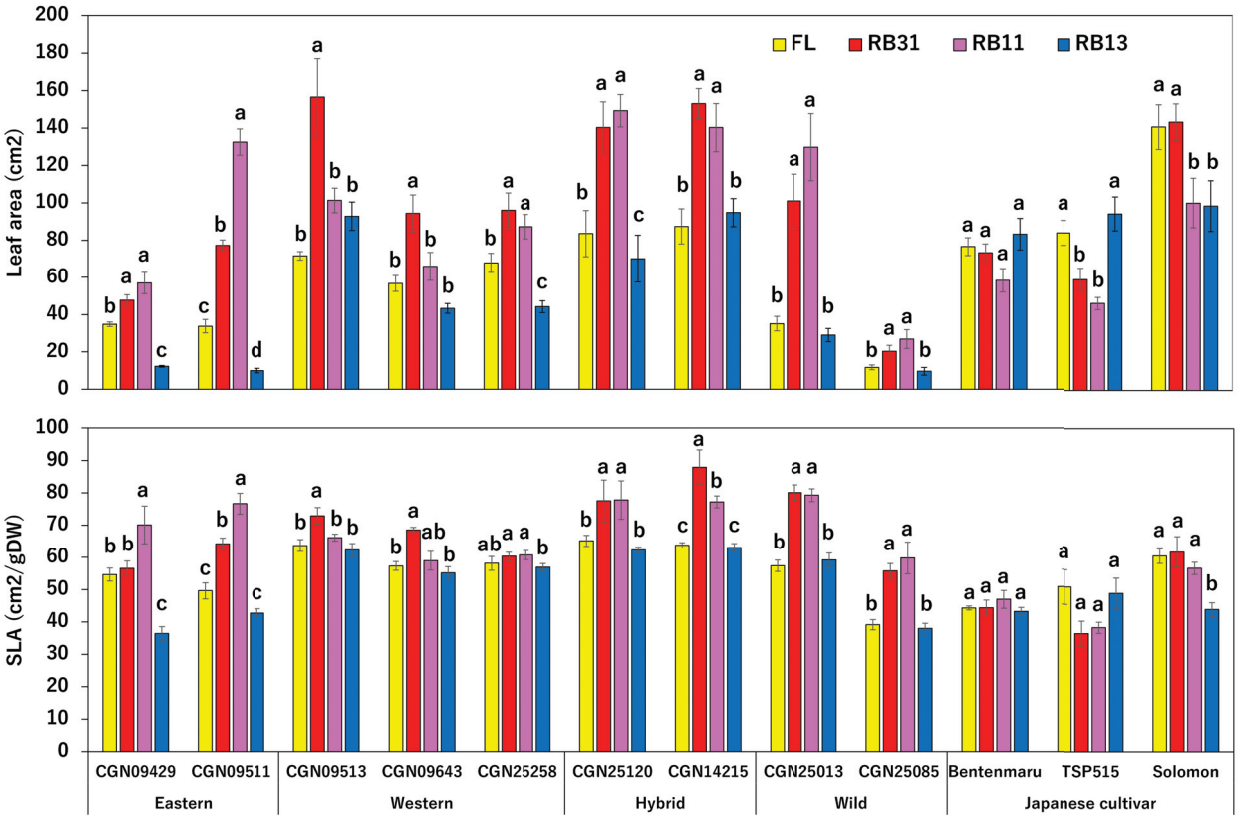


Figure 2. Effects of different light conditions on the leaf area and the specific leaf area (SLA) of spinach accessions and wild relatives (n = 3). Error bars represent the standard error (±SE). A one-way ANOVA was performed to determine significant differences in the effect of light on each accession. Different letters denote significant differences within one single accession by the post-hoc SNK test ($p < 0.05$).

2.2. Phytopigment Content

The concentrations of chlorophyll a and chlorophyll b were highest in the eastern accessions and 'CGN14215' under the RB13 condition (Figure 3 and Table S1). The two Japanese cultivars, 'TSP515' and 'Bentenmaru', recorded the highest values for both types of chlorophyll under RB11 and RB31, respectively. In contrast, the chlorophyll concentrations in 'CGN09643', 'CGN25013', and 'CGN25085' were the lowest under the RB31 irradiation condition. There was no significant variation in the chlorophyll content of 'CGN09513', 'CGN25258', 'CGN25120', and 'Solomon'.

Regarding carotenoid concentrations, both genetic factors (accession) and environmental factors (light condition) had a significant impact on total carotenoid content per unit area (Figure 3). However, upon closer examination, only the concentration of β-carotene was affected by both factors and their interaction. Additionally, while genetic factors, along with their interaction with environmental factors, significantly influenced the concentrations of lutein and violaxanthin, the level of neoxanthin was affected solely by genetic factors. Notably, the RB13 condition enhanced the concentrations of β-carotene and lutein in the eastern accessions, including 'CGN09429' and 'CGN09511' (Figure 3 and Table S1). The RB11 condition significantly reduced the concentrations of β-carotene, lutein, and violaxanthin in 'CGN14215'. In contrast, the RB11 condition notably increased the concentrations of lutein and violaxanthin in 'TSP515'. Among the three red-to-blue ratios, both RB31 and RB11 significantly enhanced the concentration of lutein and violaxanthin per unit area, whereas RB13 had the opposite effect compared to the control condition. Significant variation was not recorded in other accessions.

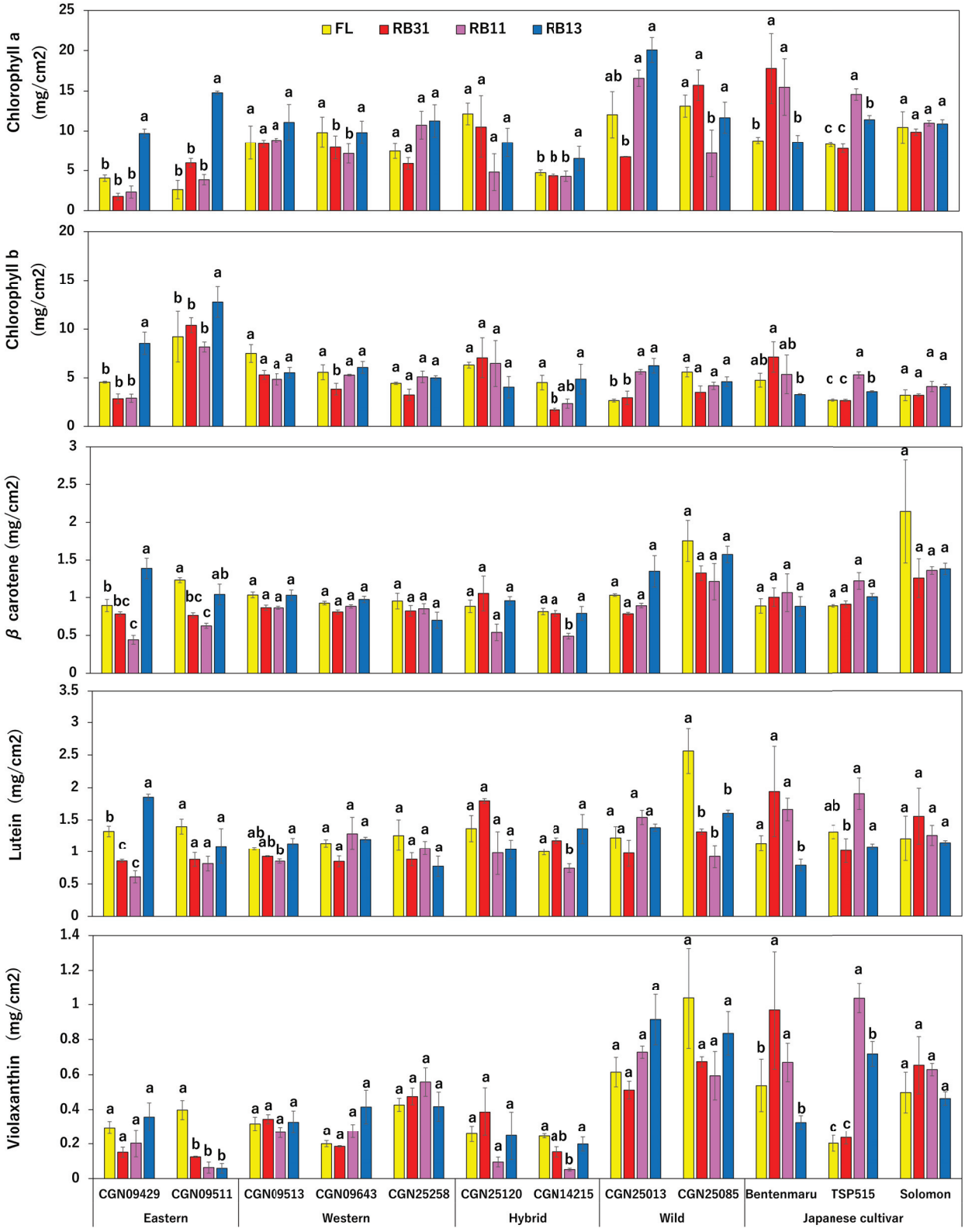


Figure 3. Effects of different light conditions on the phytopigment content of spinach accessions (n = 3). Error bars represent the standard error (±SE). A one-way ANOVA was performed to determine significant differences in the effect of light on each accession. Different letters denote significant differences within one single accession by the post-hoc SNK test ($p < 0.05$).

2.3. Sugar Content

Different groups with varying accessions exhibited diverse trends in sugar accumulation. Three Japanese cultivars displayed high levels of glucose and sucrose (Figure S3), whereas the wild accessions had a significantly lower sugar content than those of the other groups. The sugar concentrations in hybrid and wild accessions remained unchanged under the four examined treatments (Figure 4). In other accessions, RB31 and RB11 treatments tended to suppress glucose and sucrose content. Glucose levels were reduced in two Japanese cultivars, 'Bentenmaru' and 'TSP515', under RB11 irradiation. Additionally, RB11 decreased the sucrose concentration in 'CGN09429', 'CGN09511', 'CGN25258', and 'TSP515'. Conversely, RB13 increased the concentration of all sugars in 'CGN09511' and sucrose levels in 'CGN09429' and 'Solomon'.

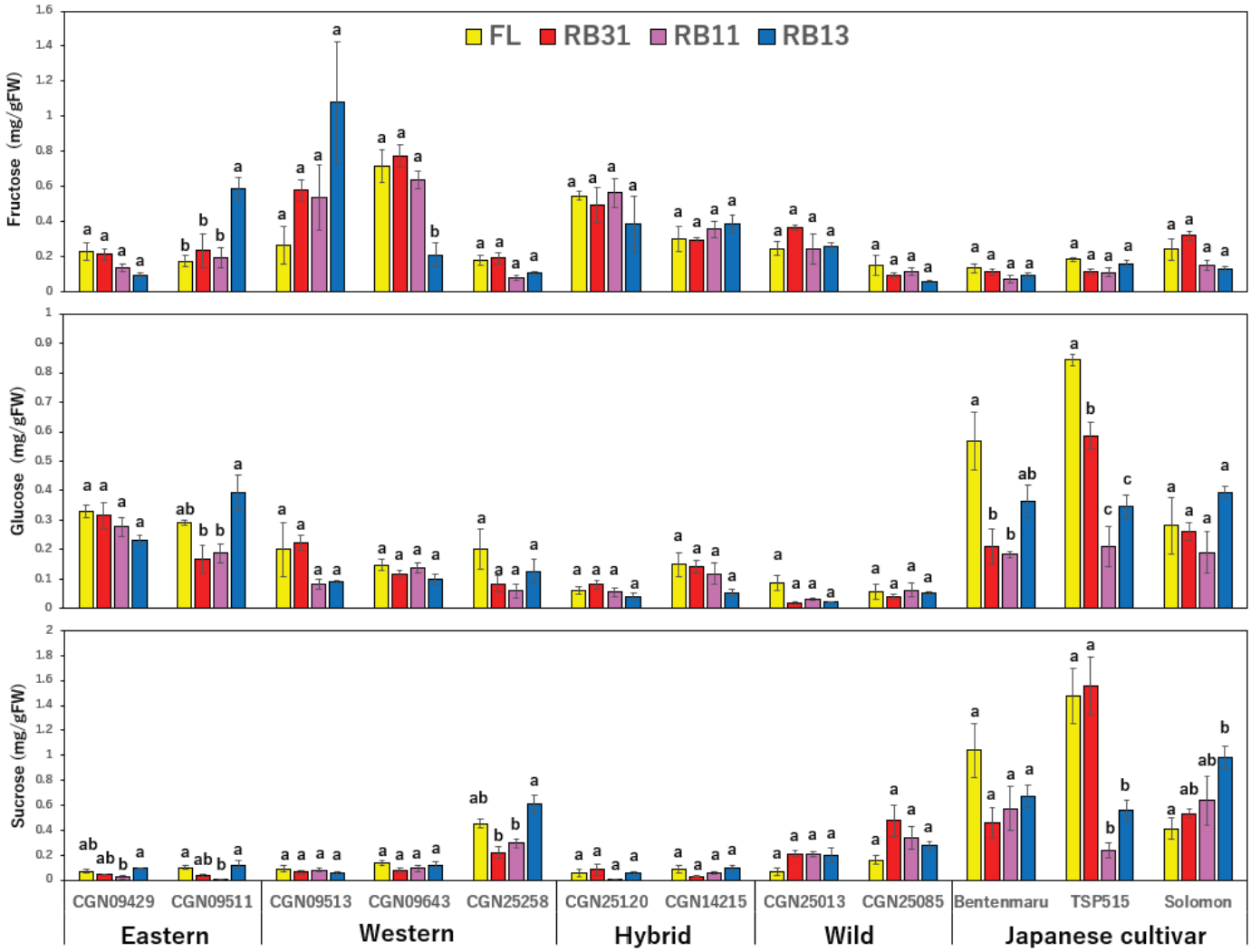


Figure 4. Effects of different light conditions on the sugar content of spinach accessions and wild relatives (n = 3). Error bars represent the standard error (±SE). The one-way ANOVA was performed to determine significant differences in the effect of light on each accession. Different letters denote significant differences within one single accession by the post-hoc SNK test ($p < 0.05$). FL: fluorescent irradiation; RB31: red/blue = 3/1; RB11: red/blue = 1/1; RB13: red/blue = 1/3.

2.4. Amino Acid Content

There were significant differences in the amino acid content among the twelve *Spinacia* accessions (Table S2). It was also indicated that changing red:blue ratios can modify the biosynthesis of amino acids in spinach. Remarkably, the impact of the interaction between

accession and light condition was significant in all examined amino acids, leading to the varying responses of accessions to specific light condition. Light conditions did not significantly affect the amino acid content in Japanese cultivars and wild species. However, in spinach accessions from the eastern group, the amino acid content was greatly influenced, particularly by the RB11 ratio. Irradiation with the RB11 ratio resulted in a notable increase in several amino acids, including glycine, isoleucine, lysine, phenylalanine, threonine, tyrosine, and valine. Additionally, the concentrations of histidine and proline increased in 'CGN09429', along with rises in alanine, asparagine, and GABA levels in 'CGN09511' (Figure 5). In contrast, aspartic acid and glutamine concentrations in 'CGN09511' were lowest under the RB11 ratio and highest under the RB13 ratio. The hybrid accessions showed trends similar to those in the eastern group, with RB11 enhancing the production of alanine, glycine, histidine, isoleucine, lysine, phenylalanine, threonine, and valine in 'CGN14215'. In 'CGN25120', all amino acids increased in concentration under RB11 irradiation, except for aspartic acid, glutamic acid, and glutamine (Figure 5). In the western accession group, only GABA concentrations rose with the RB31 ratio in 'CGN09513' and 'CGN09643'. On the other hand, 'CGN25258' showed the highest accumulation of several amino acids under irradiation with the RB13 ratio.

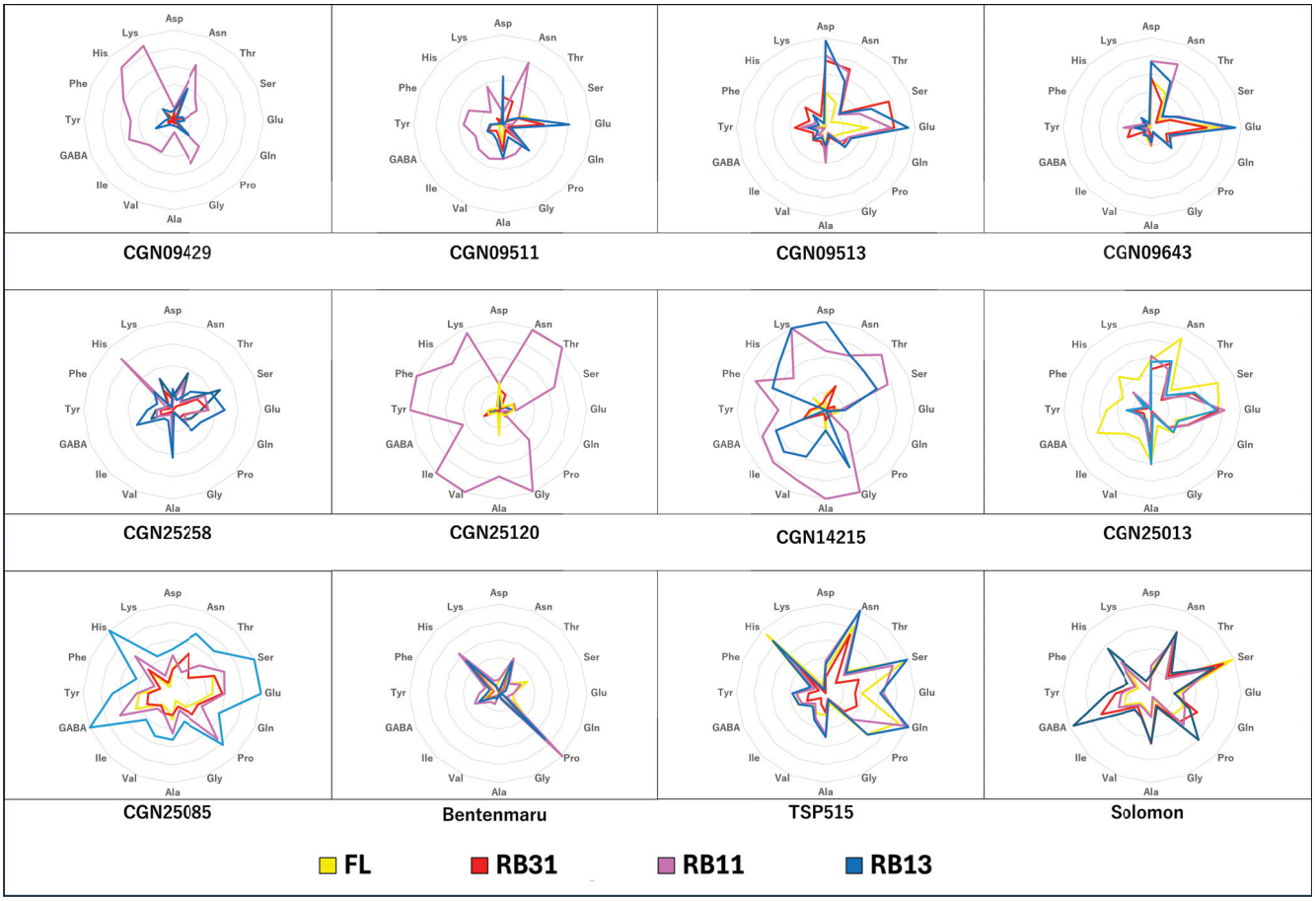


Figure 5. Changes in amino acid content in each spinach accession under different light conditions. FL: fluorescent irradiation; RB31: red/blue = 3/1; RB11: red/blue = 1/1; RB13: red/blue = 1/3. Asp: aspartic acid; Asn: asparagine; Thr: threonine; Ser: serine; Glu: glutamic acid; Gln: glutamine; Pro: proline; Gly: glycine; Ala: alanine; Val: valine; Ile: isoleucine; GABA: gama aminobutyric acid; Tyr: tyrosine; Phe: phenylalanine; His: histidine; Lys: lysine.

3. Discussion

3.1. Growth Features

The interaction between light conditions and each spinach accession reveals a complex and nuanced relationship, highlighting the significant role of genetic background in shaping responses to varying red:blue light ratios. Among the twelve accessions, cultivated varieties such as 'Solomon' and 'CGN25120' consistently exhibited higher fresh weights, demonstrating their superior adaptability to light conditions compared to the wild accession 'CGN25085', which showed the lowest yield across all treatments. Light conditions significantly influenced growth, with most CGN accessions achieving optimal fresh weights under RB11 and RB31, suggesting that balanced or red-dominated light spectra are generally favorable for spinach growth. For instance, 'CGN09513' and 'CGN09643' thrived under RB31, while 'CGN09511' performed best under RB11, indicating accession-specific optima for light conditions. These results align with the findings of prior studies [14,16], and can be explained by the widely recognized growth-promoting impact of red light [17]. Red light interacts with specific photoreceptors, known as phytochromes, which play a critical role in regulating plant development. Upon absorbing red photons, phytochrome molecules transition from their inactive Pr form to the active Pfr form, triggering the activation of genes responsible for cell expansion. This process promotes the development of new leaves, enhances light capture, and ultimately increases photosynthesis rates. Exceptions such as 'TSP515', a Japanese cultivar, showed reduced fresh weight under both RB31 and RB11, suggesting its unique sensitivity to changes in red:blue ratios.

On the other hand, strong blue light led to a decline in fresh weight in eight out of nine CGN accessions. Research has shown that while blue light has the potential to enhance photosynthetic efficiency per unit leaf area, it may also reduce overall radiation capture, thereby limiting plant growth and productivity when combined with red light, as observed in lettuce cultivation [18]. A reduction in radiation absorption and subsequent growth inhibition typically occur when blue light is combined with other wavelengths [19]. These different responses between plants grown under monochromatic blue light and those exposed to blue and red dichromatic light are attributed to complex phytochrome–cryptochrome interactions, which regulate gene expression, plant growth, and development [20]. Additionally, blue photons are partially absorbed by inactive (e.g., anthocyanin) and accessory (e.g., carotenoids) pigments that do not contribute to energy transfer to chlorophyll reaction centers, resulting in lower photosynthetic efficiency as compared to red photons [21]. Moreover, studies on single-leaf photosynthesis have demonstrated that blue photons are utilized less efficiently than red photons [22]. The consensus is that blue light primarily affects photosynthetic efficiency through photomorphogenesis, which was shown clearly in this study. Most accessions, including all CGN accessions and 'Solomon', showed decreased leaf area under RB13. The absorption of the blue light by the photoreceptors cryptochrome and phototropin usually causes a decrease in leaf area and stem elongation by inhibiting cell division and expansion [17,23,24]. The effect of blue light on leaf morphology was also reflected by the decrease in specific leaf area (SLA) value in ten *Spinacia* accessions under the RB13 condition, indicating thicker or denser leaves under high blue light.

These findings collectively demonstrate that the interaction between light conditions and accessions is highly accession-specific, with each genotype exhibiting distinct optima and sensitivities to light spectra. This underscores the importance of the relationship between light environments and the genetic background of each accession to maximize growth and productivity, particularly in controlled agricultural systems such as greenhouses or vertical farms.

3.2. Phytopigment Content

Chlorophylls and carotenoids are the two main phytopigments found in plants. They are essential for capturing light, which is crucial for the process of photosynthesis. Chlorophylls primarily absorb light from the red and blue regions of the spectrum, while carotenoids are particularly effective at absorbing blue and green light. Agarwal noted that total chlorophyll content, the chlorophyll a to chlorophyll b ratio, carotenoid content, and the chlorophyll to carotenoid ratio remained stable under red to blue (R:B) light ratios of 25:75, 50:50, and 75:25 [13]. When nitrogen was adequately supplied, various combinations of blue, red, and green light did not significantly affect the carotenoid and chlorophyll content in spinach [25]. However, in this study, we evaluated chlorophyll and carotenoid content in terms of concentration per unit area. The results indicated that phytopigments tended to accumulate at higher densities under a blue-dominant light source in certain accessions. This accumulation can be attributed to the lower specific leaf area (SLA) observed under the R:B ratio of 1:3, which resulted in thicker and more compact leaves, leading to a higher concentration of phytopigments on the leaf surface. This finding is supported by previous research on the impact of different doses of blue light on cucumber seedlings [26]. According to the ANOVA results, the contents of three carotenoids—lutein, neoxanthin, and violaxanthin—were not significantly affected by the light source. However, the levels of lutein and violaxanthin varied when considering the interaction between genetic factors and light sources, contributing to the overall variation in total carotenoid content.

The twelve *Spinacia* accessions exhibited different responses to varying red-to-blue light ratios. The eastern accessions, along with 'CGN14215', may have a genetic predisposition that allows them to optimize chlorophyll synthesis under high blue light conditions. In contrast, the Japanese cultivars ('TSP515' and 'Bentenmaru') displayed a preference for either balanced (RB11) or red-dominant (RB31) light, suggesting they are better adapted to environments with lower availability of blue light. Some accessions showed low chlorophyll content under RB31, which may indicate photo-inhibition or a reduction in chlorophyll synthesis when exposed to red-dominant light, a condition that is less efficient for producing chlorophyll b. Additionally, the reduction in carotenoid levels observed under RB11 in 'CGN14215' may reflect a stress response or a shift in pigment allocation in balanced light conditions. The lower carotenoid content noted under RB13 in some accessions could suggest a trade-off between light capture and photoprotection, since exposure to blue light can also lead to photo-inhibition if it is not properly balanced with red light.

3.3. Sugar Content

Cultivated accessions, particularly the three Japanese cultivars, exhibited higher levels of glucose and sucrose compared to wild accessions, underscoring their suitability for commercial use due to their enhanced sweetness. In contrast, wild accessions consistently showed lower sugar content, reflecting their genetic predisposition for reduced sweetness. The red:blue (R:B) ratios had a notable but accession-specific impact on sugar accumulation. While fructose content remained relatively stable across light treatments, the interaction between accession and light condition significantly influenced fructose, glucose, and

sucrose levels, indicating the importance of genetic background in shaping responses to light spectra.

Among the cultivated accessions, RB31 and RB11 generally suppressed glucose and sucrose content. For example, glucose levels decreased in the Japanese cultivars 'Bentenmaru' and 'TSP515' under RB11, while sucrose concentrations declined in 'CGN09429', 'CGN09511', 'CGN25258', and 'TSP515' under the same treatment. This suggests that balanced or red-dominated light conditions may inhibit sugar accumulation in certain accessions, possibly due to altered metabolic pathways or resource allocation under these spectra. In contrast, RB13, which emphasizes blue light, increased sugar content in specific accessions. For instance, 'CGN09511' showed elevated levels of all sugars under RB13, while 'CGN09429' and 'Solomon' exhibited higher sucrose concentrations. This indicates that blue light may stimulate sugar accumulation in some accessions, potentially by enhancing the activity of enzymes involved in carbohydrate metabolism, such as fructose biphosphate (FBP) enzymes [27,28]. These enzymes play a critical role in gluconeogenesis and are known to be regulated by light [29], which could explain the observed variations in fructose and sucrose levels under different light conditions.

3.4. Amino Acid Content

The biosynthesis of amino acids was notably modified by changes in red:blue light ratios, with the interaction between accession and light condition playing a critical role in shaping these responses. While light conditions did not significantly affect amino acid content in Japanese cultivars and wild species, accessions from the eastern and western groups, as well as hybrid accessions, exhibited pronounced changes in amino acid accumulation under specific light treatments. These findings highlight the complex interplay between genetic background and environmental factors in regulating amino acid metabolism.

The RB11 ratio had a particularly strong impact, significantly increasing the concentrations of several amino acids, including glycine, isoleucine, lysine, phenylalanine, threonine, tyrosine, and valine (Figure 6). 'CGN09429' showed elevated levels of histidine and proline under RB11, while 'CGN09511' exhibited increased alanine, asparagine, and GABA concentrations. However, 'CGN09511' also displayed contrasting responses, with aspartic acid and glutamine levels being lowest under RB11 and highest under RB13, suggesting that intense blue light may enhance the biosynthesis of these specific amino acids in this accession. Hybrid accession 'CGN25120' showed increased concentrations of nearly all amino acids under RB11, except for aspartic acid, glutamic acid, and glutamine, which were unaffected. In contrast, the western group exhibited more limited responses, with only GABA concentrations increasing under the RB31 ratio in 'CGN09513' and 'CGN09643'. Interestingly, 'CGN25258' accumulated the highest levels of several amino acids under RB13, indicating that this accession may have a unique metabolic adaptation to strong blue light.

The observed variations in amino acid content can be linked to the roles of key amino acids in metabolic pathways and flavor profiles. Aspartic acid, glutamic acid, GABA, and glutamine were identified as the most abundant amino acids in spinach, with glutamic acid and aspartic acid contributing to the savory flavor and playing critical roles in nitrogen metabolism. Glutamic acid, glutamine, and GABA are interconnected through the GABA shunt cycle, which is closely tied to the TCA cycle, a central pathway for energy production and growth [30,31]. Aspartic acid, on the other hand, serves as a key nitrogen source and is linked to the TCA cycle via its conversion to oxaloacetate [32]. The promotion of amino acid biosynthesis under RB11 and RB13 conditions suggests that these light ratios enhance the activity of metabolic pathways

involved in amino acid production. The differential responses of accessions to light conditions can be attributed to variations in the activation of key enzymes, such as glutamate dehydrogenase (GDH) and glutamate decarboxylase (GAD), which are involved in the biosynthesis of glutamic acid and GABA. In accessions like 'CGN09511' and 'CGN25258', intense blue light (RB13) may suppress the activity of these enzymes, reducing the production of succinic acid and α-ketoglutarate and thereby decreasing TCA cycle efficiency and growth. In contrast, accessions like 'CGN25120' and 'CGN14215' may possess metabolic adaptations that allow them to maintain or enhance amino acid biosynthesis under RB11 and RB13 without compromising growth.

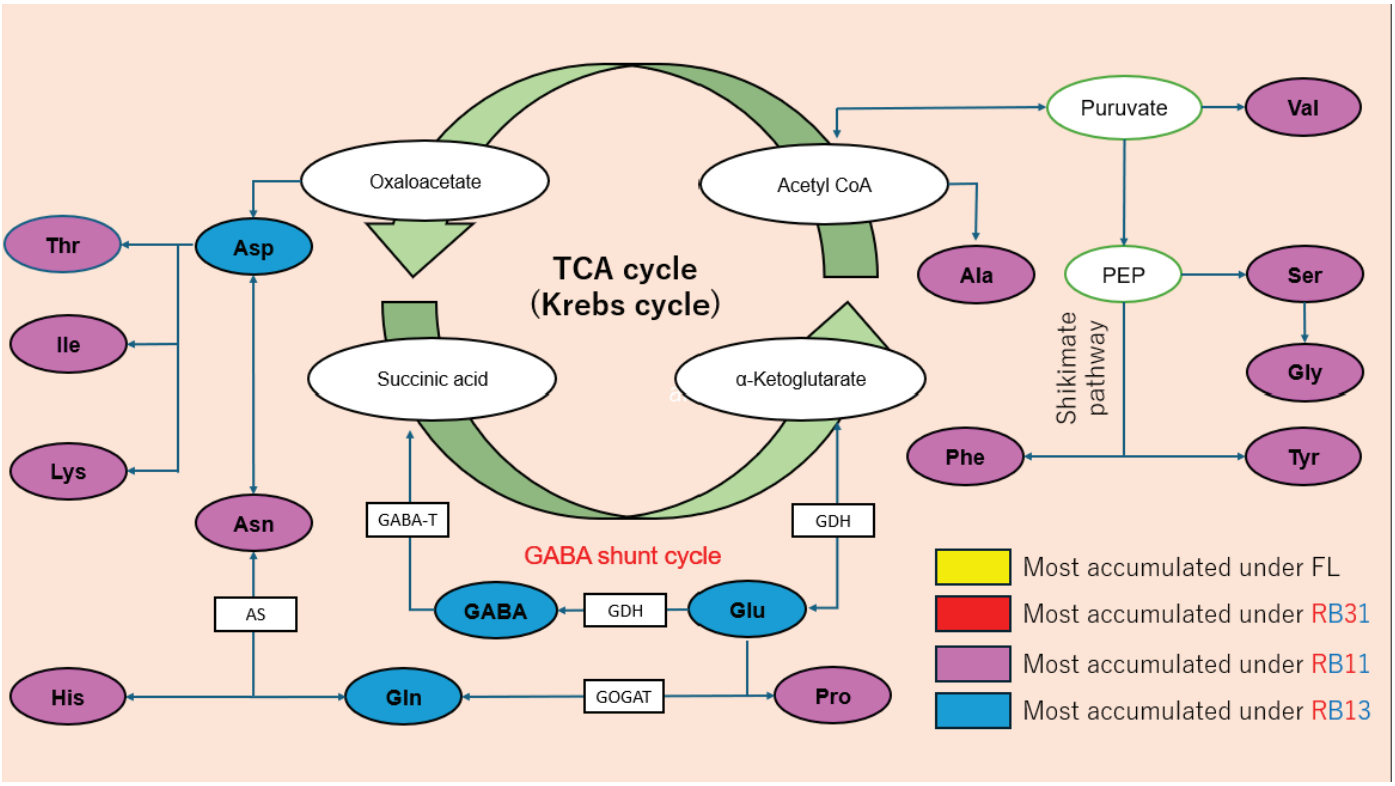


Figure 6. Relationship between the TCA cycle and the biosynthesis pathways of amino acids. Different colors indicate the light condition in which a specific amino acid was most accumulated. Squares represent relevant enzymes.

3.5. Overall Review

The results of this study showed that the interaction between accession and light can significantly affect the growth and the biosynthesis of functional compounds in spinach (Figure 7), and the response of spinach accessions to different red:blue light ratios varied significantly based on genetic background (Figure 8). The combinations of hybrid accessions with the RB11 condition, 'CGN25120-RB11' and 'CGN14215-RB11', resulted in the highest values for biomass and amino acid content across all combinations. A notable increase in biomass accumulation was also observed in 'Solomon-RB31', 'Solomon-FL', 'Solomon-RB11', 'CGN09513-RB31', 'CGN25120-RB31', 'CGN09511-RB11', and 'CGN14215-RB31'. The highest chlorophyll content was recorded in 'CGN25085-FL', while the highest carotenoid content was found in 'CGN09511-RB13'. 'TSP515-RB31' had the highest sugar concentration and exhibited a remarkable level of biomass accumulation. In general, RB11 can be considered to be the optimal ratio for all tested CGN *Spinacia* accessions, which promoted the growth and induced the synthesis of functional compounds at a certain level. RB31 and RB13 increased some parameters in specific accessions, suggesting that

those results can be used to control the productivity and flavor of spinach to meet the requirements of the producers.



Figure 7. Results of the two-way ANOVA, demonstrating the *p*-values of genetic factor (Accession), environmental factor (Light), and their interaction. Red highlight indicates significance ($p < 0.05$). Asterisks denote significance level; '***': $p = 0$–0.001; '**': $p = 0.0011$–0.01; '*': $p = 0.011$–0.05; ns: no significant difference.

Wild accession 'CGN25085' (*S. tetrandra*) showed minimal responsiveness, maintaining consistent biomass, sugar, and amino acid content across all light treatments, likely due to its adaptation to stable natural environments. In contrast, 'CGN25013' (*S. turkestanica*) increased fresh weight and elevated chlorophyll and carotenoid levels under the irradiation of RB31 and RB11, making it a valuable genetic resource for breeding.

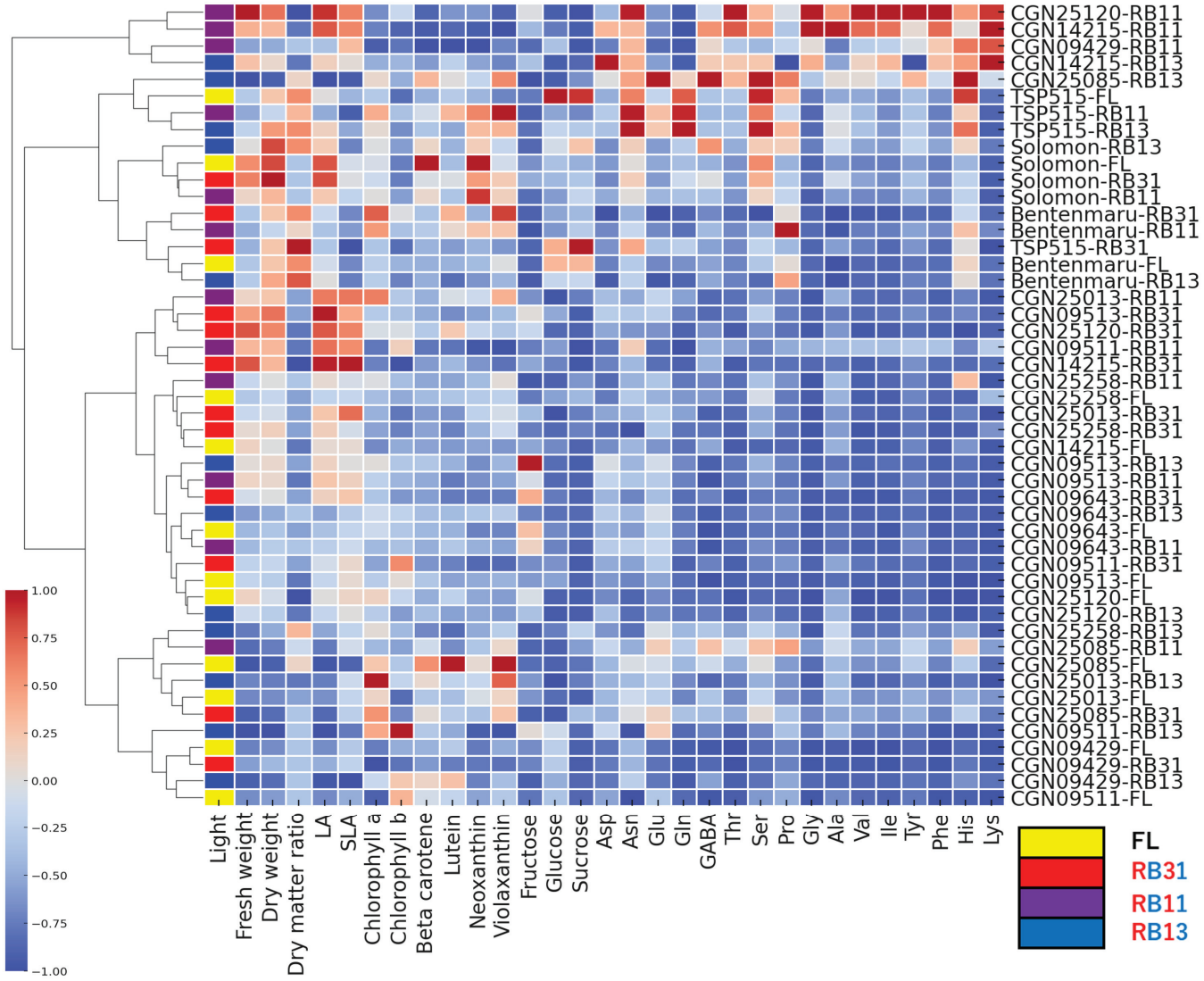


Figure 8. Overall assessment of *Spinacia* accessions across light conditions.

4. Materials and Methods

4.1. Plant Materials

Nine spinach accessions from the Center for Genetic Resources, The Netherlands were chosen from the gene bank at Wageningen University and Research in The Netherlands (Table 1). In order to maximize the level of genetic diversity, accessions were selected based on their geographical origins. These included seven accessions of spinach (*Spinacia oleracea* L.), including 'CGN09429', 'CGN09511', 'CGN09513', 'CGN09643', 'CGN25258', 'CGN14215', and 'CGN25120', and two accessions of closely related wild species, 'CGN25013' (*Spinacia turkestanica*) and 'CGN25085' (*Spinacia tetrandra*). Additionally, three Japanese cultivars (Jpn cultivar), 'Bentenmaru'and 'TSP515' from Takii & Co., Ltd., and 'Solomon' from The Sakata Seed Corporation, were included for comparison. The eastern and western groups were distinguished by their morphological differences (Figure S4). Accessions in the eastern group had narrow, hastate leaves, while those in the western group featured round leaves with a savoy texture. The accessions in the hybrid group are the offspring of hybrids between eastern and western spinach.

Table 1. List of twelve spinach accessions and their population group.

Accession	Population Group [x]	Scientific Name	Origin [y]
CGN09429	Eastern group	*Spinacia oleracea*	The Netherlands
CGN09511	Eastern group	*Spinacia oleracea*	Ethiopia
CGN09513	Western group	*Spinacia oleracea*	France
CGN09643	Western group	*Spinacia oleracea*	Iran
CGN25258	Western group	*Spinacia oleracea*	Ukraine
CGN25120	Hybrid group	*Spinacia oleracea*	Azerbaijan
CGN14215	Hybrid group	*Spinacia oleracea*	China
CGN25013	Wild group	*Spinacia turkestanica*	Uzbekistan
CGN25085	Wild group	*Spinacia tetrandra*	Georgia
Bentenmaru	Japanese cultivar	*Spinacia oleracea*	Japan
TSP515	Japanese cultivar	*Spinacia oleracea*	Japan
Solomon	Japanese cultivar	*Spinacia oleracea*	Japan

[x] Categorized by the Center for Genetic Resources, Wageningen University & Research. [y] The country where the sample was collected or derived.

4.2. Growing Conditions

The experiment took place in a deep-flow hydroponic system at the plant factory on Yoshida Campus, Yamaguchi University. The hydroponic solution used the Otsuka SA formula with an electrical conductivity (EC) of 2.0 dS/m and a pH level of 5.5–6.5. CO_2 was added to the cultivation chamber using an air pump at a consistent concentration of 1200 ppmv, while the room temperature and relative humidity were maintained at 20 °C and 60% (±10%), respectively, with an air conditioning system installed within the plant factory.

4.3. Irradiation Pattern

To estimate the effect of red and blue LED light on spinach, three red:blue ratios equaling 3:1, 1:1, and 1:3 (RB31, RB11, and RB13, respectively) were selected to irradiate simultaneously for 12 h (Figure 9). The light sources were red and blue LED lights from Union Electronics (#-01-OR). Red light peaked at 650 nm, whereas the peak wavelength of blue light was 450 nm. Fluorescent light (FHF32EX-N-H, Panasonic) with peaks ranging from 436 nm to 615 nm was used as a controlled treatment (FL). PPFD was set at 160 µmol/m^2/s in all plots. To ensure uniform germination due to the high dormancy of *S. turkestanica* and *S. tetrandra*, before sowing, all seed coats were carefully removed using pliers. The seeds were then placed in wet towels inside trays, which were covered with plastic wrap that had a small gap for seed respiration. The trays were kept in a dark area within the cultivation room of the plant factory. Five days after sowing, germinated seeds were temporarily planted in urethane foam for three days under fluorescent illumination. Spinach seedlings were transplanted into hydroponic beds and exposed to four different light conditions with a 12 h day length eight days after planting. The plants were harvested on the 32nd day after sowing (32DAS) (Figure S5).

4.4. Plant Growth Measurement

Six to ten plants of the same size were selected from each irradiation plot on 32DAS. Their fresh weight (FW) was determined immediately after harvesting. Then, all samples were freeze-dried using a VD-250R Freeze Dryer for 72 h to collect dry matter and measure the dry weight (DW). The samples were ground into dry powder and used for subsequent experiments. ImageJ 1.54g and Agisoft Metashape 2.2.0 were utilized to measure leaf area (LA) from 3D phenotyping figures and images, then the specific leaf area (SLA) was determined as the ratio of leaf area to dry weight.

4.5. Phytopigment Content Measurement

A total of 20 mg of powder was measured into a 15 mL tube, and 2.5 mL of 100% acetone was added. The sample was then vortexed for 2 min, homogenized for 20 min, and centrifuged at 5000 rpm for 5 min. The supernatant was collected in a 5 mL light-shielded glass sample tube and filtered through a 0.20 µm membrane filter (Toyo Seisakusho Kaisha, Ltd., Chiba, Japan). Samples were stored in a freezer at −25 °C and used for analysis within three days. Identification of chlorophyll a, chlorophyll b, lutein, β-carotene, violaxanthin, and neoxanthin was based on HPLC retention time using a LiChroCART 250-4.0 LiChrospher 100 RP-18 (5 µm) column and a UV-VIS Detector L-7420 (Hitachi High-Tech Corporation, Ibaraki, Japan). The injected volume for each sample was 50 µL. The column temperature was maintained at 30 °C, and the flow rate was 1.0 mL/min. For the first 20 min, the mobile phase was 80% methanol, and for the next 30 min, a mixed solution of 80% methanol:ethanol = 1:1 was passed through the column. The detection wavelength was set at 435 nm.

4.6. Sugar Content Measurement

Ten mg of the sample was measured and placed in a 15 mL tube. Then, 2 mL of 70% ethanol was added. The tube was vortexed for 5 min, heated in a block constant temperature chamber set at 75 °C for 15 min, and sonicated for 5 min. The supernatant liquid was collected with a Pasteur pipette, filtered through a 0.45 µm membrane filter (Toyo Seisakusho Kaisha, Ltd., Chiba, Japan), collected in a vial, and used as the sample solution for HPLC analysis. The sample solution was stored at −25 °C. The HPLC analysis utilized the LiChrospher 100 NH2 250-4.0 column (KANTO CHEMICAL Co., Inc., Saitama, Japan) and the RID-10A detector (Shimadzu Corporation, Kyoto, Japan) . The injected volume for each sample was 50 µL. The column temperature was maintained at 35 °C, and the flow rate was 0.8 mL/min. The mobile phase was 80% acetonitrile.

4.7. Amino Acid Content Measurement

Five mg of each sample was measured in 2 mL tubes, and then 1 mL of pH 2.2 lithium citrate (FUJIFILM Wako Pure Chemical Corporation, Hyogo, Japan) was added as the buffer solution. Samples were vortexed for 5 min and sonicated for 10 min. The supernatant was collected with a Pasteur pipette, filtered through a 0.20 µm membrane filter (Toyo Seisakusho Kaisha, Ltd., Chiba, Japan) , and collected in a vial as the sample solution. The instrument used was the Shimadzu high-performance liquid chromatogram amino acid analysis system, with the RF-20A Spectro fluorescence detector (Shimadzu Corporation, Kyoto, Japan) used as the detector and the Li-type post-column derivatization method used as the internal standard method. Calibration curves were prepared for each measurement based on standard samples. The sample solutions were stored at −4 °C. Thirty-nine amino acids were analyzed, and those with a significant amount were selected for statistical analysis, including aspartic acid (Asp), asparagine (Asn), glutamic acid (Glu), glutamine (Gln), gamma-aminobutyric acid (GABA), serine (Ser), histidine (His), proline (Pro), tyrosine (Tyr), alanine (Ala), phenylalanine (Phe), glycine (Gly), lysine (Lys), isoleucine (Ile), valine (Val), and threonine (Thr).

The HPLC conditions were set as follows:

- **Column:** Shim-pack Amino-Li
- **Mobile phase:** Amino acid analysis mobile phase kit LI type
- **Mobile phase A:** Lithium ion, citric acid, 2-methoxyethanol, perchloric acid
- **Mobile phase B:** Lithium ion, citric acid, boric acid, hydroxide ion
- **Mobile phase C:** Lithium ion, hydroxide ion

- **Reaction solution A:** Sodium carbonate, boric acid, potassium sulfate, sodium hypochlorite
- **Reaction solution B:** Sodium carbonate, boric acid, potassium sulfate, OPA, ethanol, N-acetyl-L-cysteine
- **Flow rate (initial conditions):** 0.6 mL/min
- **Column temperature (initial conditions):** 39 °C
- **Detector:** Spectro fluorescence detector RF-20Axs
- **Detection wavelength:** 450 nm
- **Gradient:** Shimadzu high-performance liquid chromatography prominence amino acid analysis system

4.8. Statistical Analysis

The items measured and analyzed were subjected to analysis of variance using the statistical analysis software R 4.4.2. The significance of the impact of genetic factors (twelve *Spinacia* accessions) and the environmental factor (irradiation conditions), as well as their interaction, was tested by two-way ANOVA. Results (*p*-values) of the two-way ANOVA were visualized with a heat map to clarify the significant impact of each factor on parameters. Then, a one-way ANOVA was performed for each single accession, followed by the Student-Newman-Keuls (SNK) post-hoc test to determine which light condition made a significant difference in the examined parameters. For overall assessment of all accession–light condition combinations, a heat map was drawn with the normalized average values (ranging from −1.00 to 1.00). The heat maps were released with Python 3.13.2 (programming language).

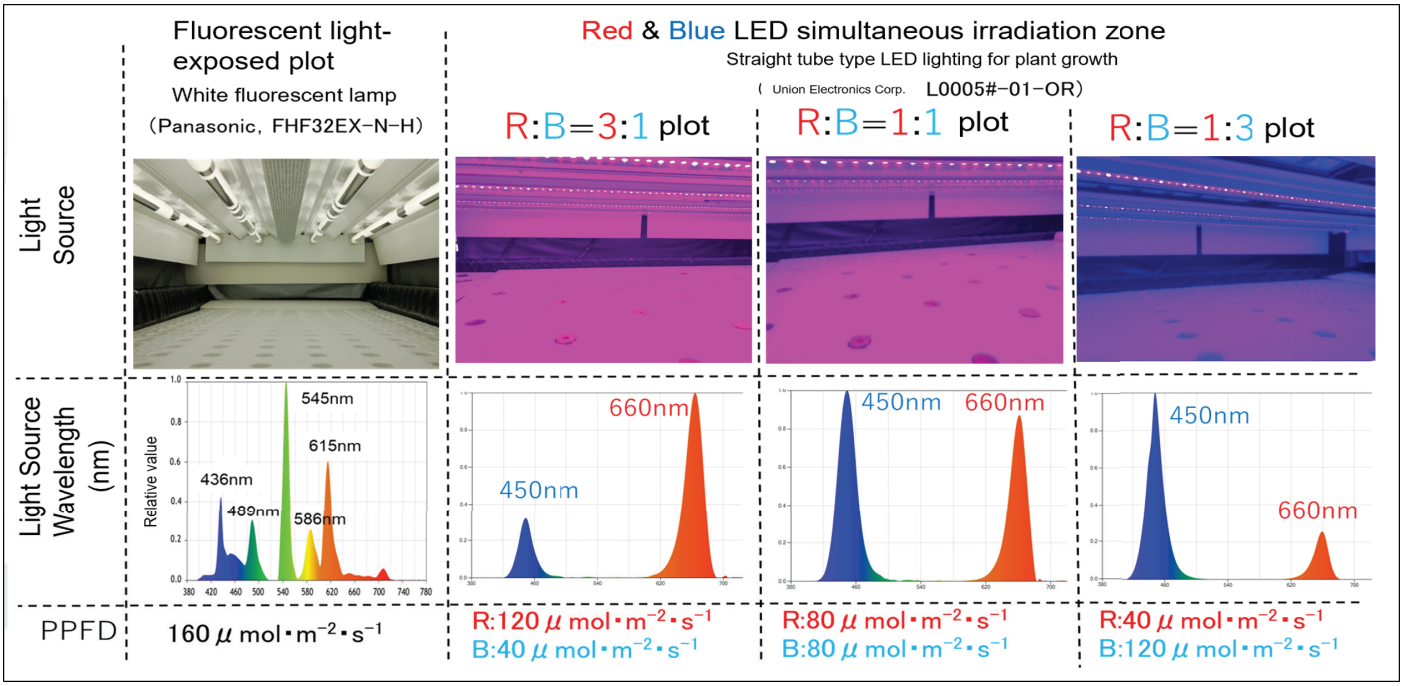


Figure 9. Spectral composition of the four irradiation treatments.

5. Conclusions

This study highlights the significant influence of red-to-blue LED light ratios on the growth performance and functional compound accumulation in spinach and its wild relatives under controlled environments. Fresh weight was maximized when red light comprised 50–70% of the spectra, emphasizing the critical role of red light in enhancing biomass production through phytochrome-mediated pathways. In contrast,

a high proportion of blue light generally suppressed growth, likely due to its effects on photomorphogenesis regulation. The study revealed notable variations in phytopigment content, with specific accessions responding differently to light treatments. There was no significant impact on the growth of the wild spinach 'CGN25085' (*S. tetrandra*) or Japanese cultivars 'Bentenmaru' and 'Solomon', and a growth-suppression effect of RB31 and RB11 was observed in 'TSP515'. The response to light conditions varied among different accessions for various functional compounds. Notably, 'CGN09429', 'CGN09511', and wild spinach 'CGN25013' (*S. turkestanica*) were most influenced by different red/blue ratios. It was suggested that the variations in functional compound biosynthesis could be attributed to the impact of spectral photons on the activation of key enzymes in metabolic pathways. These findings are expected to enhance our knowledge of how light affects spinach. This could help determine the optimal red and blue light ratios for each spinach accession, ultimately aiding in developing specialized spinach varieties for plant factory cultivation.

Supplementary Materials: The following supporting information can be downloaded at: https://www.mdpi.com/article/10.3390/plants14050700/s1, Figure S1: Growth features of 12 spinach accessions; Figure S2: Phytopigment content of 12 spinach accessions; Figure S3: Sugar content of 12 spinach accession; Figure S4: Morphological difference of twelve spinach accessions; Figure S5: Growing schedule; Table S1: Phytopigment content; Table S2: Amino acid content.

Author Contributions: Conceptualization, H.A. and M.S.; Methodology, Y.I. (Yasuomi Ibaraki); Formal analysis, T.M.L. and Y.S.; Investigation, T.M.L., K.H., K.A. and Y.I. (Yuichi Ishizaki); Resources, C.K., R.v.T. and T.v.H.; Data curation, T.M.L. and C.K.; Writing—original draft, T.M.L.; Writing—review & editing, Y.S., Y.I. (Yasuomi Ibaraki), M.A., C.K., R.v.T., T.v.H. and M.S.; Supervision, M.S.; Project administration, K.H., K.A., Y.I. (Yuichi Ishizaki), H.A. and M.S.; Funding acquisition, H.A. and M.S. All authors have read and agreed to the published version of the manuscript.

Funding: This research was funded by Nichirei Foods Inc. as part of the bridge research initiative aimed at developing new frozen vegetables by linking Genebank resources.

Data Availability Statement: Data are contained within the article and Supplementary Materials.

Acknowledgments: The authors would like to acknowledge the support of Nichirei Foods Inc. gratefully. We also extend our heartfelt thanks to Natsumi Kido and Nanaka Yamate (former undergraduate students in the faculty of agriculture, Yamaguchi University) for their contributions to the experimental work. Their dedication and expertise were instrumental in the successful completion of this study.

Conflicts of Interest: Authors Kazuhiro Harada, Kenta Arai, Yuichi Ishizaki, Hitoshi Aoki were employed by the company Nichirei Foods Inc. The remaining authors declare that the research was conducted in the absence of any commercial or financial relationships that could be construed as a potential conflict of interest.

References

1. Croce, R.; van Amerongen, H. Natural strategies for photosynthetic light harvesting. *Nat. Chem. Biol.* **2014**, *10*, 492–501. [CrossRef] [PubMed]
2. Roberts, J.L.; Moreau, R. Functional properties of spinach (*Spinacia oleracea* L.) phytochemicals and bioactives. *Food Funct.* **2016**, *7*, 3337–3353 . [CrossRef] [PubMed]
3. Morelock, T.E.; Correll, J.C., Spinach. In *Vegetables I: Asteraceae, Brassicaceae, Chenopodicaceae, and Cucurbitaceae*; Springer: New York, NY, USA, 2008; pp. 189–218. [CrossRef]
4. Ribera, A.; van Treuren, R.; Kik, C.; Bai, Y.; Wolters, A.M.A. On the origin and dispersal of cultivated spinach (*Spinacia oleracea* L.). *Genet. Resour. Crop Evol.* **2021**, *68*, 1023–1032. [CrossRef]
5. Van der Vossen, H. *Spinacia oleracea* L. In *PROTA 2: Vegetables/Légumes* ; PROTA: Wageningen, The Netherlands, 2004; Volume 2.
6. Xu, C.; Jiao, C.; Sun, H.; Cai, X.; Wang, X.; Ge, C.; Zheng, Y.; Liu, W.; Sun, X.; Xu, Y.; et al. Draft genome of spinach and transcriptome diversity of 120 *Spinacia* accessions. *Nat. Commun.* **2017**, *8*, 15275. [CrossRef]

7. Ribera, A.; Bai, Y.; Wolters, A.M.A.; van Treuren, R.; Kik, C. A review on the genetic resources, domestication and breeding history of spinach (*Spinacia oleracea* L.). *Euphytica* **2020**, *216*, 48. [CrossRef]
8. Wang, J.; Lu, W.; Tong, Y.; Yang, Q. Leaf Morphology, Photosynthetic Performance, Chlorophyll Fluorescence, Stomatal Development of Lettuce (*Lactuca sativa* L.) Exposed to Different Ratios of Red Light to Blue Light. *Front. Plant Sci.* **2016**, *7*, 250 . [CrossRef]
9. Gao, W.; He, D.; Ji, F.; Zhang, S.; Zheng, J. Effects of Daily Light Integral and LED Spectrum on Growth and Nutritional Quality of Hydroponic Spinach. *Agronomy* **2020**, *10*, 1082. [CrossRef]
10. Vaštakaitė-Kairienė, V.; Brazaitytė, A.; Miliauskienė, J.; Runkle, E.S. Red to Blue Light Ratio and Iron Nutrition Influence Growth, Metabolic Response, and Mineral Nutrients of Spinach Grown Indoors. *Sustainability* **2022**, *14*, 12564. [CrossRef]
11. Naznin, M.T.; Lefsrud, M.; Gravel, V.; Azad, M.O.K. Blue Light added with Red LEDs Enhance Growth Characteristics, Pigments Content, and Antioxidant Capacity in Lettuce, Spinach, Kale, Basil, and Sweet Pepper in a Controlled Environment. *Plants* **2019**, *8*, 93. [CrossRef]
12. Son, K.H.; Oh, M.M. Leaf shape, growth and antioxidant phenolic compounds of two lettuce cultivars grown under various combinations of Red and Blue LED. *Hortic. Environ. Biotechnol.* **2015**, *56*, 639–653. [CrossRef]
13. Battistoni, B.; Amorós, A.; Tapia, M.L.; Escalona, V. Effect of LED lights on the antioxidants properties of baby spinach leaves. *Rev. FCA UNCuyo* **2021**, *53*, 98–108. [CrossRef]
14. Gyawali, S.; Bhattarai, G.; Shi, A.; Kik, C.; du Toit, L.J. Genetic Diversity, Structure, and Selective Sweeps in *Spinacia turkestanica* Associated With the Domestication of Cultivated Spinach. *Front. Genet.* **2021**, *12*, 740437. [CrossRef] [PubMed]
15. She, H.; Liu, Z.; Xu, Z.; Zhang, H.; Cheng, F.; Wu, J.; Wang, W.; Wei, Q. Comparative chloroplast genome analyses of cultivated spinach and two wild progenitors shed light on the phylogenetic relationships and variation. *Sci. Rep.* **2022**, *12*, 856. [CrossRef] [PubMed]
16. Agarwal, A.; Dutta Gupta, S.; Barman, M.; Mitra, A. Photosynthetic apparatus plays a central role in photosensitive physiological acclimations affecting spinach (*Spinacia oleracea* L.) growth in response to blue and red photon flux ratios. *Environ. Exp. Bot.* **2018**, *156*, 170–182. [CrossRef]
17. Dougher, T.A.; Bugbee, B. Long term Blue Light Effects on the Histology of Lettuce and Soybean Leaves and Stems. *J. Am. Soc. Hortic. Sci.* **2004**, *129*, 467–472. [CrossRef]
18. Snowden, M.C.; Cope, K.R.; Bugbee, B. Sensitivity of Seven Diverse Species to Blue and Green Light: Interactions with Photon Flux. *PLoS ONE* **2016**, *11*, e0163121. [CrossRef]
19. Kong, Y.; Stasiak, M.; Dixon, M.A.; Zheng, Y. Blue light associated with low phytochrome activity can promote elongation growth as shade-avoidance response: A comparison with red light in four bedding plant species. *Environ. Exp. Bot.* **2018**, *155*, 345–359. [CrossRef]
20. Wang, Q.; Liu, Q.; Wang, X.; Zuo, Z.; Oka, Y.; Lin, C. New insights into the mechanisms of phytochrome-cryptochrome coaction. *New Phytol.* **2018**, *217*, 547–551. [CrossRef]
21. Barnes, C.; Tibbitts, T.; Sager, J.; Deitzer, G.; Bubenheim, D.; Koerner, G.; Bugbee, B. Accuracy of quantum sensors measuring yield photon flux and photosynthetic photon flux. *HortScience* **1993**, *28*, 1197–1200. [CrossRef]
22. Izzo, L.G.; Mickens, M.A.; Aronne, G.; Gomez, C. Spectral effects of blue and red light on growth, anatomy, and physiology of lettuce. *Physiol. Plant* **2021**, *172*, 2191–2202. [CrossRef]
23. Akoyunoglou, G.; Anni, H. Blue light effect on chloroplast development in higher plant. In *Blue Light Effects in Biological Systems*; Springer: Berlin/Heidelberg, Germany, 1984.
24. Christie, J.M.; Briggs, W.R. Blue light sensing in higher plants. *J. Biol. Chem.* **2001**, *276*, 11457–11460. [CrossRef] [PubMed]
25. Ramezani, M.; Thompson, D.; Moreno, M.; Joshi, V. Biochemical repercussions of light spectra on nitrogen metabolism in spinach (*Spinacia oleracea*) under a controlled environment. *Front. Plant Sci.* **2023**, *14*, 1283730. [CrossRef] [PubMed]
26. Hogewoning, S.W.; Trouwborst, G.; Maljaars, H.; Poorter, H.; van Ieperen, W.; Harbinson, J. Blue light dose-responses of leaf photosynthesis, morphology, and chemical composition of *Cucumis sativus* grown under different combinations of red and blue light. *J. Exp. Bot.* **2010**, *61*, 3107–3117. [CrossRef] [PubMed]
27. Esther van Praag, D.M. Response of the carbohydrate metabolism and fructose 2, 6-bisphosphate to environmental changes. Effect of different light treatments. *Bot. Helvenia* **1997**, *106*, 103–112.
28. Lee, S.W.; Hahn, T.R. Light-regulated differential expression of pea chloroplast and cytosolic fructose-1,6-bisphosphatases. *Plant Cell Rep.* **2003**, *21*, 611–618. [CrossRef]
29. McCormick, A.J.; Kruger, N.J. Lack of fructose 2,6-bisphosphate compromises photosynthesis and growth in Arabidopsis in fluctuating environments. *Plant J.* **2015**, *81*, 670–683. [CrossRef]
30. Wilson, D.G.; King, K.W.; Burris, R.H. Transamination Reactions in Plants. *J. Biol. Chem.* **1954**, *208*, 863–874. [CrossRef]

31. Lea, P.J.; Miflin, B.J. Alternative route for nitrogen assimilation in higher plants. *Nature* **1974**, *251*, 614–616. [CrossRef]
32. Azevedo, R.A.; Lancien, M.; Lea, P.J. The aspartic acid metabolic pathway, an exciting and essential pathway in plants. *Amino Acids* **2006**, *30*, 143–162. [CrossRef]

Disclaimer/Publisher's Note: The statements, opinions and data contained in all publications are solely those of the individual author(s) and contributor(s) and not of MDPI and/or the editor(s). MDPI and/or the editor(s) disclaim responsibility for any injury to people or property resulting from any ideas, methods, instructions or products referred to in the content.

plants

MDPI

Article

Cyanobacterial Cultures, Cell Extracts, and Individual Toxins Decrease Photosynthesis in the Terrestrial Plants *Lactuca sativa* and *Zea mays*

Scott A. Heckathorn [1,*], Clare T. Muller [1], Michael D. Thomas [1], Emily P. Vining [1], Samantha Bigioni [2], Clair Elsie [3], J. Thomas Franklin [2], Emily R. New [1] and Jennifer K. Boldt [4]

[1] Department of Environmental Sciences, University of Toledo, Toledo, OH 43606, USA; clare.muller@utoledo.edu (C.T.M.); michael.thomas11@utoledo.edu (M.D.T.); emily.vining@utoledo.edu (E.P.V.); emily.new@rockets.utoledo.edu (E.R.N.)
[2] Ottawa Hills High School, Ottawa Hills, OH 43606, USA; sbigioni@gmail.com (S.B.); franklin.john.thomas@gmail.com (J.T.F.)
[3] Sylvania High School, Sylvania, OH 43560, USA; caelsie27@gmail.com
[4] Agricultural Research Service, United States Department of Agriculture, Toledo, OH 43606, USA; jennifer.boldt@usda.gov
* Correspondence: scott.heckathorn@utoledo.edu

Abstract: Cyanobacterial harmful algal blooms (cHABs) are increasing due to eutrophication and climate change, as is irrigation of crops with freshwater contaminated with cHAB toxins. A few studies, mostly in aquatic protists and plants, have investigated the effects of cHAB toxins or cell extracts on various aspects of photosynthesis, with variable effects reported (negative to neutral to positive). We examined the effects of cyanobacterial live cultures and cell extracts (*Microcystis aeruginosa* or *Anabaena flos-aquae*) and individual cHAB toxins (anatoxin-a, ANA; beta-methyl-amino-L-alanine, BMAA; lipopolysaccharide, LPS; microcystin-LR, MC-LR) on photosynthesis in intact plants and leaf pieces in corn (*Zea mays*) and lettuce (*Lactuca sativa*). In intact plants grown in soil or hydroponically, overall net photosynthesis (P_n), but not Photosystem-II (PSII) electron-transport yield (Φ_{PSII}), decreased when roots were exposed to cyanobacterial culture (whether with intact cells, cells removed, or cells lysed and removed) or individual toxins in solution (especially ANA, which also decreased rubisco activity); cyanobacterial culture also decreased leaf chlorophyll concentration. In contrast, Φ_{PSII} decreased in leaf tissue vacuum-infiltrated with cyanobacterial culture or the individual toxins, LPS and MC-LR, though only in illuminated (vs. dark-adapted) leaves, and none of the toxins caused significant decreases in in vitro photosynthesis in thylakoids. Principal component analysis indicated unique overall effects of cyanobacterial culture and each toxin on photosynthesis. Hence, while cHAB toxins consistently impacted plant photosynthesis at ecologically relevant concentrations, the effects varied depending on the toxins and the mode of exposure.

Keywords: anatoxin; beta-methyl-amino-L-alanine; harmful algal blooms; lipopolysaccharide; microcystin; photosynthetic rate

1. Introduction

Climate change and eutrophication are increasing the frequency and severity of toxin-producing cyanobacterial harmful algal blooms (cHABs) in freshwater systems [1,2]. As a result, many surface and ground-water sources may contain, or even accumulate, cyanobacterial toxins [3–5]. Chronic and acute exposure to these toxins pose a significant health risk to humans and other animals, as they may lead to illness or death [6–8]. Contaminated food sources may present a significant and growing source of toxin exposure [4,9]. Agricultural plants can accumulate cyanobacterial toxins after irrigation with contaminated water or fertilization with cyanobacteria-based bio-fertilizers, resulting in crop contamination that can

exceed safety thresholds for daily tolerable intake (e.g., the World Health Organization's adult daily tolerable intake for microcystin-LR of 0.04 μg/kg bodyweight); cyanobacterial toxins can also decrease crop productivity [9–14].

Cyanobacteria that cause freshwater HABs, such as *Microcystis* and *Anabaena* (also known as *Dolichospermum*) species, often produce an array of toxins, including microcystins (MCs), anatoxin-a (ANA), β-methyl-amino-L-alanine (BMAA), and lipopolysaccharides (LPSs) [4]. These four toxins, which are among the most common in freshwater systems, are known to have different modes of action and toxicity in animals and plants [4,9,15–17]. Because cHAB water or cyanobacterial extracts contain multiple toxins, the effects of cHAB-contaminated water or cyanobacterial extracts on plants will likely be complex and more severe compared to the effects of individual toxins (e.g., [18]). Most studies to date examining the effects of cyanobacterial toxins on plants have either treated plants with cyanobacterial extracts or individual toxins, so our understanding of the comparative effects of different toxins or cyanobacterial extracts vs. individual toxins is lacking [4,9,16].

The most common and well-studied cyanobacterial toxins are the microcystins, especially MC-LR. These cyclic heptapeptides are composed of five non-protein (or non-canonical) amino acids and 3-amino-9-methoxy-2,6,8-trimethyl-10-phenyl-4,6-decadienoic acid (ADDA), with hundreds of congeners, resulting from substitutions in the second and fourth positions of the peptide, which vary in toxicity [16,19]. MCs inhibit eukaryotic protein phosphatases 1 (PP1) and 2A (PP2A) [20], which regulate a wide array of cell functions, including in plants [21]. Hence, MCs have wide-ranging negative effects on cells, including causing hyper-phosphorylation of cellular proteins and the generation of reactive oxygen species (ROS), DNA damage, and cell death [4,13]. Many studies have investigated the effects of microcystins on plant growth and function, although few have examined the effects on photosynthesis, with the effects of microcystins ranging from positive to neutral to negative depending on the species, the growth stage, the MC congener, the quantity of the toxin, etc. (reviewed in [4,9,13,16]).

Anatoxin-a (ANA) is a neurotoxic bicyclic amine alkaloid that acts by binding to nicotinic and muscarinic acetylcholine receptors in animals, where it mimics the neurotransmitter acetylcholine [22]. Non-neuronal acetylcholine is present in plant cells, where it may interact with many cellular processes [23]. In plants, nicotinic and muscarinic receptor antagonists, in general, have been shown to reduce cell size, alter cell structure, and affect water uptake [24]. The effects of ANA specifically on plants have rarely been investigated [4,22], but it is known to negatively impact growth and function (e.g., [25–27]).

The non-canonical amino acid, BMAA, can interfere with mammalian glutamate receptors [15,17]. BMAA may also be incorporated into proteins during protein synthesis, causing proteins to function improperly; it can induce oxidative stress, and it can likely disrupt N metabolism by interfering with ammonium assimilation [15,17]. BMAA has been shown to bioaccumulate in plants, either in free or protein-associated forms [17,28–30]. The effects of BMAA on plant function have rarely been examined [4]. It is likely that BMAA interferes with glutamate receptors in plant cells, but it is difficult to predict how this might affect them, as there are many types and roles of glutamate receptors in plants [17]. One study suggests that BMAA may increase oxidative stress in the aquatic plant, *Ceratophyllum demersum*, via inhibition of oxidative stress enzymes, leading to ROS buildup [31], and another study found that BMAA decreased the growth of *Medicago sativa* seedings at extreme concentrations [32]. On the other hand, it has been hypothesized (but not proven) that BMAA may play a role in the protection of photosynthesis during stress in cyanobacteria [33], but this has not been examined in plants.

Lipopolysaccharides (LPSs) are bacterial endotoxins that comprise a lipid A moiety, a core oligosaccharide, and an O-antigen, and they are found in the cell wall of Gram-negative bacteria, including cyanobacteria. Although the LPS lipid and oligosaccharide components are highly conserved, the O-antigen varies among species, which can affect toxicity. Interestingly, Bernardova et al. found that LPSs from cyanobacteria are similar in toxicity to LPSs from heterotrophic bacteria and that LPSs from cHABs can be more

toxic due to the presence of multiple species [34]. In plants, LPSs are detected as a microbe-associated molecular pattern by cells and triggers the release of ROS, elevated intracellular Ca^{2+}, and increased expression of kinase-mediated pathways that strengthen defense and resistance to microbial pathogens (e.g., [35–37]). Plant perceptions of and reactions to LPSs vary among plant groups and depend on what LPS species is detected [38,39]. Numerous downstream effects of LPSs on of kinase signaling could impact plant function, including photosynthesis, but data on the effects of LPSs on photosynthesis are rare.

Only a small number of studies have examined the effects of cyanobacterial extracts or individual toxins on photosynthesis in general and in plants in particular [4,9,16]. Past studies have examined cHAB toxin effects (mostly microcystins or whole-cell extracts) on various aspects of photosynthesis in organisms ranging from cyanobacteria (e.g., [40]) to photosynthetic protists (e.g., [18,41,42]), aquatic plants (e.g., [25–27,43]), and terrestrial plants (e.g., [44–47]). Most past studies have examined toxin effects only on chlorophyll concentration or Photosystem-II (PSII) function, which do not necessarily reflect the effects on net photosynthesis, and only a few studies have measured the overall net photosynthesis rate (as net CO_2 uptake or O_2 evolution) [25,43–45,47]. Excluding Chen et al. [43], who examined the effects of MC-LR on rubisco activity, we are aware of no studies that have examined the effects of cHAB toxin effects on CO_2-fixation reactions in photosynthesis. The effects of cHAB toxins on photosynthesis are often dose- or time-dependent (e.g., [26,27,43]), and they can vary among species within a study (e.g., [41]), the parameters measured (e.g., [chl] vs. PSII [40]), and whole-cell extracts vs. pure toxins (e.g., [18,41]). In some past studies, the concentrations of toxins used were so extremely low or high that they rendered the results of limited usefulness, e.g., positive effects on photosynthesis at up to 1 ng/L MC [41] or negative effects of MC at 2220–100,000 μg/L [27,44,46]. In plants, cHAB toxin effects on photosynthesis are often attributed to indirect damage from ROS (e.g., [26,36,45]) or manifest after several days (e.g., [27,46]), so it is not clear if the cHAB toxins can affect plant photosynthesis directly.

To gain a clearer understanding of the impact of cHAB toxins on plant photosynthesis, we conducted multiple experiments to determine if four common cHAB toxins affect various aspects of photosynthesis (including net photosynthesis, stomatal conductance, PSII of the light reactions, rubisco activity of the CO_2-fixation reactions, and chlorophyll concentration). Two different species (corn, lettuce) were treated with live cultures, cell extracts, and/or individual pure toxins at ecologically or physiologically relevant concentrations (ANA, BMAA, LPS, MC-LR) either via uptake by the roots in soil or hydroponically grown plants or via direct application to the leaves. To our knowledge, this is the first study to examine the effects of multiple cHAB toxins and cyanobacterial cells or extracts on both light and CO_2-fixation reactions in plants exposed to toxins through the roots vs. the leaves.

2. Materials and Methods

2.1. Plant Growth

Corn (*Zea mays* L. cv 'Bicolor Sh2'), lettuce (*Lactuca sativa* L. cv 'Casey'), and tomato (*Solanum lycopersicum* L. cv 'Early Girl') (Johnny's Select Seeds, Winslow, ME, USA) were grown from seed in a greenhouse. Greenhouse temperatures ranged from ca. 20–22 °C (night-time low) to ca. 28–32 °C (day-time high) for lettuce and tomato grown in late fall to early spring and from ca. 22–26 °C (night-time low) to ca. 32–38 °C (day-time high) for corn grown in mid spring to late summer. The greenhouse photoperiod was set to 15 h using high-output lamps providing ca. 125 μmol m^{-2} s^{-1} PAR (photosynthetically active radiation) to extend the photoperiod when needed. Otherwise, most greenhouse light was provided by ambient solar radiation, up to ca. 1600 μmol m^{-2} s^{-1} PAR at midday.

Corn was grown in topsoil in drainable plastic pots (10.5-cm wide × 10.5-cm wide × 13.5-cm tall). Lettuce and tomato were grown in 5 cm deep drainable plastic flats filled with calcite clay and peat (1:3, *v:v*). Corn plants were watered as needed and fertilized twice weekly with complete nutrient solution [5 mM KNO_3, 0.5 mM NH_4Cl, 2 mM KH_2PO_4, 2 mM $CaCl_2$, 1 mM MgCl, 1 mM K_2SO_4, 50 μM Fe (as $FeSO_4$ + $FeCl_3$, or as Fe-EDTA),

50 μM H_3BO_3, 10 μM $MnCl_2$, 2.0 μM $CuSO_4$, 2.0 μM $ZnSO_4$, 0.1 μM $NaMoO_4$, and 1 mM MES buffer (pH 6.2 ± 0.2) in RO water]. Lettuce and tomato plants were watered and fertilized similarly [as above but with 4.5 mM KNO_3, 0.5 mM NH_4NO_3, 1 mM urea, 1 mM $MgSO_4$]. Corn was used in experiments after it reached the V2 or V3 stages (2 or 3 expanded green leaves), lettuce when it reached ca. 6–10 g fresh mass, and tomato when it had 3 to 5 expanded adult leaves.

For hydroponic experiments, plants were grown as above until the experiment, at which time their roots were rinsed with tap water and they were transferred to glass jars containing nutrient solution. Jars had lids with small holes though which plants were suspended with roots submerged in nutrient solutions, and jars were wrapped in opaque tape to prevent algal growth on roots during the experiment. Hydroponic experiments were conducted in the lab (ca. 22 °C and 15–25% RH) in chemical fume-hoods to prevent human exposure to toxins, and hydroponic solutions were not aerated to prevent airborne release of toxins. Plants were illuminated in the fume-hoods with a high-intensity LED grow lamp (model Pheno 440, Phantom LED, Shoemakersville, PA, USA) providing 700–800 μmol m^{-2} s^{-1} PAR and set to a 14 h photoperiod. Plants were given 7–10 days to acclimate to the lab prior to starting the experiments. During multi-day experiments, plants were rotated ca. daily to avoid position effects. Because corn did not grow well in unaerated hydroponics, we used lettuce in such experiments lasting more than 24 h.

2.2. Cyanobacterial Growth

Microcystis aeruginosa (strains LB 2385 + LB 3037, UTEX Culture Collection, utex.org, Austin, TX, USA) was either grown in the greenhouse (experiments 1 and 2, Table 1) or in the lab (experiment 4). *Anabaena flos-aquae* (strain 2557, UTEX, or 15170, Carolina Biological, Burlington, NC, USA) was grown in the lab. "Greenhouse" *M. aeruginosa* was grown in 20 L white polypropylene carboys (ca. 40% PAR transmittance), while lab-grown cultures of both species were grown in glass flasks in a sterile hood at 22–23 °C with natural light provided by a nearby window plus light from a fluorescent bulb set to a 14 h photoperiod (yielding up to 35–50 μmol m^{-2} s^{-1} PAR). Except for experiment 3 below, cultures were grown in nutrient solution containing 1 mM KNO_3, 0.1 mM NH_4Cl, 0.1 mM KH_2PO_4, 250 μM $CaCl_2$, 125 μM MgCl, 125 μM K_2SO_4, 10 μM $FeSO_4$, 50 μM H_3BO_3, 10 μM $MnCl_2$, 2.0 μM $CuSO_4$, 2.0 μM $ZnSO_4$, 0.1 μM $NaMoO_4$, and 1 mM HEPES buffer (pH 7.3 ± 0.2) in RO water. For experiment 3 below, cyanobacteria were grown in river water (Ottawa River, University of Toledo, Toledo, OH, USA), filtered as below, to which was added 0.08 g commercial plant food (Miracle-Gro water-soluble plant food for vegetables and herbs; Marysville, OH, USA; yielding pH 7.75 ± 0.1 and 1 mM N). Cyanobacterial cultures were continuously aerated using aquarium pumps and tubing. Cyanobacterial cultures were used in experiments when the chlorophyll (chl) concentration reached 0.04–0.10 absorbance units measured at 665 nm with a spectrophotometer (=0.56–1.4 μg/mL chl), which would represent a severe cyanobacterial bloom in coastal water [48]. To obtain cell-free culture, cells were removed by filtering through a 0.45 μm filter (model GF/F, Whatman, China). To obtain a lysed-cell and cell-free culture (containing whole-cell extracts), cells were first removed from cyanobacterial culture, and then the filters with collected cells were frozen at −70 °C. Filters were then shaken in a closed glass jar until the filters disintegrated either in deionized water or in a small volume of ethanol (25 mL per 1500 mL starting culture) followed by deionized water (100 mL) plus Tween-20 non-ionic detergent (3 drops per 1500 mL starting culture). The lysed-cell extract was then filtered as above, and this filtrate was added to the original cell-free filtrate. For the soil experiments, cyanobacterial cultures (whole-cell, cells removed, and cells lysed and removed) were adjusted to match the control nutrient solution for pH; for hydroponics and leaf-disc experiments, lysed and cell-free extract was adjusted to match the control nutrient solution for pH, NO_3, and NH_4.

Table 1. Summary of experiments and their key details.

Experiment	Treatment	Species	System	Explanation	Duration	Variables [2]
1	cyanobacterial culture	corn	whole plants in soil	roots watered with *M. aeruginosa* whole-cell culture	14 d	Φ_{PSII}, [chl], biomass
2	cyanobacterial culture	corn	whole plants in soil	roots watered with *M. aeruginosa* whole-cell vs. cell-free culture	14 d	Φ_{PSII}, [chl]
3	cyanobacterial culture	corn	whole plants in soil	roots watered with *A. flos-aquae* lysed cell-free culture	10 d	P_n, G_s, C_i, Φ_{PSII}, [chl], biomass
4	cyanobacterial culture	corn	whole plants in hydroponics	roots submerged in *A. flos-aquae* or *M. aeruginosa* lysed cell-free culture	24 h	P_n, G_s, C_i, Φ_{PSII}, [chl]
5	cyanobacterial culture	corn, lettuce	leaf tissue	vacuum-infiltrated with *A. flos-aquae* or *M. aeruginosa* lysed cell-free culture	1–3 h	Φ_{PSII}, F_v/F_m
6a and b	cyanobacterial culture and purified toxins	lettuce	whole plants in hydroponics	roots submerged in *A. flos-aquae* lysed cell-free culture (6a only) or individual toxins (ANA, BMAA, LPS, MC-LR) [1]	10 d	P_n, G_s, C_i, Φ_{PSII}, [chl], biomass, (6b only) rubisco activity
7a and b	purified toxins	lettuce	leaf tissue	vacuum-infiltrated with individual toxins (ANA, BMAA, LPS, MC-LR) [1]	1–3 h	Φ_{PSII}, F_v/F_m
8	purified toxins	tomato	thylakoid membranes	individual toxins (ANA, BMAA, LPS, MC-LR) [1]	1 h	in vitro O_2 evolution

[1] anatoxin-a = ANA; beta-methyl-amino-alanine = BMAA; lipopolysaccharide = LPS; microcystin-LR = MC-LR. [2] Φ_{PSII} = light-adapted Photosystem-II yield; [chl] = relative leaf chlorophyll concentration; F_v/F_m = dark-adapted maximum Photosystem-II efficiency; P_n = net photosynthesis (CO_2 uptake); G_s = stomatal conductance; C_i = leaf internal CO_2 concentration.

2.3. Soil-Grown Corn Treated with Cyanobacterial Culture for 10–14 d

For corn plants in soil (V2 or V3 stage), experiments were conducted in the greenhouse, during which roots were watered every three days (starting with day 0) with 300 mL cyanobacterial nutrient solution (controls) or cyanobacterial culture applied to the soil (experiment 1: *M. aeruginosa*, whole-cell culture; experiment 2: *M. aeruginosa*, whole-cell vs. cells removed; experiment 3: *A. flos-aquae* cells lysed and removed; Table 1). At the end of experiments 1 and 3, plants were harvested, separated into roots and shoots, and weighed to obtain fresh and/or dry mass (the latter after drying for 48 h at 70 °C).

2.4. Corn and Lettuce Leaves Treated with Cyanobacterial Culture or Toxins for 1–3 h

Recently expanded leaves of lettuce and corn were used for the experiments. Lettuce leaves were sampled using a circular cutter (3 cm diameter) to create uniform discs, while rectangular sections (ca. 1 × 3 cm) cut with scissors from the middle of corn leaves were used. Leaf pieces were submerged in treatment solutions containing 0.01% Tween detergent, and then leaf tissue was vacuum-infiltrated (at no more than 30 cm Hg) in a chamber for ca. 10 min until leaves were fully infiltrated (determined by color change of leaves). Infiltrated discs were then placed on top of a thin layer of treatment solution in clear plastic Petri dishes with lids, either uncovered (light-adapted) or covered with aluminum foil (dark-adapted). Because lettuce was more amenable to vacuum-infiltration, we used lettuce in most of the infiltration experiments.

For corn and lettuce treated with cyanobacterial culture (experiment 5), leaf tissue was infiltrated with cyanobacterial nutrient solution (controls) or *M. aeruginosa* or *A. flos-aquae* culture (cells lysed and removed; two separate batches of each species for lettuce). Light-adapted leaf discs were incubated for 1 or 3 h, either under 750 ± 25 μmol m^{-2} s^{-1} PAR or in the dark, after which Photosystem-II (PSII) function was measured (see below).

For lettuce treated with individual pure toxins (experiment 7), leaf tissue from greenhouse-grown plants was infiltrated with deionized water (controls) or toxins in deionized water (1 μM ANA, BMAA, MC or 50 μg mL^{-1} LPS) (experiment 7) [ANA/BMAA/MC-LR (products 14609/2387/10007188) from Cayman Chemical, Ann Arbor, MI, USA; LPS from *E. coli* (product L2630) from Sigma-Aldrich, St. Louis, MO, USA]. These ANA, BMAA, and MC-LR concentrations are towards the high end of levels found during naturally occurring HABs [4,22,33], while the LPS concentration was based on previous studies documenting plant sensitivity to the toxin [36,38,39]. Leaves were incubated under 450 μmol m^{-2} s^{-1} PAR or in the dark for 2 h. After incubation, PSII function was measured as below. To further understand the effects of toxin concentration and light dependency on PSII in lettuce leaf discs, an additional experiment was conducted in a similar fashion to the one described above. In this second experiment, leaf discs were infiltrated with either deionized water (controls), 1 μM MC-LR, 10 μM MC-LR, 50 μg mL^{-1} LPS, or 250 μg mL^{-1} LPS. Light-adapted leaf discs were incubated for 3 h, either under 750 ± 25 μmol m^{-2} s^{-1} PAR or in the dark, after which PSII function was measured.

2.5. Hydroponic Plants Treated with Cyanobacterial Culture or Individual Toxins

For corn in hydroponics, plants were grown as above to the V2 stage and then transplanted into 500 mL glass jars filled with 475 mL unaerated nutrient solution for seven days to acclimate (experiment 4). Just before initiating the treatments, the plants were transferred to fresh solutions containing either nutrient solution without toxin (controls) or lysed-cell cell-free culture of *M. aeruginosa* or *A. flos-aquae*. After 24 h of treatment, photosynthetic measurements were made on leaves of intact plants (as below).

For lettuce in hydroponics, plants were grown as above to the 4-leaf stage and then transplanted into 250 mL glass jars filled with 225 mL unaerated nutrient solution and allowed seven days to acclimate (experiment 6). Just before initiating the treatments, the initial fresh weights of the plants were obtained. Plants were then transferred to fresh solutions containing either nutrient solution without toxin (controls) or with ANA (0.5 μM), BMAA (0.5 μM), LPS (25 μg mL^{-1}), or MC-LR (0.5 μM). Solution levels in jars were maintained daily by refilling with deionized water. After seven days, photosynthetic measurements were made on leaves of intact plants (as below), and then plants were harvested to obtain the final fresh mass and calculate plant growth during the experiment (final mass minus initial mass = ΔFW). Because this experiment was conducted in a chemical fume-hood for safety, this limited the number of replicates per treatment, thereby limiting the statistical power; consequently, this entire experiment (minus the cyanobacterial extract treatment) was repeated, as discussed below.

2.6. Photosynthetic Measurements

The yield of light-adapted Photosystem-II (PSII) electron transport (Φ_{PSII}) was measured on intact plants in the fume-hoods using a portable chlorophyll fluorometer (model OS1-FL, Opti-Sciences, Hudson, NH, USA). For leaf pieces, light-adapted Φ_{PSII} and dark-adapted (>30 min) maximum PSII efficiency (F_v/F_m) was measured with a pulse-modulated bench-top chlorophyll fluorometer (model 101/103, Walz, Germany) and a flash lamp (model KL1500 LCD, Schott, Germany; 2-s flash at ca. 6000 μmol m^{-2} s^{-1} PAR). Leaf relative chlorophyll concentration [chl] was measured using a portable SPAD meter (model SPAD-502 Plus, Konica Minolta, Tokyo, Japan). Leaf gas-exchange measurements were made with a portable infra-red gas-analyzer (IRGA)-based system with a 2 × 3-cm cuvette with red/blue LED light (model LI-6400, LiCor, Lincoln, NE, USA). Net photosynthesis (P_n = net CO_2 uptake), stomatal conductance to water vapor (G_s), and internal CO_2 con-

centration (C_i) measurements were made on intact plants at 400 ppm CO_2 (excluding P_n–C_i curves discussed below), 1000 μmol m^{-2} s^{-1} PAR, and 25 or 28 °C air temperature (for lettuce and corn, respectively). For single measurements at 400 ppm CO_2, data were collected within ca. 1 min of inserting leaves into the cuvette (immediately after readings stabilized). All photosynthetic measurements were made between 11 am and 3 pm on the middle of the most recently expanded leaf (corn) or on the outer half of a recently fully expanded leaf (lettuce); all measurements except for F_v/F_m were made on leaves receiving steady-state illumination (the actinic light level for Φ_{PSII} measurements)

In vivo rubisco carboxylation activity was determined using the "A-C_i" technique [49]. Briefly, P_n and C_i were measured repeatedly on individual intact lettuce plants at each of the following CO_2 concentrations: 400, 250, 200, 150, and 100 ppm. The light level and the temperature were 1000 μmol m^{-2} s^{-1} PAR and 25 °C, respectively. Results for each plant were graphed individually, with P_n on the *Y*-axis and C_i on the *X*-axis. The initial linear slope of the P_n–C_i relationship, a measure of in vivo rubisco activity in C3 plants, was determined for 100–250 ppm CO_2 ($r^2 > 0.98$ for all curves). Data were collected after readings stabilized at each CO_2 level (within 2–3 min).

As an additional method to test for direct effects of cyanobacterial toxins on photosynthesis, the effects of toxins on in vitro O_2 evolution of thylakoid membranes were investigated (experiment 8). Partially intact thylakoids were isolated from tomato (*Solanum lycopersicum* L. 'Celebrity') leaves using a simplified version of the method described in [50]. Tomato was used because of its high concentration of chlorophyll and the ease with which chloroplasts are isolated from its leaves. Briefly, leaf tissue was homogenized in a blender with chloroplast buffer (350 mM sorbitol, 50 mM HEPES (pH 7.75), 5 mM EDTA (ethylene-diamine-tetra-acetic acid), 5 mM ascorbate, 2 mM dithiothreitol, and 2% polyvinylpyrrolidone), filtered through a cotton cloth, and centrifuged for 10 min at 500× *g* to remove intact cells and nuclei. The supernatant was layered onto 1M sucrose in 50 mM HEPES (pH 7.75) and then centrifuged in a swinging-bucket rotor for 10 min at 5000× *g*. The resulting crude chloroplast pellet was resuspended in 100 mM sucrose (resulting in hypotonic lysis, producing a thylakoid preparation) and frozen at −80 °C until further use. Isolated thylakoids were resuspended to 25 μg chlorophyll per mL in thylakoid resuspension buffer (4 mM magnesium chloride, 4 mM sodium chloride, 50 mM HEPES, and 0.01% Triton, pH 7.75). Thylakoid preparations were dispensed into 50 mL plastic "Falcon" tubes (5 replicate tubes per treatment), to which was added one of four toxins (ANA, BMAA, LPS, or MC-LR) to a final concentration of 1 μM toxin (ANA, BMAA, MC-LR) or 50 μg mL^{-1} (LPS); deionized water was added to the control group. Potassium ferricyanide ($K_3Fe(CN)_6$) was added to 4 mM to each tube as an artificial electron acceptor. After 15 min under 130–140 μmol m^{-2} s^{-1} PAR, the dissolved O_2 concentration was measured using a portable galvanic-type O_2-electrode meter (model HI 9142, Hannah Instruments, Woonsocket, RI, USA). After 25 min, another dissolved O_2 reading was taken, from which the rate of O_2 evolution was calculated.

2.7. Statistical Analysis

All statistics were computed in R version 4.3.2 [51]. Comparisons of means were analyzed with *t*-test (for two comparisons) or ANOVA (for more than two comparisons); unless otherwise stated, n = 4–6, depending on the experiment. Homogeneity of variance and normality distributions were assessed with Levene and Shapiro–Wilk tests, respectively. If variance was unequal between groups, a Welch's corrected t-test or ANOVA was performed instead (noted in the results). Fisher's LSD post hoc tests were performed for ANOVAs with a p-value ≤ 0.05. For Welch's corrected ANOVA, selected *t*-tests were used to evaluate biologically significant differences among means. Multivariate comparisons were visualized for lettuce grown hydroponically in toxins or cyanobacterial extracts using principal component analysis (PCA). Individual plant replicates were plotted on two orthogonal principal component axes. PSII yield (Φ_{PSII}) was excluded from the response variables used for PCA because it limited replicate inclusion and there were not biologically or statistically

significant differences in Φ_{PSII} among treatments. All other measured response variables were included and plotted as vectors indicating the direction and magnitude of their effects on multivariate differences among individuals. Treatment groups are indicated with hull polygons for clarity.

3. Results

3.1. Cyanobacterial Culture Effects on Plant Photosynthesis

Cyanobacterial culture treatment of soil-grown corn for 10–14 d: When roots of corn plants grown in soil were watered every 3 days for 14 days with *M. aeruginosa* culture (whole cells in nutrient solution), the plant biomass, shoot-to-root mass ratio, and leaf [chl] were reduced compared to control plants watered with only nutrient solution, while Φ_{PSII} was not affected (Figure 1). Similar results were obtained in a follow-up experiment wherein for soil-grown corn plants that were watered with either whole-cell or cell-free *M. aeruginosa* culture, leaf [chl], but not Φ_{PSII}, was reduced compared to control plants after 14 days (Figure 2). In a third experiment with soil-grown corn watered with *A. flos-aquae* culture (cells lysed and removed), P_n and G_s decreased and C_i increased within 3 days compared to the controls, while leaf [chl] did not decrease until day 6, and Φ_{PSII} did not change within 10 days (Figure 3). Decreases in P_n, G_s, and leaf [chl] became progressively larger over the course of the experiment, and they were accompanied by increases in C_i relative to the controls, indicating that decreases in P_n were not driven by decreases in G_s. Biomass was also reduced by the cyanobacteria treatment (Figure 3, inset; total plant fresh mass (g), means ± 1 S.E.: controls = 0.44 ± 0.48, + cyanobacteria = 0.35 ± 0.010).

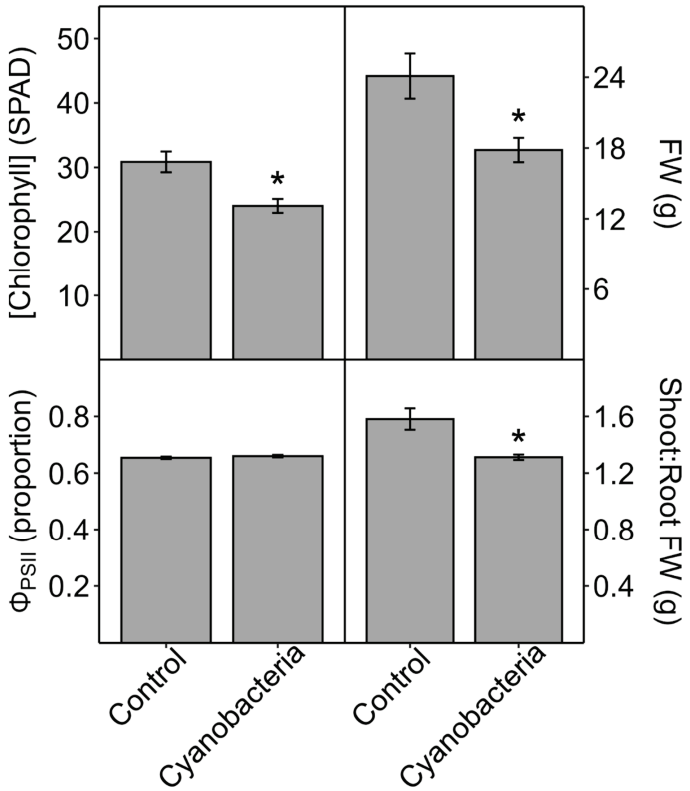


Figure 1. Effects of *Microcystis aeruginosa* culture (intact cells) on soil-grown corn (*Zea mays*) after 14 days. Roots of potted plants grown in the greenhouse were watered every third day with nutrient solution only (control) or nutrient solution containing live cyanobacteria. Just prior to harvest to obtain plant fresh weight (FW) and shoot-to-root FW ratio, yield of light-adapted Photosystem-II electron transport (Φ_{PSII}) and relative chlorophyll concentration ([chlorophyll] (SPAD)) were measured on recently expanded leaves of intact plants. Results are means ± 1 SE, n = 5–6, and significant treatment differences at $p \leq 0.05$ (t-test) are indicated with an asterisk.

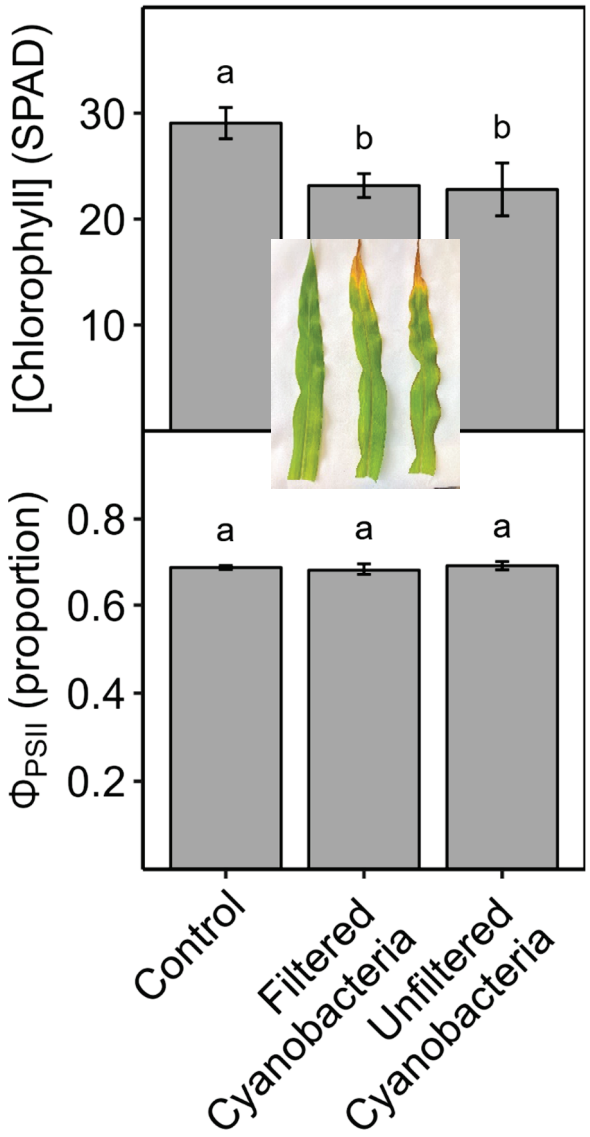


Figure 2. Effects of *Microcystis aeruginosa* culture (with or without intact cells) on soil-grown corn (*Zea mays*) plants after 14 days. Plants were grown and watered as in Figure 1 with nutrient solution only (control) or nutrient solution containing cell-free (filtered) or intact-cell (unfiltered) cyanobacterial culture. Yield of light-adapted Photosystem-II electron transport (Φ_{PSII}) and relative chlorophyll concentration ([chlorophyll] (SPAD)) were measured on recently expanded leaves of intact plants. Results are means $\pm$ 1 SE, n = 5, and significant treatment differences at $p \leq 0.05$ (ANOVA followed by LSD test) are indicated with different letters above bars. Insert photo shows leaves (ca. 3 cm wide) from each treatment after 14 d in the same order as the *X*-axis.

Cyanobacterial culture treatment of hydroponic corn treated for 24 h: When roots of young corn plants were submerged for 24 h in either *M. aeruginosa* or *A. flos-aquae* culture (cells lysed and removed), P_n and G_s decreased in *A. flos-aquae*-treated plants, while C_i increased (non-significantly for G_s and C_i); P_n, G_s, and C_i were not affected in *M. aeruginosa*-treated plants within this time frame (Figure 4). Neither Φ_{PSII} nor leaf [chl] were affected by either cyanobacterial culture within 24 h.

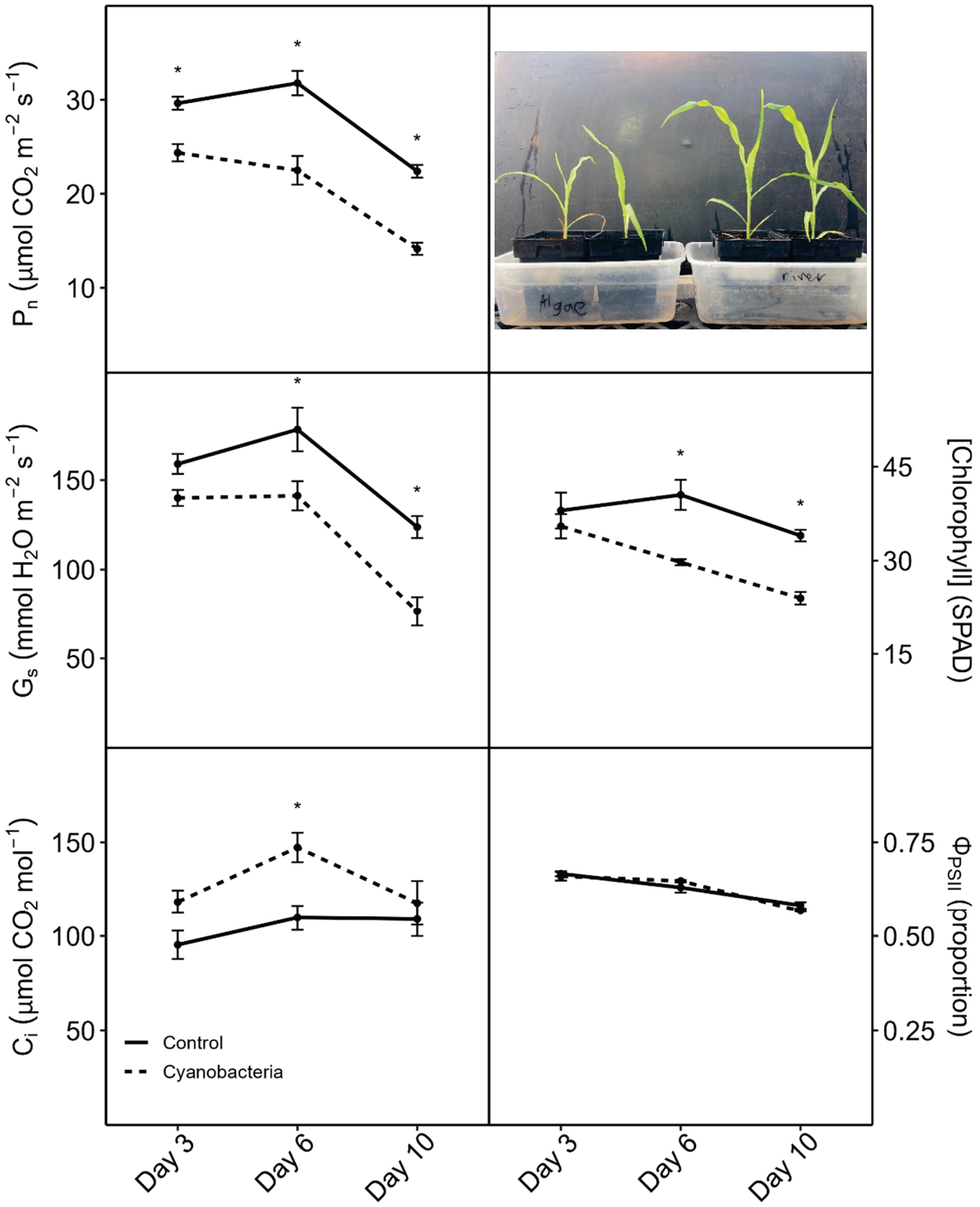


Figure 3. Effects of *Anabaena flos-aquae* culture (cells lysed and removed) on soil-grown corn (*Zea mays*) plants after 10 days. Plants were grown and watered as above with nutrient solution only (control) or nutrient solution containing cell-free (cells lysed and then filtered) cyanobacterial culture. Net photosynthesis (P_n, CO_2 uptake), stomatal conductance (G_s), internal CO_2 concentration (C_i), yield of light-adapted Photosystem-II electron transport (Φ_{PSII}), and relative chlorophyll concentration ([chlorophyll] (SPAD)) were measured on recently expanded leaves of intact plants. Results are means ± 1 SE, $n = 4$, and significant treatment differences between treatments within each day at $p \leq 0.05$ (*t*-test) are indicated with an asterisk. Insert photo shows plants from each treatment, with the control on the right.

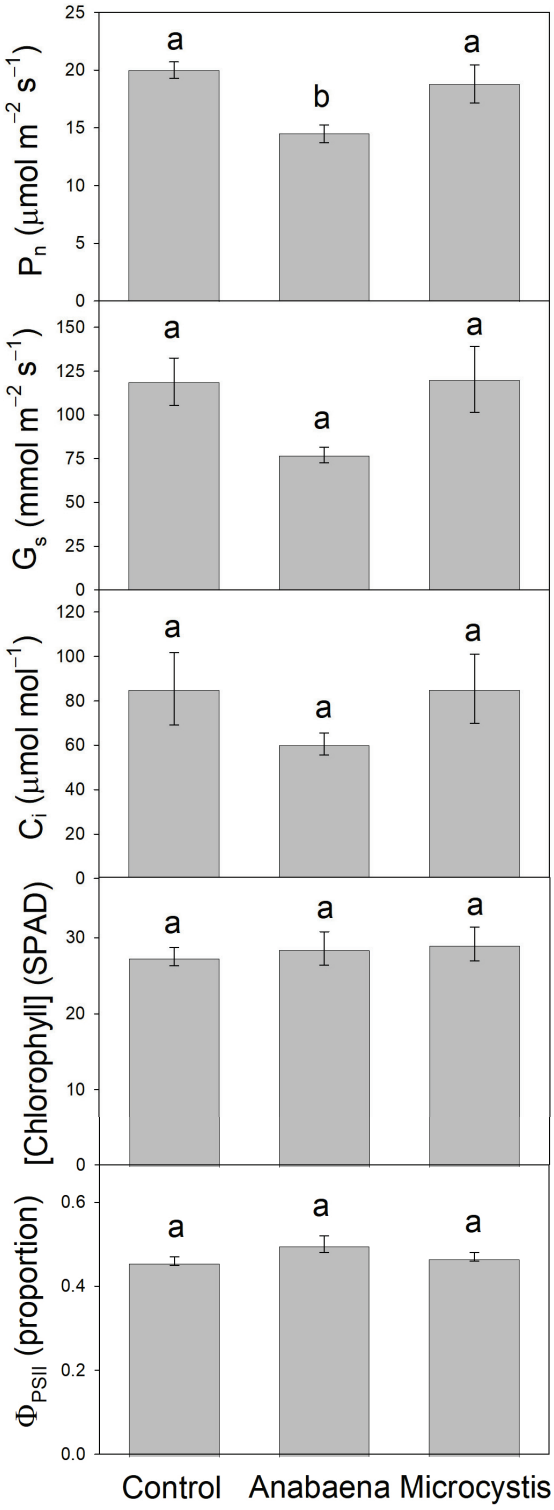


Figure 4. Effects of *Anabaena flos-aquae* or *Microcystis aeruginosa* culture (cells lysed and removed) on hydroponic corn (*Zea mays*) plants after 24 h. Plants were grown in soil and transferred to glass containers with roots submerged in nutrient solution only (control) or nutrient solution containing cell-free (cells lysed and then filtered) cyanobacterial culture. Net photosynthesis (P_n, CO_2 uptake), stomatal conductance (G_s), internal CO_2 concentration (C_i), yield of light-adapted Photosystem-II electron transport (Φ_{PSII}), and relative chlorophyll concentration ([chlorophyll] (SPAD)) were measured on recently expanded leaves of intact plants. Results are means ± 1 SE, n = 4–6, and significant treatment differences at $p \leq 0.05$ (ANOVA followed by LSD test) are indicated with different letters above the bars.

Cyanobacterial culture treatment of infiltrated corn and lettuce leaves for 1–3 h: When leaf discs of corn and lettuce were vacuum-infiltrated with either *M. aeruginosa* or *A. flos-aquae* culture (cells lysed and removed), Φ_{PSII} was reduced compared to controls within 3 h in corn treated with *A. flos-aquae* but not with *M. aeruginosa* (Figure 5). In lettuce, Φ_{PSII} was reduced compared to controls within 1 h in both *M. aeruginosa* and *A. flos-aquae* treated plants.

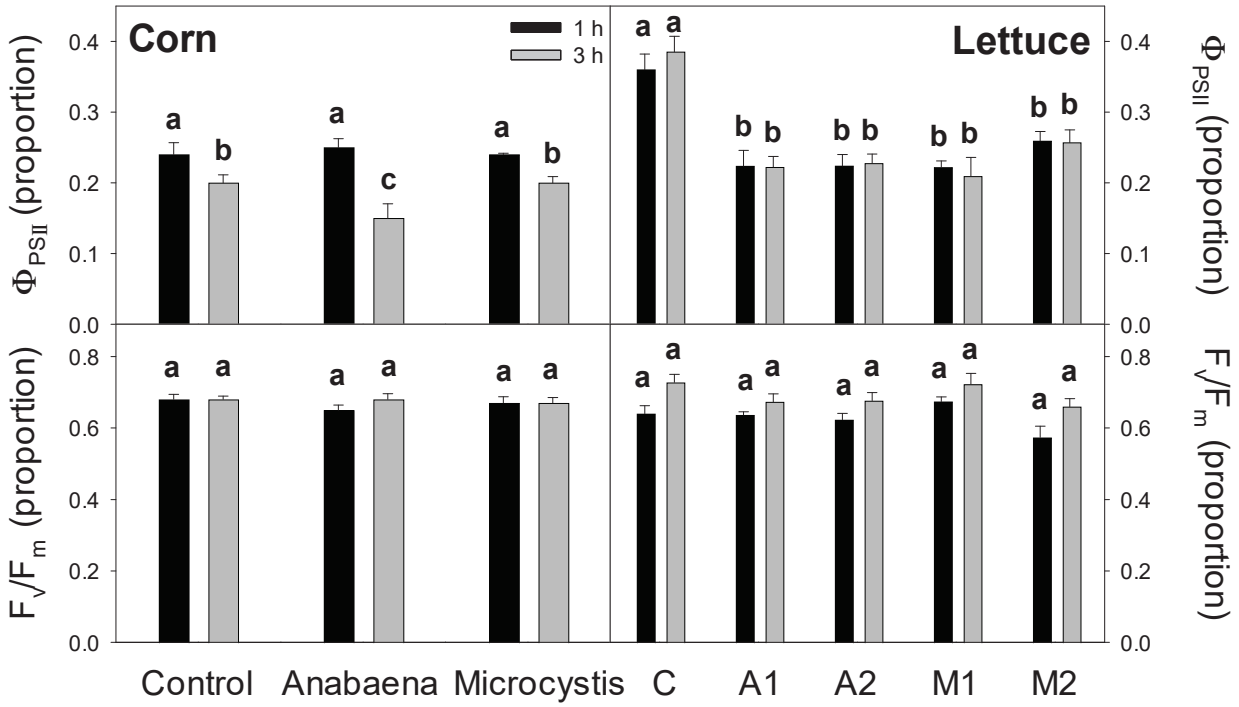


Figure 5. Effects of *Anabaena flos-aquae* or *Microcystis aeruginosa* culture (cells lysed and removed) on leaf pieces of corn (*Zea mays*) or lettuce (*Lactuca sativa*) after 1 or 3 h. Leaf pieces were vacuum-infiltrated with nutrient solution only (control, C) or nutrient solution containing cyanobacterial culture (*Anabaena*, A; *Microcystis*, M). For lettuce, two independent cultures of each species were tested (A1, A2; M1, M2). The yields of light-adapted Photosystem-II (PSII) electron transport (Φ_{PSII}) and dark-adapted maximum PSII efficiency (F_v/F_m) were measured on leaf tissue from recently expanded leaves (for Φ_{PSII}, 750 $\pm$ 25 μmol m^{-2} s^{-1} PAR). Results are means + 1 SE, n = 5, and significant treatment differences at $p \leq 0.05$ (ANOVA followed by LSD test) are indicated with different letters above bars.

3.2. Individual Toxin Effects on Plant Photosynthesis

Individual toxin (and cyanobacterial-culture) treatments of hydroponic lettuce for 10 d: When roots of young lettuce plants were submerged for 10 days in either *A. flos-aquae* culture (cells lysed and removed) or individual pure toxins (ANA, BMAA, LPS, or MC-LR), P_n was reduced compared to the controls (the decreases were significant only with cyanobacterial culture and anatoxin, wherein P_n decreased by 41%) (Figure 6). Large but non-significant decreases in G_s were observed with anatoxin and MC-LR, and G_s increased non-significantly with BMAA. Small non-significant changes in C_i were observed for anatoxin (decrease) and BMAA (increase); otherwise, there were no meaningful differences between treatments and controls. None of the treatments had significant effects on Φ_{PSII}, leaf [chl], or growth (increase in fresh mass, ΔFM), though non-significant decreases in leaf [chl] were observed with cyanobacterial culture and anatoxin, and non-significant increases in growth were observed with BMAA and LPS. Because the number of replicates per treatment (and hence the power) was constrained in this experiment by logistics, we then included all of the response parameters in a clustering analysis (PCA) and found that all treatments except LPS caused divergence from the controls, especially cyanobac-

terial culture, anatoxin, and MC-LR, while the two-dimensional space for LPS expanded compared to the controls (Figure 7).

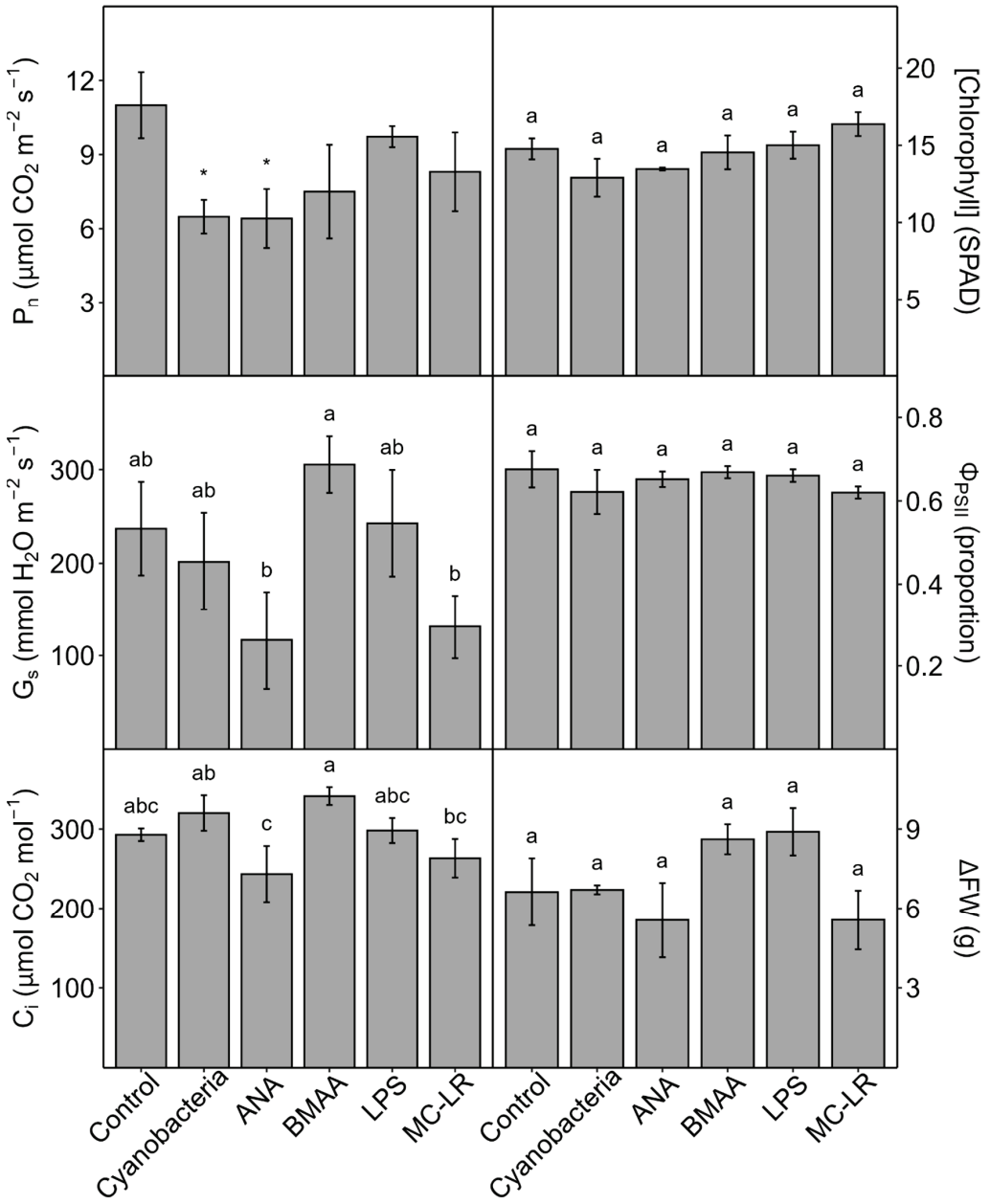


Figure 6. Effects of *Anabaena flos-aquae* culture or pure cyanobacterial toxins on hydroponic lettuce (*Lactuca sativa*) plants after 10 days. Plants were grown in soil and transferred to glass containers with roots submerged in nutrient solution only (control), cyanobacterial culture (cells lysed and removed from nutrient solution), or individual toxins in nutrient solution (0.5 µM: anatoxin-a, ANA, beta-methyl-amino-alanine, BMAA, microcystin-LR; 25 µg mL^{-1}: lipopolysaccharide, LPS). Just prior to harvest to obtain the increase in plant fresh weight during treatment (ΔFW), net photosynthesis (P_n, CO_2 uptake), stomatal conductance (G_s), internal CO_2 concentration (C_i), yield of light-adapted Photosystem-II electron transport (Φ_{PSII}), and relative chlorophyll concentration ([chlorophyll] (SPAD)) were measured on recently expanded leaves of intact plants. Results are means ± 1 SE, $n = 4$. Significant treatment differences at $p \leq 0.05$ (ANOVA followed by LSD test) are indicated with different letters above bars, except for P_n, where significant differences (Welch's ANOVA and *t*-test) from the control are indicated with asterisks (see Section 2).

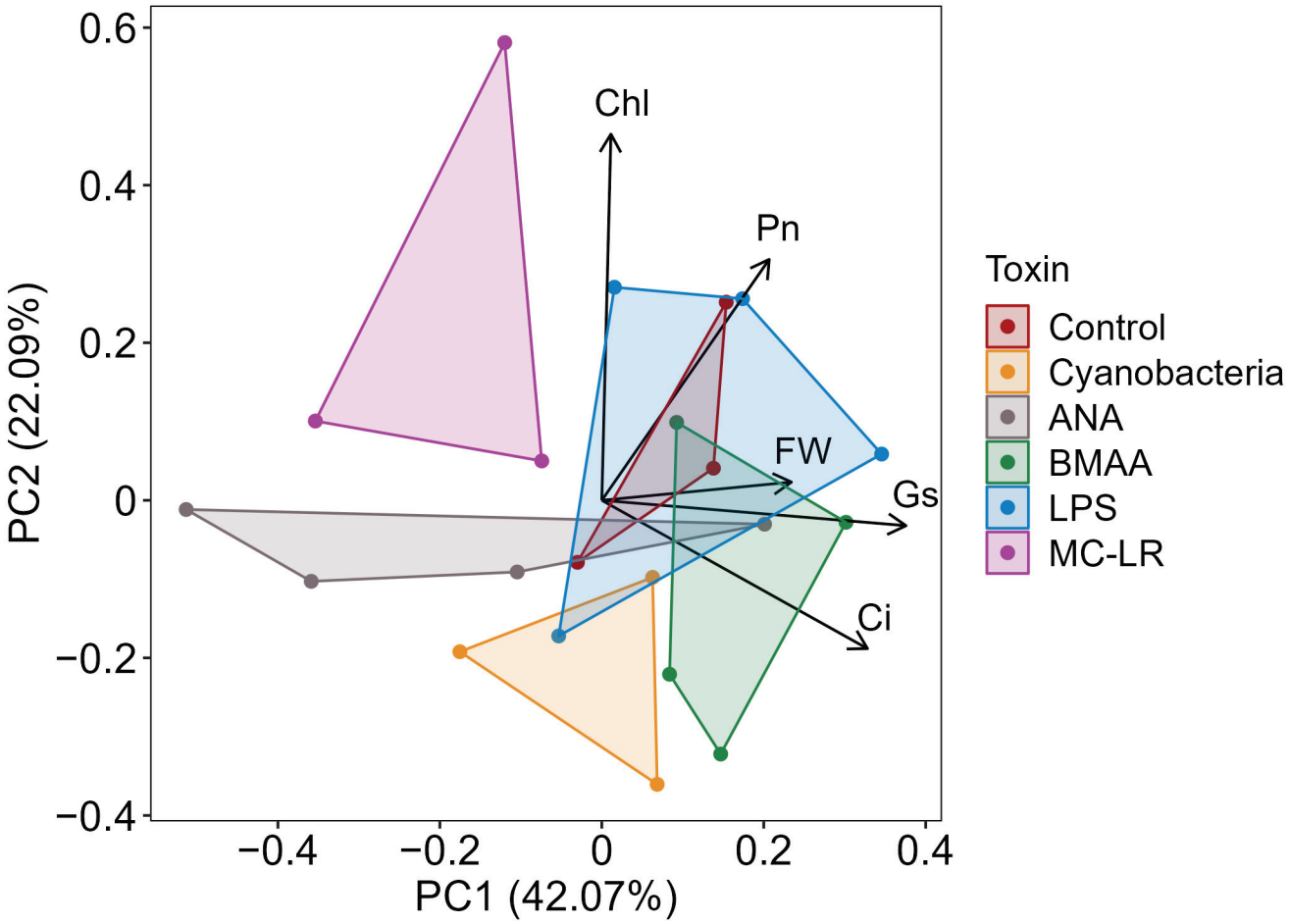


Figure 7. Principal components analysis (PCA) visualizing overall differences in the responses of lettuce (*Lactuca sativa*) to *Anabaena flos-aquae* culture and individual toxins from Figure 6. Vectors represent relative chlorophyll concentration (Chl), net photosynthesis (P_n), increase in fresh weight (FW), stomatal conductance (G_s), and internal CO_2 concentration (C_i). Points represent eigen-values of individual replicate plants. Differences in replicates are visualized based on their position on two orthogonal principal component axes. The direction and magnitude of response-variable vectors indicate their direction and degree of effect on the replicate position. Treatments are indicated by color: nutrient solution only (control); cyanobacterial culture, cells lysed and removed from nutrient solution (Cyanobacteria); or individual toxins in nutrient solution (0.5 µM: anatoxin-a, ANA, beta-methyl-amino-alanine, BMAA, microcystin-LR, MC-LR; 25 µg mL^{-1}: lipopolysaccharide, LPS).

The above experiment was then independently replicated (minus the cyanobacterial-extract treatment) to investigate the effects of individual toxins on in vivo rubisco activity, an indication of toxin effects on CO_2-fixation reactions, and to confirm the general effects of toxins on P_n, G_s, and C_i. In this second experiment, ANA reduced rubisco activity by 19.5%, while BMAA and LPS caused smaller (non-significant) reductions, and MC-LR caused no reduction (Figure 8). As in the first experiment, in the repeat experiment, P_n measured at 400 µmol/mol CO_2 was reduced the most by ANA (35%), with smaller (non-significant) reductions for BMAA, LPS, and MC-LR; no significant effects of toxins on G_s and C_i were observed (Supplemental Table S1). To confirm the above effects of ANA on rubisco activity, we then measured the effects of ANA vs. the control on rubisco activity in another (third) independent experiment and found that ANA reduced rubisco activity by 17%.

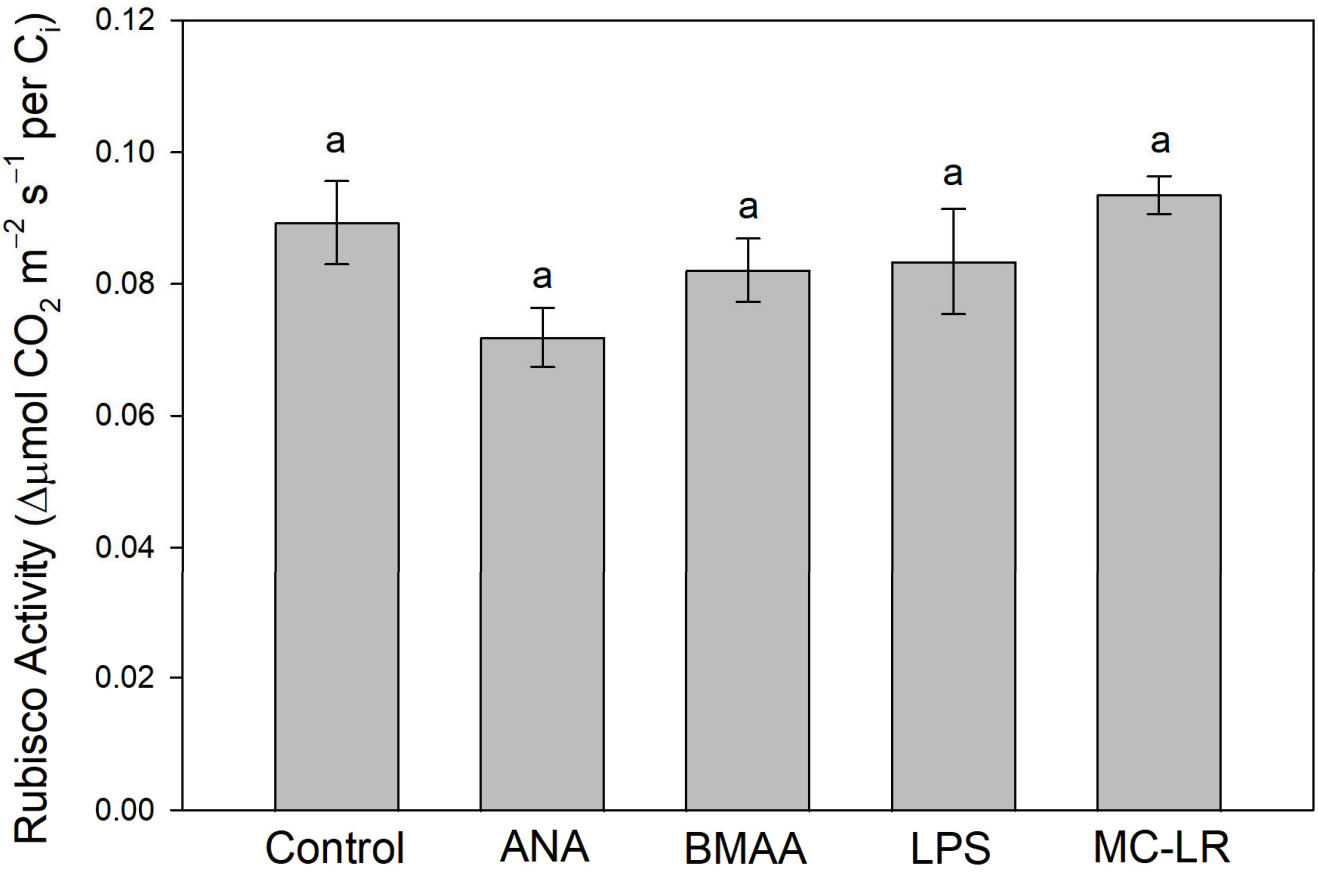


Figure 8. Effects of pure cyanobacterial toxins on in vivo rubisco activity in hydroponic lettuce (*Lactuca sativa*) plants after 10 days. Plants were grown and treated as in Figure 6, with roots submerged in nutrient solution only (control) or individual toxins in nutrient solution (0.5 μM: anatoxin-a, ANA, beta-methyl-amino-alanine, BMAA, microcystin-LR, MC-LR; 25 μg mL^{-1}: lipopolysaccharide, LPS). Rubisco activity was determined from the initial slope of the photosynthesis–CO_2 response curve, measured in recently expanded attached leaves at 1000 μmol m^{-2} s^{-1} PAR and 25 °C. Results are means ± 1 SE, n = 4. There were no significant treatment differences with ANOVA (p = 0.12), as indicated by the same letters above the bars, but ANA differed from the control with one-tailed t-test (p = 0.03).

Individual toxin treatment of infiltrated lettuce leaves infiltrated for 2–3 h: When leaf discs of lettuce were vacuum-infiltrated with individual pure toxins, neither dark-adapted F_v/F_m (maximum PSII efficiency) nor light-adapted Φ_{PSII} (PSII yield) was significantly affected after 2 h, although the values for LPS and MC-LR were lowest among all treatments (Figure 9). In a follow-up experiment, when leaves were vacuum-infiltrated with LPS or MC-LR at a higher concentration, Φ_{PSII} decreased after 3 h (significant for MC-LR), but F_v/F_m did not (Figure 10).

Individual toxin treatment of tomato chloroplast membranes for ca. 1 h: When chloroplast membranes were treated with individual pure toxins, none of the toxins significantly affected photosynthetic O_2 evolution, although the BMAA was lower than all other treatments (Figure 11).

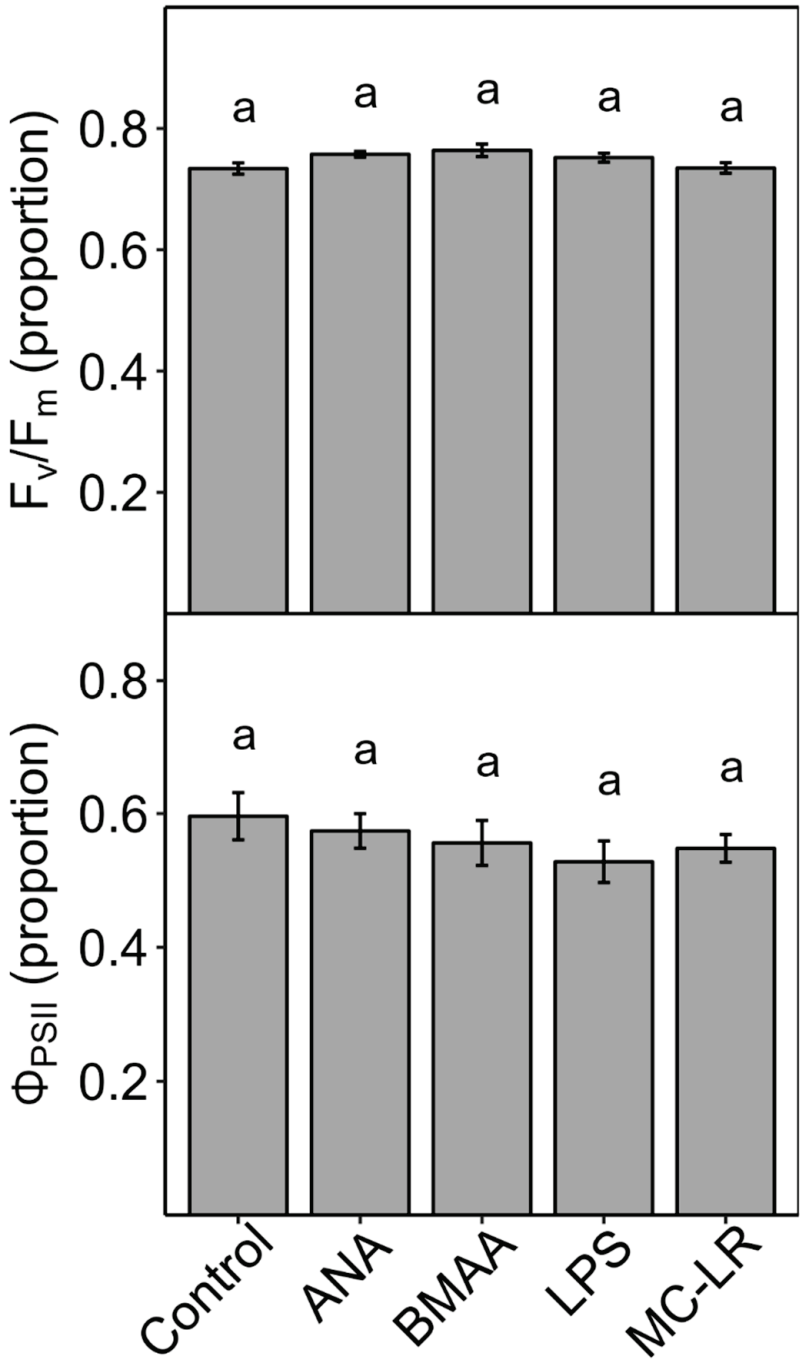


Figure 9. Effects of individual cyanobacterial toxins on detached leaves of lettuce (*Lactuca sativa*) after 2 h. Leaf pieces were vacuum-infiltrated with deionized water only (control) or individual toxins in deionized water (1 μM: anatoxin-a, ANA, beta-methyl-amino-alanine, BMAA, microcystin-LR, MC-LR; 50 μg mL^{-1}: lipopolysaccharide, LPS). Leaves were then incubated for 2 h under 450 ± 25 μmol m^{-2} s^{-1} PAR or in the dark, after which the yield of light-adapted Photosystem-II (PSII) electron transport (Φ_{PSII}) or dark-adapted maximum PSII efficiency (F_v/F_m) was measured. Results are means ± 1 SE, n = 5. There were no significant effects of toxins on Φ_{PSII} or F_v/F_m (ANOVA, $p > 0.05$), as indicated by the same letters above the bars.

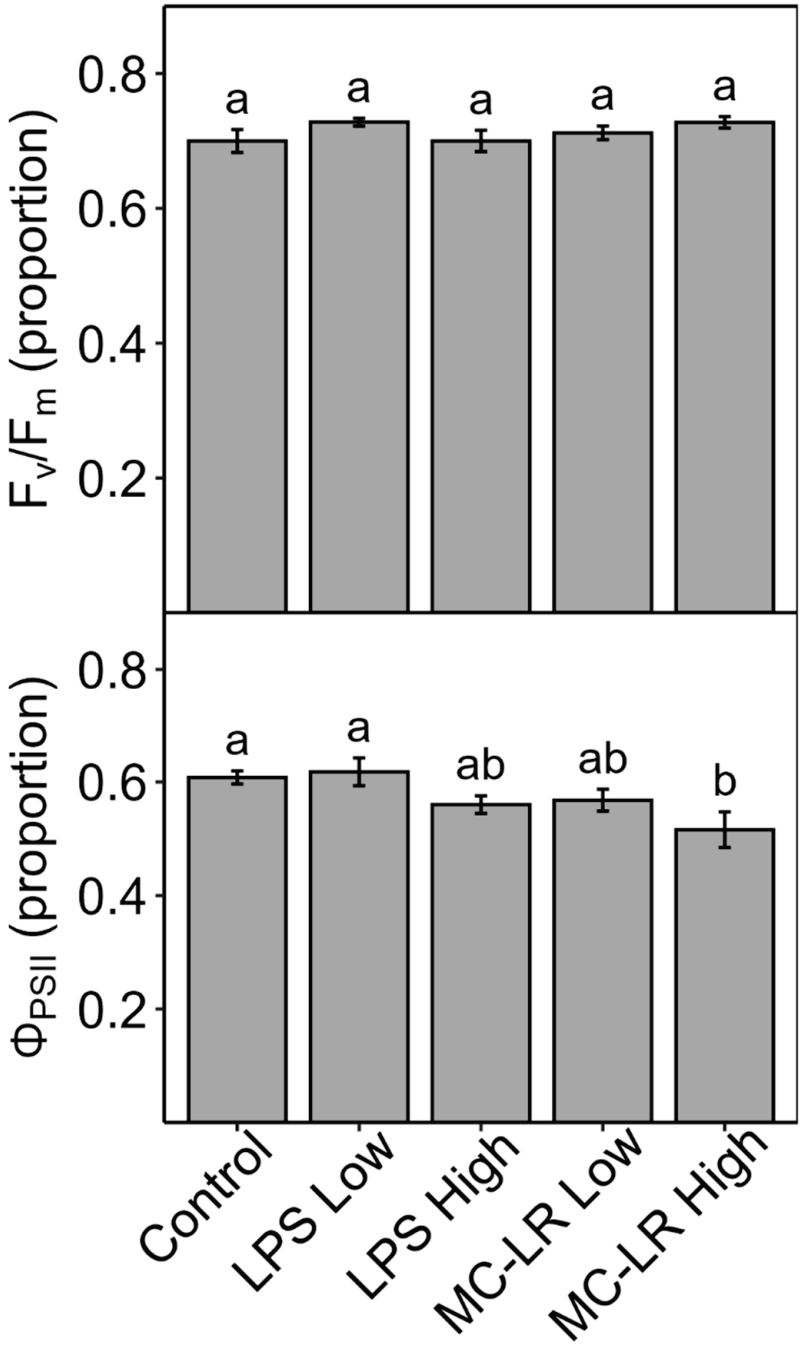


Figure 10. Effects of low vs. high concentrations of the cyanobacterial toxins, lipopolysaccharide (LPS), and microcystin-LR (MC-LR) on detached leaves of lettuce (*Lactuca sativa*) after 3 hours. Leaf pieces were vacuum-infiltrated with deionized water only (control) or 1 μM MC-LR (MC-LR Low), 10 μM MC-LR (MC-LR High), 50 μg mL^{-1} LPS (LPS Low), or 250 μg mL^{-1} LPS (LPS High). Leaves were then incubated for 3 h under 750 ± 25 μmol m^{-2} s^{-1} PAR or in the dark, after which the yield of light-adapted Photosystem-II (PSII) electron transport (Φ_{PSII}) or dark-adapted maximum PSII efficiency (F_v/F_m) was measured. Results are means ± 1 SE, $n = 5$, and significant treatment differences at $p \leq 0.05$ (ANOVA followed by LSD test) are indicated with different letters above bars.

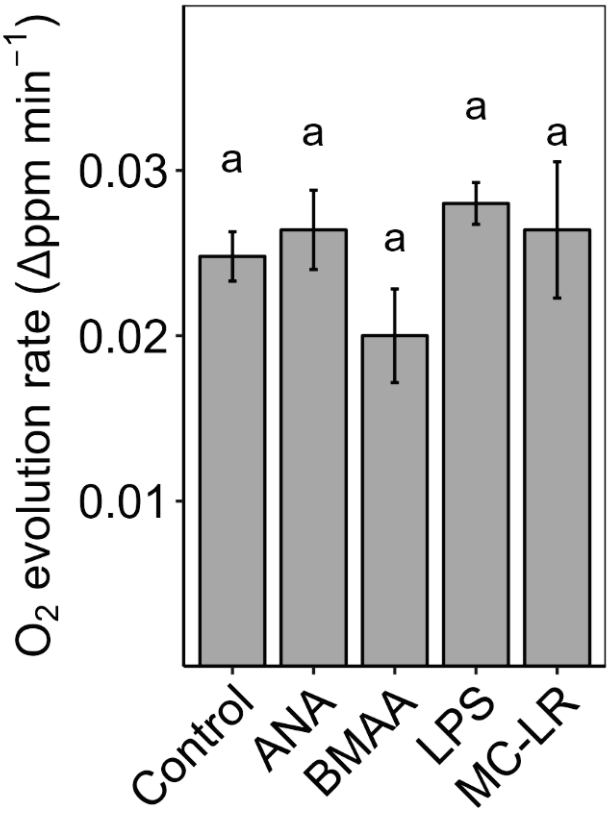


Figure 11. The effects of cyanobacterial toxins on in vitro O_2 evolution of thylakoid membranes. Chloroplasts were isolated from tomato (*Solanum lycopersicum*) leaves and lysed to obtain thylakoids. Thylakoids were treated with either deionized water or individual toxins (1 μM: anatoxin-a, ANA, beta-methyl-amino-alanine, BMAA, microcystin-LR, MC-LR; 50 μg mL^{-1}: lipopolysaccharide, LPS). Results are means ± 1 SE, $n = 5$. There were no significant effects of toxins on O_2 evolution (ANOVA, $p > 0.05$), as indicated by the same letters above the bars.

4. Discussion

A limited number of previous studies have reported variable effects (negative to neutral to positive) of cHAB cell-extracts or toxins on one or more aspects of photosynthesis in cyanobacteria, eukaryotic algae, and aquatic and terrestrial plants (e.g., [4,9,16]). However, because these studies often differed in study organisms, toxins, dosage, duration, mode of exposure, and the photosynthetic response variable measured, it is not clear which cHAB toxins affect photosynthesis and how. To clarify if and how cHAB toxins affect photosynthesis in terrestrial plants, we investigated short-term and longer-term effects of cHAB extracts from two different cHAB species and four individual toxins on multiple aspects of photosynthesis in two different plant species exposed to toxins through roots or leaves.

When corn plants were grown in soil and watered with cHAB culture or extract, plant growth (Figures 1 and 3), leaf chlorophyll concentration (Figures 1–3), and net (overall) photosynthesis (P_n, Figure 3) were reduced significantly, but the PSII yield (Φ_{PSII}) was not affected (Figures 1–3). The effects were observed with either *M. aeruginosa* or *A. flos-aquae* cyanobacteria and with whole-cell culture in nutrient solution, culture with cells removed, or culture with cells lysed and removed (the latter is functionally equivalent to cyanobacterial extract used in other studies). These cHAB-caused decreases in P_n were accompanied by decreases in stomatal conductance (G_s, an index of stomatal opening), but the increases in leaf internal CO_2 concentration (C_i) indicate that declines in P_n were caused by damage to photosynthetic metabolism rather than stomatal closure. Because Φ_{PSII} is determined by PSII efficiency and electron transport downstream from PSII [52], the lack of toxin effects on Φ_{PSII} indicates that photosynthetic electron transport was not impacted in

these experiments. Hence, the damage to photosynthesis was likely due to CO_2-fixation (i.e., the Calvin Cycle) and/or due to the loss of chlorophyll. Because Φ_{PSII} reflects the relative performance of existing PSII centers independent of their concentration in the leaf, and this did not decrease, then the loss of chlorophyll per unit leaf area indicates a reduction in the concentration of PSII per unit area, which would contribute to a decrease in P_n (confirmed in Figure 3). However, decreases in P_n occurred prior to decreases in leaf [chl], indicating that some of the decrease in P_n was attributable to damage to the Calvin Cycle (e.g., rubisco activity, Figure 8). Similarly to this study, a decrease in P_n (measured as O_2 evolution after 42 d of exposure) was observed in soil-grown spinach (*Spinacia oleracea*) watered with cHAB extract derived from *M. aeruginosa* and *Aphanizomenon flos-aquae* containing 0.5 μg/L MC-LR [45]. In contrast, cHAB extract derived from *M. aeruginosa* containing up to 22,000 μg/L MC-LR decreased the maximum PSII efficiency (dark F_v/F_m; measured after 30 d) in sand-grown tomato [46], while an *M. aeruginosa* extract containing up to 10 μg/L MC-LR increased P_n (measured after 15 d) in lettuce grown in bark and vermiculite [47].

Importantly, our experiments with soil-grown plants could not determine if the effects of cHAB cultures or extracts on photosynthesis were direct primary or indirect secondary effects, as decreases in leaf [chl] or P_n were not observed until after three or more days of treatment. To investigate if cHAB extracts had short-term, and thus possibly direct, effects on photosynthesis, we examined the effects on photosynthesis in (1) hydroponic corn plants with roots immersed for only 24 h in cHAB extract, and (2) corn and lettuce leaf tissue vacuum-infiltrated with cHAB extract for only 1 or 3 h. In the hydroponic corn, P_n, G_s, and C_i all decreased within 24 h, and leaf [chl] and Φ_{PSII} were unaffected (Figure 4). In the vacuum-infiltrated leaf tissue, light-adapted Φ_{PSII} decreased, but dark-adapted F_v/F_m did not (Figure 5), indicating that damage to PSII was from photo-inhibition (light-dependent photo-oxidation). Interestingly, in these experiments, lettuce was sensitive to extracts from both *M. aeruginosa* and *A. flos-aquae*, while corn was sensitive to only *A. flos-aquae* extract. Rapid ($\leq$1 h) effects of cHAB extracts on photosynthesis (i.e., Φ_{PSII}) in some eukaryotic algae have also been observed [18,41]. Our results above indicate that some cHAB toxins can have rapid negative effects on photosynthesis in plants, but that the effects can differ depending on the mode of exposure (roots vs. leaves), which has relevance for the method used when irrigating crops with cHAB-contaminated water (e.g., drip vs. spray, as in [11]).

Because cHAB irrigation water, lab cultures, or cell extracts likely contain many toxins, including rarely measured toxic peptides besides MCs [19], any cHAB effects on photosynthesis cannot be attributed to any single toxin without additional investigation. Consequently, we then conducted several experiments wherein we treated plants with individual pure cHAB toxins. In hydroponic lettuce plants with roots exposed to cHAB extract or individual toxins for 10 d, P_n decreased (although not always significantly) in all treatments, especially cHAB (*A. flos-aquae*) extract and pure anatoxin-a ("Cyanobacteria" and "ANA" treatments in Figure 6 and Table S1). These decreases were not associated with damage to photosynthetic electron transport, except possibly in Cyanobacteria and MC-LR treatments (which had small non-significant decreases in Φ_{PSII}) or due to loss of chlorophyll, except possibly in Cyanobacteria and ANA treatments (which had small non-significant decreases). The decreases in P_n were also not associated with stomatal closure, with the possible exception of ANA (Figure 6), BMAA, (Table S1), and MC-LR (Figure 6 and Table S1), as indicated by small non-significant decreases in C_i. Damage to the CO_2-fixation reactions of photosynthesis was suggested by non-significant increases in C_i with Cyanobacteria and BMAA treatments (Figure 6), and by decreases in rubisco activity with ANA (and, to a lesser extent, BMAA and LPS) (Figure 8). Results from the two replicate experiments with hydroponic lettuce indicate that (1) cHAB extract and all four cHAB toxins negatively affected photosynthesis in some way; (2) neither cHAB extract nor any individual toxin had a single main lesion to photosynthesis; and (3) all five treatments (cHAB extract and four toxins) each affected photosynthesis in different ways. The latter conclusion was confirmed with a multi-variate statistical analysis (PCA), which showed that Cyanobacteria (extract), ANA, BMAA, MC-LR, and the control sorted almost

completely independently of each other, and LPS overlapped with the control but had an expanded two-dimensional space (Figure 7). Our results are consistent with past studies, most of which observed negative effects of individual cHAB toxins on photosynthesis, e.g., MC-RR in cyanobacteria (decrease in chl a, phycocyanin; [40]); MC-LR, -RR, -YR, and -LF in various eukaryotic algae (decrease in Φ_{PSII}; [18,41]); MC-LR in soybean (*Glycine max*) (decrease in P_n; [44]) and cat-tail (*Typha angustifolia*) (decreases in P_n, G_s, C_i, chl, in vitro rubisco activity; [43]); ANA in *Lemna* species (decrease in P_n, chl; [25,27]) and *Ceratophyllum demersum* (decrease in chl; [26]); and LPS in *Arabidopsis thaliana* (decrease in F_v/F_m; [36]).

As with our experiments with cHAB extract, we conducted experiments with individual cHAB toxins in which we vacuum-infiltrated leaf tissue to determine if any of the toxins had short-term effects on photosynthesis (i.e., Φ_{PSII}). At relatively low concentrations of toxin (50 μg mL^{-1} LPS, 1 μM ANA/BMAA/MC-LR) and light (450 ± 25 μmol m^{-2} s^{-1} PAR), neither light-adapted Φ_{PSII} nor dark-adapted F_v/F_m were significantly affected, although Φ_{PSII} was lowest in LPS and MC-LR (Figure 9). To follow up, we then examined the effects of LPS and MC-LR at higher concentrations (250 μg mL^{-1} LPS, 10 μM MC-LR) and with brighter light (750 ± 25 μmol m^{-2} s^{-1} PAR), which resulted in larger decreases in Φ_{PSII} but (still) no effects on F_v/F_m (Figure 10). Hence, as with cHAB extract, the negative effects of LPS and MC-LR on PSII were associated with photo-inhibitory damage to PSII, and this damage increased with the dosage. Similarly to this study, Perron et al. [18] found that MC caused little decrease in maximum PSII efficiency (equivalent to our F_v/F_m) in all four species of eukaryotic algae examined but large decreases in PSII yield (equivalent to our Φ_{PSII}) and that damage to Φ_{PSII} was dose-dependent. Also, as noted above, Shang-Guan et al. [36] found that LPS decreased PSII function, although, in their case, F_v/F_m.

Because neither cHAB extracts nor individual toxins affected the maximum PSII efficiency (dark-adapted F_v/F_m) and only affected the PSII yield (light-adapted Φ_{PSII}), there was no indication of a direct immediate effect of cHAB toxins on photosynthesis in our experiments. To confirm this, we exposed isolated chloroplast thylakoids to individual toxins (ANA/BMAA/LPS/MC-LR), and none of the toxins decreased in vitro photosynthetic O_2 evolution significantly (Figure 11). Therefore, our experiments indicated that the negative effects of cHAB toxins were not the consequence of direct immediate effects on photosynthetic metabolism but were rather due to indirect secondary effects, such as decreases in plant N status leading to decreases in the concentration of chlorophyll and other photosynthetic machinery, oxidative stress, such as photo-inhibition, and/or stomatal closure limiting CO_2 uptake. As with cHAB extracts noted above, some past studies have found that individual cHAB toxins can have rapid ($\leq$1 h) effects on photosynthesis. For example, both Perron et al. [18] and Garcia-Espin et al. [41] observed rapid effects of MC on Φ_{PSII} in eukaryotic algae, and Abe et al. [27] and Kaminski et al. [44] observed such effects on P_n in soybean with MC and *Lemna triscula* with ANA, respectively. Hence, direct effects of cHAB toxins on photosynthetic machinery cannot be ruled out yet.

As we expected, in our experiments, there were indications that whole-cell cHAB culture or extract had more severe effects on photosynthesis than individual toxins. First, decreases in Φ_{PSII} were greater for cHAB extract than for any individual toxin (Figure 5 vs. Figures 9 and 10). Second, decreases in P_n were greatest for cHAB extract compared to all individual toxins except for ANA (which caused a similar decrease) (Figure 6). In contrast, Perron et al. [18] found similar decreases in the green alga, *Chlorella vulgaris*, in Φ_{PSII} for pure MC-LR and an amount of *M. aeruginosa* extract containing an equal concentration of MC-LR (and no significant levels of other MCs). Garcia-Espin et al. [41] also found that decreases in Φ_{PSII} were greater for two different cHAB extracts than for pure MC-LR in the four eukaryotic algae species examined.

In general, the two species examined in our study, corn and lettuce, showed similar photosynthetic responses to cHAB toxins, with some exceptions. In hydroponic plants of both species, cHAB extract from *A. flos-aquae* decreased P_n significantly, with smaller or no effects on Φ_{PSII} (Figure 4 vs. Figure 6), and it decreased Φ_{PSII} significantly in vacuum-

infiltrated leaf tissue (Figure 5). However, as noted above, Φ_{PSII} in lettuce was more sensitive than in corn to cHAB extract from *M. aeruginosa* (Figure 5). It should also be noted that growth in soil-grown corn was very sensitive to cHAB extract (Figures 1 and 3) but was unaffected in hydroponic lettuce, despite similar decreases in P_n (Figure 3 vs. Figure 6). Both Perron et al. [18] and Garcia-Espin et al. [41] found that sensitivity of Φ_{PSII} to cHAB toxins varied among species of eukaryotic algae, and Pflugmacher et al. [45] found variation among spinach varieties as far as sensitivity of P_n to cHAB extract.

5. Conclusions

Research to date has yielded conflicting results regarding the effects of cyanobacterial toxins on photosynthesis. We investigated short- to longer-term effects of cyanobacterial cultures/extracts and four individual toxins (anatoxin-a, beta-methyl-L-amino alanine, lipopolysaccharides, microcystin-LR) on multiple aspects of photosynthesis in two species of terrestrial plants (corn/*Zea mays*, lettuce/*Lactuca sativa*) exposed to toxins through roots or leaves. We found that at ecologically relevant concentrations, (1) cyanobacterial culture/extract and all four toxins negatively affected photosynthesis, although in different ways; (2) neither cyanobacterial culture/extract nor any individual toxin had a single main lesion to photosynthesis; (3) the mode of toxin exposure mattered, as the exposure of roots to toxins decreased photosynthetic CO_2-fixation (i.e., the Calvin Cycle) and/or chlorophyll concentration but not photosynthetic electron transport (P_{et}), while direct treatment of leaves reduced P_{et} in a light-dependent manner (photo-inhibition); and (4) in general, photosynthesis in corn and lettuce responded similarly to cyanobacterial cultures and toxins. These results improve our understanding of the negative effects of cyano-toxins on plants, which has implications for both growers and consumers of crops irrigated with cHAB water.

Supplementary Materials: The supporting information (Table S1) can be downloaded at: https://www.mdpi.com/article/10.3390/plants13223190/s1. Table S1: Results from Experiment 6b-Effects of pure toxins on leaf-level photosynthesis (Pn; μmol CO_2 m^{-2} s^{-1}), stomatal conductance (Gs; mmol m^{-2} s^{-1}), and internal [CO_2] (mol/mol) in hydroponic lettuce (Lactuca sativa) plants after 10 days.

Author Contributions: Conceptualization and methodology, S.A.H., C.T.M. and M.D.T.; investigation and analysis, S.A.H., C.T.M., M.D.T., E.P.V., S.B., C.E., J.T.F. and E.R.N.; writing—original draft preparation, S.A.H., M.D.T. and C.T.M.; writing—review and editing, S.A.H. and J.K.B.; supervision, S.A.H.; project administration, S.A.H.; funding acquisition, S.A.H. and J.K.B. All authors have read and agreed to the published version of the manuscript.

Funding: This research was funded by the U.S. Department of Agriculture (NACA 58-5082-1-009). Mention of trade names or commercial products in this publication is solely for the purpose of providing specific information and does not imply recommendation or endorsement by the U.S. Department of Agriculture. The USDA is an equal opportunity provider and employer.

Data Availability Statement: Datasets are available upon request.

Acknowledgments: The authors thank Steven Murphy for his assistance with greenhouse maintenance.

Conflicts of Interest: The authors declare no conflicts of interest.

References

1. Visser, P.M.; Verspagen, J.M.H.; Sandrini, G.; Stal, L.J.; Matthijs, H.C.P.; Davis, T.W.; Paerl, H.W.; Huisman, J. How Rising CO_2 and Global Warming May Stimulate Harmful Cyanobacterial Blooms. *Harmful Algae* **2016**, *54*, 145–159. [CrossRef] [PubMed]
2. Igwaran, A.; Kayode, A.J.; Moloantoa, K.M.; Khetsha, Z.P.; Unuofin, J.O. Cyanobacteria Harmful Algae Blooms: Causes, Impacts, and Risk Management. *Water. Air. Soil Pollut.* **2024**, *235*, 71. [CrossRef]
3. Chen, W.; Song, L.; Gan, N.; Li, L. Sorption, Degradation and Mobility of Microcystins in Chinese Agriculture Soils: Risk Assessment for Groundwater Protection. *Environ. Pollut.* **2006**, *144*, 752–758. [CrossRef] [PubMed]
4. Corbel, S.; Mougin, C.; Bouaïcha, N. Cyanobacterial Toxins: Modes of Actions, Fate in Aquatic and Soil Ecosystems, Phytotoxicity and Bioaccumulation in Agricultural Crops. *Chemosphere* **2014**, *96*, 1–15. [CrossRef] [PubMed]

5. Yang, Z.; Kong, F.; Zhang, M. Groundwater Contamination by Microcystin from Toxic Cyanobacteria Blooms in Lake Chaohu, China. *Environ. Monit. Assess.* **2016**, *188*, 280. [CrossRef]
6. Nielsen, M.C.; Jiang, S.C. Can Cyanotoxins Penetrate Human Skin during Water Recreation to Cause Negative Health Effects? *Harmful Algae* **2020**, *98*, 101872. [CrossRef]
7. Plaas, H.E.; Paerl, H.W. Toxic Cyanobacteria: A Growing Threat to Water and Air Quality. *Environ. Sci. Technol.* **2021**, *55*, 44–64. [CrossRef]
8. Lad, A.; Breidenbach, J.D.; Su, R.C.; Murray, J.; Kuang, R.; Mascarenhas, A.; Najjar, J.; Patel, S.; Hegde, P.; Youssef, M.; et al. As We Drink and Breathe: Adverse Health Effects of Microcystins and Other Harmful Algal Bloom Toxins in the Liver, Gut, Lungs and Beyond. *Life* **2022**, *12*, 418. [CrossRef]
9. Machado, J.; Campos, A.; Vasconcelos, V.; Freitas, M. Effects of Microcystin-LR and Cylindrospermopsin on Plant-Soil Systems: A Review of Their Relevance for Agricultural Plant Quality and Public Health. *Environ. Res.* **2017**, *153*, 191–204. [CrossRef]
10. Corbel, S.; Mougin, C.; Nélieu, S.; Delarue, G.; Bouaïcha, N. Evaluation of the Transfer and the Accumulation of Microcystins in Tomato (*Solanum lycopersicum* Cultivar MicroTom) Tissues Using a Cyanobacterial Extract Containing Microcystins and the Radiolabeled Microcystin-LR (14 C-MC-LR). *Sci. Total Environ.* **2016**, *541*, 1052–1058. [CrossRef]
11. Lee, S.; Jiang, X.; Manubolu, M.; Riedl, K.; Ludsin, S.A.; Martin, J.F.; Lee, J. Fresh Produce and Their Soils Accumulate Cyanotoxins from Irrigation Water: Implications for Public Health and Food Security. *Food Res. Int.* **2017**, *102*, 234–245. [CrossRef] [PubMed]
12. World Health Organization. Guidelines for Drinking-Water Quality. Available online: https://iris.who.int/bitstream/handle/10665/352532/9789240045064-eng.pdf?sequence=1 (accessed on 12 September 2024).
13. Melaram, R.; Newton, A.R.; Chafin, J. Microcystin Contamination and Toxicity: Implications for Agriculture and Public Health. *Toxins* **2022**, *14*, 350. [CrossRef] [PubMed]
14. Weralupitiya, C.; Wanigatunge, R.P.; Gunawardana, D.; Vithanage, M.; Magana-Arachchi, D. Cyanotoxins Uptake and Accumulation in Crops: Phytotoxicity and Implications on Human Health. *Toxicon* **2022**, *211*, 21–35. [CrossRef] [PubMed]
15. Delcourt, N.; Claudepierre, T.; Maignien, T.; Arnich, N.; Mattei, C. Cellular and Molecular Aspects of the β-N-Methylamino-l-Alanine (BMAA) Mode of Action within the Neurodegenerative Pathway: Facts and Controversy. *Toxins* **2017**, *10*, 6. [CrossRef] [PubMed]
16. Campos, A.; Redouane, E.M.; Freitas, M.; Amaral, S.; Azevedo, T.; Loss, L.; Máthé, C.; Mohamed, Z.A.; Oudra, B.; Vasconcelos, V. Impacts of Microcystins on Morphological and Physiological Parameters of Agricultural Plants: A Review. *Plants* **2021**, *10*, 639. [CrossRef]
17. Koksharova, O.A.; Safronova, N.A. Non-Proteinogenic Amino Acid β-N-Methylamino-L-Alanine (BMAA): Bioactivity and Ecological Significance. *Toxins* **2022**, *14*, 539. [CrossRef]
18. Perron, M.-C.; Qiu, B.; Boucher, N.; Bellemare, F.; Juneau, P. Use of Chlorophyll a Fluorescence to Detect the Effect of Microcystins on Photosynthesis and Photosystem II Energy Fluxes of Green Algae. *Toxicon* **2012**, *59*, 567–577. [CrossRef]
19. Janssen, E.M.-L. Cyanobacterial Peptides beyond Microcystins—A Review on Co-Occurrence, Toxicity, and Challenges for Risk Assessment. *Water Res.* **2019**, *151*, 488–499. [CrossRef]
20. MacKintosh, C.; Beattie, K.A.; Klumpp, S.; Cohen, P.; Codd, G.A. Cyanobacterial Microcystin-LR Is a Potent and Specific Inhibitor of Protein Phosphatases 1 and 2A from Both Mammals and Higher Plants. *FEBS Lett.* **1990**, *264*, 187–192. [CrossRef]
21. Luan, S. Protein Phosphatases in Plants. *Annu. Rev. Plant Biol.* **2003**, *54*, 63–92. [CrossRef]
22. Christensen, V.G.; Khan, E. Freshwater Neurotoxins and Concerns for Human, Animal, and Ecosystem Health: A Review of Anatoxin-a and Saxitoxin. *Sci. Total Environ.* **2020**, *736*, 139515. [CrossRef] [PubMed]
23. Tretyn, A.; Kendrick, R.E. Acetylcholine in Plants: Presence, Metabolism and Mechanism of Action. *Bot. Rev.* **1991**, *57*, 33–73. [CrossRef]
24. Wessler, I.; Kilbinger, H.; Bittinger, F.; Kirkpatrick, C.J. The Non-Neuronal Cholinergic System. *Jpn. J. Pharmacol.* **2001**, *85*, 2–10. [CrossRef] [PubMed]
25. Mitrovic, S.M.; Pflugmacher, S.; James, K.J.; Furey, A. Anatoxin-a Elicits an Increase in Peroxidase and Glutathione S-Transferase Activity in Aquatic Plants. *Aquat. Toxicol.* **2004**, *68*, 185–192. [CrossRef] [PubMed]
26. Ha, M.-H.; Pflugmacher, S. Phytotoxic Effects of the Cyanobacterial Neurotoxin Anatoxin-a: Morphological, Physiological and Biochemical Responses in Aquatic Macrophyte, *Ceratophyllum demersum*. *Toxicon* **2013**, *70*, 1–8. [CrossRef]
27. Kaminski, A.; Chrapusta, E.; Adamski, M.; Bober, B.; Zabaglo, K.; Bialczyk, J. Determination of the Time-Dependent Response of *Lemna trisulca* to the Harmful Impact of the Cyanotoxin Anatoxin-a. *Algal Res.* **2016**, *16*, 368–375. [CrossRef]
28. Esterhuizen, M.; Pflugmacher, S.; Downing, T.G. β-N-Methylamino-l-Alanine (BMAA) Uptake by the Aquatic Macrophyte *Ceratophyllum demersum*. *Ecotoxicol. Environ. Saf.* **2011**, *74*, 74–77. [CrossRef]
29. Contardo-Jara, V.; Schwanemann, T.; Pflugmacher, S. Uptake of a Cyanotoxin, β-N-Methylamino-l-Alanine, by Wheat (*Triticum aestivum*). *Ecotoxicol. Environ. Saf.* **2014**, *104*, 127–131. [CrossRef]
30. Li, B.; Yu, S.; Li, G.; Chen, X.; Huang, M.; Liao, X.; Li, H.; Hu, F.; Wu, J. Transfer of a Cyanobacterial Neurotoxin, β-Methylamino-l-Alanine from Soil to Crop and Its Bioaccumulation in Chinese Cabbage. *Chemosphere* **2019**, *219*, 997–1001. [CrossRef]
31. Esterhuizen-Londt, M.; Pflugmacher, S.; Downing, T.G. The Effect of β-N-Methylamino-l-Alanine (BMAA) on Oxidative Stress Response Enzymes of the Macrophyte *Ceratophyllum demersum*. *Toxicon* **2011**, *57*, 803–810. [CrossRef]

32. Samardzic, K.; Steele, J.R.; Violi, J.P.; Colville, A.; Mitrovic, S.M.; Rodgers, K.J. Toxicity and Bioaccumulation of Two Non-Protein Amino Acids Synthesised by Cyanobacteria, β-N-Methylamino-L-Alanine (BMAA) and 2,4-Diaminobutyric Acid (DAB), on a Crop Plant. *Ecotoxicol. Environ. Saf.* **2021**, *208*, 111515. [CrossRef] [PubMed]
33. Zhang, Y.; Whalen, J.K. Production of the Neurotoxin Beta-N-Methylamino-l-Alanine May Be Triggered by Agricultural Nutrients: An Emerging Public Health Issue. *Water Res.* **2020**, *170*, 115335. [CrossRef] [PubMed]
34. Bernardová, K.; Babica, P.; Maršálek, B.; Bláha, L. Isolation and Endotoxin Activities of Lipopolysaccharides from Cyanobacterial Cultures and Complex Water Blooms and Comparison with the Effects of Heterotrophic Bacteria and Green Alga. *J. Appl. Toxicol.* **2008**, *28*, 72–77. [CrossRef] [PubMed]
35. Jones, J.D.G.; Dangl, J.L. The Plant Immune System. *Nature* **2006**, *444*, 323–329. [CrossRef]
36. Shang-Guan, K.; Wang, M.; Htwe, N.M.P.S.; Li, P.; Li, Y.; Qi, F.; Zhang, D.; Cao, M.; Kim, C.; Weng, H.; et al. Lipopolysaccharides Trigger Two Successive Bursts of Reactive Oxygen Species at Distinct Cellular Locations. *Plant Physiol.* **2018**, *176*, 2543–2556. [CrossRef]
37. Hussan, R.H.; Dubery, I.A.; Piater, L.A. Identification of MAMP-Responsive Plasma Membrane-Associated Proteins in *Arabidopsis thaliana* Following Challenge with Different LPS Chemotypes from *Xanthomonas campestris*. *Pathogens* **2020**, *9*, 787. [CrossRef]
38. Ranf, S. Immune Sensing of Lipopolysaccharide in Plants and Animals: Same but Different. *PLoS Pathog.* **2016**, *12*, e1005596. [CrossRef]
39. Tinte, M.M.; Steenkamp, P.A.; Piater, L.A.; Dubery, I.A. Lipopolysaccharide Perception in Arabidopsis Thaliana: Diverse LPS Chemotypes from *Burkholderia cepacia*, *Pseudomonas syringae* and *Xanthomonas campestris* Trigger Differential Defence-Related Perturbations in the Metabolome. *Plant Physiol. Biochem.* **2020**, *156*, 267–277. [CrossRef]
40. Hu, Z.; Liu, Y.; Li, D. Physiological and Biochemical Analyses of microcystin-RR Toxicity to the Cyanobacterium *Synechococcus elongatus*. *Environ. Toxicol.* **2004**, *19*, 571–577. [CrossRef]
41. García-Espín, L.; Cantoral, E.A.; Asencio, A.D.; Aboal, M. Microcystins and Cyanophyte Extracts Inhibit or Promote the Photosynthesis of Fluvial Algae. Ecological and Management Implications. *Ecotoxicology* **2017**, *26*, 658–666. [CrossRef]
42. Pereira, A.L.; Santos, C.; Azevedo, J.; Martins, T.P.; Castelo-Branco, R.; Ramos, V.; Vasconcelos, V.; Campos, A. Effects of Two Toxic Cyanobacterial Crude Extracts Containing Microcystin-LR and Cylindrospermopsin on the Growth and Photosynthetic Capacity of the Microalga *Parachlorella kessleri*. *Algal Res.* **2018**, *34*, 198–208. [CrossRef]
43. Chen, G.; Zheng, Z.; Bai, M.; Li, Q. Chronic Effects of Microcystin-LR at Environmental Relevant Concentrations on Photosynthesis of *Typha angustifolia* Linn. *Ecotoxicology* **2020**, *29*, 514–523. [CrossRef] [PubMed]
44. Abe, T.; Lawson, T.; Weyers, J.D.B.; Codd, G.A. Microcystin-LR Inhibits Photosynthesis of *Phaseolus vulgaris* Primary Leaves: Implications for Current Spray Irrigation Practice. *New Phytol.* **1996**, *133*, 651–658. [CrossRef]
45. Pflugmacher, S.; Aulhorn, M.; Grimm, B. Influence of a Cyanobacterial Crude Extract Containing microcystin-LR on the Physiology and Antioxidative Defence Systems of Different Spinach Variants. *New Phytol.* **2007**, *175*, 482–489. [CrossRef]
46. El Khalloufi, F.; El Ghazali, I.; Saqrane, S.; Oufdou, K.; Vasconcelos, V.; Oudra, B. Phytotoxic Effects of a Natural Bloom Extract Containing Microcystins on *Lycopersicon esculentum*. *Ecotoxicol. Environ. Saf.* **2012**, *79*, 199–205. [CrossRef]
47. Bittencourt-Oliveira, M.D.C.; Cordeiro-Araújo, M.K.; Chia, M.A.; Arruda-Neto, J.D.D.T.; Oliveira, Ê.T.D.; Santos, F.D. Lettuce Irrigated with Contaminated Water: Photosynthetic Effects, Antioxidative Response and Bioaccumulation of Microcystin Congeners. *Ecotoxicol. Environ. Saf.* **2016**, *128*, 83–90. [CrossRef]
48. Schalles, J.F. Optical Remote Sensing Techniques to Estimate Phytoplankton Chlorophyll a Concentrations in Coastal Waters with Varying Suspended Matter and CDOM Concentrations. In *Remote Sensing of Aquatic Coastal Ecosystem Processes*; Richardson, L.L., LeDrew, E.F., Eds.; Springer: Dordrecht, The Netherlands, 2006; pp. 27–79. ISBN 978-1-4020-3968-3.
49. Long, S.P. Gas Exchange Measurements, What Can They Tell Us about the Underlying Limitations to Photosynthesis? Procedures and Sources of Error. *J. Exp. Bot.* **2003**, *54*, 2393–2401. [CrossRef]
50. Heckathorn, S.A.; Mueller, J.K.; LaGuidice, S.; Zhu, B.; Barrett, T.; Blair, B.; Dong, Y. Chloroplast Small Heat-shock Proteins Protect Photosynthesis during Heavy Metal Stress. *Am. J. Bot.* **2004**, *91*, 1312–1318. [CrossRef]
51. R Core Team. *R: A Language and Environment for Statistical Computing*; R Core Team: Vienna, Austria, 2023; Available online: https://www.R-project.org/ (accessed on 14 August 2024).
52. Maxwell, K.; Johnson, G.N. Chlorophyll Fluorescence—A Practical Guide. *J. Exp. Bot.* **2000**, *51*, 659–668. [CrossRef]

Disclaimer/Publisher's Note: The statements, opinions and data contained in all publications are solely those of the individual author(s) and contributor(s) and not of MDPI and/or the editor(s). MDPI and/or the editor(s) disclaim responsibility for any injury to people or property resulting from any ideas, methods, instructions or products referred to in the content.

plants

MDPI

Article

Salicylic Acid Priming Improves Cotton Seedling Heat Tolerance through Photosynthetic Pigment Preservation, Enhanced Antioxidant Activity, and Osmoprotectant Levels

Ashim Kumar Das [1,†], Protik Kumar Ghosh [2,†], Sheikh Arafat Islam Nihad [3], Sharmin Sultana [4], Sanjida Sultana Keya [5], Md. Abiar Rahman [1], Totan Kumar Ghosh [6], Munny Akter [2], Mehedi Hasan [7], Umme Salma [8], Md. Mahadi Hasan [9,*] and Md. Mezanur Rahman [1,5,*]

1 Department of Agroforestry and Environment, Bangabandhu Sheikh Mujibur Rahman Agricultural University, Gazipur 1706, Bangladesh; ashimbsmrau@gmail.com (A.K.D.); abiar@bsmrau.edu.bd (M.A.R.)
2 Department of Agronomy, Bangabandhu Sheikh Mujibur Rahman Agricultural University, Gazipur 1706, Bangladesh; protikbsmrau@gmail.com (P.K.G.); munny@bsmrau.edu.bd (M.A.)
3 Plant Pathology Division, Bangladesh Rice Research Institute, Gazipur 1701, Bangladesh; nihad402@gmail.com
4 Institute of Biotechnology and Genetic Engineering, Bangabandhu Sheikh Mujibur Rahman Agricultural University, Gazipur 1706, Bangladesh; sharminomi87@gmail.com
5 Institute of Genomics for Crop Abiotic Stress Tolerance, Department of Plant and Soil Science, Texas Tech University, Lubbock, TX 79409, USA; skeya@ttu.edu
6 Department of Crop Botany, Bangabandhu Sheikh Mujibur Rahman Agricultural University, Gazipur 1706, Bangladesh; totan@bsmrau.edu.bd
7 Department of Agriculture, Bangabandhu Sheikh Mujibur Rahman Science and Technology University, Gopalganj 8100, Bangladesh; mhjackey26@gmail.com
8 Department of Biochemistry and Molecular Biology, Primeasia University, Dhaka 1213, Bangladesh; ummesalma.jubmb15@gmail.com
9 State Key Laboratory of Grassland Agro-Ecosystems, College of Ecology, Lanzhou University, Lanzhou 730000, China
* Correspondence: hasanmahadikau@gmail.com (M.M.H.); mdmerahm@ttu.edu (M.M.R.)
† These authors equally contribute to this work.

Abstract: The escalating global temperatures associated with climate change are detrimental to plant growth and development, leading to significant reductions in crop yields worldwide. Our research demonstrates that salicylic acid (SA), a phytohormone known for its growth-promoting properties, is crucial in enhancing heat tolerance in cotton (*Gossypium hirsutum*). This enhancement is achieved through modifications in various biochemical, physiological, and growth parameters. Under heat stress, cotton plants typically show significant growth disturbances, including leaf wilting, stunted growth, and reduced biomass. However, priming cotton plants with 1 mM SA significantly mitigated these adverse effects, evidenced by increases in shoot dry mass, leaf-water content, and chlorophyll concentrations in the heat-stressed plants. Heat stress also prompted an increase in hydrogen peroxide levels—a key reactive oxygen species—resulting in heightened electrolyte leakage and elevated malondialdehyde concentrations, which indicate severe impacts on cellular membrane integrity and oxidative stress. Remarkably, SA treatment significantly reduced these oxidative stresses by enhancing the activities of critical antioxidant enzymes, such as catalase, glutathione *S*-transferase, and ascorbate peroxidase. Additionally, the elevated levels of total soluble sugars in SA-treated plants enhanced osmotic regulation under heat stress. Overall, our findings reveal that SA-triggered protective mechanisms not only preserve photosynthetic pigments but also ameliorate oxidative stress and boost plant resilience in the face of elevated temperatures. In conclusion, the application of 1 mM SA is highly effective in enhancing heat tolerance in cotton and is recommended for field trials before being commercially used to improve crop resilience under increasing global temperatures.

Keywords: antioxidant enzymes; osmotic balance; photosynthetic pigments; reactive oxygen species; salicylic acid

1. Introduction

The marked increase in both frequency and severity of abiotic stresses—including heat waves, cold snaps, droughts, and floods—substantially compromises crop yields and threatens the sustainability of agriculture [1,2]. Global warming, characterized by elevated environmental temperatures, is predicted to intensify these challenges, with more severe and frequent heat stress episodes anticipated in the future [3–5]. Heat stress impairs plant performance, adversely affecting growth, photosynthesis, mineral uptake, and yield [6–9]. In addition, heat stress disrupts cellular homeostasis, leading to an overwhelming upsurge in reactive oxygen species (ROS). This results in a cascade of oxidative burden, which is characterized by an excessive accumulation of hydrogen peroxide (H_2O_2), which in turn leads to an increase in malondialdehyde (MDA) production [10,11]. Indeed, plants have evolved sophisticated physiological, biochemical, cellular, and molecular regulatory mechanisms to meticulously orchestrate their responses to heat stress [12]. The mechanisms involved reduced water loss, maintaining the integrity of the cell membrane, scavenging ROS, and strengthening both enzymatic and non-enzymatic antioxidant defense systems [13,14]. Despite these adaptive mechanisms, the rising global temperature and erratic climatic patterns exacerbate heat stress impact on a wide range of crops, including cotton (*Gossypium* spp.), highlighting the urgent need for innovative strategies to improve plant resilience [3].

Cotton has been considered the preeminent plant for natural fibers, accounting for 35% of the global market share, making it an indispensable commercial crop worldwide [15]. *Gossypium hirsutum*, the primary species of cotton, is grown in over 95% of the world's cotton-producing areas, supplying vital natural fibers for the textile industry and yielding important by-products, including biofuels, food products, and edible oils [16–18]. Although cotton plants can withstand temperatures up to 43 °C without apparent adverse effects when soil moisture is adequate, prolonged heat stress significantly impairs their growth, development, yield, and the quality of the fiber produced [18–20]. Decades-long endeavors have been devoted to breeding and utilizing biotechnological strategies to develop cotton varieties with enhanced heat tolerance. Despite these efforts, achieving significant progress remains a formidable challenge, necessitating substantial investment of both time and resources [21]. Recently, the application of phytohormones, such as salicylic acid (SA), has gained scientific attention as a means of alternative and promising strategy for enhancing resilience against multiple abiotic stresses [22–25]. SA is recognized for its crucial role in modulating a multitude of key physiological and biochemical processes, including optimizing the acquisition of nutrients, enhancing the retention of water, coordinating the closure of stomata, stimulating the activity of photosynthesis, accumulating osmolytes, and detonating the activation of antioxidant defense mechanisms. These mechanisms endow plants with an extraordinary ability to withstand abiotic stresses, including the effect of scorching heat [26–28]. A plethora of research has demonstrated that applications of SA have improved the drought tolerance in canola (*Brassica napus* L.) [29], heat tolerance in maize (*Zea mays*) [30], cold stress in wheat (*Triticum aestivum*) [31], cadmium stress in rice (*Oryza sativa*) [32], and salinity stress in sorghum (*Sorghum bicolor*) [33].

Given the myriad benefits of SA, we anticipated that the supplementation of SA could play a crucial role in nullifying the pernicious consequences of heat stress on cotton plants. This intervention is expected to regulate a multitude of mechanisms associated with morphological, physiological, and biochemical features. Considering this, the present study delved into the pivotal functions of SA in alleviating heat stress-induced damage in the CB-12 cotton variety, a widely acclaimed upland cotton cultivar extensively grown in the cotton-rich regions of Bangladesh. Our study focused on a thorough investigation of diverse morpho-physiological and biochemical parameters. These encompassed a comprehensive assessment of (i) plant growth characteristics and subsequent biomass accumulation, (ii) abundance of diverse photosynthetic pigments, (iii) heat-induced H_2O_2 accumulation

and their consequential impact on membrane lipid peroxidation and electrolyte leakages in leaves, (iv) levels and/or activities of essential non-enzymatic and enzymatic antioxidants, and (v) accumulation of various osmoprotectants, and their remarkable role in maintaining plant water status.

2. Results

2.1. Salicylic Acid Positively Modulated the Growth and Phenotype of Heat-Stressed Cotton Plants

To assess the effects of SA and water pretreatment on cotton plants subjected to heat stress, we evaluated various growth features along with the phenotypic appearance (Figure 1A–F). Phenotypic inspections revealed that heat stress led to significant alterations, such as leaf wilting and shrinking in plants subjected only to heat ('Heat') compared with untreated control ('Control') (Figure 1A–C). In contrast, plants pretreated with SA before experiencing heat stress ('SA+Heat') displayed a noticeable improvement in their phenotypic traits relative to the 'Heat' group (Figure 1A–C). Correspondingly, 'Heat' plants displayed a significant decrease in shoot height, shoot fresh weight (FW), shoot dry weight (DW), root FW, and root DW by 15.72%, 62.97%, 24.45%, 61.53%, and 20.20%, respectively, in relation to 'Control' plants (Figure 1D–H). Remarkably, SA pretreatment ('SA+Heat') significantly improved shoot height by 36.05%, shoot FW by 232.75%, shoot DW by 100.72%, root FW by 216.67%, and root DW by 63.29%, compared with the plants exposed solely to heat stress ('Heat') (Figure 1D–F). Additionally, plants that underwent SA pretreatment alone ('SA') showed significant improvements in shoot height by 15.58%, shoot FW by 35.72%, shoot DW by 75.27%, root FW by 42.30%, and root DW by 46.97%, in relation to 'Control' plants (Figure 1D–F).

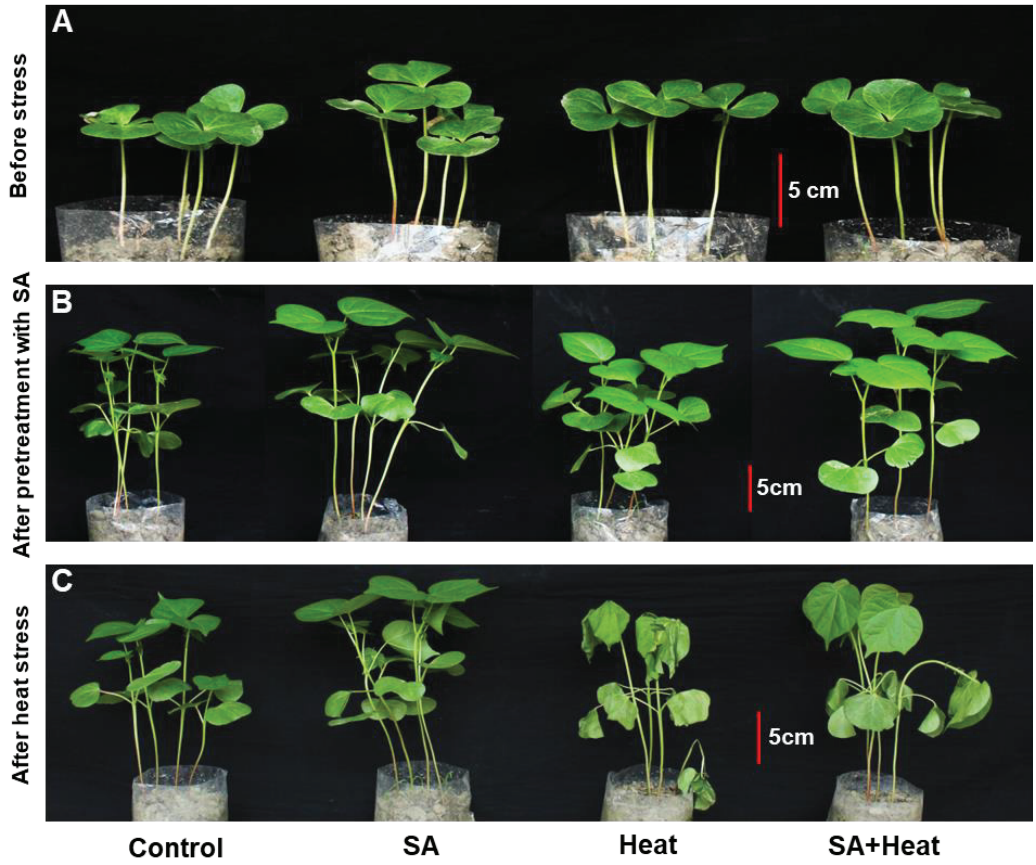


Figure 1. *Cont.*

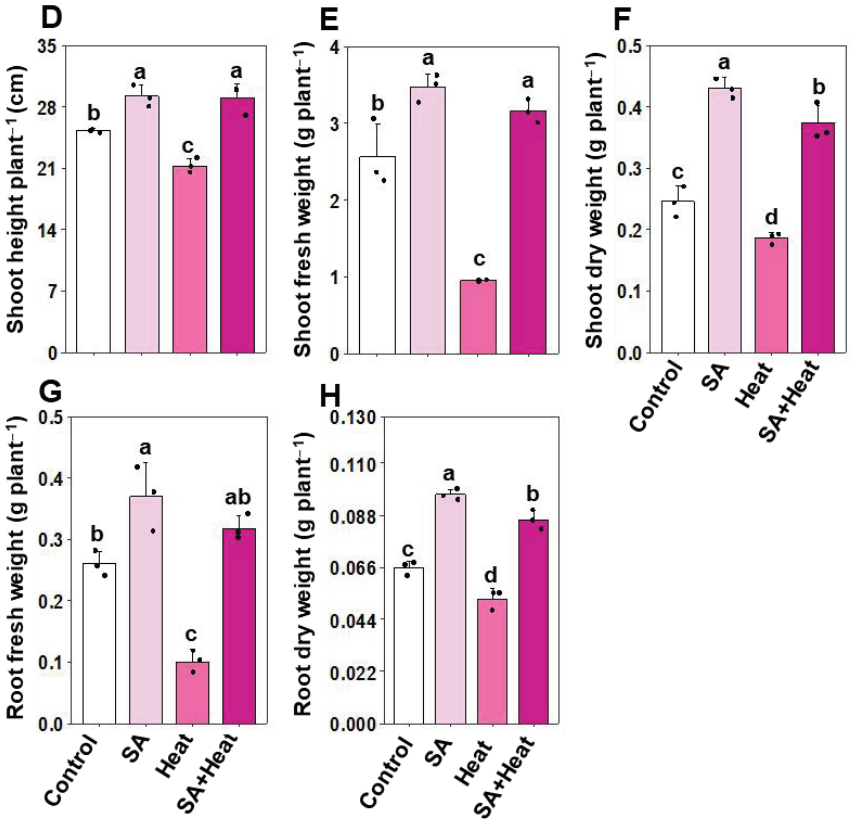


Figure 1. Impact of exogenously applied salicylic acid (SA, 1 mM) on growth-related characteristics of cotton plants subjected to 48 h of heat stress. Representative images of cotton plants captured at different stages: (**A**) before priming with 1 mM SA (pretreatment), (**B**) after 10 days of 1 mM SA priming (pre-stress), and (**C**) following exposure to 48 h of heat stress. Growth parameters assessed include (**D**) shoot height per plant, (**E**) shoot fresh weight per plant, (**F**) shoot dry weight per plant, (**G**) root fresh weight per plant, and (**H**) root dry weight per plant under different treatments. Data are presented as mean values with standard deviations (n = 3). Statistically significant treatment differences, as assessed by the least significant difference (LSD) test ($p < 0.05$), are indicated by distinct letters above the bars. Treatments include water-treated non-stressed plants (Control), 1 mM SA-primed non-stressed plants (SA), water-treated heat-exposed plants (Heat), and 1 mM SA-primed heat-exposed plants (SA+Heat).

2.2. Comparative Analysis of Photosynthetic Pigments and Flavonoids in Salicylic Acid-Treated and Heat-Stressed Cotton

To thoroughly assess the impact of SA on the preservation of photosynthetic pigments and flavonoid levels under heat stress conditions, we conducted a detailed quantification of total chlorophylls, chlorophyll *a*, chlorophyll *b*, carotenoids, and total flavonoids (Figure 2A–E). Our analysis revealed that heat stress substantially reduced the levels of chlorophyll *a* by 29.83%, total chlorophylls by 34.16%, carotenoids by 25.09%, and total flavonoids by 43.25% in 'Heat' plants compared with the 'Control' plants. Interestingly, chlorophyll *b* levels remained relatively consistent between the 'Heat' and 'Control' plants (Figure 2A–E). Conversely, 'SA+Heat' plants exhibited a noteworthy increase in the quantities of chlorophyll *a* (by 32.37%), total chlorophylls (42.19%), and carotenoids (28.51%) in comparison to 'Heat' plants, while changes in leaf chlorophyll *b* and total flavonoid levels were not statistically significant (Figure 2A–E). 'SA' plants, on the other hand, displayed a substantial enhancement in chlorophyll *b* (by 59.96%), total chlorophylls (24.95%), and carotenoid levels (26.61%), compared with the 'Control' plants, albeit with a 34.15% reduction in total flavonoids (Figure 2B–E). Despite the treatment, the chlorophyll content in plants treated with salicylic acid ('SA') remained unchanged and was comparable to the

levels found in the control plants ('Control'), indicating that SA did not significantly alter chlorophyll concentration under non-stress conditions (Figure 2A).

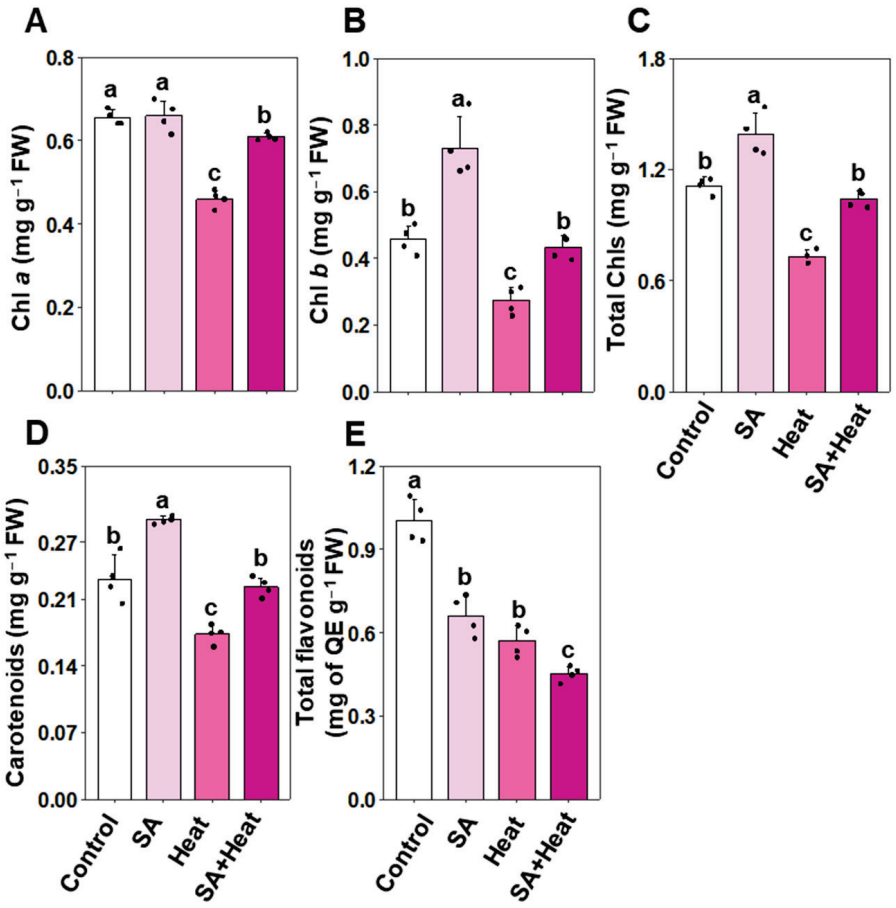


Figure 2. Impact of exogenously applied salicylic acid (SA, 1 mM) on the levels of photosynthetic pigments and flavonoids in cotton leaves subjected to 48 h of heat stress. (**A**) Chlorophyll *a* (Chl *a*), (**B**) chlorophyll *b* (Chl *b*), (**C**) total chlorophylls (total Chls), (**D**) carotenoids, and (**E**) total flavonoids in cotton leaves. Data are presented as mean values with standard deviations ($n = 4$). Statistically significant treatment differences, as assessed by the least significant difference (LSD) test ($p < 0.05$), are indicated by distinct letters above the bars. The treatments compared include water-treated non-stressed plants (Control), 1 mM SA-primed non-stressed plants (SA), water-treated heat-exposed plants (Heat), and 1 mM SA-primed heat-exposed plants (SA+Heat). Fresh weight (FW), quercetin equivalent (QE).

2.3. Salicylic Acid Reduced Heat-Induced Oxidative Stress in Cotton Plants

To explore the potential of SA in alleviating heat-induced oxidative injury, we quantified MDA and H_2O_2 concentrations, along with the percentage of electrolyte leakage in cotton leaves (Figure 3A–C). Compared with 'Control', leaves from plants exposed to heat stress ('Heat') demonstrated a notable increase in MDA (by 89.69%) and H_2O_2 (772.40%), alongside a 61.44% rise in electrolyte leakage (Figure 3A–C). Remarkably, SA priming before heat stress ('SA+Heat') significantly reduced MDA levels by 39.49%, H_2O_2 levels by 82.06%, and electrolyte leakage by 33.99% in comparison to the 'Heat' group (Figure 3A–C). Furthermore, leaves from plants treated with SA alone ('SA') displayed a substantial reduction in electrolyte leakage by 40.36%, although the levels of MDA and H_2O_2 remained comparable, similar to the 'Control' group (Figure 3A–C).

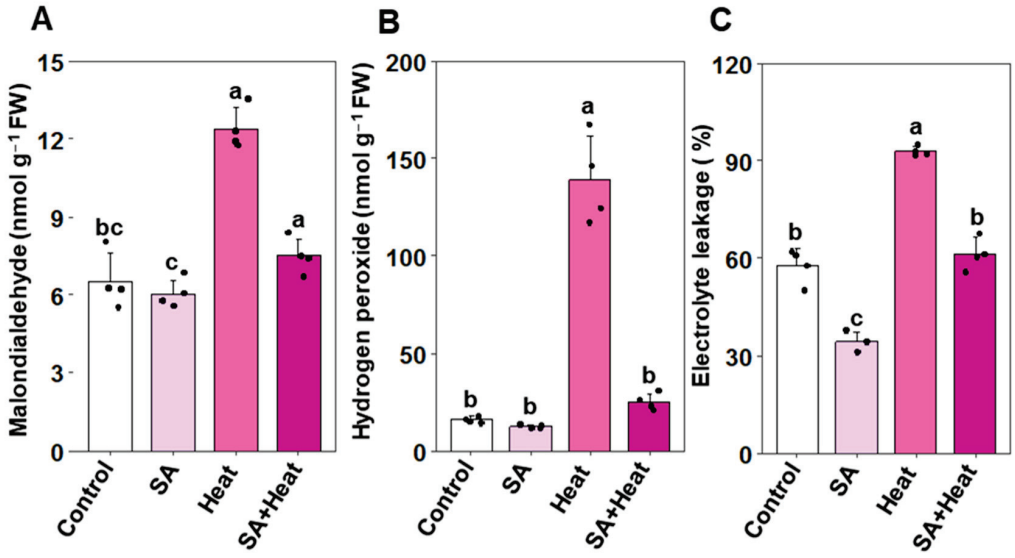


Figure 3. Impact of exogenously applied salicylic acid (SA, 1 mM) on oxidative stress markers in cotton leaves subjected to 48 h of heat stress. (**A**) Malondialdehyde content, (**B**) hydrogen peroxide content, and (**C**) electrolyte leakage percentage in cotton leaves. Data are presented as mean values with standard deviations ($n = 4$). Statistically significant treatment differences, as assessed by the least significant difference (LSD) test ($p < 0.05$), are indicated by distinct letters above the bars. Treatments include water-treated non-stressed plants (Control), 1 mM SA-primed non-stressed plants (SA), water-treated heat-exposed plants (Heat), and 1 mM SA-primed heat-exposed plants (SA+Heat).

2.4. Differential Antioxidant Enzyme Responses to Salicylic Acid and Heat Stress in Cotton

To elucidate the effect of SA on enhancing antioxidant defense mechanisms, we evaluated the activities of several crucial antioxidant enzymes, namely GST, APX, POD, and CAT (Figure 4A–D). Heat stress substantially improved POD and GST activities by 106.61% and 64.09%, respectively, in 'Heat' plants compared with 'Control' plants. Conversely, APX activity was reduced by 36.69%, while CAT activity remained comparable in 'Heat' and 'Control' plants (Figure 4A–D). Remarkably, 'SA+Heat' plants showed a notable improvement in CAT (by 1243.08%), APX (102.66%), and GST (35.88%) activities, and a notable decrease in POD activity (46.99%) relative to 'Heat' plants (Figure 4A–D). Additionally, the activities of POD, APX, and GST in salicylic acid-treated ('SA') plants were comparable to those in control ('Control') plants. However, CAT activity was markedly higher, showing an increase of 237.14% in 'SA' plants compared with 'Control' plants (Figure 4A–D).

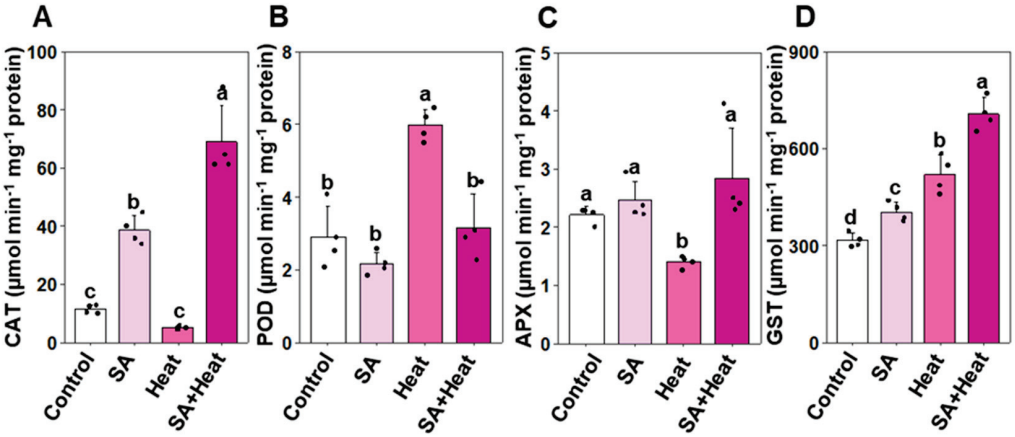


Figure 4. Impact of exogenously applied salicylic acid (SA, 1 mM) on the activities of key antioxidant enzymes in cotton leaves subjected to 48 h of heat stress. (**A**) Catalase (CAT), (**B**) peroxidase (POD),

(**C**) ascorbate peroxidase (APX), and (**D**) glutathione *S*-transferase (GST) activities in cotton leaves. Data are presented as mean values with standard deviations ($n = 4$). Statistically significant treatment differences, as assessed by the least significant difference (LSD) test ($p < 0.05$), are indicated by distinct letters above the bars. Treatments include water-treated non-stressed plants (Control), 1 mM SA-primed non-stressed plants (SA), water-treated heat-exposed plants (Heat), and 1 mM SA-primed heat-exposed plants (SA+Heat).

2.5. Salicylic Acid's Role in Enhancing Water Status and Osmoprotectant Balance in Cotton Plants under Heat Stress

To evaluate whether salicylic acid (SA) aids in maintaining water status under heat stress conditions, we measured the relative water content (RWC) and analyzed the concentrations of total soluble sugars, proline, total carbohydrates, and total free amino acids in the leaves of cotton plants (Figure 5A–E). Plants exposed to heat stress ('Heat') experienced a substantial reduction in RWC by 39.52% compared with control plants ('Control'). Additionally, these heat-stressed plants exhibited significant increases in proline levels (378.08%), total carbohydrates (275.29%), and total free amino acids (130.22%). In contrast, the levels of total soluble sugars remained unchanged when compared with the 'Control' group (Figure 5A–E). Conversely, SA-primed ('SA+Heat') plants showed a notable decrease in proline levels (by 59.36%) and total carbohydrates (34.90%), alongside improvement in RWC (30.59%) and total soluble sugars (116.30%) relative to 'Heat' plants (Figure 5A–D). However, there was no significant difference in the total free amino acid content between the 'SA+Heat' plants and those subjected to 'Heat' treatment alone (Figure 5E). Compared with the 'Control' plants, those treated with salicylic acid ('SA') demonstrated a significant enhancement in leaf RWC, showing an increase of 9.59%. However, the levels of osmoprotectants remained largely unchanged between the 'Control' and 'SA' plants (Figure 5A–E).

2.6. Visualizing the Differential Impact of Heat and Salicylic Acid Treatments on Cotton Plants: A Detailed Heatmap and Principal Component Analysis Approach

To succinctly visualize the impact of different treatment compositions on cotton plants at a glance, we generated a heatmap that delineated four distinct clusters of parameters (Figure 6A). In 'Heat' plants, parameters within the cluster-I displayed an increasing trend compared with 'Control' plants, with an unexpected further increase observed in 'SA+Heat' plants (Figure 6A). Conversely, variables in cluster-II increased significantly in 'Heat' plants relative to 'Control' plants but demonstrated a decrease in 'SA+Heat' plants (Figure 6A). Notably, the parameter in cluster-III uniquely exhibited an increasing trend in 'Control' plants compared to all other treatments (Figure 6A). In contrast, the cluster-IV variables showed a decrease in the 'Heat' plants but exhibited an increase in the 'SA+Heat' plants compared with the 'Heat' plants (Figure 6A). Subsequently, we utilized principal component analysis (PCA) to investigate the relationships between the various treatments and the measured parameters. This analytical approach allowed us to discern patterns and correlations within the data, providing deeper insights into the effects of different treatments on the observed variables (Figure 6B). The analysis revealed that the majority of variability was explained by PC1 (72.5%) and PC2 (22.50%), cumulatively accounting for 95.00% of the observed variability. Intriguingly, cluster-I parameters were strongly associated with the 'SA+Heat' treatment, while cluster-II variables correlated closely with the 'Heat' treatments (Figure 6A,B). 'Control' plants predominantly aligned with the cluster-III parameter (Figure 6A,B), whereas variables from cluster-IV were closely linked to the 'SA' treatment (Figure 6A,B).

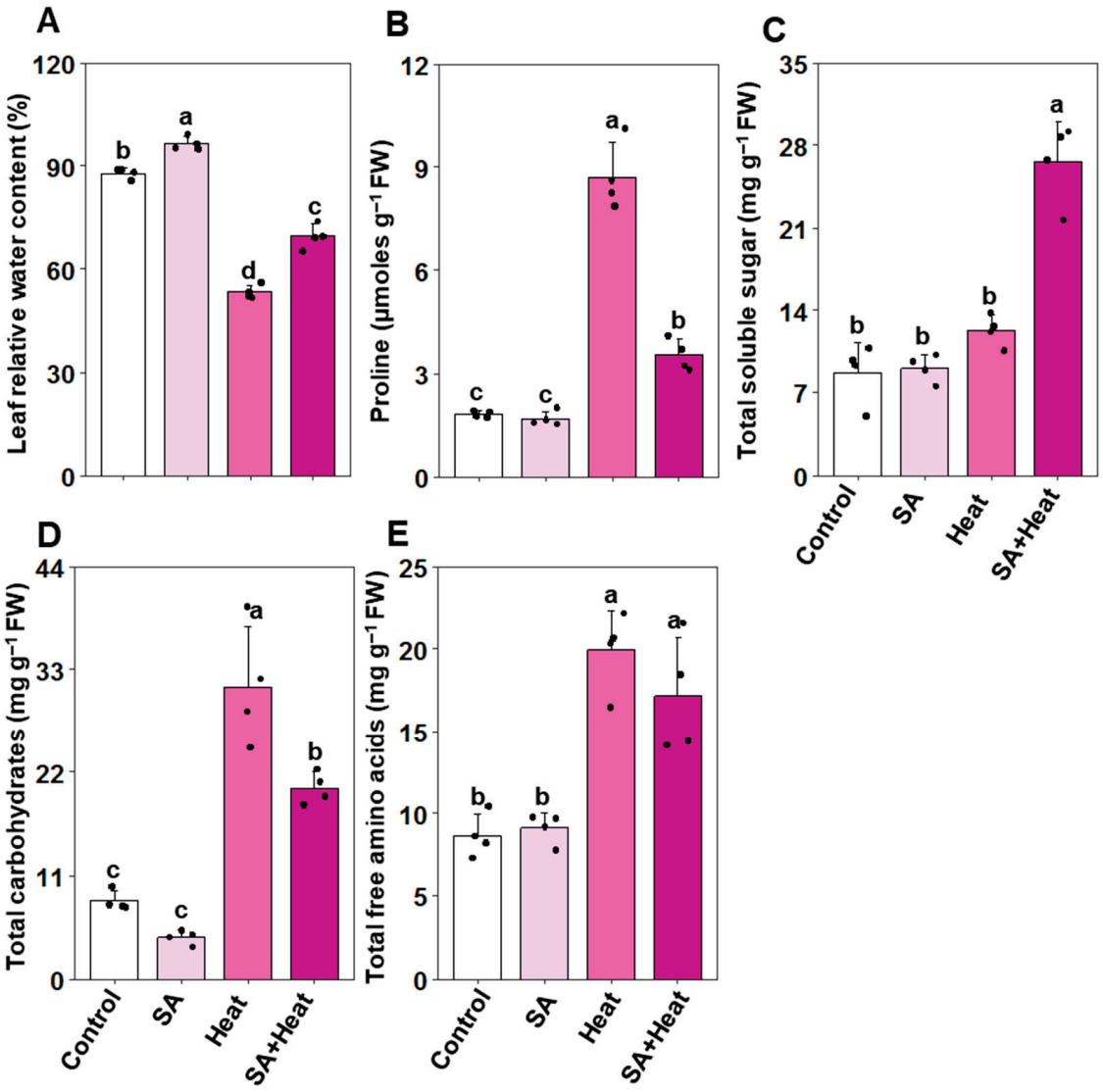


Figure 5. Impact of exogenously applied salicylic acid (SA, 1 mM) on various physiological and biochemical parameters in cotton leaves subjected to 48 h of heat stress. (**A**) Leaf relative water content, (**B**) proline, (**C**) total soluble sugars, (**D**) total carbohydrates, and (**E**) total free amino acid levels in cotton leaves. Data are presented as mean values with standard deviations ($n = 4$). Statistically significant treatment differences, as assessed by the least significant difference (LSD) test ($p < 0.05$), are indicated by distinct letters above the bars. Treatments include water-treated non-stressed plants (Control), 1 mM SA-primed non-stressed plants (SA), water-treated heat-exposed plants (Heat), and 1 mM SA-primed heat-exposed plants (SA+Heat). Fresh weight (FW).

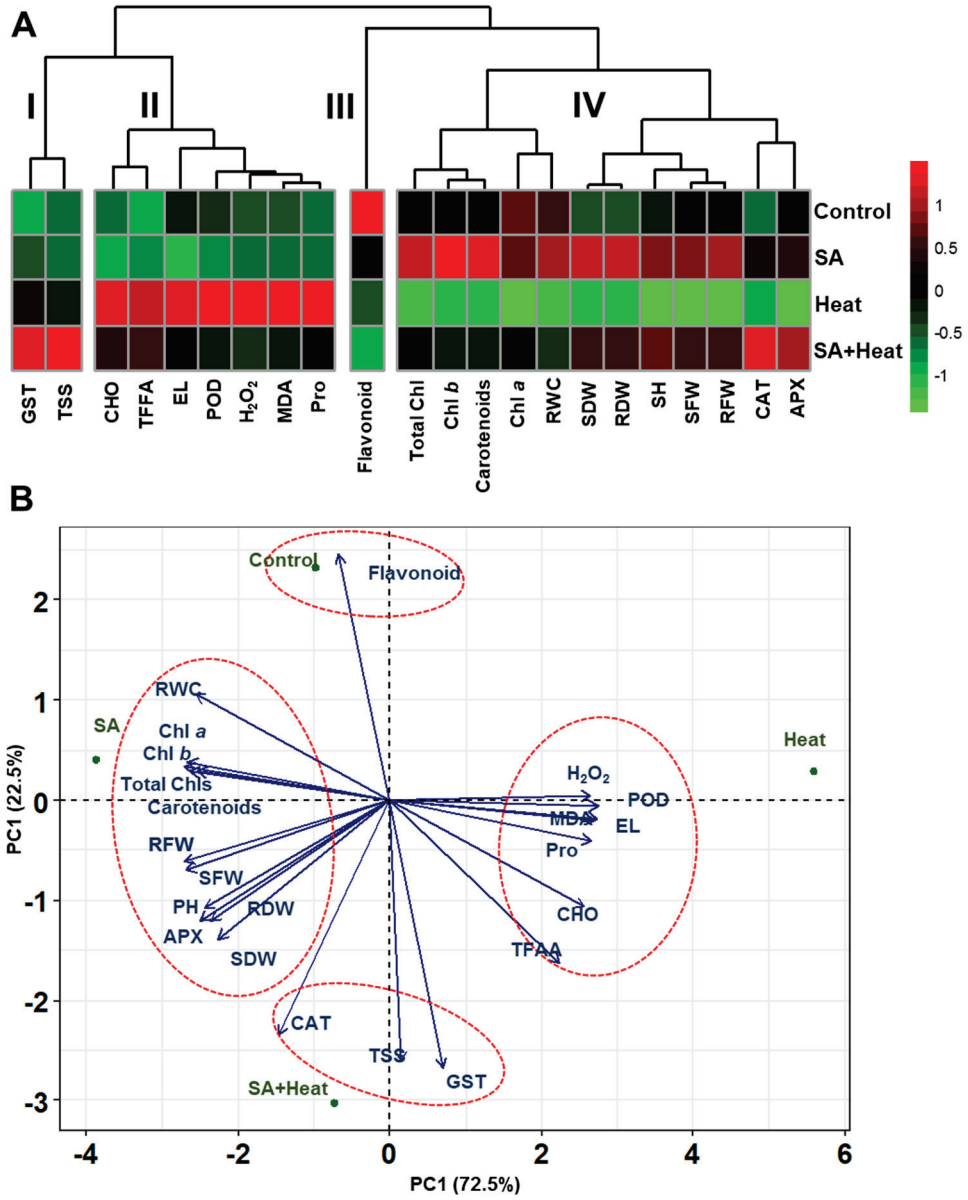


Figure 6. Clustering heatmap and biplot principal component analysis (PCA) illustrating the impact of salicylic acid (SA) priming on heat stress tolerance in cotton plants. (**A**) Clustering heatmap of normalized mean values showing the responses of various morphophysiological and biochemical parameters under different treatment combinations: water-treated non-stressed plants (Control), 1 mM SA-primed non-stressed plants (SA), water-treated heat-exposed plants (Heat), and 1 mM SA-primed heat-exposed plants (SA+Heat). The heatmap provides a comprehensive overview of the divergence in parameter responses across treatments. (**B**) Biplot PCA depicts correlations between parameters and treatments, with the first two principal components (PC1 and PC2) explaining 94.6% of the total variability in the dataset. Vector lines indicate the strength and direction of relationships between morphophysiological and biochemical parameters and treatments, with tiny angles denoting weak associations and wide angles indicating strong associations. Key parameters include plant height (PH), chlorophyll *a* (Chl *a*), shoot dry weight (SDW), chlorophyll *b* (Chl *b*), shoot fresh weight (SFW), root dry weight (RDW), root fresh weight (RFW), total chlorophylls (Total Chls), ascorbate peroxidase (APX), total free amino acids (TFAA), peroxidase (POD), total flavonoids (Flavonoid), glutathione *S*-transferase (GST), malondialdehyde (MDA), total carbohydrates (CHO), hydrogen peroxide (H_2O_2), electrolyte leakage (EL), proline (Pro), relative water content (RWC), and total soluble sugars (TSS).

3. Discussion

Global cotton growth and production are severely perturbed by high-temperature stress, a challenge increasingly prevalent in many regions worldwide [34]. SA has long been deemed as an unwavering warrior, safeguarding plants from the pernicious consequences imposed by a multitude of abiotic stresses in a diverse array of crop species, including rice (*Oryza sativa*), cotton, maize (*Zea mays*), and wheat (*Triticum aestivum*) [25,35–37]. Our study demonstrated that the supplementation of SA markedly enhances the heat tolerance of cotton plants. This conclusion is supported by SA's significant role in mitigating heat-induced phenotypic abnormalities, including leaf wilting and shrinkage. The observed reduction in these stress symptoms is likely correlated with the notable improvements in overall growth and biomass yield in SA-treated plants (Figure 1A–F). It is well-recognized that under high-temperature stress, plants need to preserve root plasticity to efficiently explore the surrounding and deeper layers of soil to extract the water to cool the plant's overall temperature [19,38–40]. Therefore, robust root growth under elevated temperatures is one of the paramount traits that enhances the heat tolerance of plants. Our investigation displayed that the root biomass of heat-stressed plants was substantially reduced; nonetheless, SA supplementation successfully promoted robust root growth and amplified biomass (Figure 1F). This finding indirectly suggests that the profound root system in SA-supplemented plants enabled them to eagerly absorb copious amounts of water from the soil, ultimately resulting in vigorous growth under high-temperature conditions. In support of our investigation in enhancing plant growth and biomass, we concurrently observed that the supplementation of SA enhanced photosynthetic pigment levels, such as chlorophyll *a*, chlorophyll *b*, total chlorophylls, and carotenoids, in cotton leaves subjected to both non-stressed and heat-stressed conditions (Figure 2A–D). These outcomes indicate that SA may be involved in either stimulating the production or inhibiting the breakdown of photosynthetic pigments, or perhaps both, consequently leading to an enhancement in biomass production (Figure 2A–D). Our PCA analysis also revealed a positive correlation with SA-treated plants in growth features and photosynthetic pigment contents (Figure 6A,B).

A substantial body of research has consistently demonstrated that the decrease in biomass observed under heat stress conditions is intricately connected to the initiation of oxidative damage. This damage is predominantly driven by the elevated production of ROS, which disrupts cellular homeostasis and impairs various physiological processes critical for plant growth and development [41–44]. In the present investigation, we observed substantially higher levels of EL percentage, MDA, and H_2O_2 in heat-exposed cotton plants, unequivocally demonstrating the profound impact of heat stress on inducing severe oxidative stress and membrane dysfunction in cotton plants (Figure 3A–C). Furthermore, SA priming followed by heat stress exposure led to a reduced accumulation of H_2O_2, along with lower levels of MDA and EL. This indicates that SA effectively mitigates cell membrane damage by preventing the excessive production of H_2O_2 and curtailing lipid peroxidation product (MDA) in heat-stressed leaves. The findings of our PCA also indicate that oxidative stress markers, including H_2O_2 and MDA, were intricately associated with 'Heat' treatment (Figure 6A,B). This observation aligns with recent studies, which have shown that SA can mitigate oxidative damage in cotton leaves under salt stress and in tomato (*Solanum lycopersicum*) under heat stress, as well as plays a role in regulating leaf senescence and promoting shoot growth [26,45]. Furthermore, our findings unequivocally displayed that those plants supplemented with SA exhibited a robust antioxidant defense system that effectively mitigated the oxidative burden imposed by H_2O_2 and consequential effects derived from EL and lipid peroxidation under heat stress conditions. We observed that cotton plants primed with SA and subsequently exposed to heat stress triggered a momentous upsurge in the activities of CAT, APX, and GST, which played a pivotal role in efficiently detoxifying the heat-stress-induced H_2O_2, ensuring plant survival and resilience under such challenging conditions (Figures 3B and 4A,C,D). Similar to our findings, Janda et al. [46] also revealed that SA treatment bolstered GST activity in *Brachypodium*

distachyon plants under heat-stress conditions. Our PCA also revealed a strong association in heightened levels of antioxidant enzyme activities with the 'SA+Heat' treatment (Figure 6A,B).

Plants facing stressful conditions encounter a formidable challenge as their water uptake capacity diminishes, resulting in a disruptive balance of water at the cellular level [47]. In response, an arsenal of osmoprotectants, such as proline, is mobilized to mitigate this imbalance [25,48]. Our study revealed that cotton plants subjected to heat stress exhibited escalated proline levels while concurrently experiencing significantly diminished leaf RWC in comparison to control plants (Figure 5A,B). These compelling outcomes suggest that proline accumulation alone may not suffice to maintain optimal water status under heat stress. Intriguingly, SA priming effectively minimized water loss in heat-stressed cotton plants without significantly increasing proline levels, as opposed to the traditional view that proline accumulation directly correlates with stress severity and suggested alternative mechanisms for preserving leaf RWC under heat stress [25,48–50]. Remarkably, we also noted a surge in total free amino acid levels in heat-exposed plants, in contrast to SA-primed heat-stressed plants; nonetheless, even this surge proved inadequate in sustaining the plant's water status (Figure 5E). Additionally, we observed that heat-stressed plants treated with SA exhibited a significantly higher accumulation of total soluble sugars compared to those treated with water. This increased sugar accumulation likely plays a crucial role in maintaining plant water status, as indicated by the higher RWC in the leaves (Figure 5A,C). However, we observed a pronounced reduction in RWC in heat-stressed plants. Apart from heat stress, this sharp decline is likely attributable to insufficient irrigation intended to mitigate water stress, alongside minor yet significant variations in relative humidity inside the growth chamber. These factors necessitate meticulous monitoring and control in the design and execution of heat stress experiments. Furthermore, scientific evidence explicitly highlights the profound impact of amplified total soluble sugar accumulation in meeting the crucial nitrogen and carbon demands to maintain optimal plant metabolic functions under stress circumstances [51]. Remarkably, Zhang et al. [52] have also extensively reported the protective role of heightened total soluble sugars in counteracting the adverse effects induced by heat stress in rice plants. In addition, the reduced carbohydrate content in SA-primed cotton plants may enhance osmotic regulation by providing additional sugars for osmoprotection. This balance could be achieved through the interconversion of starch to sugars via hydrolytic enzymes and/or by supplying ATP to energize stressed cells through an elevated respiration rate (Figure 5C,D) [53,54].

4. Materials and Methods

4.1. Plant Species and Treatment Compositions

CB-12 cotton seeds, renowned for their high yield potential in Bangladesh (seed cotton yield: 4.52 tons ha^{-1}), were pre-soaked overnight in darkness before being sown in polybags (19 cm in length and 15 cm in width) containing 800 g of soil. These polybags were subsequently placed in a growth chamber (GC-560H, Firstek Scientific, Taiwan), where conditions were carefully controlled to simulate extended daylight. The chamber maintained a 16-h day and an 8-h night photoperiod, with the temperature set at 28 °C, relative humidity at 70%, and lighting at 500 µmol m^{-2} s^{-1} lights. Once uniformly germinated, the seedlings (four per polybag) were categorized into two main groups. One group received treatment with SA (Fujifilm Wako Pure Chemical Corporation, Osaka, Japan), while the control group was treated with tap water.

SA treatments were administered by applying 10 mL of a 1 mM SA solution directly to the root zone of each plant, totaling 40 mL for four seedlings in each polybag. This was performed at two developmental stages, seven and twelve days after germination, based on the optimal dose identified in a previous study conducted by Keya et al. [25]. Control plants received an equal volume of tap water. Seventeen days post-germination, which includes four days following the last SA and tap water application, plants were subdivided into four groups, each consisting of five polybags to serve as five replications.

These groups were then subjected to different treatments: (i) water-treated, non-stressed plants (Control), (ii) 1 mM SA-primed, non-stressed plants (SA), (iii) water-treated, heat-exposed plants (Heat), and (iv) 1 mM SA-primed, heat-exposed plants (SA+Heat). Heat stress was induced by exposing the plants to 42 °C temperature and 70% humidity for 48 h. To mitigate water stress, 30 mL of water was added to each of the heat-stressed polybags at 12-h intervals, totaling 4 times applications over the stress tenure. To ensure its reliability, research was conducted three times. The 3rd leaves, counting from the base, of 19-day-old plants were collected for the analysis of various morphological, physiological, and biochemical parameters.

4.2. Growth Parameter Assessment

Height, shoot dry weight (DW), and root biomass were assessed from three plants randomly selected from each treatment group, following the comprehensive methodologies described by Rahman et al. [47].

4.3. Methodical Approach to Evaluating Water Content and Cellular Integrity in Cotton Leaves

To measure the relative water content (RWC) of cotton leaves, we followed a systematic procedure. First, we weighed the fresh leaves (FW). Then, the leaves were soaked in deionized water for twelve hours to achieve full turgidity, after which they were reweighed to obtain the turgid weight (TW). The leaves were subsequently dried at 75 °C for 72 h to determine their dry weight (DW) [51]. The RWC was calculated using the formula: RWC (%) = $[(FW - DW)/(TW - DW)] \times 100$. To determine the electrolyte leakage (EL), we adopted a specific method. We submerged 0.2 g of leaf tissue in 20 milliliters of tap water. The initial electrical conductivity of the solution (EC1) was measured. After heating the samples at 100 °C for thirty minutes, the electrical conductivity was measured again (EC2) after cooling the sample. The EL was then calculated using the formula EL (%) = $[(EC1 - EC0)/(EC2 - EC0)] \times 100$, with EC0 representing the conductivity of the tap water [48].

4.4. Assessment of Photosynthetic Pigments and Flavonoid Contents

Pigments were extracted from 0.2 g of freshly harvested cotton leaves using chilled 80% acetone (v/v). The suspension was centrifuged at 10,000× g for 10 min at 4 °C. The concentrations of the supernatant were then quantified using a spectrophotometer. For carotenoids, the quantification was based on equations from Lichtenthaler and Wellburn [55], while chlorophyll *a*, chlorophyll *b*, and total chlorophyll levels were measured using methods established by Arnon [56]. Furthermore, we evaluated the total flavonoid content in fresh leaf samples using the detailed protocol described by Das et al. [48].

4.5. Assessment of Hydrogen Peroxide, Malondialdehyde, and Proline

To quantify the biochemical markers indicative of oxidative stress, we utilized the 3rd bottommost leaves from freshly harvested cotton plants. Spectrophotometric methods, as detailed by Kim et al. [57] for malondialdehyde (MDA) determination, were employed. Briefly, leaf samples (0.2 g) were homogenized in 800 µL of 0.1% trichloroacetic acid (TCA). The homogenate underwent centrifugation at 14,000× g for 20 min at 4 °C to isolate the supernatant. Subsequently, 500 µL of the supernatant was reacted with 1.5 mL of 0.5% thiobarbituric acid in 20% TCA. The reaction mixture was then heated to 95 °C for 30 min. Following incubation, the mixture was promptly cooled on ice and centrifuged at 10,000× g for 5 min. The absorbance of the resulting supernatant was measured at 532 nm and 600 nm using a GENESYS 10S UV–VIS spectrophotometer (Thermo Scientific, San Jose, CA, USA). MDA concentrations were precisely calculated using an extinction coefficient of 156 mM^{-1} cm^{-1}. For the determination of hydrogen peroxide (H_2O_2), fresh plant tissues (0.1 g) were pulverized in 2 mL of 0.1% (w/v) trichloroacetic acid (TCA) under pre-chilled conditions using an ice bath. The homogenate was then subjected to centrifugation at 12,000× g for 15 min. The supernatant (0.5 mL) was subsequently aliquoted and mixed

with 0.5 mL of potassium phosphate buffer (pH 7.0) and 1 mL of potassium iodide solution. The resultant mixture was vigorously vortexed, and the absorbance was quantitatively measured at 390 nm, with 0.1% TCA serving as the blank [58]. Additionally, to evaluate the proline content, which serves as a vital osmoprotectant and stress biomarker in plants, we employed the protocol established by Bates et al. [59].

4.6. Extraction of Antioxidant Enzymes and Quantification of Enzyme Activities

Following the methodology detailed by Rahman et al. [47], we extracted enzymes from cotton leaf samples to evaluate the activities of several key antioxidant enzymes. These enzymes included glutathione *S*-transferase (GST), peroxidase (POD), catalase (CAT), and ascorbate peroxidase (APX).

4.7. Quantification Techniques for Soluble Sugars, Amino Acids, and Carbohydrate Levels

To conduct biochemical analyses, we carefully excised the third leaf from the base of each plant. The quantification of soluble sugar levels was conducted using Somogyi's method [60]. Briefly, an extraction buffer was prepared by mixing 80 mL of ethanol with 20 mL of water. For the anthrone reagent, dissolve anthrone powder in sulfuric acid (2.5 mL acid: 5 mg anthrone) on ice, stirring until completely dissolved. Standard glucose stock was prepared by dissolving 20 mg of glucose in 20 mL of water (1000 μg/mL) and then diluting accordingly. Homogenize 0.2 g of fresh leaf sample in 1.5 mL of 80% ethanol, centrifuge at 11,500× *g* for 15 min at 4 °C and collect the supernatant. Dilute 40 μL of the supernatant with 160 μL of water. Slowly add 2.5 mL of the anthrone reagent to the mixture, then vortex and incubate at 90 °C for 15 min. Cool immediately on ice, then measure the absorbance at 620 nm using the anthrone reagent as the blank. Free amino acids were measured following the technique described by Lee and Takahashi [61]. An extraction buffer was prepared by mixing 80 mL of ethanol with 20 mL of distilled water. For the reaction mixture (RM), combine citrate buffer (0.5 M, pH 5.5), 1% ninhydrin reagent (prepared by dissolving ninhydrin in citrate buffer), and 55% glycerol solution, stirring with a magnetic stirrer. For each sample, 0.2 mL of 1% ninhydrin reagent, 0.2 mL of citrate buffer, and 1.2 mL of 55% glycerol are required to prepare the RM. Homogenize 0.2 g of fresh leaf sample in 1 mL of 80% ethanol. Centrifuge the mixture at 11,500× *g* at 4 °C for 15 min and collect the supernatant. Mix 0.1 mL of the supernatant with 1.6 mL of RM. For the blank, mix 0.1 mL of 80% ethanol with 1.6 mL of RM. Vortex and heat the mixture in a boiling water bath for 30 min until a purple color develops. After cooling, measure the absorbance at 570 nm using a spectrophotometer. Additionally, we determined total carbohydrate content using the protocol established by Dubois et al. [62].

4.8. Statistical Methodologies and Visualization Tools for Data Interpretation

The data were statistically analyzed using Statistix 10 software (Analytical Software, 2105 Miller Landing Rd, Tallahassee, FL 32312, USA). We applied a one-way analysis of variance (ANOVA) to evaluate differences across all datasets, and significant variations between treatments were identified using the least significant difference (LSD) post hoc test with a significance level of $p < 0.05$. The results, presented as means ± standard deviations (SDs), were based on three biological replicates for morphological data and four biological replicates for biochemical data per treatment. To further explore the data, we employed cluster heatmap and principal component analysis (PCA) techniques, utilizing various R software packages (RStudio version 2023.06.1+524). This approach followed the methodology outlined by Ghosh et al. [63], enabling us to visualize complex patterns and relationships within the dataset effectively.

5. Conclusions

Our findings demonstrated that salicylic acid (SA) significantly enhances cotton growth under optimal conditions and improves its resilience against heat stress (Figure 7). This underscores SA pretreatment's potential as a novel strategy to increase heat tolerance

in crops. Specifically, SA pretreatment led to notable improvements in key heat tolerance mechanisms, including increased shoot and root biomass, preservation of essential photosynthetic pigments, effective reduction of H_2O_2, EL, and MDA-mediated oxidative damage through the strengthening of the antioxidant defense system, and a remarkable increase in osmoprotectant levels to maintain water balance (Figure 7). Future research should aim to decipher the specific regulatory pathways that SA targets and modulates to impart heat tolerance in cotton and other essential fiber crops through comprehensive genetic and molecular investigations. Additionally, conducting field trials and economic assessments of SA treatments are critical next steps to mitigate heat stress impacts and minimize catastrophic losses in crop yields.

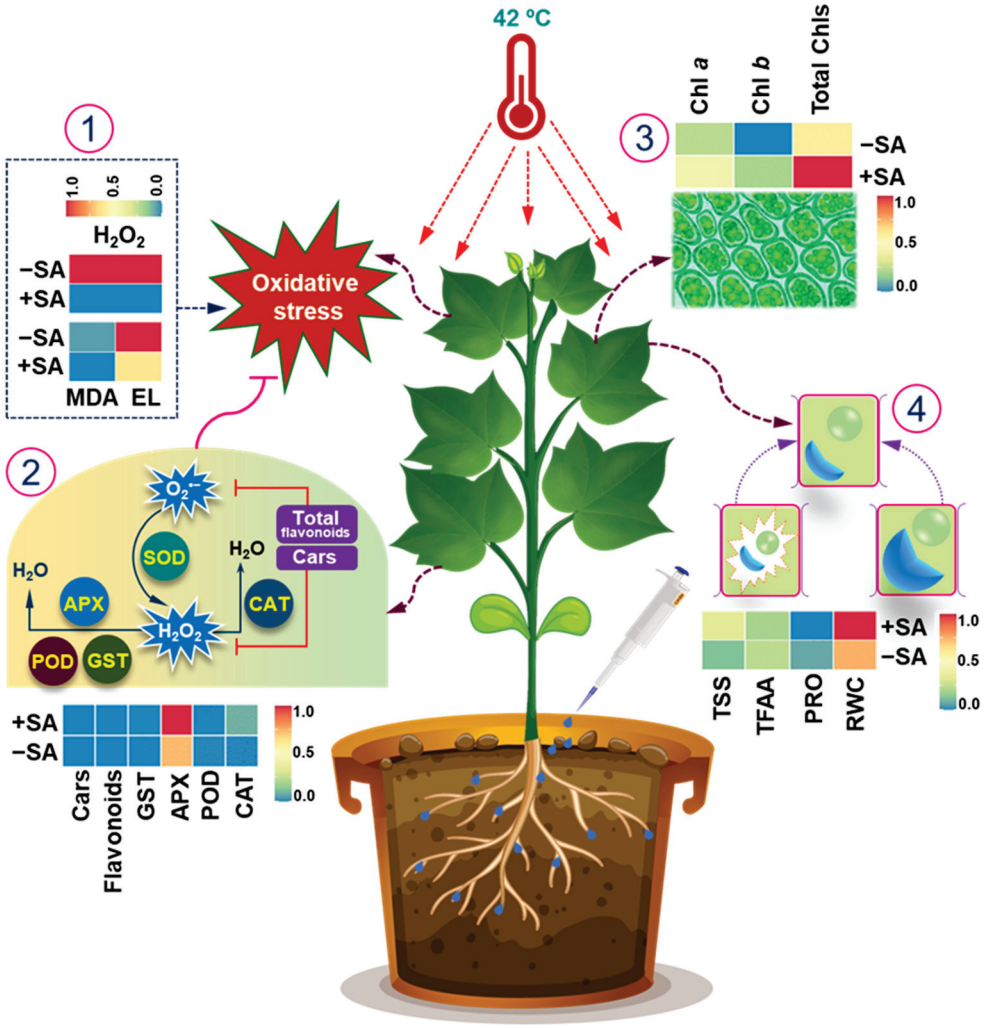


Figure 7. Mechanistic overview of salicylic acid (SA) priming in enhancing heat stress tolerance in cotton plants. SA priming significantly reduces the levels of oxidative stress indicators such as malondialdehyde (MDA), which is a marker of lipid peroxidation, electrolyte leakage (EL), which indicates cell membrane damage, and hydrogen peroxide (H_2O_2), a reactive oxygen species. Concurrently, SA priming enhances the activities of several key antioxidant enzymes that play vital roles in mitigating oxidative damage. These enzymes include glutathione *S*-transferase (GST), which is involved in detoxification processes; ascorbate peroxidase (APX), which helps in the reduction of H_2O_2 to water; catalase (CAT), which decomposes H_2O_2 into water and oxygen; and peroxidase (POD), which catalyzes the oxidation of various substrates using H_2O_2 (1, 2). This robust antioxidant defense mechanism alleviates oxidative damage, thereby preserving photosynthetic efficiency, as evidenced by higher levels of photosynthetic pigments (chlorophyll *a*, chlorophyll *b*, and Cars) (3).

Additionally, SA-primed plants demonstrate a superior ability to maintain higher relative water content (RWC), which is crucial for sustaining cellular functions and overall plant turgor under stress conditions. These plants also accumulate significantly greater amounts of total soluble sugars (TSS), which act as osmoprotectants and energy sources, aiding in stress mitigation. The levels of proline (PRO), an amino acid known for its role in osmotic adjustment, protection of cellular structures, and scavenging of free radicals, are also elevated. Furthermore, SA priming leads to an increase in total free amino acids (TFAA), which contribute to protein synthesis, stress signaling, and metabolic adjustments during heat stress (4). The depicted interactions underscore the multifaceted role of SA in modulating physiological and biochemical responses to heat stress in cotton plants. Cars, carotenoids.

Author Contributions: Conceptualization, M.M.R.; methodology, M.M.R. and A.K.D.; experimental work, A.K.D., P.K.G. and S.S.; software, S.A.I.N., M.H. and P.K.G.; formal analysis, A.K.D. and P.K.G.; validation, M.M.R.; investigation, M.M.R. and M.A.R; data curation, A.K.D., S.S.K. and M.M.R.; writing—original draft preparation, S.S.K., S.A.I.N., U.S., M.A. and P.K.G.; writing—review and editing, M.M.R. and M.M.H.; supervision, M.M.R., M.A.R. and T.K.G.; provided materials, M.A.R. and T.K.G. All authors have read and agreed to the published version of the manuscript.

Funding: This research did not receive any grant from funding agencies in the public, commercial, or not-for-profit sectors.

Institutional Review Board Statement: Not applicable.

Data Availability Statement: Data will be available upon request.

Conflicts of Interest: The authors declare no conflicts of interest.

References

1. Soualiou, S.; Duan, F.; Li, X.; Zhou, W. Crop production under cold stress: An understanding of plant responses, acclimation processes, and management strategies. *Plant Physiol. Biochem.* **2022**, *190*, 47–61. [CrossRef]
2. Rivero, R.M.; Mittler, R.; Blumwald, E.; Zandalinas, S.I. Developing climate-resilient crops: Improving plant tolerance to stress combination. *Plant J.* **2022**, *109*, 373–389. [CrossRef] [PubMed]
3. Desaint, H.; Aoun, N.; Deslandes, L.; Vailleau, F.; Roux, F.; Berthomé, R. Fight hard or die trying: When plants face pathogens under heat stress. *New Phytol.* **2021**, *229*, 712–734. [CrossRef] [PubMed]
4. Arias, P.; Bellouin, N.; Coppola, E.; Jones, R.; Krinner, G.; Marotzke, J.; Naik, V.; Palmer, M.; Plattner, G.-K.; Rogelj, J. Intergovernmental Panel on Climate Change (IPCC). Technical summary. In *Climate Change 2021: The Physical Science Basis. Contribution of Working Group I to the Sixth Assessment Report of the Intergovernmental Panel on Climate Change*; Cambridge University Press: Cambridge, UK, 2023; pp. 35–144.
5. Zenda, T.; Wang, N.; Dong, A.; Zhou, Y.; Duan, H. Reproductive-stage heat stress in cereals: Impact, plant responses and strategies for tolerance improvement. *Int. J. Mol. Sci.* **2022**, *23*, 6929. [CrossRef] [PubMed]
6. Zandalinas, S.I.; Mittler, R.; Balfagón, D.; Arbona, V.; Gómez-Cadenas, A. Plant adaptations to the combination of drought and high temperatures. *Physiol. Plant.* **2018**, *162*, 2–12. [CrossRef] [PubMed]
7. Hu, S.; Ding, Y.; Zhu, C. Sensitivity and responses of chloroplasts to heat stress in plants. *Front. Plant Sci.* **2020**, *11*, 520328. [CrossRef] [PubMed]
8. Khan, M.A.; Asaf, S.; Khan, A.L.; Jan, R.; Kang, S.-M.; Kim, K.-M.; Lee, I.-J. Thermotolerance effect of plant growth-promoting Bacillus cereus SA1 on soybean during heat stress. *BMC Microbiol.* **2020**, *20*, 175. [CrossRef] [PubMed]
9. Rai, K.K.; Pandey, N.; Rai, S.P. Salicylic acid and nitric oxide signaling in plant heat stress. *Physiol. Plant.* **2020**, *168*, 241–255. [CrossRef] [PubMed]
10. Ahmad, M.; Waraich, E.A.; Zulfiqar, U.; Ullah, A.; Farooq, M. Thiourea application improves heat tolerance in camelina (*Camelina sativa* L. Crantz) by modulating gas exchange, antioxidant defense and osmoprotection. *Ind. Crop. Prod.* **2021**, *170*, 113826.
11. Alam, M.N.; Yang, L.; Yi, X.; Wang, Q.; Robin, A.H.K. Role of melatonin in inducing the physiological and biochemical processes associated with heat stress tolerance in tall fescue (*Festuca arundinaceous*). *J. Plant Growth Regul.* **2022**, *41*, 2759–2768. [CrossRef]
12. Xu, X.; Wang, Q.; Li, W.; Hu, T.; Wang, Q.; Yin, Y.; Liu, X.; He, S.; Zhang, M.; Liang, Y. Overexpression of SlBBX17 affects plant growth and enhances heat tolerance in tomato. *Int. J. Biol. Macromol.* **2022**, *206*, 799–811. [CrossRef] [PubMed]
13. Yu, B.; Ming, F.; Liang, Y.; Wang, Y.; Gan, Y.; Qiu, Z.; Yan, S.; Cao, B. Heat stress resistance mechanisms of two cucumber varieties from different regions. *Int. J. Mol. Sci.* **2022**, *23*, 1817. [CrossRef] [PubMed]
14. Asthir, B. Mechanisms of heat tolerance in crop plants. *Biol. Plant.* **2015**, *59*, 620–628. [CrossRef]

15. Abdelraheem, A.; Esmaeili, N.; O'Connell, M.; Zhang, J. Progress and perspective on drought and salt stress tolerance in cotton. *Ind. Crop. Prod.* **2019**, *130*, 118–129. [CrossRef]
16. Hou, S.; Zhu, G.; Li, Y.; Li, W.; Fu, J.; Niu, E.; Li, L.; Zhang, D.; Guo, W. Genome-wide association studies reveal genetic variation and candidate genes of drought stress related traits in cotton (*Gossypium hirsutum* L.). *Front. Plant Sci.* **2018**, *9*, 1276. [CrossRef]
17. An, M.; Wang, X.; Chang, D.; Wang, S.; Hong, D.; Fan, H.; Wang, K. Application of compound material alleviates saline and alkaline stress in cotton leaves through regulation of the transcriptome. *BMC Plant Biol.* **2020**, *20*, 462. [CrossRef] [PubMed]
18. Zhang, Y.; Zhou, X.; Dong, Y.; Zhang, F.; He, Q.; Chen, J.; Zhu, S.; Zhao, T. Seed priming with melatonin improves salt tolerance in cotton through regulating photosynthesis, scavenging reactive oxygen species and coordinating with phytohormone signal pathways. *Ind. Crop. Prod.* **2021**, *169*, 113671. [CrossRef]
19. Majeed, S.; Rana, I.A.; Mubarik, M.S.; Atif, R.M.; Yang, S.-H.; Chung, G.; Jia, Y.; Du, X.; Hinze, L.; Azhar, M.T. Heat stress in cotton: A review on predicted and unpredicted growth-yield anomalies and mitigating breeding strategies. *Agronomy* **2021**, *11*, 1825. [CrossRef]
20. Mercado Alvarez, K.; Bertero, H.D.; Paytas, M.J.; Ploschuk, E.L. Mesophyll conductance modulates photosynthetic rate in cotton crops exposed to heat stress under field conditions. *J. Agron. Crop Sci.* **2022**, *208*, 53–64. [CrossRef]
21. Anwar, A.; Kim, J.-K. Transgenic breeding approaches for improving abiotic stress tolerance: Recent progress and future perspectives. *Int. J. Mol. Sci.* **2020**, *21*, 2695. [CrossRef]
22. Pan, Q.; Zhan, J.; Liu, H.; Zhang, J.; Chen, J.; Wen, P.; Huang, W. Salicylic acid synthesized by benzoic acid 2-hydroxylase participates in the development of thermotolerance in pea plants. *Plant Sci.* **2006**, *171*, 226–233. [CrossRef]
23. Saleem, M.; Fariduddin, Q.; Castroverde, C.D.M. Salicylic acid: A key regulator of redox signalling and plant immunity. *Plant Physiol. Biochem.* **2021**, *168*, 381–397. [CrossRef] [PubMed]
24. Jha, U.C.; Nayyar, H.; Siddique, K.H. Role of phytohormones in regulating heat stress acclimation in agricultural crops. *J. Plant Growth Regul.* **2022**, *41*, 1041–1064. [CrossRef]
25. Keya, S.S.; Mostofa, M.G.; Rahman, M.M.; Das, A.K.; Sultana, S.; Ghosh, P.K.; Anik, T.R.; Ahsan, S.; Rahman, M.A.; Jahan, N.; et al. Salicylic acid application improves photosynthetic performance and biochemical responses to mitigate saline stress in cotton. *J. Plant Growth Regul.* **2023**, *42*, 5881–5894. [CrossRef]
26. Jahan, M.S.; Wang, Y.; Shu, S.; Zhong, M.; Chen, Z.; Wu, J.; Sun, J.; Guo, S. Exogenous salicylic acid increases the heat tolerance in Tomato (*Solanum lycopersicum* L.) by enhancing photosynthesis efficiency and improving antioxidant defense system through scavenging of reactive oxygen species. *Sci. Hortic.* **2019**, *247*, 421–429. [CrossRef]
27. Wassie, M.; Zhang, W.; Zhang, Q.; Ji, K.; Cao, L.; Chen, L. Exogenous salicylic acid ameliorates heat stress-induced damages and improves growth and photosynthetic efficiency in alfalfa (*Medicago sativa* L.). *Ecotoxicol. Environ. Saf.* **2020**, *191*, 110206. [CrossRef] [PubMed]
28. Yang, J.; Duan, L.; He, H.; Li, Y.; Li, X.; Liu, D.; Wang, J.; Jin, G.; Huang, S. Application of exogenous KH_2PO_4 and salicylic acid and optimization of the sowing date enhance rice yield under high-temperature conditions. *J. Plant Growth Regul.* **2022**, *41*, 1532–1546. [CrossRef]
29. Tanveer, S.; Akhtar, N.; Ilyas, N.; Sayyed, R.; Fitriatin, B.N.; Perveen, K.; Bukhari, N.A. Interactive effects of Pseudomonas putida and salicylic acid for mitigating drought tolerance in canola (*Brassica napus* L.). *Heliyon* **2023**, *9*, e14193. [CrossRef]
30. Li, Y.; Han, X.; Ren, H.; Zhao, B.; Zhang, J.; Ren, B.; Gao, H.; Liu, P. Exogenous SA or 6-BA maintains photosynthetic activity in maize leaves under high temperature stress. *Crop J.* **2023**, *11*, 605–617. [CrossRef]
31. Wang, W.; Wang, X.; Lv, Z.; Khanzada, A.; Huang, M.; Cai, J.; Zhou, Q.; Huo, Z.; Jiang, D. Effects of cold and salicylic acid priming on free proline and sucrose accumulation in winter wheat under freezing stress. *J. Plant Growth Regul.* **2022**, *41*, 2171–2184. [CrossRef]
32. Huang, Q.; Xu, R.; Zhang, Y.; Yan, Z.; Chen, H.; Shao, G. Salicylic acid ameliorates cadmium toxicity by increasing nutrients uptake and upregulating antioxidant enzyme activity and uptake/transport-related genes in *Oryza sativa* L. indica. *J. Plant Growth Regul.* **2023**, *42*, 1158–1170. [CrossRef]
33. Jangra, M.; Devi, S.; Satpal; Kumar, N.; Goyal, V.; Mehrotra, S. Amelioration effect of salicylic acid under salt stress in *Sorghum bicolor* L. *Appl. Biochem. Biotechnol.* **2022**, *194*, 4400–4423. [PubMed]
34. Zafar, M.M.; Jia, X.; Shakeel, A.; Sarfraz, Z.; Manan, A.; Imran, A.; Mo, H.; Ali, A.; Youlu, Y.; Razzaq, A. Unraveling heat tolerance in upland cotton (*Gossypium hirsutum* L.) using univariate and multivariate analysis. *Front. Plant Sci.* **2022**, *12*, 727835. [CrossRef] [PubMed]
35. Tahjib-Ul-Arif, M.; Siddiqui, M.N.; Sohag, A.A.M.; Sakil, M.A.; Rahman, M.M.; Polash, M.A.S.; Mostofa, M.G.; Tran, L.-S.P. Salicylic acid-mediated enhancement of photosynthesis attributes and antioxidant capacity contributes to yield improvement of maize plants under salt stress. *J. Plant Growth Regul.* **2018**, *37*, 1318–1330. [CrossRef]
36. Khan, M.S.; Akther, T.; Ali, D.M.; Hemalatha, S. An investigation on the role of salicylic acid alleviate the saline stress in rice crop (*Oryza sativa* (L.)). *Biocatal. Agric. Biotechnol.* **2019**, *18*, 101027. [CrossRef]
37. Loutfy, N.; Sakuma, Y.; Gupta, D.K.; Inouhe, M. Modifications of water status, growth rate and antioxidant system in two wheat cultivars as affected by salinity stress and salicylic acid. *J. Plant Res.* **2020**, *133*, 549–570. [CrossRef] [PubMed]

38. Nieto-Sotelo, J.; Martínez, L.M.; Ponce, G.; Cassab, G.I.; Alagón, A.; Meeley, R.B.; Ribaut, J.-M.; Yang, R. Maize HSP101 plays important roles in both induced and basal thermotolerance and primary root growth. *Plant Cell* **2002**, *14*, 1621–1633. [CrossRef]
39. Sarwar, M.; Saleem, M.F.; Ullah, N.; Ali, S.; Rizwan, M.; Shahid, M.R.; Alyemeni, M.N.; Alamri, S.A.; Ahmad, P. Role of mineral nutrition in alleviation of heat stress in cotton plants grown in glasshouse and field conditions. *Sci. Rep.* **2019**, *9*, 13022. [CrossRef]
40. Ul Hassan, M.; Rasool, T.; Iqbal, C.; Arshad, A.; Abrar, M.; Abrar, M.M.; Habib-ur-Rahman, M.; Noor, M.A.; Sher, A.; Fahad, S. Linking plants functioning to adaptive responses under heat stress conditions: A mechanistic review. *J. Plant Growth Regul.* **2022**, *41*, 2596–2613. [CrossRef]
41. EL Sabagh, A.; Hossain, A.; Islam, M.S.; Barutcular, C.; Ratnasekera, D.; Gormus, O.; Amanet, K.; Mubeen, M.; Nasim, W.; Fahad, S.; et al. Drought and Heat Stress in Cotton (*Gossypium hirsutum* L.): Consequences and Their Possible Mitigation Strategies. In *Agronomic Crops: Volume 3: Stress Responses and Tolerance*; Hasanuzzaman, M., Ed.; Springer: Singapore, 2020; pp. 613–634.
42. Ahmad, F.; Perveen, A.; Mohammad, N.; Ali, M.A.; Akhtar, M.N.; Shahzad, K.; Danish, S.; Ahmed, N. Heat Stress in Cotton: Responses and Adaptive Mechanisms. In *Cotton Production and Uses: Agronomy, Crop Protection, and Postharvest Technologies*; Ahmad, S., Hasanuzzaman, M., Eds.; Springer: Singapore, 2020; pp. 393–428.
43. Azhar, M.T.; Wani, S.H.; Chaudhary, M.T.; Jameel, T.; Kaur, P.; Du, X. Heat Tolerance in Cotton. In *Heat Stress Tolerance in Plants: Physiological, Molecular and Genetic Perspectives*; Wani, S.H., Kumar, V., Eds.; John Wiley & Sons Inc.: Hoboken, NJ, USA, 2020; pp. 1–22.
44. Qamer, Z.; Chaudhary, M.; Du, X.; Hinze, L.; Azhar, M.T. Review of oxidative stress and antioxidative defense mechanisms in *Gossypium hirsutum* L. in response to extreme abiotic conditions. *J. Cotton Res.* **2021**, *4*, 9. [CrossRef]
45. Ahanger, M.; Mir, R.; Alyemeni, M.; Ahmad, P. Combined effects of brassinosteroid and kinetin mitigates salinity stress in tomato through the modulation of antioxidant and osmolyte metabolism. *Plant Physiol. Biochem.* **2019**, *147*, 31–42. [CrossRef] [PubMed]
46. Janda, T.; Lejmel, M.; Molnar, A.; Majláth, I.; Pál, M.; Quang Trung, N.; Nguyen, N.; Le, V.N.; Szalai, G. Interaction between elevated temperature and different types of Na-salicylate treatment in *Brachypodium dystachion*. *PLoS ONE* **2020**, *15*, e0227608. [CrossRef] [PubMed]
47. Rahman, M.M.; Mostofa, M.G.; Rahman, M.A.; Islam, M.R.; Keya, S.S.; Das, A.K.; Miah, M.G.; Kawser, A.Q.M.R.; Ahsan, S.; Hashem, A.; et al. Acetic acid: A cost-effective agent for mitigation of seawater-induced salt toxicity in mung bean. *Sci. Rep.* **2019**, *9*, 15186. [CrossRef] [PubMed]
48. Das, A.K.; Touhidur Rahman, A.; Rahman, M.M.; Sanjida Sultana, K.; Islam, M.R.; Rahman, M.A.; Sultana, S.; Ghosh, P.K.; Khan, S.; Ahamed, T.; et al. Ethanol treatment enhances physiological and biochemical responses to mitigate saline toxicity in soybean. *Plants* **2022**, *11*, 272. [CrossRef] [PubMed]
49. Rahman, M.M.; Mostofa, M.G.; Das, A.K.; Anik, T.R.; Keya, S.S.; Ahsan, S.M.; Khan, M.A.R.; Ahmed, M.; Rahman, M.A.; Hossain, M.M.; et al. Ethanol positively modulates photosynthetic traits, antioxidant defense and osmoprotectant levels to enhance drought acclimatization in soybean. *Antioxidants* **2022**, *11*, 516. [CrossRef] [PubMed]
50. Keya, S.S.; Mostofa, M.G.; Mezanur Rahman, M.; Das, A.K.; Abiar Rahman, M.; Anik, T.R.; Sultana, S.; Arifur Rahman Khan, M.; Robyul Islam, M.; Watanabe, Y.; et al. Effects of glutathione on waterlogging-induced damage in sesame crop. *Ind. Crop. Prod.* **2022**, *185*, 115092. [CrossRef]
51. Rahman, M.M.; Mostofa, M.G.; Rahman, M.A.; Miah, M.G.; Saha, S.R.; Karim, M.A.; Keya, S.S.; Akter, M.; Islam, M.; Tran, L.S.P. Insight into salt tolerance mechanisms of the halophyte *Achras sapota*: An important fruit tree for agriculture in coastal areas. *Protoplasma* **2018**, *256*, 181–191. [CrossRef]
52. Zhang, C.X.; Feng, B.H.; Chen, T.T.; Zhang, X.F.; Tao, L.X.; Fu, G.F. Sugars, antioxidant enzymes and IAA mediate salicylic acid to prevent rice spikelet degeneration caused by heat stress. *Plant Growth Regul.* **2017**, *83*, 313–323. [CrossRef]
53. Parida, A.K.; Jha, B. Inductive responses of some organic metabolites for osmotic homeostasis in peanut (*Arachis hypogaea* L.) seedlings during salt stress. *Acta Physiol. Plant.* **2013**, *35*, 2821–2832. [CrossRef]
54. Parida, A.K.; Veerabathini, S.K.; Kumari, A.; Agarwal, P.K. Physiological, anatomical and metabolic implications of salt tolerance in the halophyte *Salvadora persica* under hydroponic culture condition. *Front. Plant Sci.* **2016**, *7*, 184129. [CrossRef]
55. Lichtenthaler, H.K.; Wellburn, A.R. Determinations of total carotenoids and chlorophylls a and b of leaf extracts in different solvents. *Biochem. Soc. Trans.* **1983**, *11*, 591–592. [CrossRef]
56. Arnon, D.I. Copper enzymes in isolated chloroplasts. polyphenoloxidase in *Beta vulgaris*. *Plant Physiol.* **1949**, *24*, 1–15. [CrossRef] [PubMed]
57. Kim, T.Y.; Ku, H.; Lee, S.-Y. Crop enhancement of cucumber plants under heat stress by shungite carbon. *Int. J. Mol. Sci.* **2020**, *21*, 4858. [CrossRef] [PubMed]
58. Velikova, V.; Yordanov, I.; Edreva, A. Oxidative stress and some antioxidant systems in acid rain-treated bean plants: Protective role of exogenous polyamines. *Plant Sci.* **2000**, *151*, 59–66. [CrossRef]
59. Bates, L.S.; Waldren, R.P.; Teare, I.D. Rapid determination of free proline for water-stress studies. *Plant Soil.* **1973**, *39*, 205–207. [CrossRef]
60. Smogyi, M. Notes on sugar determination. *J. Biol. Chem.* **1952**, *195*, 19–23. [CrossRef] [PubMed]
61. Lee, Y.-P.; Takahashi, T. An improved colorimetric determination of amino acids with the use of ninhydrin. *Anal. Biochem.* **1966**, *14*, 71–77. [CrossRef]

62. Dubois, M.; Gilles, K.; Hamilton, J.K.; Rebers, P.A.; Smith, F. A colorimetric method for the determination of sugars. *Nature* **1951**, *168*, 167. [CrossRef]
63. Ghosh, P.K.; Sultana, S.; Keya, S.S.; Nihad, S.A.I.; Shams, S.-N.-U.; Hossain, M.S.; Tahiat, T.; Rahman, M.A.; Rahman, M.M.; Raza, A. Ethanol-mediated cold stress tolerance in sorghum seedlings through photosynthetic adaptation, antioxidant defense, and osmoprotectant enhancement. *Plant Stress* **2024**, *11*, 100401. [CrossRef]

Disclaimer/Publisher's Note: The statements, opinions and data contained in all publications are solely those of the individual author(s) and contributor(s) and not of MDPI and/or the editor(s). MDPI and/or the editor(s) disclaim responsibility for any injury to people or property resulting from any ideas, methods, instructions or products referred to in the content.

plants

MDPI

Review

Complex Signaling Networks Underlying Blue-Light-Mediated Floral Transition in Plants

Yun Kong and Youbin Zheng *

School of Environmental Science, University of Guelph, 50 Stone Road East, Guelph, ON N1G 2W1, Canada; yunkong@uoguelph.ca
* Correspondence: yzheng@uoguelph.ca

Abstract: Blue light (BL) is important in regulating floral transition. In a controlled environment production system, BL can be manipulated easily and precisely in aspects like peak wavelength, intensity, duration, and co-action with other wavelengths. However, the results of previous studies about BL-mediated floral transition are inconsistent, which implies that an in-depth critical examination of the relevant physiological mechanisms is necessary. This review consolidates the recent findings on the role of BL in mediating floral transition not only in model plants, such as *Arabidopsis thaliana*, but also in crops, especially horticultural crops. The photoreceptors, floral integrator proteins, signal pathways, and key network components involved in BL-mediated floral transition are critically reviewed. This review provides possible explanations for the contrasting results of previous studies on BL-mediated flowering; it provides valuable information to explain and develop BL manipulation strategies for mediating flowering, especially in horticultural plants. The review also identifies the knowledge gaps and outlines future directions for research in related fields.

Keywords: flower induction; photoreceptors; signal pathways; physiological mechanisms; future directions

1. Introduction

Floral transition is a crucial developmental phase that determines the reproductive success of plants and significantly impacts the timing of harvest and marketability in horticultural crops [1]. This transition involves two core features: the induction of floral signals in leaves and their subsequent transport to the shoot apical meristem (SAM), where vegetative growth shifts to reproductive development [2]. For successful flowering, the SAM must finish a transition from an incompetent to a competent state for the formation of floral meristems.

Light spectral quality is one of the important environmental cues regulating floral transition, acting through internal light perception systems [3]. While the role of red and far-red (FR) light has been well-established [4], blue light (BL; 400–500 nm) seems to be a versatile but crucial regulator of flowering [5]. For example, we found that even under 24 h modest-intensity lighting, pure BL promoted flowering of short-day (SD) plants in marigold (*Tagetes erecta*) compared with red light; however, impure BL containing a low level of red light failed to induce flowering, and adding a low level of FR light to the impure BL restored the flowering-promoting effect [6,7]. It appears that BL influences flowering not only through photoperiodism but also by interacting with other light wavelength(s) and intensity [8]. Generally, BL-mediated flowering involves the light signal's

perception by its photoreceptors, which initiate downstream signaling cascades influencing the expression of key flowering genes, such as *CONSTANS (CO)* and *FLOWERING LOCUS T (FT)*, to control floral transition [9,10].

In recent years, advances in light-emitting diode (LED) technology have enabled precise manipulation of light spectral quality, particularly BL, in controlled environment agriculture (CEA). Blue LEDs alone, or their combination with other wavelengths, are increasingly used for night interruption, day extension, supplemental, and sole-source lighting strategies to regulate flowering in various crops [8]. Compared to FRLEDs, blue LEDs are more cost-effective and widely accessible, making them a practical choice for commercial applications [11]. In *Arabidopsis thaliana* (hereafter *Arabidopsis*), BL has been shown to effectively promote flowering via stabilization of the CO protein under long-day (LD) conditions [9,12]. However, conflicting results have been reported across plant species and even within the same species [8]. For example, in LD plants, while LD treatment with BL promoted flowering in petunia (*Petunia* × *hybrida*), like *Arabidopsis* [13], it had negligible effects in *Gypsophila paniculata* [14]. In the SD plant chrysanthemum (*Chrysanthemum morifolium*), LD treatment with BL failed to inhibit flowering in growth chambers across a wide range of light intensities [15–18] but suppressed flowering in greenhouse conditions only when the light intensity exceeded a threshold [19,20]. These variable BL-mediated flowering responses (dependent on plant species, environmental conditions, and light intensities) suggest the involvement of a complex underlying molecular signaling mechanism.

Despite growing interest, a comprehensive understanding of the molecular signaling mechanism involved in BL-mediated floral regulation remains limited, especially in economically important horticultural crops. Shibuya [9] has proposed two signaling pathways for BL-promoted flowering in terms of photoreceptors: FKF1 and CRY2. However, light can regulate plant flowering through at least three pathways, photoperiod, shade, and light quantity pathways [21], and BL signals can be precepted by multiple receptors other than FKF1 and CRY2 [5]. This suggests that more than two pathways can be involved in BL-mediated flowering. Also, most mechanistic insights have been derived from model species under idealized conditions, which may not translate directly to crop production systems. Moreover, even in the model plant, *Arabidopsis*, there is insufficient clarity on how the BL signaling network specifically regulates flower transition, despite documentation on light regulation.

This review aims to consolidate current knowledge on the mechanisms underlying light-mediated flowering, with a focus on BL, in both model species and important crops (e.g., horticultural plants). We identify and discuss key photoreceptors, signaling pathways, and gene expression networks involved in this process. Additionally, we try to use the knowledge on the underlying mechanisms to explain the previous conflicting findings on BL-mediated flowering. Finally, we highlight existing knowledge gaps and propose future research directions to improve the application of BL for flowering control in CEA.

2. Photoreceptors and Photosynthetic Pigments

BL serves as not only an environmental signal to mediate plant flowering through photoreceptors but also an energy source to drive photosynthesis and produce sugar to affect plant flowering through photosynthetic pigments [22]. These photoreceptors and photosynthetic pigments can sense blue light, together with other signals, to mediate plant flowering (Figure 1).

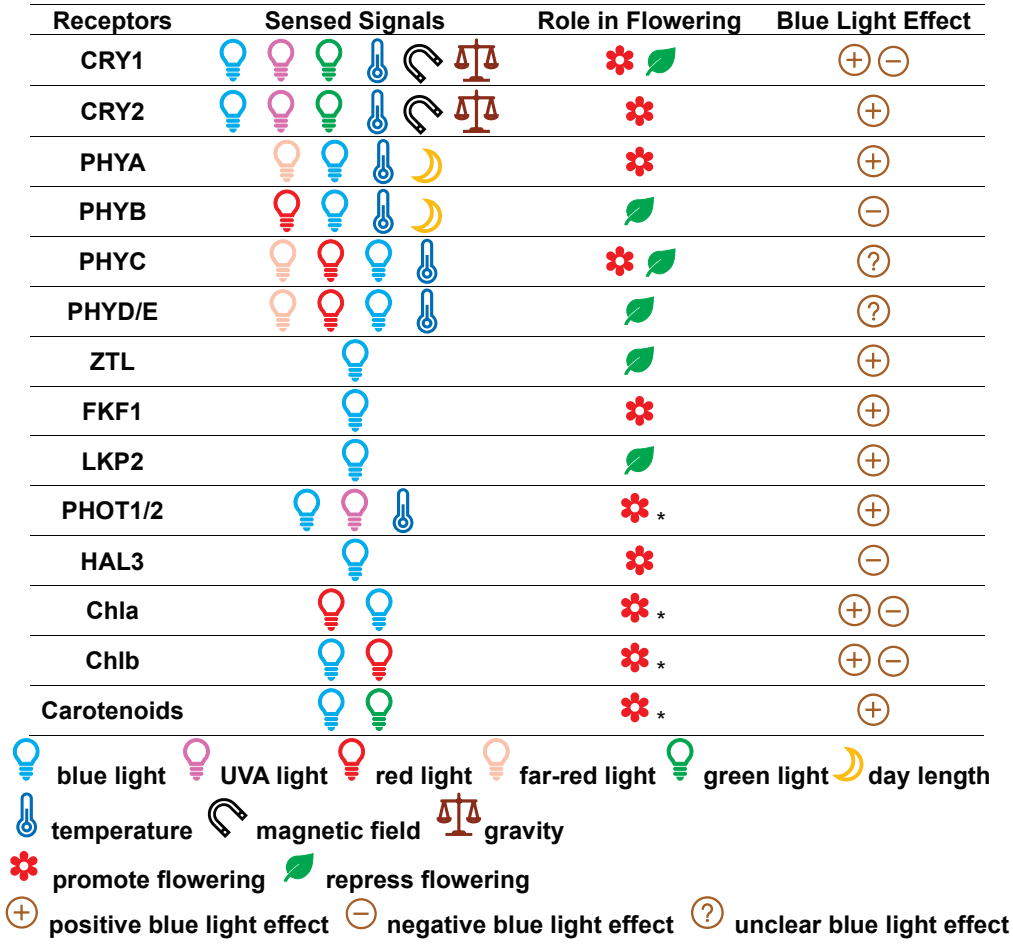


Figure 1. An illustration of the functions of photoreceptors and photosynthetic pigments involved in blue-light-mediated flowering in terms of their sensed signals, role in flowering, and response to blue light. CRY1/2 = cryptochrome1/2; PHYA/B/C/D/E = phytochrome A/B/C/D/E; ZTL = ZEITLUPE; FKF1 = FLAVIN-BINDING, KELCHREPEAT, F-BOX; LKP2 = LOV KELCH PROTEIN2; PHOT1/2 = phototropin1/2; HAL3 = Halotolerance protein; and Chl = Chlorophyll. If both flowering promotion and repression are shown together, this indicates that the role of this receptor depends on environmental conditions or plant genotypes. If both the positive and negative effects of blue light are shown together, this indicates that the blue light effect may vary with light intensity or background light. * indicates that there is only indirect evidence.

2.1. Photoreceptors

BL can be perceived by plants through various light-responsive proteins (termed photoreceptors), such as cryptochromes (CRYs), phytochromes (PHYs), phototropins (PHOTs), and ZEITLUPE (ZTL) family proteins [5,23]. The activation of the BL photoreceptors is sensitive not only to the wavelength but also to the fluence rate (intensity) and photoperiod [24,25]. These photoreceptors are like a series of switches and dimmers, each modulating the activity of a network that controls a specific pathway to flowering [25,26]. Also, the BL receptors interact in synergistic, antagonistic, and redundant ways with each other [24,26].

2.1.1. Cryptochromes (CRYs)

CRYs are primarily photoreceptors of BL and UVA light as well as greenlight, but they can also coordinate or modulate the perception of other environmental signals, such as temperature, magnetic field, and gravity [5,27–29].

Like *Arabidopsis*, almost all higher plants studied have two CRY members, CRY1 and CRY2, despite having more than two genes [28,30]. For example, tomato (*Solanum*

lycopersicum) and barley (*Hordeum vulgare*) each have at least three CRY genes, *CRY1a*, *CRY1b*, and *CRY2* [31,32]. There is now evidence for CRY3 in *Arabidopsis*, but its function is presently unknown [33,34]. CRY1 is stably expressed in the BL and biologically activated at a higher light intensity, but CRY2 is degraded upon exposure to BL, and it has a more specialized role under conditions of limiting BL intensity [34,35]. In *Arabidopsis*, CRY1 functions in both the nucleus and the cytoplasm, whereas CRY2 seems to be an exclusively nuclear protein that completes its post-translational cycle in the nucleus [34]. In onion (*Allium cepa*), AcCRY1 demonstrates cytoplasmic localization under BL conditions, while it localizes in the nucleus during darkness, indicating a strong dependence on BL for its subcellular distribution [36]. In addition, CRY2 forms photobodies in the nucleus in response to BL, and CRY2 function and degradation closely correlate with the formation of photobodies, which have been proposed as sites for CRY2 signal transduction and/or CRY2 degradation [35].

The CRYs are in an inactive monomeric state in the dark and potentially change to an active oligomeric state under BL [37]. The rate of CRY oligomerization reaction in light is much faster than that of the CRY monomerization in darkness. Photoactivation of CRYs begins with photoexcitation, which results in conformational changes and formation of the CRY homooligomers that interact with CRY-interacting proteins to alter gene expression and plant development [28]. During the process of photoactivation, either CRY1 or CRY2 undergoes blue-light-dependent phosphorylation to transduce the signal to the downstream component of the CRY signaling relay [35]. The phosphorylation of CRYs closely correlates with the intensity and duration of BL exposure [35]. This may partly explain why the effect of BL on plant flowering varies with the amount of light [8]. For example, BL can influence flowering only when delivered with sufficiently high intensities as night interruption (NI) lighting but is ineffective in regulating flowering at low intensities [19,20]. Additionally, photoactivation of CRYs can also be influenced by the presence of light wavelength(s) other than BL due to their interaction on the photoreceptors or cross-talk between photoreceptors [29,38]. This is supported by varying plant responses to blue LED in combination with other different LEDs [7,39–42].

Photoactivation of CRYs by BL can trigger a negative feedback reaction by increasing the BLUE-LIGHT INHIBITOR OF CRY (BIC) proteins to prevent excessive accumulation of active CRYs and maintain sustainable photosensitivity of the cell [28,43,44]. The BICs can inhibit blue-light-induced CRY1 activation, as well as BL-induced CRY2 degradation [28,44]. Also, the BICs appear to function only in BL, but not in other wavelengths, such as red light or FR light; however, the mRNA expressions of both *BIC1* and *BIC2* genes are induced by light in a wavelength-independent manner and are mediated by both CRYs and PHYs [43,45]. In the past, our lab has found that sole-source lighting with low- or modest-intensity blue LED light, which is associated with a low PPS value (low PHYB activity), resulted in low CRY1 activity but high CRY2 activity [38]. In this case, whether a balance of photoactivation and inactivation of CRYs is disrupted by the blue LED light through overexpression of the BIC due to co-action of CRYs and PHYs is unknown.

CRY2 is a major photoreceptor regulating BL-mediated photoperiodic flowering, but its effect on flowering varies with spectral quality (i.e., co-action of BL with other light wavelengths) and plant genotype. In *Arabidopsis*, CRY2 promotes flowering under long-day (LD) conditions [35]. However, in our recent study on *Arabidopsis* under constant sole-source lighting, the *cry2* mutant did not delay flowering under blue LED, but it did under blue + FR LED compared with wild plants [38]. Moreover, overexpression of *CRY2* did not affect flowering time under either blue or blue + FR LED. It appears that the role of CRY2 in BL control of flowering time is also affected by light spectral quality and,

possibly, the expression of CRY2 can maintain a sufficiently activated level under blue + FR LED light [38]. In rice (*Oryza sativa*), the knockdown of *CRY2*, but not of *CRY1*, delays flowering both in LD and short-day (SD) conditions [46]. However, a recent study indicates that overexpression of *CRY2* in rice with a photoperiod-insensitive genetic background does not affect the flowering time, although the *OsiCRY2 Arabidopsis* overexpressors exhibited early flowering [47], suggesting the effect of genetic background on the CRY2's function. Furthermore, for tomatoes under LD conditions, *CRY2* overexpression delayed flowering [48].

CRY1 also plays a role in BL-mediated photoperiodic flowering, with the importance of the role varying with environmental conditions and plant genotype. In *Arabidopsis*, the *cry1* mutant exhibited a pronounced late-flowering phenotype at 16 °C, but not at 23 °C, suggesting that temperature influences the role of CRY1 in the photoperiodic regulation of flowering time [35,49]. It appears that the role of CRY1 in *Arabidopsis* flowering control is limited due to the evident effect only under specific environmental conditions [35]. In contrast to *Arabidopsis*, CRY1a rather than CRY2a in soybean (*Glycine max*) is a major regulator of photoperiodic flowering, and it exhibits circadian rhythmicity in varying photoperiods and strongly promotes floral initiation [46,50]. Also, sorghum (*Sorghum bicolor*) CRY1b can rescue the late-flowering phenotype of the *Arabidopsis cry1/cry2* double mutant, indicating a similar role to *Arabidopsis* CRY2 as a major regulator of photoperiodic flowering [46,51]. Additionally, in onions, overexpression of CRY1 leads to a significant acceleration of flowering time [36].

There are overlapping functions of CRY1 and CRY2 in regulating photoperiodic flowering. In tomatoes, both CRY2 and CRY1a likely function to repress flowering; the knockout of a single *CRY* gene, whether *CRY2* or *CRY1a*, does not affect flowering time, but the simultaneous knockout of both *CRY1a* and *CRY2* results in an earlier onset of flowering [46,52]. In *Arabidopsis*, the *cry1cry2* double mutant flowers later than either the *cry1* or *cry2* single mutants under LD or continuous BL conditions [53]. In our recent study on *Arabidopsis* under constant sole-source lighting with blue LED, neither the *cry1* nor the *cry2* mutant delayed flowering, but the *cry1cry2* double mutant inhibited flower initiation compared with wild plants [38]. The overlapping roles of CRY1 and CRY2 in regulating photoperiodic flowering are partly attributed to their shared downstream pathway components, such as COP1/SPA and PIF [54]. However, CIB is a specific downstream pathway component that accounts for CRY2′s roles in BL-mediated flowering, which is a key distinction between CRY1 and CRY2 [54]. Detailed information can be found in Section 4.1.

2.1.2. Phytochromes (PHYs)

The PHYs are primarily photoreceptors of red and FR light, but they also perceive other light wavelengths, including BL, due to small absorption peaks [5,55]. Furthermore, PHYs are also able to sense changes in ambient temperature as well as day length and the difference between day and night [26,56,57].

In *Arabidopsis*, PHYs are encoded by five different genes (*PHYA* to *PHYE*) [22,57]. Most seed plants possess three PHYs: PHYA, PHYB, and PHYC [58]. PHYD and PHYE probably originated from duplications of PHYB in angiosperms and only in Brassicaceae, respectively [57]. However, some flowering plants lack PHYC (e.g., *Populus trichocarpa*) or PHYE (e.g., monocots) [58]. Several species, such as maize (*Zea mays*) and tomato, have two copies of PHYB, i.e., PHYB1 and PHYB2 [57,59]. Generally, in the majority of dicotyledonous plants, PHYs are encoded by five gene families (*PHYA* to *PHYE*), but, in monocotyledonous plants, PHYs are encoded by three genes, *PHYA*, *PHYB*, and *PHYC* [60]. PHYA is mainly activated by FR light, as well as BL [55], whereas PHYB-E are activated by red light and deactivated by foliar shade, as well as BL [22,61].

PHYs can be classified into different types or statuses according to certain features. Based on photolability, PHYs can be grouped into two types: type I photolabile forms and type II photostable forms [62]. PHYA is classified as a type I photolabile PHY and is unstable under light, but PHYB to PHYE are classified as type II PHYs and are relatively stable under prolonged light exposure [22,62]. Also, according to biological activity, PHYs exist in two forms: a biologically inactive red-light-absorbing form (Pr) and a biologically active FR-light-absorbing form (Pfr). The inactive Pr PHY is assembled in the cytosol, and, once converted to Pfr, PHYs move from the cytoplasm into the nucleus, where most signaling functions occur [22]. The inactive Pr state can partly photoconvert to the active Pfr state upon exposure to light (including BL), with the greatest conversion by red light, and the Pfr is partly inactivated under FR light or in the dark through a process of temperature-dependent thermal relaxation called thermal reversion [56,62].

Although BL can stimulate PHYs to some degree, it is less efficient than red light [63]. Plants grown under any light wavelengths have both Pfr and Pr, and the PHY activity can be indicated by the value of the phytochrome photostationary state [PPS; PPS = Pfr/(Pfr + Pr)] [64]. Active PHYB responses normally occur when PPS > 0.6, but active PHYA responses do so at much lower values, e.g., PPS < 0.2 [56,64]. The PPS value for plants growing under light can be calculated based on the light spectrum, and its absorption values can be calculated based on PHY [65]. Pure BL from narrow-band LED light normally has a low PPS value of around 0.5 depending on peak wavelength, but impure BL from traditional lighting sources, such as blue fluorescent light, has a high PPS value above 0.6 [66]. The blue LED in combination with a low level of red LED light increases the PPS value up to 0.7, but its combination with a low level of another light wavelength from UVA, UVB, green, or FR LED light still has a low PPS value below 0.6 [67,68].

The activation of PHYs induces conformational changes that trigger PHY-regulated responses [62,69]. In the activation process, the activity of PHYs greatly relies on their nuclear localization [22,62], and it is regulated by dephosphorylation and phosphorylation [70], as well as the formation of photobodies [22]. A photobody is an assembly of active PHY, Pfr, into large subnuclear compartments, which is a key step in PHY signaling [22]. Photobodies can act to enhance PHYB activity [22]. Red light increases Pfr stabilization and promotes photobody formation, while BL, as well as FR light, high temperature, and darkness, cause its disassembly [71]. This partly supports our lab's reports that blue LED light causes low PHY activity [7,42].

A promotive role in flowering is played by PHYA. In *Arabidopsis*, the *phyA* mutant flowers later than wild type plants under LD and quasi-LD conditions, such as with night breaks or day extensions, and transgenic plants overexpressing *PHYA* flower earlier in both SD and quasi-LD conditions [72]. In *Arabidopsis*, PHYA, together with CRY1 and CRY2, also functions redundantly in mediating BL promotion of flowering. Monogenic *cry1*, *cry2*, or *phyA* mutants flowered at about the same time as the wild type, but a double mutant impaired in any two of the three photoreceptors or the *cry1cry2phyA* triple mutant flowered significantly later than the wild type when grown under continuous BL [73].

The PHYB generally inhibits floral initiation. *Arabidopsis phyB* mutant flowered earlier compared to the wild type in both LD and SD conditions, with a more pronounced effect under SD conditions, and similar flowering responses were observed in *phyB* mutations in pea (*Pisum sativum* L.) and sorghum [53,72]. This indicates that PHYB inhibits flowering in both LD and SD plants, with stronger inhibition in the photoperiod that typically suppresses flowering [72]. Despite its role as a floral inhibitor, PHYB's function in floral initiation is likely more complex. For instance, transgenic *Arabidopsis* plants overexpressing *PHYB* also flowered earlier than the wild type, a phenomenon that is not easily explained [72].

The interaction between PHYA and PHYB demonstrates that PHYB inhibits flowering under both LD and SD conditions, a suppression necessary for the expression of PHYA's promotive effect [74]. PhyA is exclusively responsible for promoting flowering through NI lighting, while PHYB plays a crucial role in detecting light quality during end-of-day light treatments, night breaks, and day extensions. Notably, PHYB functions differently and is subsequent to PHYA in controlling flower induction [74]. The subsequent role of the two photoreceptors was partly supported by a recent study on chrysanthemum, where plant flowering was not inhibited under prolonged photoperiod lighting with blue LEDs, despite increased expression of both PHYA and PHYB [16].

Besides PHYA and PHYB, other PHYs (PHYC/D/E) also play roles in plant flowering. PHYC plays distinct roles in the regulation of flowering time in different plant species [75]. In rice and *Arabidopsis*, PHYC appears to function as a flowering repressor under non-inductive photoperiods [76,77]. However, in wheat (*Triticum aestivum*), PHYC promotes flowering under inductive photoperiods [75]. Like PHYB, both PHYD and PHYE inhibit photoperiodic flowering, but they play redundant roles with PHYB. The *phyD* or *phyE* mutant shows no changes in flowering time, unless in a *phyB* mutant background where flowering is earlier in double mutants [72]. PHYD, PHYE, and PHYB are also redundantly involved in mediating flowering as a shade avoidance response (SAR).

PHY seems to play a less important role in flowering's response to BL compared to red light or white light, where an interaction between PHYs and CRYs is necessary. Our study on *Arabidopsis* indicated that a quintuple phytochrome mutant (*phyA phyB phyC phyD phyE*) did not change the flowering time under low-PPS BL (blue LED or 94% B + 6% R + FR LED), but it flowered earlier under high-PPS BL (94%B + 6% R LED) compared with wild type plants [78]. This suggests that PHY is not indispensable for BL-mediated flowering but contributes to the flowering response to BL under high-PPS background light conditions. However, under blue-containing light, such as white light, the interaction of PHYB and CRY2 is necessary to control fundamental processes (e.g., flowering time and circadian rhythm) in *Arabidopsis*, where the regulation of floral induction is mediated by the antagonistic actions of CRY2 and PHYB [53,63,79].

2.1.3. ZEITLUPE (ZTL) Family Members

Another group of BL photoreceptors is ZTL family proteins [80,81]. ZTL family proteins are activated by illumination with BL; they undergo structural changes upon BL exposure that modulate protein activity [80,82,83]. ZTL family proteins transduce light signals primarily by altering the activity of the SCF E3 ligase complex [61,83]. ZTL family proteins did not show dark recovery as PHOT did in early studies [80], but later studies indicated that they did return to the dark state, despite slow adduct decay (occurring in the order of hours to days) [84,85].

The ZTL family comprises three proteins: ZTL protein, FLAVIN-BINDING, KELCHREPEAT, F-BOX (FKF1) protein, and LOV KELCH PROTEIN2 (LKP2) [81–83,86]. ZTL family proteins have an important role in the photoperiodic control of floral transition [81,82]. Despite the partly overlapping roles of these proteins, generally, ZTL exerts control over circadian rhythms, and FKF1 controls the transition to flowering, while LKP2 is required for both processes [83].

(1) ZTL

ZTL is a negative regulator of flowering, but it plays a predominant role in the control of the circadian clock, which can affect photoperiodic flowering [82]. ZTL itself is positioned in interconnected clocks in plants [61]. Also, ZTL plays some roles in the clock input of light by mediating the components of the circadian clock [87]. Furthermore, ZTL interacts with the clock component in a BL-enhanced manner, contributing to ZTL

protein stabilization and accumulation by the end of the light period [82]. Additionally, ZTL photocycle kinetics are crucial in determining the circadian period length [82]. ZTL can sense BL fluence to mediate circadian timing [84]. ZTL mutants exhibit a fluence-dependent effect on the circadian period, resulting in a maximal circadian period of 36 h under low-light conditions (0.6–8 μmol m^{-2} s^{-1}). Above 8 μmol m^{-2} s^{-1}, the circadian period collapses to near wild type (28 h), indicating that ZTL circadian function may be limited to low-light conditions [84]. ZTL's role in light intensity recognition suggests it is important in resetting the plant clock and contributes to the clock's acceleration with increased light fluence [82]. ZTL also functions in temperature compensation of the circadian clock due to its involvement in warm-temperature responses [88]. Intriguingly, ZTL and CRYs play opposite roles in thermo-responses; the mechanism and potential physiological significance of this remain to be explored [88]. Although ZTL is a major protein within the group for circadian clock regulation, the ZTL homologs, LKP2 and FKF1, also contribute to controlling the pace and robustness of the circadian clock [89].

(2) FLAVIN-BINDING, KELCHREPEAT, F-BOX (FKF1)

FKF1 acts as a positive regulator of flowering in a light-dependent manner, particularly in the afternoon [61,87,89]. FKF1 plays a role in detecting LD signals and activating the photoperiodic flowering pathway [86]. BL seems to have a predominant role in FKF1's function in flowering regulation [80]. Despite its transcripts oscillating with a circadian rhythm, FKF1 does not appear to have any intrinsic clock function but likely operates as part of the clock's output [80]. Also, FKF1 is required for CRY-interacting factors, such as CIB3, to promote flowering in response to BL [90]. In *Arabidopsis*, FKF1 is activated by BL and promotes flowering under inductive LD conditions [91]. In rice, FKF1 not only has a similar role in photoperiod-mediated flowering relative to *Arabidopsis* but also promotes flowering independent of photoperiod [91].

(3) LOV KELCH PROTEIN2 (LKP2)

The LKP2 mediates both the circadian clock and flowering. Like ZTL, the LKP2 also plays a role in the regulation of the circadian clock by mediating the clock's components [87]. The phenotypic parallelism observed in *ztl lkp2* double mutants compared to *ztl* mutants suggests that LKP2 functions in an intricate manner [87]. Also, LKP2, as well as ZTL, are involved in the suppression of flowering [92]. Although LKP2 does not function as a major regulator of the circadian clock and flowering time due to its low physiological expression, it binds the substrates of ZTL and FKF1 in vitro and partially contributes to the circadian clock and flowering [93]. Overexpression of LKP2 or ZTL, as well as deficiency of FKF1, result in late flowering in *Arabidopsis* under LD conditions [92].

2.1.4. Other Photoreceptors

(1) Phototropins (PHOTs)

PHOTs act as BL photoreceptors, but they can also sense UVA light and temperature signals [81,83]. PHOTs are known for their central role in plant phototropism, but they can also indirectly contribute to plant flowering [94–96].

In the dark, PHOTs lack activity until the absorption of BL [83]. Multiple phosphorylation leads to dimerization and activation of PHOTs [83,94,97]. As a result, the activated PHOTs transmit this signal to downstream components within the signaling pathway [94]. However, in the dark, the photoreceptor reverts to the inactive state within several tens or hundreds of seconds [83].

Higher plants, including *Arabidopsis*, possess two isoforms of PHOTs: PHOT1 and PHOT2 [86,97]. BL triggers both PHOTs, but in different manners. It stimulates PHOT2 and downregulates PHOT1 [81]. For example, in *Arabidopsis* plants exposed to 3 h of lighting at

40 μmol m^{-2} s^{-1} after 16 h of dark adaption, both blue and red light downregulated PHOT1 transcript abundance but upregulated the PHOT2 level compared to the dark treatment [98]. Compared to red light, BL upregulated PHOT1, but it did not affect PHOT2 [98]. The PHOT1 is photostable, but PHOT2 is photolabile [83,97]. PHOT1 can be activated under much lower BL intensity than PHOT2 [80,97]. For example, under a BL of 10 μmol m^{-2} s^{-1}, over 85% of PHOT1 is activated, but only 40% of PHOT2 is activated [97]. Also, the dark reversion of PHOT2 is about 10 times faster than that of PHOT1 [80].

Limited information is available about the role of PHOT1 and PHOT2 in flowering mediated by BL. Our recent study on *phot* mutants in *Arabidopsis* has indicated that both PHOT1 and PHOT2 are partly involved in the promotion of plant flowering mediated by BL in association with low PHY activity [96]. However, it is still unclear whether the PHOTs directly or indirectly contribute to this process.

(2) Halotolerance protein (HAL3)

In rice, Sun et al. [99] found that OsHAL3, a highly conserved Flavin mononucleotide (FMN)-binding protein, serves as a new BL sensor. OsHAL3 is structurally inactivated by light, especially BL, through photo-oxidation and direct interaction with photons. Also, OsHAL3 has been identified as a positive regulator of flowering in rice; OsHAL3 overexpression lines exhibited an early flowering phenotype, whereas downregulation of OsHAL3 expression through RNA interference delayed flowering under an inductive photoperiod (i.e., SD conditions) [100]. OsHAL3 directly binds to the promoter of *Hd3a* and forms a complex with Hd1 to positively regulate flowering under SD conditions, especially at around 4 h before light onset, but the interaction is inhibited by blue or white light [100,101].

2.2. Photosynthetic Pigments

Despite not being protein-based receptors, photosynthetic pigments can indeed act as an additional group of receptors [25,102]. The photosynthetic pigments are essential for capturing and transferring light energy during photosynthesis [102]. Also, these molecules can respond to light signals and exert effects on plant physiology, including flowering [25]. The photosynthetic pigments mainly absorb photosynthetically active radiation (400–700 nm), although they can also absorb UVA with very low quantum efficiency due to the flavonoid shield [63]. Among PAR wavelengths, BL results in greater energy loss during the light reaction in photosynthesis than red or green light due to a higher frequency or energy [63]. Photosynthetic pigments may sense changes in BL quantity to affect photosynthesis and thus the availability of assimilates [21]. The photosynthetic pigments include the various chlorophylls and carotenoids [63].

2.2.1. Chlorophylls (Chls)

The Chls are essential pigments required by all photosynthetic organisms to absorb light energy, and they play a key role in acclimation to environments with a varied light spectrum. Terrestrial plants only possess Chl a and Chl b. Chl a is the most abundant form of Chl in terrestrial plants, and Chl a has the highest absorption peak at 665 nm (red light) and is the main collector of light energy transferred to the photosynthetic reaction centers [63,103]. Chl b, with the highest absorption peak at 450 nm (BL), is only found in the antennae of the light-harvesting complexes [103]. Chl b has a critical role in harvesting light at lower light intensities as well as photoprotection [104]. A high Chl a/b ratio indicates greater acclimation to high light intensities and an enhancement in photosynthetic electron transport, whereas a low Chl a/b ratio indicates shade tolerance [103]. In many species, monochromatic BL causes a decrease in chlorophyll content and an increase in the Chl a/b ratio compared to those under multispectral light, despite a positive role of BL in combination with another wavelength (e.g., red light) [63].

There is no direct evidence of a relationship between chlorophyll accumulation and flowering time; however, studies on plants with altered chlorophyll metabolism showed that flowering time is changed compared to wild type plants [105]. In Chl b-less mutants, besides the imbalances in photosynthesis and growth, plants show a delay in the onset of flowering [104]. The complex pathways involved in regulating chlorophyll biosynthesis and breakdown may interact with the pathways regulating flowering [105]. However, as chlorophyll contents affect sugar biosynthesis [106], additional research will be required to disentangle the effects of chlorophyll and sugars in the regulation of the floral transition.

2.2.2. Carotenoids

Carotenoids are principally thought to protect chlorophylls by quenching their triplet state via the transformation of excitation energy into heat [103]. Carotenoids absorb light strongly in the range of 480–580 nm, where chlorophylls have low absorption [25]. BL stimulates the accumulation of carotenoids in leaves when compared to red light, especially at higher irradiances (>200 μmol m^{-2} s^{-1}), thus contributing to the leaf's photoprotective capacity [63]. Carotenoids are less abundant than chlorophylls, with a carotenoid to chlorophyll ratio usually ranging from 0.1 to 0.5, depending on the species and environmental conditions [63,107].

Despite there being no direct relationship between carotenoid accumulation and plant flowering, Fibrillins (FIB/FBN/FIN), carotenoid-associated proteins, play a vital role in environmental-stress-induced flowering. It has been found that overexpression of pepper (*Capsicum annuum*) FIB in tobacco (*Nicotiana tabacum*) accelerated flowering when grown under high light [103].

2.3. Integration of Multiple Photoreceptors and Photosynthetic Pigments

There is a complex network of interactions between different photoreceptors, as well as between photoreceptors and photosynthetic pigments. For example, within different photoreceptors, CRY1 and PHYB appear to be the main photoreceptors involved in the regulation of *PHOT1* transcript accumulation, and the expression of *PHOT2* is dependent on both CRYs and PHYA [98]. The interactions between photosynthetic pigments and photoreceptors are implied by significant overlapping of their absorption spectra [94]. Also, the interactions can be attributed to the fact that photosynthesis mediated by photosynthetic pigments requires coordinated regulation of the nuclear and plastidic genomes [81]. On one hand, a variety of intermediates from chloroplastic metabolic pathways, such as carbohydrates and reactive oxygen species, have been identified as signals emitted by the chloroplast to deliver information to the nucleus to affect photoreceptor action [108]. On the other hand, the expression of numerous nuclear genes involved in plastid transcription and photosynthesis is controlled by CRYs in response to BL [24].

The final expressions of different photoreceptors and the accumulation of photosynthetic pigments under BL are the results of their interactions. For *Arabidopsis* grown under sole-source lighting at a PPFD of 120 μmol m^{-2} s^{-1} and a photoperiod of 16 h, plants had earlier flowering under blue LED than white LED and white fluorescent light [109]. In this case, blue LED significantly reduced *PHYA*, *PHYD*, and *CRY1* mRNA levels and slightly decreased *PHYB*, *PHYE*, and *PHOT1* mRNA levels but did not change the mRNA levels of *PHYC*, *CRY2*, and *PHOT2* compared with the white fluorescent light. Blue LED did not affect mRNA levels of *PHYD*, *CRY2*, and *PHOT2* but reduced those of other photoreceptors compared with white LED. The reduction of photoreceptor gene expression manifests the reduced sensitivity of light-sensing molecules and their regulatory properties toward BL [110]. Also, plants under blue LED and white LED had similar content of the main

photosynthetic pigments per dry weight unit, but they had lower content than those under white fluorescent light [109].

Despite interaction between multi-photoreceptors, it is possible that the contribution of different photoreceptors to BL-mediated flowering varies with plant species. For three SD plants, chrysanthemum, perilla (*Perilla frutescens*), and kalanchoe (*Kalanchoe blossfeldiana*), NI lighting with BL did not inhibit flowering in chrysanthemum, but it did in perilla, and BL had a secondary effect on the control of flowering of kalanchoe while red light played the main role [8,111,112]. Possibly, two light-regulating systems through PHY and CRY function at the same time in perilla, but only one system (PHY) functions in chrysanthemum, and a greater role was played by PHY than CRY in kalanchoe [112]. In *Phalaenopsis* orchids (*Phalaenopsis* spp.), whether spiking is improved by daytime supplemental lighting depends on the relative amount of active PHY [113].

Additionally, the contribution of different photoreceptors to BL-mediated flowering varies with other light wavelength(s) co-acted with BL. This is supported by the impact of shifts in the spectral quality of light on gene expression in chrysanthemums by NI lighting with blue and other LEDs [114]. The NI lighting sequentially with FR and blue LED promoted flowering associated with higher expression of flowering inducer genes *PHYA* and *CRY1*. However, NI lighting sequentially with blue and red light failed to induce flowering due to higher expression of *PHYB* and *ANTI-FLORIGENIC FT/TFL1 FAMILY PROTEIN (AFT)*, despite high expression of *CRY1* and *FLOWERING LOCUS T-LIKE (FTL)*. It appears that the co-action of BL with different light wavelengths can change the balance of both photoreceptors and floral integrator proteins, where the FTL and AFT positively and negatively regulate flowering, respectively.

3. Floral Integrator Proteins

Floral integrators are specifically a group of genes that act as "decision-makers" for flowering because they function as "hubs" in the flowering network by integrating environmental and intrinsic signals that are sensed by different upstream pathways [115]. These floral integrators can be roughly grouped into two types in terms of their function in floral induction: positive floral integrators (the proteins they encode act as floral activators) and negative floral integrators (the proteins they encode act as floral inhibitors) (Figure 2).

Floral integrators	Role in Flowering	Blue Light Effect
FT	✿	⊕⊖
SOC1	✿	⊕⊖
AGL24	✿	?
SPL	✿	?
FUL	✿	?
LFY	✿	?
TFL1	🍃	⊕⊖
FLC	🍃	?
SVP	🍃	?
TEM1	🍃	?
FLM	🍃	?

✿ promote flowering 🍃 repress flowering
⊕ positive blue light effect ⊖ negative blue light effect ? unclear blue light effect

Figure 2. An illustration of the characterization of floral integrator proteins in terms of their role in flowering and their response to blue light. FT = FLOWERING LOCUS T; SOC1 = SUPPRESSOR OF OVEREXPRESSION OF CONSTANS 1; AGL24 = AGAMOUS-LIKE 24; SPL = SQUAMOSA PROMOTER BINDING-LIKE; FUL = FRUITFULL; LFY = LEAFY; TFL1 = TERMINAL FLOWER 1; FLC = FLOWERING LOCUS C; SVP = SHORT VEGETATIVE PHASE; TEM1 = TEM-PRANILLO1; and FLM = FLOWERING LOCUS M. If both positive and negative effects of blue light are shown together, this indicates the blue light effect may vary with plant genotype and the application of blue light.

3.1. Floral Activators

The major floral activators in *Arabidopsis* include FLOWERING LOCUS T (FT), SUPPRESSOR OF OVEREXPRESSION OF CONSTANS 1 (SOC1)/AGAMOUS-LIKE 20 (AGL20), AGAMOUS-LIKE 24 (AGL24), SQUAMOSA PROMOTER BINDING-LIKE (SPL), FRUITFULL (FUL)/AGL8, LEAFY (LFY), and other relevant regulators [115,116]. FT exerts a positive influence on SOC1, with this FT-to-SOC1 module occupying a central role in plant flowering, exhibiting evolutionary conservation across diverse plant species [117]. In *Arabidopsis*, FT emerges as a direct downstream target of both CONSTANS (CO) within the photoperiod pathway and FLOWERING LOCUS C (FLC) in the vernalization/autonomous pathway [115]. SOC1, on the other hand, is under the direct sway of SPL in the aging pathway, alongside FLC and DELLA proteins within the gibberellin (GA) pathway [117]. Therefore, FT and SOC1 are the two key components among the major floral activators.

3.1.1. FLOWERING LOCUS T (FT)

FT is the earliest identified florigen, a floral activator, in *Arabidopsis* [116]. Florigen is ubiquitous in flowering plants, but the number and name of FT homologs vary with plant species [118], and all *FT* homologous genes within each species do not play an equally important role in flowering regulation [119]. For example, specific major FT homologs regulating flowering in other crops include HEADING DATE 3a (Hd3a) and RICE FLOWERING LOCUS T 1 (RFT1) in rice, ZEA MAYS CENTRORADIALIS 8 (ZCN8) in maize, GLYMA.16G150700 (GmFT2a) and GLYMA.16G044100 (GmFT5a) in soybean, SINGLE-FLOWER TRUSS (SFT) in tomato, and FLOWERING LOCUS T-LIKE 3 (FTL3) in chrysanthemum [118,120,121]. In rice, Hd3a and RFT1 are essential for promoting rice flowering under SD conditions, while RFT1 functions as a floral activator under LD conditions [119].

In *Arabidopsis*, FT is produced in the vascular leaf bundle and transferred via the phloem to the shoot apical meristem (SAM) to induce the floral transition [118]. In the SAM cells, FT binds to a 14-3-3 protein in the cytoplasm, enters the nucleus, and interacts with FLOWERING LOCUS D (FD), creating a florigen activation complex (FAC) [118,122,123]. The FAC then induces the expression of floral meristem identity genes, such as *APETALA 1 (AP1)*, *SOC1*, and *FUL*, leading to floral induction [26]. In rice, similarly to *Arabidopsis* FT, both Hd3a and RFT1 are expressed in the vascular tissue of leaves and move to the SAM, where they enhance the expression of floral meristem identity genes, such as *OsMADS14* and *OsMADS15*, and trigger flowering [119,124,125].

BL's effect on *FT* gene expression varies with plant species, lighting source, lighting duration, and time of the day, which is associated with varying flowering responses to BL. In *Arabidopsis* under BL, CRY2 binds with CIB proteins, which directly bind to the promoter of *FT* and promote its transcription [54,126]. In day-neutral-type strawberries (*Fragaria* × *ananassa*), FvFT1 was induced by blue LED light and exclusively expressed in the veins of older leaves [127], which may partly explain the promotional effects of blue LED light on the number of flower clusters and final strawberry yield [128]. In sweet pepper (*Capsicum annuum*), sole-source daytime lighting with blue LED light induced the expression of CaFT1 and CaFT2 and caused earlier flowering compared with white light [129]. In rice, NI lighting with impure BL suppressed Hd3a expression through activating PHYB and delayed flowering [130]; however, blue LED light in the morning induced Hd3a expression to promote flowering by activating Ehd1 expression [131]. In petunia, PehFT expression was higher on the first day but lower on the seventh day under blue vs. red LED light, suggesting that it may not be the major contributor to BL-promoted flowering in this species [132].

3.1.2. SUPPRESSOR OF OVEREXPRESSION OF CONSTANS 1 (SOC1)

SOC1 plays regulatory roles in integrating multiple flowering signals for floral transition and reproductive development in *Arabidopsis* [133]. SOC1 interacts with AGL24 to promote the differentiation of primordia into floral meristems via upregulating LFY [134]. SOC1 expression is directly regulated by FT positively and by FLC negatively [115,134]. The role of SOC1 in floral induction has also been found in other species, such as cotton (*Gossypium hirsutum*) [133]. Also, the *Brassica rapa* genome possesses three *SOC1* genes, and *BrSOC1-1* and *BrSOC1-2* function redundantly in flowering time regulation [115].

The BL effects on SOC1 and other floral integrator proteins vary with plant species, cultivars, and reference light. Prolonged photoperiod lighting with BL promoted flowering through the induction of FT and SOC1 expression in *Arabidopsis* but not in another LD plant, *Gypsophila paniculata*, where both GpFTs and GpSOC1 expressions were low with BL induction [14]. In *Gypsophila paniculata*, two cultivars showed different expressions of GpFT and GpSOC1, which was associated with their contrasting flowering responses to blue light [11]. In petunia, *FLORAL BINDING PROTEIN 28 (FBP28)*, a SOC1-like gene, not only had a role in transmitting the BL signal from the FT protein to induce floral bud formation but also increased expression under blue LED light compared with red LED light [13]. In LD plant lisianthus (*Eustoma grandiflorum*) under SD conditions, overnight lighting with low-intensity blue LEDs promoted flowering compared to no lighting, and this is associated with increased expression of *EgFTL* and *EgSOC1L* [135]. However, later and lower expression of these genes was induced by blue LED compared to FR LED, suggesting weaker promotion of flowering by BL than FR light in lisianthus.

3.1.3. Other Floral Activators

Despite the existence of some other floral activators, limited information is available about their response to BL. In *Arabidopsis*, the expression of an *SPL* gene, *AtSPL8*, is positively regulated by CRYs [136]. However, whether blue LED lighting affects its expression associated with the flowering response is unknown.

3.2. Floral Inhibitors

The major floral inhibitors in *Arabidopsis* include TERMINAL FLOWER 1 (TFL1), FLOWERING LOCUS C (FLC), SHORT VEGETATIVE PHASE (SVP), TEMPRANILLO1 (TEM1), and FLOWERING LOCUS M (FLM) [120,137–139]. These negative regulators act antagonistically to positive regulators by controlling parallel signaling pathways [26]. For example, FLC acts with its partner SVP to repress transcription of the flowering-promoting genes *FT*, *FD*, and *SOC1* [115]. TEM1 acts within the leaf to repress FT, while FLC works both within the leaf and in the SAM, acting on different targets [26]. SVP delays the floral transition by regulating *SOC1*, *FT*, and *FLC* genes [139]. FLM interacts with SVP and forms a complex to prevent flowering [120]. Among these floral inhibitors, information about their involvement in BL-mediated flowering response is available for only TFL1 so far.

TFL1 is a closely related FT homolog, and it has been identified as an anti-florigen, a floral inhibitor, in *Arabidopsis* [118]. From other crops, the identified anti-florigens include ANTI-FLORIGENIC FT/TFL1 FAMILY PROTEIN (AFT) in chrysanthemum, RICE CENTRORADIALIS (RCN) in rice, and SELF PRUNING (SP) in tomatoes [26,118,120,121,140].

The BL effect on TFL1 may vary with plant species, even from the same photoperiod response group. In SD plant chrysanthemum, AFT (CsAFT) is induced by the coincidence of PHY signals (i.e., activated PHYB) with the photosensitive phase set by the dusk signal under non-flowering-inductive conditions (e.g., NI lighting with red light and LD conditions) [141]. Plant flowering occurred only when night length exceeded the photosensitive phase for CsAFT induction. This may partly explain why prolonged photoperiod lighting

with blue LEDs did not prevent flowering in this species [15–18], as PHYB cannot be activated by blue LEDs to induce AFT. Differing from chrysanthemum, in SD-type strawberry, end-of-day (EOD) lighting with BL or FR light could induce greater expression of FvTFL1, the repressor of floral induction [142].

3.3. Co-Action of Floral Integrator Proteins

In *Arabidopsis*, FT and TFL1 function oppositely and play antagonistic roles in the determination of flowering time [120,143]. TFL1 forms a complex with FD and acts to repress flowering by modulating FD-dependent transcriptional regulation [120,143]. In rice, RCN (a TFL1 homolog) inhibits flowering by competing with Hd3a (a FT homolog) for 14-3-3 binding to form a florigen repression complex (FRC), and the balance between FRC and the florigen activation complex (FAC) regulates the development of the SAM [118,144]. Similarly, other FT/TFL1-like proteins, such as SFT/SP in tomatoes and FTL3/AFT in chrysanthemum, act as activators/repressors of flowering and determine the timing of flowering in coordination [120,121,145].

BL can affect the balance of floral integrator proteins as well as other flowering regulators. In strawberries, associated with promoted flowering by blue LED light in LD conditions, the expression of an LD-specific floral activator FaFT1 was stimulated, while that of a flowering suppressor FaTFL1 was inhibited, resetting the balance of expression between these two opposite flowering regulators [146]. In kalanchoe, supplementing white LEDs with low-intensity blue LEDs at the end of the day increased flower bud formation under both SD and LD conditions [147]. This was associated with higher expression of the flowering promoter genes (*KfPHYA*, *KfCRY1*, *KfFT*, and *KfFPF-1*) and lower expression of the flowering suppressor gene (*KfPHYB*).

The BL application method, photoperiod, and leaf age can affect flowering by modulating both positive and negative floral integrator proteins (as well as other flowering regulators) in chrysanthemums. For example, when two light wavelengths were sequentially applied, the NI lighting treatments ended with BL (NI-RB and NI-WB) induced flowering, but those that ended with red or white light (NI-BR and NI-BW) did not [114]. For the latter treatments, despite high levels of *CRY1* and *FTL* gene expression, there was also greater expression of flowering inhibitor genes, like *PHYB* and *AFT*, suggesting that the balance of overall expression patterns of the above genes affects the flowering response [110]. Also, chrysanthemum flowering was promoted by exposure to low-intensity blue LEDs as either 4 h EOD SL or NI under SD conditions but only as 4 h EOD SL under LD conditions [148]. The flowering-promotion treatments were associated with greater gene expression of the florigen gene *CmFTL3*, floral meristem identity genes *APETALA1 (CDM111)*, *FRUITFULL (CmAFL1)*, and *LEAFY (CmFL)*, and two photoreceptor genes, *CmPHYA* and *CmCRY1*, but lower expression of anti-florigenic gene *CmAFT* and the photoreceptor gene *CmPHYB*. Additionally, the youngest leaf showed greater sensitivity to BL, influencing gene expression more effectively than other parts [148].

4. Signal Transduction Pathways

Light, as one of the environmental cues, regulates flowering through quality, quantity, and duration. From light receptors to floral integrator proteins, there are at least three signal transduction pathways for flowering mediated by light (including BL): the photoperiod pathway, the light quality pathway (or shade pathway), and the light quantity pathway (or photosynthesis pathway) [21]. For some species, the BL seems to promote flowering as a strong stimulus or signal over the critical day length [149], which implies that BL can affect plant flowering initiation in more than the photoperiod pathway, at least for these species. Intensive molecular genetic and genomic studies in *Arabidopsis* have provided

significant insights to distinguish the three pathways for flowering regulation, despite many cross-talks between these pathways, as well [21].

4.1. Photoperiod Pathway

The photoperiod pathway controls flowering in response to day length and especially night length [5]. In this pathway, photoreceptors entrain and interact with the circadian clock to activate clock-associated genes at different times of the day, enabling plants to measure photoperiod length [21,137,150]. In turn, the circadian clock regulates the rhythmic expression of downstream flowering genes, such as *GIGANTEA (GI)*, *CO*, and *FT* [5,21,137] (Figure 3).

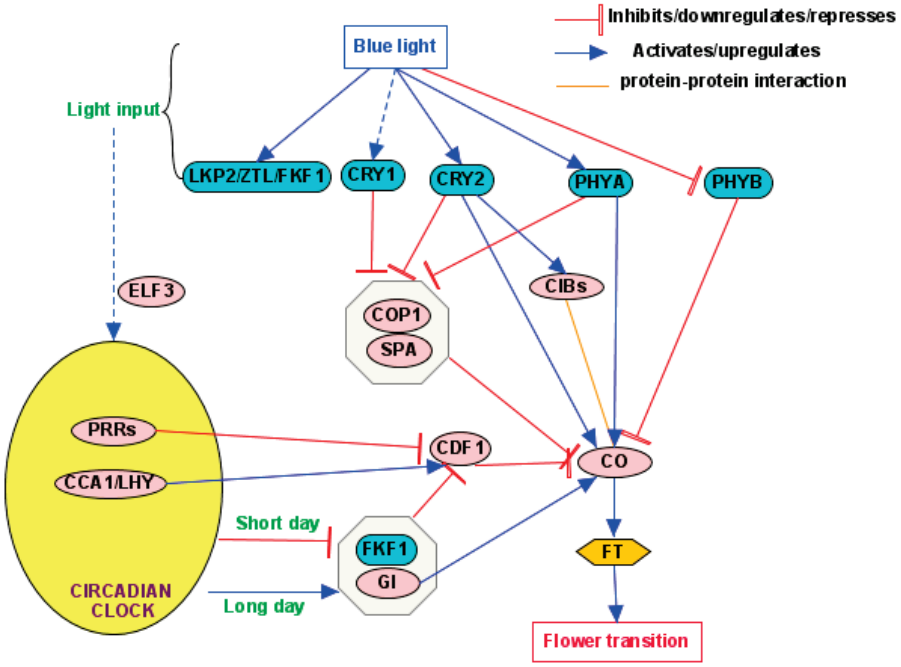


Figure 3. A simplified diagram of the photoperiod pathway in blue-light-mediated floral transition in *Arabidopsis thaliana*. FT = FLOWERING LOCUS T, a florigen; CO = CONSTANS, a central transcription factor in photoperiod pathway. The involved main blue light photoreceptors include CRY1/2 = cryptochrome 1/2; PHYA/B = phytochrome A/B; ZTL = ZEITLUPE, FKF1 = FLAVIN-BINDING, KELCHREPEAT, F-BOX1; and LKP2 = LOV KELCH PROTEIN2. The involved key circadian clock components include GI = GIGANTEA, an important clock output member; ELF3 = EARLY FLOWERING 3, an important clock input member; PRRs = PSUEDO RESPONSE REGULATORs, core clock components; and CCA1/LHY = CIRCADIAN CLOCK ASSOCIATED 1/LATE ELONGATED HYPOCOTYL, two core clock components. Other involved key transcription factors include CDF1 = CYCLING DOF FACTOR1; CIBs = CRYPTOCHROME-INTERACTING basic helix–loop–helixes; and COP1/SPA = CONSTITUTIVE PHOTOMORPHOGENIC1/SUPPRESSOR OF PHYA-105. Each gray hexagon with two transcription factors inside indicates a protein complex. Under long day conditions, GI and FKF1 form a complex, leading to the degradation of CDF and thus an increase in CO transcript abundance; however, under short day conditions, the expression of GI precedes that of FKF1, which disrupts the formation of the GI–FKF1 complex and thus reduces the abundance of CO [151]. The dashed lines indicate that the action can be affected by many factors or the involved detailed action mechanism is still unclear. To be clear, only the key pathway components are presented in the diagram, and information about other pathway components can be found in the manuscript's text. Also, the regulations at the transcriptional and translational levels are not distinguished in the figure for simplification, and the relevant information can be found in the text.

In the photoperiodic flowering pathway, both PHYs and CRYs act as main photoreceptors, with ZTL and FKF1 acting as accessory photoreceptors contributing to clock

entrainment and signal integration [21,150]. Specifically, in the photoperiodic pathway of BL-mediated flowering, CRY1 and CRY2 are the primary photoreceptors, supported by FKF1 and ZTL [5]. PHYA and PHYB also participate in BL signaling and are known to directly and physically interact with CRYs [95]. In *Arabidopsis*, photoperiodic flowering is primarily regulated by the expression of FT, which acts as a florigen [21]. The detailed pathway from photoreceptors to FT may vary with plant species. Taking the PHYs' pathway as an example, the regulation of photoperiodic flowering in soybeans acts through PHYA-LUXE1-FT and is different from the PHYB-CO-FT flowering pathway in many nonlegume plants [150,152]. Also, normally, there is more than one pathway from a certain photoreceptor to FT. In *Arabidopsis*, CRY-mediated photoperiodic flowering follows at least three main pathways [35]. (1) Entrainment of the circadian clock by CRY1 and CRY2 and modulation of CO expression [153]. (2) CO protein stabilization by CRY1 and CRY2 (while CRY2 plays a primary role) under LD conditions [35]. (3) Activation of CIB transcription factors by CRY2 to promote FT expression [126,154,155]. Among the numerous components in the photoperiodic flowering pathway, CO is a central regulator of FT expression in *Arabidopsis* [156]. Normally, CO has a positive role in flowering induction in LD; CO binds directly to the *FT* promoter, upregulating FT expression [156,157]. In *Arabidopsis*, CO is regulated by the integrated signals from the circadian clock, day length, and light quality [115,157]. Due to the mediation of the circadian clock, the CO transcription level varies daily, with a minimum in the morning and a maximum in the evening under LD conditions [115]. Meanwhile, CO protein is stabilized in LD conditions but degraded in SD conditions [156]. Under LD conditions, CO protein accumulation coincides with increased CO transcripts in the afternoon to promote FT activation and floral transition [115]. Additionally, CO protein accumulation is regulated by light quality through photoreceptors [115]. In the dark, CO is degraded due to the COP1/SPA1 complex [26]. In the morning to noon, CO is degraded by CYCLING DOF FACTORS (CDFs) in a PHYB-dependent manner due to the greater red light percentage, while in the afternoon to evening, CO is gradually stabilized by the photoreceptors PHYA, FKF1, and CRY2 due to the gradually increased percentage of blue and FR light [26,60,119,158].

It is well-established that CDFs are key factors in the photoperiod pathway in *Arabidopsis* by controlling expression patterns of key flowering regulators, such as CO and FT [159]. In *Arabidopsis*, the CDFs can repress CO and FT expression redundantly and delay the flowering time [160]. In particular, CDF1 negatively regulates CO in the morning by interacting with the TOPLESS (TPL) co-repressor [137,161]. CDF protein stability is reduced in LD afternoon due to the degradation by a GI–FKF1 protein complex [159]. Furthermore, the gene expression level of *CDF1* is regulated sequentially from morning to evening by the circadian clock's core components [160].

The GI serves as a key mediator between the circadian clock and the master flowering regulators (CO and FT) in the photoperiod pathway. GI is a gating factor in the output pathway of the circadian clock [162]. Also, GI promotes flowering by increasing the expression of CO and thus FT [163]. Under LD conditions, GI and FKF1 form a complex, leading to the degradation of CDF and thus the increase in CO transcript abundance; however, under SD conditions, the expression of GI precedes that of FKF1, which disrupts the formation of the GI–FKF1 complex and thus reduces the abundance of CO [151]. In addition to the CO-dependent regulation of FT, GI can independently regulate FT [164,165].

In addition to GI, the core circadian clock components also mediate daily variations of CO levels. Upon sensing the light of dawn, the core clock components CIRCADIAN CLOCK ASSOCIATED 1 (CCA1) and LATE ELONGATED HYPOCOTYL (LHY) activate the CDF to repress CO transcription [115]. During the afternoon and evening, CDF expression is repressed by the clock component PSUEDO RESPONSE REGULATORs (PRRs) [115].

Also, the PRR proteins directly stabilize CO proteins; PRR9 contributes to CO accumulation in the morning, whereas PRR5, PRR7, and TOC1 (PPR1) function in the evening [156,166]. Additionally, PRRs and FKF1 can form a protein complex and repress the transcription of CDFs to stabilize CO proteins [156,167].

As a key component of the input pathway of the circadian clock, EARLY FLOWERING 3 (ELF3) shows sensitivity to photoperiod changes and is regulated by the circadian clock while mediating flowering by affecting GI and CO levels [168–170]. Increasing day length increases the nuclear accumulation of ELF3, but increased darkness causes the degradation of ELF3 to an undetectable level [170]. In *Arabidopsis*, the *ELF3* genes are highly expressed during the evening time and downregulated in the early morning [168]. ELF3 promotes the degradation of GI through COP1, thus repressing flowering [171]. ELF3 and CO interact by preventing CO from building up in the late afternoon and early evening and causing late flowering in plants [168]. So, the opposing expression and regulation of ELF3 and CO work together to create a finely tuned regulatory loop, allowing for optimal flowering time [168].

Several signaling hub components convey BL signals from photoreactors to downstream components. CONSTITUTIVE PHOTOMORPHOGENIC1/SUPPRESSOR OF PHYA-105 (COP1/SPA) acts as a key repressor of light signaling downstream of photoreceptors [95]. COP1/SPA is active primarily in darkness [172], but, upon BL perception, photoreceptors (such as CRYs) directly interact with the COP1/SPA complex to suppress its activity [95]. A pivotal function of COP1/SPA in the regulation of flowering time by photoperiod involves the transcription factor CO [172]. In darkness, CO is degraded via COP1/SPA, which causes a delay in *Arabidopsis* flowering under non-inductive SD conditions and therefore allows for the adjustment of flowering time to seasons [172]. COP1 also suppresses flowering by promoting the degradation of GI, a circadian-clock-associated protein, in an ELF3-dependent manner, and it functions as an integrator of photoperiod and circadian signals [153]. In addition to COP1, the other two transcription factors, PIFs and HY5, can also convey BL signaling perceived by photoreceptors to regulate the circadian clock or directly to mediate floral integrator genes to affect flowering. Detailed information can be found in Sections 4.2 and 5.3.

Despite the above general pathway, the specific involvement of the pathway components may be different depending on the methods of applying BL to plants. For example, at the end of the day, in response to BL, CRY2 interacts with SPA and suppresses COP1 activity, which decreases CO degradation and promotes FT expression [5]. When sensing BL under LD conditions in *Arabidopsis*, FKF1 interacts with GI, and the resulting FKF1–GI complex mediates BL-dependent degradation of CDF proteins that repress the transcription of *CO* and *FT* genes [5,173]. FKF1 also interacts physically with CO in a BL-dependent manner, and the FKF1-CO complex increases CO stability in LD conditions [174]. When BL is applied at the beginning of the day, PHYA may play a role in the plant's responses. PHYA has been identified as a sensitive detector of both dawn and short photoperiods [175]. PHYA protein accumulates during the night, especially in short photoperiods; at dawn, PHYA activation by light results in a burst of gene expression, with consequences for physiological processes [175].

4.2. Light Quality/Shade Pathway

Flowering is accelerated, besides increased elongation growth, for plants growing under shade conditions, which is normally indicated by altered light quality, such as decreased R/FR ratios and lower BL levels [21,176]. This light-quality-regulated flowering response is actually a shade-avoidance response (SAR), which has a pathway independent of photoperiodism [21]. In this case, the light quality pathway for flowering regulation can also be called the shade pathway.

For the shade pathway, CRY1 seems to be the most important photoreceptor involved in BL-mediated flowering, despite unignored contributions from PHYs (especially PHYB). PHYB is a major photoreceptor in the SARs induced by decreased R/FR ratios, but there is redundancy with PHYD and PHYE [21,177]. A characteristic of this pathway is that the early flowering phenotype in the absence of PHYB is temperature sensitive, and the sensitivity lies in a flowering-specific branch of the PHYB signaling pathway rather than other aspects of SARs [21]. In addition, PHYA is a positive regulator of shade-regulated flowering time [177], although PHYA can also inhibit SAS in deep shade conditions, where FR light is much enriched and dominant [178]. CRY1 is the primary photoreceptor controlling the low-BL-induced SAR in adult plants [35]. There is a synergistic interaction between PHY and CRY signals, and the presence of both of these signals has more severe effects than either of these alone [179]. Due to a low PPS value, continuous sole-source lighting with blue LED at low to modest intensity can induce low activity of both PHYB and CRY1 [38,78]. This might accelerate flowering as one of the SARs, regardless of the photoperiodism type of the plant species [7].

Like the photoperiod pathway, shade-pathway-regulated flowering in *Arabidopsis* also mainly acts through the regulation of the florigen, FT [21,132] (Figure 4). This was confirmed by studying the effect of shade on flowering acceleration in 1001 *Arabidopsis* accessions, revealing that natural variation within the FT locus is the primary cause of shade-induced flowering [26,180]. The photoreceptors act through FT, implying that the shade pathway is leaf-based, which is supported by the fact that FT expression was suppressed by PHYB expressed in mesophyll cells [181].

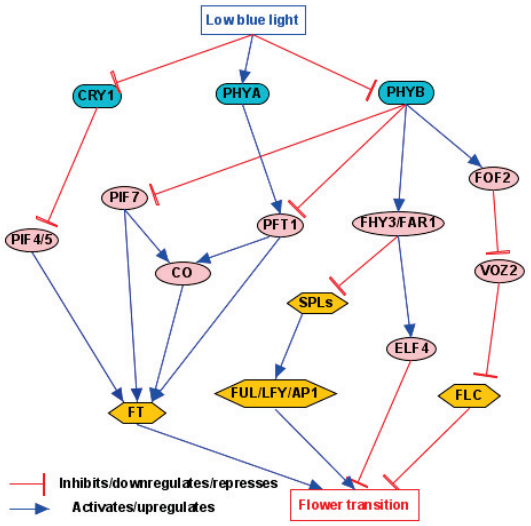


Figure 4. A simplified diagram of the light quality pathway (or shade pathway) in blue-light-mediated floral transition in *Arabidopsis thaliana*. The involved floral integrator proteins include FT = FLOWERING LOCUS T, a florigen; SPL = SQUAMOSA PROMOTER BINDING-LIKE; FUL/LFY/AP1 = FRUITFULL/LEAFY/APETALA1; and FLC = FLOWERING LOCUS C. The involved main blue light photoreceptors include CRY1 = cryptochrome 1; and PHY A/B = phytochrome A/B. The involved key transcription factors include PIF4/5/7 = PHYTOCHROME INTERACTING FACTOR4/5/7, an important group in the shade pathway; CO = CONSTANS, a central component in the photoperiod pathway; ELF4 = EARLY FLOWERING 4, an important clock component; PFT1 = PHYTOCHROME AND FLOWERING TIME 1; FHY3/FAR1 = HYPOCOTYL3/FAR-RED IMPAIRED RESPONSE1; FOF2 = F-box of Flowering 2; and VOZ2 = VASCULAR PLANT ONE-ZINC FINGER 2. To be clear, only the key pathway components are presented in the diagram, and information about other pathway components can be found in the manuscript's text. Also, the regulations at the transcriptional and translational levels are not distinguished in the figure for simplification, and the relevant information can be found in the text.

PIFs are very important components in the shade pathway, and, for flowering regulated by shade, the most common pathway is PHY/CRY-PIFs-FT. Shade causes the inactivation of PHYB and/or CRY1, leading to the accumulation of PIFs, and an increase in PIF abundance leads to the induction of FT and its close homolog TWIN SYSTER OF FT (TSF) [26,182]. Among the PIF members, PIF4, PIF5, and PIF7 play a predominant role in shade-induced flowering by directly upregulating FT/TSF while downregulating Pri-miR156E/F [182]. It is worthwhile to note that different PIFs are involved in the CRY- and PHY-mediated SAR [35], as PIF4/5 predominantly regulates the CRY-mediated SAR but PIF7 exerts the predominant effect on the PHY-mediated SAR [35,176]. There is an antagonistic relationship between the photoreceptors and PIFs. Taking the relationship between CRY1 and PIF4/5 as an example, when BL is abundant, CRY1 suppresses the action of PIF4/5 by directly binding to them; however, in low BL conditions under shade, this repression is lifted, and the PIFs are able to promote SARs [179].

In addition to PIFs, the CO is also partly involved in the flowering regulated by shade in the PHY-FT pathway. Shade-triggered flowering involves the promoted expression and protein stability of CO, which acts to induce the expression of FT and TSF [182]. CO together with PIF7 plays an additive role in the promotion of flowering under shade conditions; however, LONG HYPOCOTYL IN FAR-RED1 (HFR1), a negative regulator of SAR response, is involved in the interaction with and inactivation of CO and thus the suppression of flowering, balancing the action of PIF7 [156,177,183]. Additionally, PHYA likely affects flowering time by regulating the protein stability of CO, showing a function independent of PIF7 [177]. It has also been found that CO contributes to shade-induced FT activation synergistically with the ATP-dependent chromatin remodeling factor, PICKLE [26,184].

PHYTOCHROME AND FLOWERING TIME 1 (PFT1) is also involved in flowering regulation by shade in the PHYB-FT pathway [21]. PFT1 is essential for PHYB regulation of flowering time [185] and primarily regulates flowering downstream of PHYB in a photoperiod-independent pathway [158]. PFT1 is equally able to promote flowering by modulating both CO-dependent (PHYB-PFT1-CO-FT) and CO-independent (PHYB-PFT1-FT) pathways, supported by the role of PFT1 as an activator of CO transcription and also FT transcription in a CO-independent manner [186]. Although PFT1 also regulates floral transition downstream of PHYA [55], this may be an indirect effect of changes in the PHYB pathway due to interaction between PHYA and PHYB [185].

Besides the PHYB-FT pathway, another pathway, PHYB-SPLs-FUL/LFY/AP1, is also involved in flowering regulated by shade. For this pathway, FAR-RED ELONGATED HYPOCOTYL3 (FHY3) and FAR-RED IMPAIRED RESPONSE1 (FAR1) act downstream of PHYB/D/E and are positively regulated by these photoreceptors [182,187]. Meanwhile, FHY3 and FAR1 interact with SPL3/4/5, flowering-promoting TFs, and inhibit their binding to key flowering regulatory genes, such as *FUL*, *LFY*, *AP1*, and miR172C, thereby delaying flowering [182]. Shade decreases FHY3 and FAR1 levels and prevents the above process, leading to early flowering [188]. Additionally, FHY3 and FAR1 delay flowering time under both LD and SD conditions by transcriptionally upregulating Early Flowering4 (ELF4) [189], and they were shown to interact with PIF3/5 and act as negative regulators of SAS [182].

Recently, the PHYB-FLC pathway has also been identified to regulate flowering by shade. In this pathway, F-box of Flowering 2 (FOF2) functions downstream of PHYB to promote FLC expression and inhibit flowering under simulated shade conditions, which are partially dependent on VASCULAR PLANT ONE-ZINC FINGER 2 (VOZ2) proteins [190]. Under the mimic shade, PHYB mediates the stabilization of FOF2 and leads to the degradation of VOZ2. This suggests a novel mechanism whereby plants fine-tune flowering

time through a PHYB–FOF2–VOZ2 module that regulates FLC expression in response to shade [190,191].

4.3. Light Quantity/Photosynthesis Pathway

The quantity of light, including BL, can also influence plant flowering. Normally, increased light levels usually have a positive effect on flowering, despite varying responses among plant species [21]. The light quantity pathway is particularly crucial during early development, especially in herbaceous species with a distinct juvenile phase; it has been found in petunia that lower irradiances prolong the juvenile phase [21,192].

In general, flowering responses to light quantity are assumed to be linked to photosynthesis and the availability of assimilates, so the light quantity pathway is also called the photosynthesis pathway [21,193]. A strong irradiance dependence on flowering in *Brassica campestris* can be eliminated by supplying sucrose [21]. Because photosynthesis contributes to flowering regulated by the light quantity pathway, in this case, the photoreceptors are photosynthetic pigments [21,193] (Figure 5). As receptors for the regulation of flowering, photosynthetic pigments may sense a change in light quantity to affect photosynthesis and thus the availability of assimilates [105]. The contribution of the light quantity pathway to BL-mediated flowering results from the effects of BL on photosynthesis, which are associated with a very high absorbance of BL by photosynthetic pigments [63]. BLs also act on chloroplast movement within the plant cell to improve photosynthesis efficiency through its photoreceptor, PHOT [5,63].

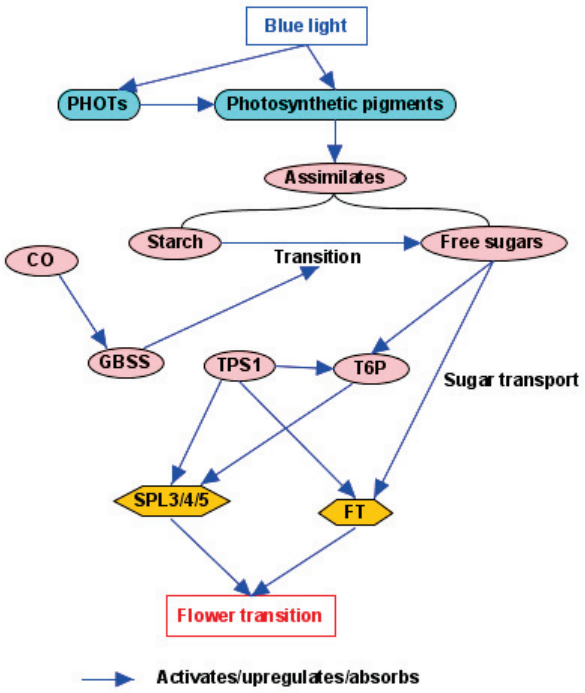


Figure 5. A simplified diagram of the light quantity pathway (or photosynthesis pathway) in blue-light-mediated floral transition. FT = FLOWERING LOCUS T, a florigen; SPL/3/4/5 = SQUAMOSA PROMOTER BINDING-LIKE 3/4/5, a group of positive floral integrator proteins. PHOTs = phototropins, blue light photoreceptors. CO = CONSTANS, a central component in the photoperiod pathway; T6P = trehalose-6-phosphate, a carbohydrate from sucrose; TPS1 = T6P synthase1; GBSS = GRANULE BOUND STARCH SYNTHASE. To be clear, only the key pathway components are presented in the diagram, and information about other pathway components can be found in the manuscript's text. Also, the regulations at the transcriptional and translational levels are not distinguished in the figure for simplification, and the relevant information can be found in the text.

For the light quantity pathway, assimilates act as part of a complex flowering signal [21]. The signals from assimilates may differ depending on the amount of light. Starch metabolism was differentially regulated during the floral transition in response to the amount of light, and the distribution of sugar and starch is linked to the floral transition [105,194,195]. As major assimilates, free sugars serve as important signaling molecules to regulate plant flowering [196]. Exposure to different light amounts changes the sugar content in *Ranunculus asiaticus*, showing a positive correlation between early flowering and higher accumulation of free sugars [197]. As a signal to initiate flowering, sugar type also varies across plant species [105]. For example, sucrose accumulation in the phloem increased during floral induction in *Sinapis alba* [198], but *Arabidopsis* has a higher demand for glucose and fructose than sucrose in the reproductive stage [199].

In addition to sucrose, glucose, and fructose, other carbohydrates may also play a role in the floral transition [105]. For example, trehalose-6-phosphate (T6P) accumulation is induced by sucrose, and T6P content is regulated in plants by T6P synthase (TPS) and T6P phosphatase (TPP) [200]. T6P signaling regulates flowering time in two different tissues; one is in the leaf where TPS1 is responsible for the induction of FT and TSF in response to photoperiod, and another one is in the SAM, where TPS1 and T6P signaling regulates the floral transition by controlling the transcription level of SPL3/4/5 via the age pathway, independent of the photoperiod pathway [105,201]. This indicates that, at least through T6P, the light quantity pathway can be integrated into other signal pathways.

Besides T6P, the light quantity pathway can potentially interact with the photoperiod pathway through light signal and/or pathway components. The amount of light is directly related to the photoperiod. The photoperiod can regulate starch metabolism differentially during the floral transition, and a disturbance in starch metabolism causes a change in flowering time [202,203]. CO may play a crucial role in the balance between free sugars and starch during floral transition by controlling the timing and the expression levels of GRANULE BOUND STARCH SYNTHASE (GBSS) [105]. Additionally, as an important photoreceptor in the photoperiod pathway, PHYA's action is mediated partly and indirectly through photosynthesis, as flowering was delayed under low irradiance in *phyA* mutants but not at higher irradiances [21,193]. A recent study on chrysanthemum has also found that plant flowering responds to the intensity of prolonged photoperiod lighting (e.g., NI lighting) with BL, suggesting the co-regulation of photosynthetic carbon assimilation and differential photoreceptors in flowering [204].

Although assimilates themselves are part of a complex flowering signal, it is also possible that a sufficient mass flow of assimilates can contribute to the delivery of mobile flowering signals like FT [21]. In this case, besides sugar accumulation, carbohydrate transport is an important factor during the floral transition [105]. For example, chrysanthemum treated with exogenous sucrose showed a high induction of CmFTLs and FT homologs and flowered early under both LD and SD conditions [205]. Nevertheless, the precise molecular mechanisms through which light quantity, potentially through photosynthetic assimilation, modifies the length of the juvenile phase remain less clear.

5. Key Midstream Pathway Components

In the above three flowering pathways, after the reception of light signals by the photoreceptors, many midstream network components are involved in further transducing light signals to floral integrator proteins and eventually inducing flower initiation. The roles of some key midstream network components and their responses to BL are summarized as follows (Figure 6).

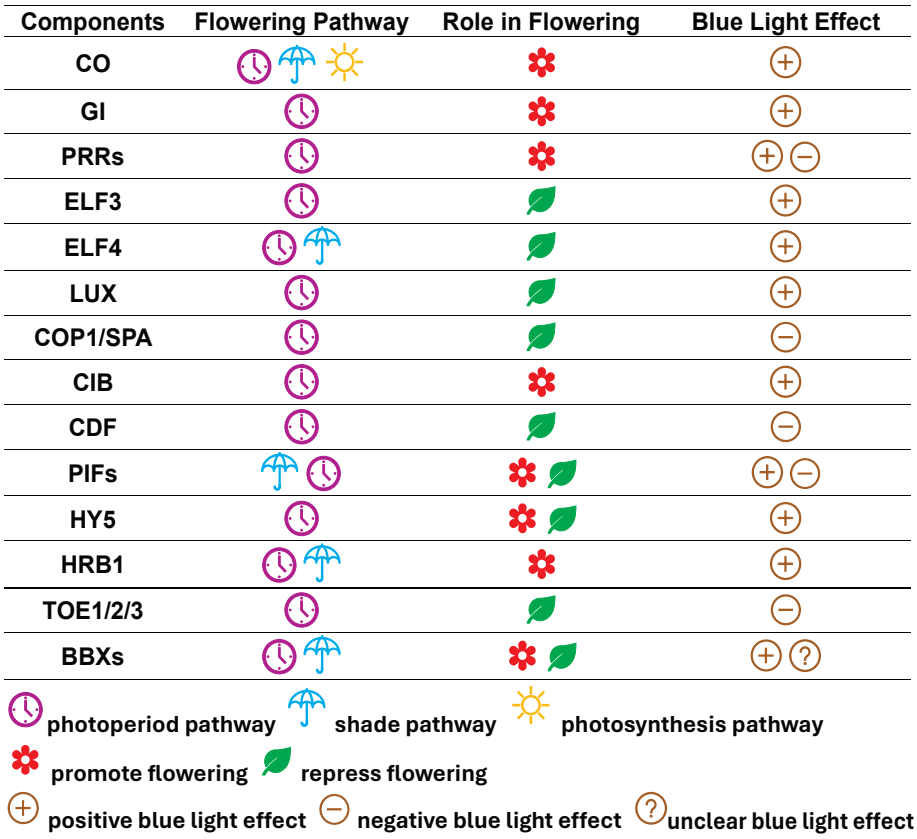


Figure 6. An illustration of the functions of key pathway components in blue-light-mediated flowering in terms of their involved flowering pathways, roles in flowering, and response to blue light. CO = CONSTANS; GI = GI-GANTEA; PRRs = PSUEDO RESPONSE REGULATORS; ELF3/4 = EARLY FLOWERING3/4; LUX = LUX ARRHYTHMO; COP1/SPA = CONSTITUTIVE PHOTOMORPHOGENIC 1/SUPPRESSOR OF PHYTOCHROME A; CIB = CRYPTOCHROME-INTERACTING basic helix–loop–helix; CDF = CYCLING DOF FACTOR; PIFs = PHYTOCHROME INTERACTING FACTORS; HY5 = ELONGATED HYPOCOTYL 5; HRB1 = Hypersensitive to red and blue protein; TOE1/2/3 = TARGET OF EAT1/2/3; and BBXs = B-box containing proteins. If both flowering promotion and repression are shown together, this indicates that the role of this pathway component depends on specific pathway or member. If both positive and negative effects of blue light are shown together, this indicates that the blue light effect may vary with light intensity or component member. For BBXs, although some members show positive responses to blue light, other members are unknown.

5.1. CONSTANS (CO)

CO is an important component in the photoperiodic flowering pathway, but the role of CO in photoperiodic flowering may vary with photoperiod, plant species, and light quality. In *Arabidopsis*, CO normally has a positive role in flowering induction in LD conditions by upregulating FT expression [156,157]. However, CO also has a negative role in flowering induction in SD conditions [206], where CO can inhibit flowering hypothetically through the flowering repressor TFL1, ensuring an alternative mechanism that prevents *Arabidopsis* from flowering in the wrong season [26]. In other plant species, proteins with a structure like that of CO (COL proteins) have been identified and studied in diverse crops, including ornamental plant, such as *Petunia hybrida* and *Pharbitis nil*, and economically important crops, including rice, barley, wheat, maize, sorghum, cotton, hemp (*Cannabis sativa* L.), tomato, grapevine (*Vitis vinifera*), and strawberry [157]. For example, in rice, there are two important COL transcription factors: Heading date1 (Hd1), an ortholog of the *Arabidopsis* CO, and Early heading date1 (Ehd1), which is unique in rice [119]. Ehd1 always acts

as an inducer of florigen genes (*Hd3a* in SD conditions or *RFT1* in LD conditions), and its expression is upregulated by BL in the morning; however, Hd1 acts as a repressor in noninductive LD [157]. In strawberries, although both blue and FR light treatments trigger flowering through the FvFT1 cascade, BL operates through FvFT1 and is partially independent of FvCO, while FR light operates completely independently of FvCO [127].

BL, like FR light, enhances the stability of CO proteins, but red light promotes the degradation of CO [156,158]. For example, in *Hippeastrum hybridum* under RB-LED lighting with 10% or 90% B, RB-LED with 90% B compared with white LED advanced flowering time and extended the duration of the flowering period, which was associated with greater expression of the *HpCOL* gene [207]. The stabilization of CO by BL is a balanced result of the contribution of several BL receptors. FKF1, identified as a CDF-destabilizing photoreceptor, interacts directly with CO proteins to enhance their stability [156]. FKF1 also prevents COP1 homodimer formation, reducing COP1-dependent CO degradation [208]. Additionally, FKF1 competes with AP2-like proteins (TOE1, TOE2, TOE3), known FT repressors, for CO protein stabilization [156,209]. The FKF1's role in CDF degradation and CO protein stabilization is crucial for photoperiodic sensitivity [210]. Similarly to FKF1, BL photoreceptors CRY1 and CRY2 can also enhance the stability of CO proteins by physically impairing TOE1, TOE2, and the COP1–SPA complex [156]. However, ZTL leads to CO degradation [173], although the mechanism remains unclear.

5.2. Circadian Clock

Photoreceptors influence flowering time indirectly by modulating the circadian clock [193], a gene and protein network producing 24 h oscillations synchronized to environmental cycles [211]. This internal timing system allows plants to anticipate and adapt to daily changes in the environment [212]. The circadian clock comprises complicated components, and BL can regulate the clockwork and its components to regulate plant flowering.

5.2.1. Clock Components

The plant circadian clock is composed of three main parts: (1) input pathways that perceive and transmit environmental signals, (2) a central oscillator that generates 24 h rhythms, and (3) output pathways that regulate physiological processes [158]. In *Arabidopsis*, the identified core clock proteins include at least morning-expressed proteins CIRCADIAN CLOCK ASSOCIATED 1 (CCA1) and LATE ELONGATED HYPOCOTYL (LHY); midday regulators PSEUDORESPONSE REGULATOR 9 (PRR9), PRR7, and *PRR5*; and evening-expressed components EARLY FLOWERING 3 (ELF3), ELF4, and LUX ARRHYTHMO (LUX), which are called the evening complex, and Timing of CAB2 Expression 1 (TOC1) [213]. These components, together with GI, form an interlocked feedback loop to control circadian rhythms (Figure 7). The function of these core circadian components is largely conserved among *Arabidopsis* and crops like rice, maize, and duckweed (*Lemna gibba*) [119]. Among these clock components, CCA1, LHY, ELF3, ELF4, and LUX act as flowering repressors, but PRR9, PRR7, PRR5, and TOC1 positively regulate flowering in *Arabidopsis* [163].

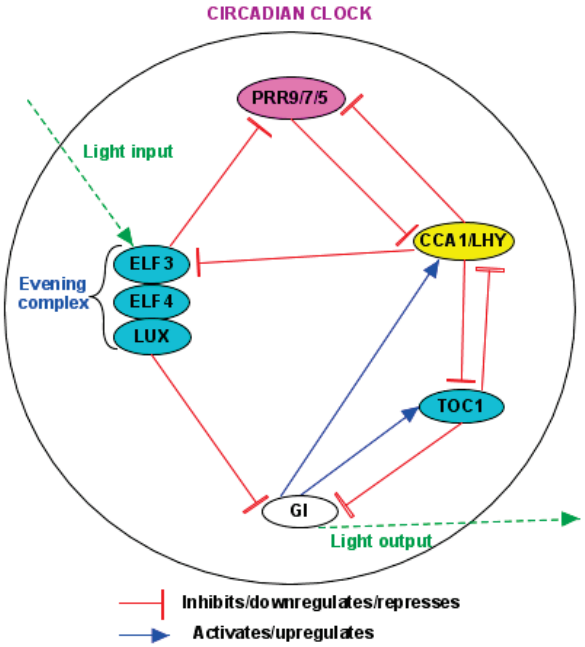


Figure 7. A simplified diagram of the main components of the circadian clock in *Arabidopsis thaliana*. The figure is adapted and modified from the literature [170]. CCA1/LHY = CIRCADIAN CLOCK ASSOCIATED 1/LATE ELONGATED HYPOCOTYL; PRR9/7/5 = PSUEDO RESPONSE REGULATOR9/7/5; TOC1 = Timing of CAB2 Expression 1; LUX = LUX ARRHYTHMO; ELF3/4 = EARLY FLOWERING 3/4; GI = GIGANTEA. Among these clock components, ELF3 and GI are important clock input and output members, respectively. In the diagram, the yellow components are expressed in the morning, purple components are expressed midday, and blue components are expressed in the evening.

5.2.2. Regulation of Clockwork by BL

Blue light entrains the circadian oscillator by adjusting its pace and phase. In *Arabidopsis*, the circadian period shortens under BL compared to darkness (where the plant has a circadian period of 30 to 36 h), with increased intensity accelerating the rhythm (or shortening the circadian period [72,170,214].

Photoreceptors CRY1, CRY2, and PHYA serve as primary BL sensors for the clock's entrainment [82]. Normally, PHYA is most important in low-intensity blue light, CRY2 in low-intensity BL, and CRY1 in high- or low-intensity BL [215]. For example, PHYA is necessary to re-entrain the oscillator in response to a BL pulse at the end of the night, which shifts the phase of the clock [82]. Additionally, some other BL photoreceptors, such as the ZTL family, have also been shown to regulate clock components [193]. The mechanism linking BL perception to the core of the circadian clock is still not fully understood. In *Arabidopsis*, CRYs have been revealed to affect the circadian period through photo-signaling hub factors, PIFs, COP1, or other transcription factors [214]. For example, CRY2 binding to several core clock gene promoters for fine-tuning the oscillator could be modulated by PIF due to a proven interaction between CRYs and PIFs [176]. COP1, acting at the crossroads of multiple light wavelengths, also conveys BL information to the circadian clock [82]. Also, BL can repress the transcription of *COLD REGULATED GENE 27 (COR27)* and *COR28* but stabilize COR27 and COR28 proteins, which bind to the promoters of *PRR5* and *TOC1* and repress their transcription [216]. Additionally, HY5, induced by BL, binds directly to clock gene promoters, including *CCA1*, *PRR9*, and *LUX*, integrating BL perception with clock function [82,189,211]

5.2.3. Responses of Key Clock Components to BL

(1) BL and GI

GI serves as a core component that transmits BL signals for circadian rhythm resetting while overseeing floral initiation [162]. In *Arabidopsis*, under BL conditions, GI can bind to ZTL and establish a GI–ZTL protein complex to stabilize ZTL expression [217]. In the BL signaling system, GI binding to ZTL as well as LKP2 to orchestrate the degradation of TOC1 and PRR5, contributing to correct oscillation of the plant's circadian clock [93,162,218]. BL also induces the formation of an FKF1–GI protein complex to promote CO and FT expression and flowering in LD conditions [219,220], as mentioned in Section 4.1. In rice, OsGI plays a critical gatekeeper role in BL induction of Ehd1, a CO-like protein, resulting in early flowering under SD conditions [131,221]. In chrysanthemums, CsGI can control photoperiodic flowering by shaping the gate for light induction of CsAFT, an anti-florigen [121], but the specific response of CsGI to BL is unknown.

(2) BL and PRRs

PRR9 and PRR7 act redundantly not only as a crucial circadian output hub to control photoperiodic flowering time but also participate in the light input pathway [214,222]. Specifically, PRR9 mainly mediates BL signal input, while PRR7 acts in red light input [222]. Recently, it has been found that photoreceptor CRY2 mediates BL input to the circadian clock by directly interacting with PRR9 in a BL-dependent manner [214]. Given the labile nature of CRY2 in strong BL, BL triggers CRY2 turnover in proportion to its intensity, which accordingly releases PRR9 to fine-tune circadian speed [214].

(3) BL and evening complex (EC)

ELF3 is involved in BL-mediated circadian regulation [168]. Under continuous blue or red light conditions, overexpression of ELF3 led to a significant extension of the circadian period across a wide range of fluence rates, resembling the fluence response curves observed in plants lacking functional CRY1 and CRY2 [223]. ELF3 is also part of the BL signaling pathway through its interaction with COP1, and some, but not all, inputs of PHYs to the clock depend on ELF3 [170]. So far, no BL receptors have been identified that directly interact with ELF3 [224]. However, BL can promote the localization of ELF3 to foci independent of ELF4 [225]. ELF4 also negatively regulates flowering by affecting the biological activity of the GI. In petunia, two ELF4-like genes, *PhELF4-1* and *PhELF4-2*, are under photoperiodic control involving the circadian clock and implicated in signal transduction from one or more BL photoreceptors [10]. Both genes exhibit a rhythmic expression pattern, with higher expression under blue LED light compared to red LED light, peaking 12 h into a 14 h photoperiod. *PhELF4-1* shows higher amplitude and higher peak expression than *PhELF4-2*. *PhELF4-1* maintains its expression rhythm for two days under continuous blue LED light, indicating a circadian rhythm, and shifts phases after transfer to short days with an 8 h photoperiod [10].

LUX acts as a flowering repressor [158,163]. The expression of LUX is activated by BL, in addition to cold temperatures and red light [225]. The activation of LUX expression by blue and red light occurs through HY5, and, in this process, BL has a major effect, while red light has a minor effect [225].

5.3. Other Key Transcription Factors/Regulators

5.3.1. CONSTITUTIVE PHOTOMORPHOGENIC 1/SUPPRESSOR OF PHYTOCHROME A (COP1/SPA)

As a downstream pathway component after photoreceptors, the COP1/SPA complex is a master repressor of light signaling by ubiquitinating and subsequently degrading many light-regulated transcription factors (e.g., CO, PIFs, and HY5) in darkness [95]. Under

light conditions, photoreceptors, such as CRYs and PHYs, suppress the activity of the COP1/SPA complex [172]. For the COP1/SPA complex, SPA proteins are required for the light-induced nuclear exclusion of COP1 and thereby contribute to the light-induced inhibition of COP1 [226]; however, blue or red light leads to dissociation of the COP1–SPA1 interaction, likely a very important mechanism of light-induced inhibition of COP1/SPA activity [172]. In *Arabidopsis* under BL, COP1/SPA activity is inhibited by CRY1 and CRY2, FKF1, and PHYA [95]. In addition to FKF1, the other members of the ZEITLUPE family, such as ZTL and LKP2, also interact with COP1 [95,208]. This leads to the stabilization of the CO protein, followed by early flowering under LD conditions [208]. Following this mechanism, these BL photoreceptors may act in parallel or together in promoting flowering via CO [95]. Moreover, COP1/SPA facilitates the light-induced degradation of PIFs by associating with PHYs [172]. In *Arabidopsis*, COP1/SPA ubiquitinating HY5 is suppressed by BL through CRYs; however, in *Marchantia polymorpha*, MpCRY is not an inhibitor of this process under BL, although COP1/SPA ubiquitinating HY5 is conserved in this species [227].

5.3.2. CRYPTOCHROME-INTERACTING Basic Helix–Loop–Helix (CIB) Proteins

The CIBs, belonging to basic helix–loop–helix (bHLH) proteins, are important downstream components after photoreceptors in the photoperiodic flowering pathway, and BL mediates CIB proteins through its photoreceptors to regulate flowering. CRY2 mediates the BL stimulation of CIB1 activation, which promotes the transcription of the *FT* gene, and three CIB1-like proteins (CIB2/4/5) also interact with photoactivated CRY2 and bind to the *FT* promoter [28]. Furthermore, CIB proteins directly interact with CO to promote floral initiation, suggesting that CRY2 might influence the CIB–CO interaction and *FT* transcription [228]. In the dark or under red light, CIB proteins (CIB1/4/5) are degraded by the 26S proteasome; however, BL suppresses their degradation through ZTL and LKP2, rather than through CRYs [28].

5.3.3. CYCLING DOF FACTOR (CDF)

As an important component of the photoperiod pathway, the CDF family members (especially CDF1) act as floral repressors under LD conditions by inhibiting CO expression in the first part of the light period [137]. In the LD afternoon, a protein complex formed by GI and FKF1 is required to degrade the CDF proteins, releasing the repression of CO and FT transcription [159]. In *Arabidopsis*, FKF1 and GI form a complex in a BL-dependent manner, which mediates the degradation of the CDF1 protein [219]. The function of FKF1 depends on the interaction between GI and CDF1, and GI also interacts with ZTL and LKP2 and synergistically degrades CDF2 protein [160,173,174].

5.3.4. PHYTOCHROME INTERACTING FACTORS (PIFs)

The PIFs, belonging to bHLHs, can also mediate flowering by binding their genes to floral integrator proteins as well as other flowering regulators, such as AP1, SVP, LFY, AGAMOUS (AG), and SEP3 (SEPALLATA3) in *Arabidopsis* [229]. In addition to *Arabidopsis*, in rice, *ospil13*, one of the putative PIF4 homologs, mutants were reported to head earlier compared to the wild type, indicating that OsPIL13 might regulate floral development in rice [230,231].

The PIFs are involved in multiple flowering pathways, including the shade pathway and the photoperiod pathway, as mentioned before. PIF7 functions as the major regulator alongside PIF1/3/4/5 in orchestrating shade avoidance syndrome (SAS) and thus indirectly mediating flowering [232]. Also, PIFs interact with circadian clock components like TOC1 to modulate the timing of gene expression, which ensures that flowering time regulators are expressed in coordination with the circadian rhythm [229]. PIF7, together with CO,

plays an additive role in the promotion of flowering under shade conditions through the induction of FT expression [26,177]. Additionally, the PIFs are also involved in other signaling pathways to regulate flowering. For example, when there is an increase in the ambient temperature, PIF4 is stabilized, and it directly binds to the promoter of *FT* and induces its expression, indicating that FT can also induce flowering in a temperature-dependent manner via PIF4 [230]. PIF1 suppresses the floral transition in *Arabidopsis* under LD conditions by interacting with gibberellins (GAs) and floral integrators, such as *FT*, *SOC1*, and *LFY* [233]. Furthermore, under shade conditions, GA-mediated degradation of DELLA relieves their inhibition of PIF4, which in turn activates *FT* transcription to promote flowering [182].

BL-activated PHYA induces the degradation of PIF1 [234], a suppressor of floral transition, and thus possibly promotes flowering. However, no evidence supports BL-triggered, CRY-induced degradation of PIF1 [235]. Also, CRYs directly interact with PIFs, and this interaction modulates the activity of PIFs, thereby affecting flowering [182]. It has been shown that PIF4 and PIF5 are CRY-interacting proteins and that PIF4, PIF5, and CRY2 bind to common chromatin regions of target genes [176].

5.3.5. ELONGATED HYPOCOTYL 5 (HY5)

The HY5 is a signaling hub component acting downstream of several photoreceptors [211]. HY5 regulates the circadian clock by binding to specific promoter elements of the majority of clock genes [236]. Also, HY5 interacts with histone deacetylase HDA9 to epigenetically regulate flowering time in *Arabidopsis* by repressing the expression of *PIF4* and *COL5* [237,238].

Under BL, activated CRYs interact with and inhibit COP1, which targets HY5 for degradation, which leads to the stabilization and accumulation of HY5 [236]. BL is more efficient than red light in inducing the accumulation of HY5 at transcriptional and post-transcriptional levels, and HY5-mediated signaling to the clock is most pronounced in BL [211]. Therefore, BL could efficiently modulate the pace of the circadian clock by governing the abundance of HY5 [211].

5.3.6. Hypersensitive to Red and Blue Protein (HRB1)

The HRB1 is a downstream component after photoreceptors to regulate flowering in at least the photoperiod pathway and the shade pathway. The *hrb1* mutant flowers late under both LD and SD conditions, whereas *HRB1* overexpression leads to early flowering under SD conditions due to altered *FT* expression [158]. HRB1 regulates CRY-mediated BL responses as well as PHYB-mediated red light responses and is localized to the nucleus [158]. HRB1 may regulate *FT* expression and flowering downstream of CRY2 in LD conditions and modulate the PHYB-mediated shade pathway to regulate flowering in both LD and SD conditions [239]. HRB1 is essential for the proper expression of *PIF4* under red light and BL, suggesting that HRB1 and PIF4 may be crucial intersection points for red light and BL signaling pathways [158]. Additionally, *HRB1* expression is regulated by the circadian clock, similarly to other flowering genes [158].

5.3.7. TARGET OF EAT1/2/3 (TOE1/2/3)

At least involved in the photoperiod pathway, the APETALA2 (AP2)-like proteins, TOE1/2/3, are well-known FT repressors and compete with FKF1 for CO, resulting in CO destabilization due to a lack of access to FKF1 proteins [209]. Similarly to FKF1, CRY1 and CRY2 physically impair TOE1 and TOE2 under BL [156,240].

5.3.8. B-Box Containing Proteins (BBXs)

The BBXs are transcription factors essential in plant flowering [241]. The first BBX protein characterized and identified in *Arabidopsis* was CO/BBX1 [242]. The following BBXs mean proteins other than CO/BBX1.

The BBXs can not only inhibit photoperiod-mediated flowering but also regulate the shade avoidance response (SAR) to control flowering. For example, BBX10, BBX14, BBX15, BBX16, BBX17, BBX19, BBX30, and BBX31 interact with CO to inhibit its expression, while BBX32 forms heterodimers with BBX4 to bind and repress the *FT* promoter, and BBX7 inhibits the expression of both *CO* and *FT* [241,243]. Also, BBX21 upregulates genes involved in PHYB, BR, and auxin signaling to inhibit SAR, while BBX24 and BBX25 promote SAR in a COP1-dependent manner and BBX24 interacts with DELLAs and JAZ3 to modulate PIF4 activity and DELLA suppression, promoting SAR [241].

BL can affect levels of BBXs in plants. In *Arabidopsis*, BBX17, as a flowering repressor under LD conditions, is degraded in the dark but stabilized under BL as well as white, red, or FR light [242]. In strawberries, among the identified BBX proteins, the downregulated FaBBX29 plays an important role in the flowering promoted by sole-source lighting with blue vs. white light [160]. In *Arabidopsis*, CRY2, activated by BL, competes with HY5 to interact with COP1, thereby stabilizing HY5 protein, which directly targets the promoters of *BBX7* and *BBX8* to positively regulate their expression [244]. The CRY2-COP1-HY5-BBX7/8 module regulates BL-dependent cold acclimation, but whether the module can also mediate flowering is unknown.

6. Concluding Remarks and Future Perspectives

Floral transition is a crucial physiological process in plants, and regulation of this process directly affects the productivity of many crops [1,245]. Although significant progress has been made in understanding BL-mediated flowering, further mechanistic research is essential to deepen our scientific knowledge in this area. Much of our current understanding comes from studies on the model plant *Arabidopsis*, which, while valuable, has no direct agricultural importance and offers limited insight for SD or day-neutral crops. In contrast, only fragmental information is available on horticultural crops, as well as field/agronomic crops, which can be found in different sections of this manuscript and has also been summarized in Table 1. This limits the application of BL to flowering regulation, especially in horticultural crops, which are the most common crops produced in a controlled environment.

Table 1. Summarized mechanistic studies related to blue-light-mediated flowering in horticultural crops and field/agronomic crops in this review.

Common Name	Scientific Name	Main Results	Reference(s)
1. Horticultural crops			
Chrysanthemum	*Chrysanthemum morifolium*	Blue light (BL) did not inhibit floral transition under long day (LD), despite increased expression of both *PHYA* and *PHYB*.	[16]
		Shifts in the sequence of blue and other LEDs for night interruption (NI) lighting caused varying flowering responses associated with different expressions of related genes, such as *PHYA*, *CRY1*, *PHYB*, *AFT*, and *FTL*.	[114]

Table 1. *Cont.*

Common Name	Scientific Name	Main Results	Reference(s)
		At least two distinct phytochrome responses were involved in the flowering response; daytime light quality affects the light quality required for effective NI lighting due to different effects on FLOWERING LOCUS T (CmFTL3).	[111]
		An anti-florigen gene, *AFT*, was identified to contribute to the phytochrome (PHY)-mediated response to light and to determine the obligate photoperiodic flowering response.	[141]
		Flowering-promotion responses by long day BL treatments resulted from balanced expression of a series of genes, such as *CmFTL3*, *APETALA1 (CDM111)*, *FRUITFULL (CmAFL1)*, *LEAFY (CmFL)*, *CmPHYA*, *CmCRY1*, *CmAFT*, and *CmPHYB*. Also, the youngest leaf showed greater sensitivity to BL.	[148]
		BL-promoted flowering might be due to the co-regulation of photosynthetic carbon assimilation and differential photoreceptors in flowering.	[204]
		Increased photosynthesis, carbohydrate accumulation, and antioxidant production contributed to BL-promoted flowering.	[246]
		Exogenous sucrose induced a high expression of CmFTLs, and it flowered early regardless of the photoperiod.	[205]
		CsGI controlled photoperiodic flowering by gating light-induced CsAFT.	[121]
		A high daytime phytochrome photoequilibrium prevented plants from perceiving subsequent BL as a long day.	[247]
		Plant flowering under long-day BL treatment was not observed in all short-day (SD) plants.	[248]
Baby's Breath	*Gypsophila paniculata*	BL did not induce FT and SOC1 expression and had weaker flowering promotion than far-red (FR) light.	[14]
		Genotype variation in the flowering response to blue light was associated with GpFT and GpSOC1, rather than GpFKF1 and GpGI.	[11]
Kalanchoe	*Kalanchoe blossfeldiana*	BL was not perceived as a photoperiod signal to regulate flowering, which was mainly controlled by red light.	[112]
		The BL signal at the end of day increased flower bud formation regardless of the photoperiod, which was associated with higher expression of flowering promoter genes (*KfPHYA*, *KfCRY1*, *KfFT*, and *KfFPF-1*) and lower expression of the flowering suppressor gene (*KfPHYB*).	[147]
Lisianthus	*Eustoma grandiflorum*	Prolonged photoperiod lighting with BL promoted flowering under SD, associated with increased expression of EgFTL and EgSOC1L, but there was weaker promotion compared to FR light.	[135]

Table 1. *Cont.*

Common Name	Scientific Name	Main Results	Reference(s)
Marigold	*Tagetes erecta*	Twenty-four-hour sole-source lighting with pure BL promoted flowering compared with red light; however, impure BL containing a low level of red light failed to induce flowering, and adding a low level of far-red light restored the flowering-promoting effect.	[6,7]
Petunia	*Petunia* × *hybrida*	BL influenced *PehFT* expression but not the main gene promoting flowering.	[132]
		Blue vs. red LED light increased the expression of *FBP28*, a *SOC1*-like gene, which transmitted the BL signal from the FT protein to induce flowering.	[10,249]
		Two *ELF4*-like genes, *PhELF4-1* and *PhELF4-2*, were identified to act in signal transduction from one or more BL photoreceptors.	[10]
		Lower irradiances prolonged the juvenile phase.	[192]
		Twenty-four-hour sole-source lighting with pure BL promoted flowering compared with red light; however, impure BL containing a low level of red light failed to induce flowering, and adding a low level of far-red light restored the flowering-promoting effect.	[6,7]
Phalaenopsis orchid	*Phalaenopsis* spp.	Flowering response depended on active PHY levels under supplemental lighting.	[113]
Strawberry	*Fragaria* × *ananassa*	Sole-source lighting with blue vs. white LEDs promoted flowering associated with altered expression of PHYB, PIFs, HY5, FKF1, CCA1, LHY, and CO. The downregulated FaBBX29, an identified BBX protein, played an important role in BL-promoted flowering.	[160]
		Both blue and FR light promoted flowering in day-neutral accessions through FvFT1, but BL acted partially independent of FvCO, and FR light was completely independent of FvCO. Also, BL induced the expression of FvFT1 exclusively in veins of older leaves.	[127]
		Blue LED light increased the number of flower clusters and final yield in an everbearing variety.	[128]
		End-of-day lighting with BL or FR light could induce a higher expression of FvTFL1, the repressor of floral induction, in an SD variety.	[142]
		Blue LED light promoted the flowering of an SD variety in LD conditions, associated with increased expression of FaFT1 and decreased expression of FaTFL1, as well as enhanced photosynthesis and carbohydrate production.	[146]
Sweet pepper	*Capsicum annuum*	Sole-source lighting with BL induced the expression of CaFT1 and CaFT2 compared to white light.	[129]
Tomato	*Solanum lycopersicum*	BL sensitivity differs from *Arabidopsis*; indifferent flowering response found.	[250]

Table 1. *Cont.*

Common Name	Scientific Name	Main Results	Reference(s)
		Both CRY2 and CRY1a function to repress tomato flowering: knockout of *CRY2* or *CRY1a* does not affect flowering time, but the simultaneous knockout of both *CRY1a* and *CRY2* promotes flowering.	[46,52]
		This species has at least three *CRY* genes, *CRY1a*, *CRY1b*, and *CRY2*.	[31,32]
		Under LD conditions, *CRY2* overexpression in this species delayed flowering.	[48]
2. Field/agronomic crops			
Barley	*Hordeum vulgare*	CRY1a and CRY2a were identified, and CRY1a was a major regulator of photoperiodic flowering.	[32]
Maize	*Zea mays*	PHYB2 and, to a lesser extent, PHYB1 mediated photoperiodic flowering, and the sub-functionalization might contribute to flowering variation among varieties.	[59]
Onion	*Allium cepa*	Overexpression of *AcCRY1* accelerated flowering; BL promoted cytoplasmic localization.	[36]
Rice	*Oryza sativa*	Knockdown of *CRY2*, but not *CRY1*, delayed flowering both in long- and short-day conditions.	[46]
		Overexpression of *CRY2* in plants with a photoperiod-insensitive genetic background did not affect flowering time.	[47]
		PHYC functioned as a flowering repressor under noninductive photoperiods.	[76]
		FKF1 had a similar role in photoperiod-mediated flowering relative to *Arabidopsis* and promoted flowering independent of the photoperiod.	[91]
		OsHAL3 was identified as a new BL sensor, which was structurally inactivated by light, especially BL.	[99]
		OsHAL3 was a positive regulator of flowering by directly binding to the promoter of *Hd3a* and forming a complex with Hd1 under SD conditions.	[100]
		Hd3a and RFT1 are essential for promoting rice flowering under SD conditions, while RFT1 functions as a floral activator under LD conditions.	[119]
		Both Hd3a and RFT1 are expressed in leaves and move to the SAM, where they enhance the expression of floral meristem identity genes and trigger flowering.	[119,124,125]
		NI lighting with BL suppressed Hd3a expression and delayed flowering.	[130]
		RCN (a TFL1 homolog) inhibited flowering by competing with Hd3a (a FT homolog) for 14-3-3 binding to form a florigen repression complex.	[118,144]
		There are two important COL transcription factors. These are Heading date1 (Hd1), an ortholog of the *Arabidopsis* CO, and Early heading date1 (Ehd1) which is unique in rice.	[119]

Table 1. *Cont.*

Common Name	Scientific Name	Main Results	Reference(s)
		Ehd1 always acts as an inducer of florigen genes (*Hd3a* in SD conditions or *RFT1* in LD conditions), and its expression is upregulated by BL in the morning; however, *Hd1* acts as a repressor in noninductive LD.	[157]
		OsGI plays a critical gatekeeper role in BL induction of Ehd1, a CO-like protein, resulting in early flowering under SD conditions.	[131,221]
		OsPIL13 might regulate floral development; *ospil13*, one of the putative *PIF4* homologs, mutants headed earlier compared to the wild type.	[230,231]
Sorghum	*Sorghum bicolor*	CRY2 is a major regulator of photoperiodic flowering; CRY1b can rescue the late-flowering phenotype in *Arabidopsis cry1/cry2* double mutant.	[46,51]
Soybean	*Glycine max*	CRY1a rather than CRY2a is a major regulator of photoperiodic flowering.	[46,50]
		The regulation of photoperiodic flowering through PHYA-LUXE1-FT is different from the PHYB-CO-FT flowering pathway in many nonlegume plants.	[150,152]
Wheat	*Triticum aestivum*	PHYC promoted flowering under inductive photoperiods.	[75]

Emerging evidence highlights substantial variation in BL responses between model and crop species. For instance, a recent study has revealed that tomato, a widely cultivated crop, is relatively insensitive to BL in terms of flowering, unlike *Arabidopsis*, which shows sensitive responses [250]. This discrepancy underscores the growing need to investigate BL-mediated flowering directly in agriculturally important species. Despite beginning, increased research interests have been focused on exploring mechanisms underlying BL-regulated floral transition in horticultural crops, especially chrysanthemums and strawberries.

Chrysanthemum, a quantitative SD plant, typically fails to flower under LD conditions. However, extended photoperiod lighting using blue LEDs did not inhibit floral transition and even promoted stem elongation, which is desirable for cut flower production [8]. Research from Korea has shown that BL treatment activates specific photoreceptors, enhances sugar accumulation, and increases expression of FT, all contributing to flowering responses [16,114,204,246]. Nevertheless, the effects of BL in chrysanthemums are highly dependent on environmental conditions and vary among different SD plant species [8,247,248], indicating a need for deeper exploration of the underlying regulatory mechanisms.

In strawberries, BL has also been identified as a crucial signal in flowering regulation [127,128,142,146,160]. For example, sole-source blue lighting has been shown to promote flowering more effectively than white light [160]. Under BL, genes involved in light signaling (*PHYB*, *PIFs*, and *HY5*) and the circadian clock (*FKF1*, *CCA1*, *LHY*, and *CO*) are differentially expressed. Also, the BBX family protein, FaBBX29, was found to play an important role in flowering regulation under BL. Additionally, contrasting results about the expression of FaTFL1 have been reported in short-day varieties [142,146]. This suggests that a complex signaling network may be involved in strawberry's flowering response to BL.

Overall, BL-mediated flowering involves multiple photoreceptors and intricate signaling pathways. This complexity likely contributes to the diverse flowering responses

observed under BL treatments in controlled environments. Therefore, applying BL to regulate flowering should consider many factors, such as species-specific and environmental differences. Continued in-depth mechanistic studies, particularly in horticultural crops, are essential to fully use BL as a practical tool in crop production.

Author Contributions: Conceptualization, Y.K. and Y.Z.; methodology, Y.K. and Y.Z.; investigation, Y.K.; writing—original draft preparation, Y.K.; writing—review and editing, Y.K. and Y.Z.; funding acquisition, Y.Z. All authors have read and agreed to the published version of the manuscript.

Funding: This research received no external funding.

Data Availability Statement: Data are contained within the article.

Conflicts of Interest: The authors declare no conflicts of interest.

References

1. Jung, C.; Pillen, K.; Staiger, D.; Coupland, G.; Von Korff, M. Recent advances in flowering time control. *Front. Plant Sci.* **2017**, *7*, 2011. [CrossRef]
2. Peer, L.A.; Bhat, M.Y.; Ahmad, N.; Mir, B.A. Floral induction pathways: Decision making and determination in plants to flower—A comprehensive review. *J. Appl. Biol. Biotechnol.* **2021**, *9*, 7–17.
3. Li, L.; Li, X.; Liu, Y.; Liu, H. Flowering responses to light and temperature. *Sci. China Life Sci.* **2016**, *59*, 403–408. [CrossRef] [PubMed]
4. Demotes-Mainard, S.; Peron, T.; Corot, A.; Bertheloot, J.; Le Gourrierec, J.; Pelleschi-Travier, S.; Crespel, L.; Morel, P.; Huche-Thelier, L.; Boumaza, R. Plant responses to red and far-red lights, applications in horticulture. *Environ. Exp. Bot.* **2016**, *121*, 4–21. [CrossRef]
5. Huche-Thelier, L.; Crespel, L.; Le Gourrierec, J.; Morel, P.; Sakr, S.; Leduc, N. Light signaling and plant responses to blue and UV radiations—Perspectives for applications in horticulture. *Environ. Exp. Bot.* **2016**, *121*, 22–38. [CrossRef]
6. Kong, Y.; Kamath, D.; Zheng, Y. Blue-light-promoted elongation and flowering are not artifacts from 24-h lighting: A comparison with red light in four bedding plant species. *Acta Hortic* **2020**, *1296*, 659–666. [CrossRef]
7. Kong, Y.; Schiestel, K.; Zheng, Y. Blue light associated with low phytochrome activity can promote flowering: A comparison with red light in four bedding plant species. *Acta Hortic.* **2020**, *1296*, 433–440. [CrossRef]
8. Kong, Y.; Zheng, Y. Diverse Flowering Response to Blue Light Manipulation: Application of Electric Lighting in Controlled-Environment Plant Production. *Horticulturae* **2024**, *10*, 578. [CrossRef]
9. Shibuya, T.; Kanayama, Y. Flowering response to blue light and its molecular mechanisms in Arabidopsis and horticultural plants. *Adv. Hortic. Sci.* **2014**, *28*, 179–183.
10. Fukuda, N.; Suenaga, T.; Miura, E.; Tsukamoto, A.; Olsen, J.E. The expression of ELF4-like genes is influenced by light quality in petunia. *Agronomy* **2020**, *10*, 1800. [CrossRef]
11. Shibuya, T.; Murakawa, Y.; Nishidate, K.; Nishiyama, M.; Kanayama, Y. Characterization of flowering-related genes and flowering response in relation to blue light in Gypsophila paniculata. *Hortic. J.* **2017**, *86*, 94–104. [CrossRef]
12. Eskins, K. Light-quality effects on Arabidopsis development. Red, blue and far-red regulation of flowering and morphology. *Physiol. Plant.* **1992**, *86*, 439–444. [CrossRef]
13. Fukuda, N.; Ishii, Y.; Ezura, H.; Olsen, J.E. Effects of light quality under red and blue light emitting diodes on growth and expression of *FBP28* in *Petunia*. *Acta Hortic.* **2011**, *907*, 361–366. [CrossRef]
14. Hori, Y.; Nishidate, K.; Nishiyama, M.; Kanahama, K.; Kanayama, Y. Flowering and expression of flowering-related genes under long-day conditions with light-emitting diodes. *Planta* **2011**, *234*, 321–330. [CrossRef] [PubMed]
15. Park, Y.G.; Jeong, B.R. Night interruption light quality changes morphogenesis, flowering, and gene expression in Dendranthema grandiflorum. *Hortic. Environ. Biotechnol.* **2019**, *60*, 167–173. [CrossRef]
16. Park, Y.G.; Jeong, B.R. How supplementary or night-interrupting low-intensity blue light affects the flower induction in chrysanthemum, a qualitative short-day plant. *Plants* **2020**, *9*, 1694. [CrossRef]
17. Jeong, S.W.; Hogewoning, S.W.; van Ieperen, W. Responses of supplemental blue light on flowering and stem extension growth of cut chrysanthemum. *Sci. Hortic.* **2014**, *165*, 69–74. [CrossRef]
18. Singh, M.C.; van Ieperen, W.; Heuvelink, E.P. Effect of LEDs on flower bud induction in *Chrysanthemum morifolium* cv. Zembla. *HortFlora Res. Spectr.* **2013**, *2*, 185–188.
19. Meng, Q.; Runkle, E.S. Moderate-intensity blue radiation can regulate flowering, but not extension growth, of several photoperiodic ornamental crops. *Environ. Exp. Bot.* **2017**, *134*, 12–20. [CrossRef]

20. Meng, Q.; Runkle, E.S. Low-intensity blue light in night-interruption lighting does not influence flowering of herbaceous ornamentals. *Sci. Hortic.* **2015**, *186*, 230–238. [CrossRef]
21. Thomas, B. Light signals and flowering. *J. Exp. Bot.* **2006**, *57*, 3387–3393. [CrossRef] [PubMed]
22. Pardi, S.A.; Nusinow, D.A. Out of the dark and into the light: A new view of phytochrome photobodies. *Front. Plant Sci.* **2021**, *12*, 732947. [CrossRef]
23. Shinomura, T.; Nagatani, A.; Hanzawa, H.; Kubota, M.; Watanabe, M.; Furuya, M. Action spectra for phytochrome A-and B-specific photoinduction of seed germination in Arabidopsis thaliana. *Proc. Natl. Acad. Sci. USA* **1996**, *93*, 8129–8133. [CrossRef] [PubMed]
24. Jan, M.; Liu, Z.; Rochaix, J.-D.; Sun, X. Retrograde and anterograde signaling in the crosstalk between chloroplast and nucleus. *Front. Plant Sci.* **2022**, *13*, 980237. [CrossRef] [PubMed]
25. Folta, K.M.; Carvalho, S.D. Photoreceptors and control of horticultural plant traits. *HortScience* **2015**, *50*, 1274–1280. [CrossRef]
26. Perrella, G.; Vellutini, E.; Zioutopoulou, A.; Patitaki, E.; Headland, L.R.; Kaiserli, E. Let it bloom: Cross-talk between light and flowering signaling in Arabidopsis. *Physiol. Plant.* **2020**, *169*, 301–311. [CrossRef]
27. Xu, C.; Lv, Y.; Chen, C.; Zhang, Y.; Wei, S. Blue light-dependent phosphorylations of cryptochromes are affected by magnetic fields in Arabidopsis. *Adv. Space Res.* **2014**, *53*, 1118–1124. [CrossRef]
28. Wang, Q.; Lin, C. Mechanisms of cryptochrome-mediated photoresponses in plants. *Annu. Rev. Plant Biol.* **2020**, *71*, 103–129. [CrossRef]
29. Khudyakova, A.; Kosobryukhov, A.; Pashkovskiy, P.; Kreslavski, V. Cryptochromes and Their Role in the Process of Plant Adaptation. *Russ. J. Plant Physiol.* **2024**, *71*, 42. [CrossRef]
30. Lin, C. Blue light receptors and signal transduction. *Plant Cell* **2002**, *14*, S207–S225. [CrossRef]
31. Perrotta, G.; Ninu, L.; Flamma, F.; Weller, J.L.; Kendrick, R.E.; Nebuloso, E.; Giuliano, G. Tomato contains homologues of Arabidopsis cryptochromes 1 and 2. *Plant Mol. Biol.* **2000**, *42*, 765–773. [CrossRef]
32. Perrotta, G.; Yahoubyan, G.; Nebuloso, E.; Renzi, L.; Giuliano, G. Tomato and barley contain duplicated copies of cryptochrome 1. *Plant Cell Environ.* **2001**, *24*, 991–998. [CrossRef]
33. Li, Q.H.; Yang, H.Q. Cryptochrome signaling in plants. *Photochem. Photobiol.* **2007**, *83*, 94–101. [CrossRef] [PubMed]
34. Fraikin, G.Y.; Belenikina, N.S.; Rubin, A.B. Molecular bases of signaling processes regulated by cryptochrome sensory photoreceptors in plants. *Biochemistry* **2023**, *88*, 770–782. [PubMed]
35. Yang, Z.; Liu, B.; Su, J.; Liao, J.; Lin, C.; Oka, Y. Cryptochromes orchestrate transcription regulation of diverse blue light responses in plants. *Photochem. Photobiol.* **2017**, *93*, 112–127. [CrossRef]
36. Jia, Q.; Yin, Y.; Gai, S.; Tian, L.; Zhu, Z.; Qin, L.; Wang, Y. Onion cryptochrome 1 (AcCRY1) regulates photomorphogenesis and photoperiod flowering in Arabidopsis and exploration of its functional mechanisms under blue light. *Plant Physiol. Biochem.* **2024**, *206*, 108300. [CrossRef]
37. Kruusvee, V.; Toft, A.M.; Aguida, B.; Ahmad, M.; Wenkel, S. Stop CRYing! Inhibition of cryptochrome function by small proteins. *Biochem. Soc. Trans.* **2022**, *50*, 773–782. [CrossRef]
38. Kong, Y.; Zheng, Y. Low-activity cryptochrome 1 plays a role in promoting stem elongation and flower initiation of mature Arabidopsis under blue light associated with low phytochrome activity. *Can. J. Plant Sci.* **2022**, *102*, 755–759. [CrossRef]
39. Park, Y.; Runkle, E.S. Spectral effects of light-emitting diodes on plant growth, visual color quality, and photosynthetic photon efficacy: White versus blue plus red radiation. *PLoS ONE* **2018**, *13*, e0202386. [CrossRef]
40. Meng, Q.; Boldt, J.; Runkle, E.S. Blue radiation interacts with green radiation to influence growth and predominantly controls quality attributes of lettuce. *J. Am. Soc. Hortic. Sci.* **2020**, *145*, 75–87. [CrossRef]
41. Kang, W.H.; Kim, J.; Yoon, H.I.; Son, J.E. Quantification of spectral perception of plants with light absorption of photoreceptors. *Plants* **2020**, *9*, 556. [CrossRef] [PubMed]
42. Kong, Y.; Stasiak, M.; Dixon, M.A.; Zheng, Y. Blue light associated with low phytochrome activity can promote elongation growth as shade-avoidance response: A comparison with red light in four bedding plant species. *Environ. Exp. Bot.* **2018**, *155*, 345–359. [CrossRef]
43. Wang, X.; Wang, Q.; Han, Y.J.; Liu, Q.; Gu, L.; Yang, Z.; Su, J.; Liu, B.; Zuo, Z.; He, W. A CRY–BIC negative-feedback circuitry regulating blue light sensitivity of Arabidopsis. *Plant J.* **2017**, *92*, 426–436. [CrossRef]
44. Wang, Q.; Zuo, Z.; Wang, X.; Gu, L.; Yoshizumi, T.; Yang, Z.; Yang, L.; Liu, Q.; Liu, W.; Han, Y.-J. Photoactivation and inactivation of Arabidopsis cryptochrome 2. *Science* **2016**, *354*, 343–347. [CrossRef] [PubMed]
45. Wang, Q.; Liu, Q.; Wang, X.; Zuo, Z.; Oka, Y.; Lin, C. New insights into the mechanisms of phytochrome–cryptochrome coaction. *New Phytol.* **2018**, *217*, 547–551. [CrossRef] [PubMed]
46. Fantini, E.; Facella, P. Cryptochromes in the field: How blue light influences crop development. *Physiol. Plant.* **2020**, *169*, 336–346. [CrossRef]

47. Singh, S.; Sharma, P.; Mishra, S.; Khurana, P.; Khurana, J.P. CRY2 gene of rice (*Oryza sativa* subsp. indica) encodes a blue light sensory receptor involved in regulating flowering, plant height and partial photomorphogenesis in dark. *Plant Cell Rep.* **2023**, *42*, 73–89. [CrossRef]
48. Giliberto, L.; Perrotta, G.; Pallara, P.; Weller, J.L.; Fraser, P.D.; Bramley, P.M.; Fiore, A.; Tavazza, M.; Giuliano, G. Manipulation of the blue light photoreceptor cryptochrome 2 in tomato affects vegetative development, flowering time, and fruit antioxidant content. *Plant Physiol.* **2005**, *137*, 199–208. [CrossRef]
49. Blázquez, M.A.; Ahn, J.H.; Weigel, D. A thermosensory pathway controlling flowering time in Arabidopsis thaliana. *Nat. Genet.* **2003**, *33*, 168–171. [CrossRef]
50. Zhang, Q.; Li, H.; Li, R.; Hu, R.; Fan, C.; Chen, F.; Wang, Z.; Liu, X.; Fu, Y.; Lin, C. Association of the circadian rhythmic expression of GmCRY1a with a latitudinal cline in photoperiodic flowering of soybean. *Proc. Natl. Acad. Sci. USA* **2008**, *105*, 21028–21033. [CrossRef]
51. Zhou, T.; Zhou, L.; Ma, Y.; Gao, J.; Li, W.; Piao, M.; Zeng, B.; Yang, Z.; Bian, M. Cryptochrome 1b from sweet sorghum regulates photoperiodic flowering, photomorphogenesis, and ABA response in transgenic *Arabidopsis thaliana*. *Plant Mol. Biol. Rep.* **2018**, *36*, 13–22. [CrossRef]
52. Fantini, E.; Sulli, M.; Zhang, L.; Aprea, G.; Jiménez-Gómez, J.M.; Bendahmane, A.; Perrotta, G.; Giuliano, G.; Facella, P. Pivotal roles of cryptochromes 1a and 2 in tomato development and physiology. *Plant Physiol.* **2019**, *179*, 732–748. [CrossRef]
53. Mockler, T.C.; Guo, H.; Yang, H.; Duong, H.; Lin, C. Antagonistic actions of Arabidopsis cryptochromes and phytochrome B in the regulation of floral induction. *Development* **1999**, *126*, 2073–2082. [CrossRef] [PubMed]
54. Su, J.; Liu, B.; Liao, J.; Yang, Z.; Lin, C.; Oka, Y. Coordination of cryptochrome and phytochrome signals in the regulation of plant light responses. *Agronomy* **2017**, *7*, 25. [CrossRef]
55. Klose, C.; Büche, C.; Fernandez, A.P.; Schäfer, E.; Zwick, E.; Kretsch, T. The mediator complex subunit PFT1 interferes with COP1 and HY5 in the regulation of Arabidopsis light signaling. *Plant Physiol.* **2012**, *160*, 289–307. [CrossRef] [PubMed]
56. Legris, M.; Ince, Y.Ç.; Fankhauser, C. Molecular mechanisms underlying phytochrome-controlled morphogenesis in plants. *Nat. Commun.* **2019**, *10*, 5219. [CrossRef]
57. Hernando, C.E.; Murcia, M.G.; Pereyra, M.E.; Sellaro, R.; Casal, J.J. Phytochrome B links the environment to transcription. *J. Exp. Bot.* **2021**, *72*, 4068–4084. [CrossRef]
58. Mathews, S. Evolutionary studies illuminate the structural-functional model of plant phytochromes. *Plant Cell* **2010**, *22*, 4–16. [CrossRef]
59. Sheehan, M.J.; Kennedy, L.M.; Costich, D.E.; Brutnell, T.P. Subfunctionalization of PhyB1 and PhyB2 in the control of seedling and mature plant traits in maize. *Plant J.* **2007**, *49*, 338–353. [CrossRef]
60. Lei, Y.; Ma, Q.; Zhang, Y.; Li, J.; Ning, X.; Wang, Y.; Ge, X.; Zhao, H.; Lin, H. Functional dissection of phytochrome A in plants. *Front. Plant Sci.* **2024**, *15*, 1340260. [CrossRef]
61. Paik, I.; Huq, E. Plant photoreceptors: Multi-functional sensory proteins and their signaling networks. *Semin. Cell Dev. Biol.* **2019**, *92*, 114–121. [CrossRef]
62. Cheng, M.-C.; Kathare, P.K.; Paik, I.; Huq, E. Phytochrome signaling networks. *Annu. Rev. Plant Biol.* **2021**, *72*, 217–244. [CrossRef]
63. Landi, M.; Zivcak, M.; Sytar, O.; Brestic, M.; Allakhverdiev, S.I. Plasticity of photosynthetic processes and the accumulation of secondary metabolites in plants in response to monochromatic light environments: A review. *Biochim. Et Biophys. Acta (BBA)-Bioenerg.* **2020**, *1861*, 148131. [CrossRef] [PubMed]
64. Stutte, G.W. Light-emitting diodes for manipulating the phytochrome apparatus. *HortScience* **2009**, *44*, 231–234. [CrossRef]
65. Sager, J.C.; Smith, W.O.; Edwards, J.L.; Cyr, K.L. Photosynthetic efficiency and phytochrome photoequilibria determination using spectral data. *Trans. ASAE* **1988**, *31*, 1882–1889. [CrossRef]
66. Kong, Y.; Zheng, Y. Magic Blue Light: A Versatile Mediator of Plant Elongation. *Plants* **2023**, *13*, 115. [CrossRef] [PubMed]
67. Kong, Y.; Schiestel, K.; Zheng, Y. Pure blue light effects on growth and morphology are slightly changed by adding low-level UVA or far-red light: A comparison with red light in four microgreen species. *Environ. Exp. Bot.* **2019**, *157*, 58–68. [CrossRef]
68. Kong, Y.; Zheng, Y. Growth and morphology responses to narrow-band blue light and its co-action with low-level UVB or green light: A comparison with red light in four microgreen species. *Environ. Exp. Bot.* **2020**, *178*, 104189. [CrossRef]
69. Junior, C.A.S.; D'Amico-Damião, V.; Carvalho, R.F. Phytochrome type B family: The abiotic stress responses signaller in plants. *Ann. Appl. Biol.* **2021**, *178*, 135–148. [CrossRef]
70. Han, Y.-J.; Kim, S.-H.; Kim, J.-I. Phytochrome phosphorylation in plant light signaling. *Front. Plant Sci.* **2024**, *15*, 1259720. [CrossRef]
71. Van Buskirk, E.K.; Decker, P.V.; Chen, M. Photobodies in light signaling. *Plant Physiol.* **2012**, *158*, 52–60. [CrossRef]
72. Lin, C. Photoreceptors and regulation of flowering time. *Plant Physiol.* **2000**, *123*, 39–50. [CrossRef] [PubMed]
73. Mockler, T.; Yang, H.; Yu, X.; Parikh, D.; Cheng, Y.-C.; Dolan, S.; Lin, C. Regulation of photoperiodic flowering by Arabidopsis photoreceptors. *Proc. Natl. Acad. Sci. USA* **2003**, *100*, 2140–2145. [CrossRef] [PubMed]

74. Weller, J.L.; Beauchamp, N.; Kerckhoffs, L.H.J.; Platten, J.D.; Reid, J.B. Interaction of phytochromes A and B in the control of de-etiolation and flowering in pea. *Plant J.* **2001**, *26*, 283–294. [CrossRef] [PubMed]
75. Chen, A.; Li, C.; Hu, W.; Lau, M.Y.; Lin, H.; Rockwell, N.C.; Martin, S.S.; Jernstedt, J.A.; Lagarias, J.C.; Dubcovsky, J. PHYTOCHROME C plays a major role in the acceleration of wheat flowering under long-day photoperiod. *Proc. Natl. Acad. Sci. USA* **2014**, *111*, 10037–10044. [CrossRef]
76. Takano, M.; Inagaki, N.; Xie, X.; Yuzurihara, N.; Hihara, F.; Ishizuka, T.; Yano, M.; Nishimura, M.; Miyao, A.; Hirochika, H. Distinct and cooperative functions of phytochromes A, B, and C in the control of deetiolation and flowering in rice. *Plant Cell* **2005**, *17*, 3311–3325. [CrossRef]
77. Monte, E.; Alonso, J.M.; Ecker, J.R.; Zhang, Y.; Li, X.; Young, J.; Austin-Phillips, S.; Quail, P.H. Isolation and characterization of phyC mutants in Arabidopsis reveals complex crosstalk between phytochrome signaling pathways. *Plant Cell* **2003**, *15*, 1962–1980. [CrossRef]
78. Kong, Y.; Zheng, Y. Phytochrome contributes to blue-light-mediated stem elongation and flower initiation in mature Arabidopsis thaliana plants. *Can. J. Plant Sci.* **2021**, *102*, 449–458. [CrossRef]
79. Más, P.; Devlin, P.F.; Panda, S.; Kay, S.A. Functional interaction of phytochrome B and cryptochrome 2. *Nature* **2000**, *408*, 207–211. [CrossRef]
80. Banerjee, R.; Batschauer, A. Plant blue-light receptors. *Planta* **2005**, *220*, 498–502. [CrossRef]
81. Teixeira, R.T. Distinct responses to light in plants. *Plants* **2020**, *9*, 894. [CrossRef] [PubMed]
82. Sanchez, S.E.; Rugnone, M.L.; Kay, S.A. Light perception: A matter of time. *Mol. Plant* **2020**, *13*, 363–385. [CrossRef] [PubMed]
83. Voitsekhovskaja, O. Phytochromes and other (photo)receptors of information in plants. *Russ. J. Plant Physiol.* **2019**, *66*, 351–364. [CrossRef]
84. Pudasaini, A.; Zoltowski, B.D. Zeitlupe senses blue-light fluence to mediate circadian timing in *Arabidopsis thaliana*. *Biochemistry* **2013**, *52*, 7150–7158. [CrossRef]
85. Christie, J.M.; Blackwood, L.; Petersen, J.; Sullivan, S. Plant flavoprotein photoreceptors. *Plant Cell Physiol.* **2015**, *56*, 401–413. [CrossRef]
86. Christie, J.M. Phototropin blue-light receptors. *Annu. Rev. Plant Biol.* **2007**, *58*, 21–45. [CrossRef]
87. Kumar, A.; Choudhary, A.; Kaur, N.; Kaur, H. Wake up: It's time to bloom. *Russ. J. Plant Physiol.* **2021**, *68*, 579–595. [CrossRef]
88. Li, X.; Liang, T.; Liu, H. How plants coordinate their development in response to light and temperature signals. *Plant Cell* **2022**, *34*, 955–966. [CrossRef] [PubMed]
89. Zoltowski, B.D.; Imaizumi, T. Structure and function of the ZTL/FKF1/LKP2 group proteins in Arabidopsis. *Enzymes* **2014**, *35*, 213–239.
90. Zhou, L.; Lu, Y.; Huang, J.; Sha, Z.; Mo, W.; Xue, J.; Ma, S.; Shi, W.; Yang, Z.; Gao, J. Arabidopsis CIB3 regulates photoperiodic flowering in an FKF1-dependent way. *Biosci. Biotechnol. Biochem.* **2021**, *85*, 765–774. [CrossRef]
91. Han, S.H.; Yoo, S.C.; Lee, B.D.; An, G.; Paek, N.C. Rice FLAVIN-BINDING, KELCH REPEAT, F-BOX 1 (OsFKF 1) promotes flowering independent of photoperiod. *Plant Cell Environ.* **2015**, *38*, 2527–2540. [CrossRef] [PubMed]
92. Shchennikova, A. Photoperiod-Dependent Mechanisms of Flowering Initiation in *Arabidopsis thaliana* L. and *Zea mays* L. *Russ. J. Plant Physiol.* **2022**, *69*, 43. [CrossRef]
93. Kwon, E.; Pathak, D.; Dahal, P.; Tandukar, S.; Jung, H.S.; Kim, W.-Y.; Kim, D.Y. Structural analysis of the regulation of blue-light receptors by GIGANTEA. *Cell Rep.* **2022**, *39*, 110700. [CrossRef] [PubMed]
94. Toman, E.; Käs, M.D.; Taubert, B.; Moritz, M.; Qi, J.; Bolle, C. Photosynthetic and plastid performance effects of photoreceptors. *J. Mitochondria Plast. Endosymbiosis* **2024**, *2*, 2330972. [CrossRef]
95. Ponnu, J. Molecular mechanisms suppressing COP1/SPA E3 ubiquitin ligase activity in blue light. *Physiol. Plant.* **2020**, *169*, 418–429. [CrossRef]
96. Kong, Y.; Zheng, Y. Phototropin is partly involved in blue-light-mediated stem elongation, flower initiation, and leaf expansion: A comparison of phenotypic responses between wild Arabidopsis and its phototropin mutants. *Environ. Exp. Bot.* **2020**, *171*, 103967. [CrossRef]
97. Okajima, K. Molecular mechanism of phototropin light signaling. *J. Plant Res.* **2016**, *129*, 149–157. [CrossRef]
98. Łabuz, J.; Sztatelman, O.; Banaś, A.K.; Gabryś, H. The expression of phototropins in Arabidopsis leaves: Developmental and light regulation. *J. Exp. Bot.* **2012**, *63*, 1763–1771. [CrossRef]
99. Sun, S.-Y.; Chao, D.-Y.; Li, X.-M.; Shi, M.; Gao, J.-P.; Zhu, M.-Z.; Yang, H.-Q.; Luan, S.; Lin, H.-X. OsHAL3 mediates a new pathway in the light-regulated growth of rice. *Nat. Cell Biol.* **2009**, *11*, 845–851. [CrossRef]
100. Su, L.; Shan, J.-X.; Gao, J.-P.; Lin, H.-X. OsHAL3, a blue light-responsive protein, interacts with the floral regulator Hd1 to activate flowering in rice. *Mol. Plant* **2016**, *9*, 233–244. [CrossRef]
101. Zhu, X.; Dong, Z.; Zhu, M.; Hu, W.; Hu, J.; Chen, M.; Guan, Y. The Significance of Florigen Activation Complex in Controlling Flowering in Rice. *Crit. Rev. Plant Sci.* **2023**, *42*, 300–323. [CrossRef]
102. Chamovitz, D.A.; Deng, X.W.; Lam, E. Light signaling in plants. *Crit. Rev. Plant Sci.* **1996**, *15*, 455–478. [CrossRef]

103. Simkin, A.J.; Kapoor, L.; Doss, C.G.P.; Hofmann, T.A.; Lawson, T.; Ramamoorthy, S. The role of photosynthesis related pigments in light harvesting, photoprotection and enhancement of photosynthetic yield in planta. *Photosynth. Res.* **2022**, *152*, 23–42. [CrossRef] [PubMed]
104. Voitsekhovskaja, O.; Tyutereva, E. Chlorophyll b in angiosperms: Functions in photosynthesis, signaling and ontogenetic regulation. *J. Plant Physiol.* **2015**, *189*, 51–64. [CrossRef]
105. Gawarecka, K.; Ahn, J.H. Isoprenoid-derived metabolites and sugars in the regulation of flowering time: Does day length matter? *Front. Plant Sci.* **2021**, *12*, 765995. [CrossRef]
106. Yang, L.; Xu, M.; Koo, Y.; He, J.; Poethig, R.S. Sugar promotes vegetative phase change in Arabidopsis thaliana by repressing the expression of MIR156A and MIR156C. *eLife* **2013**, *2*, e00260. [CrossRef] [PubMed]
107. Murchie, E.H.; Hubbart, S.; Chen, Y.; Peng, S.; Horton, P. Acclimation of rice photosynthesis to irradiance under field conditions. *Plant Physiol.* **2002**, *130*, 1999–2010. [CrossRef]
108. Griffin, J.H.; Toledo-Ortiz, G. Plant photoreceptors and their signalling components in chloroplastic anterograde and retrograde communication. *J. Exp. Bot.* **2022**, *73*, 7126–7138. [CrossRef]
109. Pashkovskiy, P.P.; Kartashov, A.V.; Zlobin, I.E.; Pogosyan, S.I.; Kuznetsov, V.V. Blue light alters miR167 expression and microRNA-targeted auxin response factor genes in Arabidopsis thaliana plants. *Plant Physiol. Biochem.* **2016**, *104*, 146–154. [CrossRef]
110. Dutta Gupta, S.; Pradhan, S. Regulation of gene expression by LED lighting. In *Light Emitting Diodes for Agriculture: Smart Lighting*; Dutta Gupta, S., Ed.; Springer Nature Singapore Pte Ltd.: Singapore, 2017; pp. 237–258.
111. Higuchi, Y.; Sumitomo, K.; Oda, A.; Shimizu, H.; Hisamatsu, T. Day light quality affects the night-break response in the short-day plant chrysanthemum, suggesting differential phytochrome-mediated regulation of flowering. *J. Plant Physiol.* **2012**, *169*, 1789–1796. [CrossRef]
112. Amaki, W.; Kunii, M. Effects of light quality on the flowering responses in *Kalanchoe blossfeldiana*. *Acta Hortic.* **2015**, *1107*, 279–284. [CrossRef]
113. Runkle, E. Environmental control of the flowering process of Phalaenopsis orchids. *Acta Hortic.* **2019**, *1262*, 7–12. [CrossRef]
114. Park, Y.G.; Muneer, S.; Jeong, B.R. Morphogenesis, flowering, and gene expression of Dendranthema grandiflorum in response to shift in light quality of night interruption. *Int. J. Mol. Sci.* **2015**, *16*, 16497–16513. [CrossRef] [PubMed]
115. Li, N.; Yang, R.; Shen, S.; Zhao, J. Molecular mechanism of flowering time regulation in *Brassica rapa*: Similarities and differences with *Arabidopsis*. *Hortic. Plant J.* **2024**, *10*, 615–628. [CrossRef]
116. Tsoy, O.; Mushegian, A. Florigen and its homologs of FT/CETS/PEBP/RKIP/YbhB family may be the enzymes of small molecule metabolism: Review of the evidence. *BMC Plant Biol.* **2022**, *22*, 56. [CrossRef]
117. Song, G.-q.; Liu, Z.; Zhong, G.-y. Regulatory frameworks involved in the floral induction, formation and developmental programming of woody horticultural plants: A case study on blueberries. *Front. Plant Sci.* **2024**, *15*, 1336892. [CrossRef]
118. Wang, X.; Zhou, P.; Huang, R.; Zhang, J.; Ouyang, X. A daylength recognition model of photoperiodic flowering. *Front. Plant Sci.* **2021**, *12*, 778515. [CrossRef] [PubMed]
119. Wang, F.; Han, T.; Jeffrey Chen, Z. Circadian and photoperiodic regulation of the vegetative to reproductive transition in plants. *Commun. Biol.* **2024**, *7*, 579. [CrossRef]
120. Liu, L.; Xuan, L.; Jiang, Y.; Yu, H. Regulation by FLOWERING LOCUS T and TERMINAL FLOWER 1 in flowering time and plant architecture. *Small Struct.* **2021**, *2*, 2000125. [CrossRef]
121. Oda, A.; Higuchi, Y.; Hisamatsu, T. Constitutive expression of CsGI alters critical night length for flowering by changing the photo-sensitive phase of anti-florigen induction in chrysanthemum. *Plant Sci.* **2020**, *293*, 110417. [CrossRef]
122. Colleoni, P.E.; van Es, S.W.; Winkelmolen, T.; Immink, R.G.; van Esse, G.W. Flowering time genes branching out. *J. Exp. Bot.* **2024**, *75*, 4195–4209. [CrossRef] [PubMed]
123. Lebedeva, M.; Dodueva, I.; Gancheva, M.; Tvorogova, V.; Kuznetsova, K.; Lutova, L. The Evolutionary Aspects of Flowering Control: Florigens and Anti-Florigens. *Russ. J. Genet.* **2020**, *56*, 1323–1344. [CrossRef]
124. Komiya, R.; Ikegami, A.; Tamaki, S.; Yokoi, S.; Shimamoto, K. Hd3a and RFT1 are essential for flowering in rice. *Development* **2008**, *135*, 767–774. [CrossRef]
125. Tamaki, S.; Matsuo, S.; Wong, H.L.; Yokoi, S.; Shimamoto, K. Hd3a protein is a mobile flowering signal in rice. *Science* **2007**, *316*, 1033–1036. [CrossRef] [PubMed]
126. Liu, H.; Yu, X.; Li, K.; Klejnot, J.; Yang, H.; Lisiero, D.; Lin, C. Photoexcited CRY2 interacts with CIB1 to regulate transcription and floral initiation in Arabidopsis. *Science* **2008**, *322*, 1535–1539. [CrossRef]
127. Prisca, M.; Maarten, V.; Bart, N.; Wouter, S.; Timo, H. Blue and far-red light control flowering time of woodland strawberry (Fragaria vesca) distinctively via CONSTANS (CO) and FLOWERING LOCUS T1 (FT1) in the background of sunlight mimicking radiation. *Environ. Exp. Bot.* **2022**, *198*, 104866. [CrossRef]
128. Magar, Y.; Ohyama, K.; Noguchi, A.; Amaki, W.; Furufuji, S. Effects of light quality during supplemental lighting on the flowering in an everbearing strawberry. *Acta Hortic.* **2018**, *1206*, 279–284. [CrossRef]

129. Nie, W.; Li, Y.; Chen, Y.; Zhou, Y.; Yu, T.; Zhou, Y.; Yang, Y. Spectral light quality regulates the morphogenesis, architecture, and flowering in pepper (*Capsicum annuum* L.). *J. Photochem. Photobiol. B Biol.* **2023**, *241*, 112673. [CrossRef]
130. Ishikawa, R.; Shinomura, T.; Takano, M.; Shimamoto, K. Phytochrome dependent quantitative control of Hd3a transcription is the basis of the night break effect in rice flowering. *Genes Genet. Syst.* **2009**, *84*, 179–184. [CrossRef]
131. Itoh, H.; Nonoue, Y.; Yano, M.; Izawa, T. A pair of floral regulators sets critical day length for Hd3a florigen expression in rice. *Nat. Genet.* **2010**, *42*, 635–638. [CrossRef]
132. Tsukamoto, A.; Hirai, T.; Chin, D.P.; Mii, M.; Mizoguchi, T.; Mizuta, D.; Yoshida, H.; Olsen, J.E.; Ezura, H.; Fukuda, N. The FT-like gene PehFT in petunia responds to photoperiod and light quality but is not the main gene promoting light quality-associated flowering. *Plant Biotechnol.* **2016**, *33*, 297–307. [CrossRef] [PubMed]
133. Wu, L.; Marcelis, L.F.; Kong, F.; Zhu, Y. Flowering time control in agricultural and horticultural crops. *Front. Plant Sci.* **2023**, *14*, 1116197.
134. Sohail, A. Genetic and signaling pathways of flowering regulation in rice (*Oryza sativa* L.). *Braz. J. Bot.* **2023**, *46*, 599–608. [CrossRef]
135. Shibuya, T.; Takahashi, T.; Hashimoto, S.; Nishiyama, M.; Kanayama, Y. Effects of overnight radiation with monochromatic far-red and blue light on flower budding and expression of flowering-related and light quality-responsive genes in Eustoma grandiflorum. *J. Agric. Meteorol.* **2019**, *75*, 160–165. [CrossRef]
136. Preston, J.C.; Hileman, L.C. Functional evolution in the plant SQUAMOSA-PROMOTER BINDING PROTEIN-LIKE (SPL) gene family. *Front. Plant Sci.* **2013**, *4*, 80. [CrossRef] [PubMed]
137. Osnato, M.; Cota, I.; Nebhnani, P.; Cereijo, U.; Pelaz, S. Photoperiod control of plant growth: Flowering time genes beyond flowering. *Front. Plant Sci.* **2022**, *12*, 805635. [CrossRef]
138. Wang, Y.; Severing, E.I.; Koornneef, M.; Aarts, M.G. FLC and SVP are key regulators of flowering time in the biennial/perennial species Noccaea caerulescens. *Front. Plant Sci.* **2020**, *11*, 582577. [CrossRef] [PubMed]
139. Liu, S.; Vasupalli, N.; Hou, D.; Lin, X. Ectopic expression of a bamboo SVP-like gene alters flowering time and floral organs in *Arabidopsis thaliana*. *Plant Cell Tissue Organ Cult.* **2022**, *150*, 721–732. [CrossRef]
140. Higuchi, Y. Florigen and anti-florigen: Flowering regulation in horticultural crops. *Breed. Sci.* **2018**, *68*, 109–118. [CrossRef]
141. Higuchi, Y.; Narumi, T.; Oda, A.; Nakano, Y.; Sumitomo, K.; Fukai, S.; Hisamatsu, T. The gated induction system of a systemic floral inhibitor, antiflorigen, determines obligate short-day flowering in chrysanthemums. *Proc. Natl. Acad. Sci. USA* **2013**, *110*, 17137–17142. [CrossRef]
142. Rantanen, M.; Kurokura, T.; Mouhu, K.; Pinho, P.; Tetri, E.; Halonen, L.; Palonen, P.; Elomaa, P.; Hytönen, T. Light quality regulates flowering in FvFT1/FvTFL1 dependent manner in the woodland strawberry Fragaria vesca. *Front. Plant Sci.* **2014**, *5*, 271. [CrossRef]
143. Zhu, Y.; Klasfeld, S.; Wagner, D. Molecular regulation of plant developmental transitions and plant architecture via PEPB family proteins: An update on mechanism of action. *J. Exp. Bot.* **2021**, *72*, 2301–2311. [CrossRef] [PubMed]
144. Kaneko-Suzuki, M.; Kurihara-Ishikawa, R.; Okushita-Terakawa, C.; Kojima, C.; Nagano-Fujiwara, M.; Ohki, I.; Tsuji, H.; Shimamoto, K.; Taoka, K.-I. TFL1-like proteins in rice antagonize rice FT-like protein in inflorescence development by competition for complex formation with 14-3-3 and FD. *Plant Cell Physiol.* **2018**, *59*, 458–468. [CrossRef] [PubMed]
145. Wang, S.; Yang, Y.; Chen, F.; Jiang, J. Functional diversification and molecular mechanisms of FLOWERING LOCUS T/TERMINAL FLOWER 1 family genes in horticultural plants. *Mol. Hortic.* **2022**, *2*, 19. [CrossRef] [PubMed]
146. Yang, J.; Song, J.; Jeong, B.R. Flowering and runnering of seasonal strawberry under different photoperiods are affected by intensity of supplemental or night-interrupting blue light. *Plants* **2024**, *13*, 375. [CrossRef]
147. Yang, J.; Song, J.; Jeong, B.R. Low-intensity blue light supplemented during photoperiod in controlled environment induces flowering and antioxidant production in kalanchoe. *Antioxidants* **2022**, *11*, 811. [CrossRef]
148. Yang, J.; Song, J.; Park, Y.G.; Jeong, B.R. Both the Positioned Supplemental or Night-Interruptional Blue Light and the Age of Leaves (or Tissues) Are Important for Flowering and Vegetative Growth in Chrysanthemum. *Plants* **2024**, *13*, 2874. [CrossRef]
149. YAMAZAKI, K.; ISHII, Y.; MATSUI, S.; TANAKA, I. Effects of light quality, daylength and growing temperature on flowering in morning glory (Pharbitis nil Choisy). *Environ. Control Biol.* **2003**, *41*, 211–219. [CrossRef]
150. Yuan, J.; Ott, T.; Hiltbrunner, A. Phytochromes and flowering: Legumes do it another way. *Trends Plant Sci.* **2023**, *28*, 379–381. [CrossRef]
151. Sawa, M.; Kay, S.A.; Imaizumi, T. Photoperiodic flowering occurs under internal and external coincidence. *Plant Signal. Behav.* **2008**, *3*, 269–271. [CrossRef]
152. Lin, X.; Dong, L.; Tang, Y.; Li, H.; Cheng, Q.; Li, H.; Zhang, T.; Ma, L.; Xiang, H.; Chen, L. Novel and multifaceted regulations of photoperiodic flowering by phytochrome A in soybean. *Proc. Natl. Acad. Sci. USA* **2022**, *119*, e2208708119. [CrossRef]
153. Yu, J.-W.; Rubio, V.; Lee, N.-Y.; Bai, S.; Lee, S.-Y.; Kim, S.-S.; Liu, L.; Zhang, Y.; Irigoyen, M.L.; Sullivan, J.A. COP1 and ELF3 control circadian function and photoperiodic flowering by regulating GI stability. *Mol. Cell* **2008**, *32*, 617–630. [CrossRef] [PubMed]

154. Yu, X.; Liu, H.; Klejnot, J.; Lin, C. The cryptochrome blue light receptors. *Arab. Book/Am. Soc. Plant Biol.* **2010**, *8*, e0135. [CrossRef] [PubMed]
155. Liu, Y.; Li, X.; Li, K.; Liu, H.; Lin, C. Multiple bHLH proteins form heterodimers to mediate CRY2-dependent regulation of flowering-time in Arabidopsis. *PLoS Genet.* **2013**, *9*, e1003861. [CrossRef] [PubMed]
156. Takagi, H.; Hempton, A.K.; Imaizumi, T. Photoperiodic flowering in Arabidopsis: Multilayered regulatory mechanisms of CONSTANS and the florigen FLOWERING LOCUS T. *Plant Commun.* **2023**, *4*, 100552. [CrossRef]
157. Romero, J.M.; Serrano-Bueno, G.; Camacho-Fernández, C.; Vicente, M.H.; Ruiz, M.T.; Pérez-Castiñeira, J.R.; Pérez-Hormaeche, J.; Nogueira, F.T.; Valverde, F. CONSTANS, a HUB for all seasons: How photoperiod pervades plant physiology regulatory circuits. *Plant Cell* **2024**, *36*, 2086–2102. [CrossRef]
158. Ni, M. Integration of light signaling with photoperiodic flowering and circadian rhythm. *Cell Res.* **2005**, *15*, 559–566. [CrossRef]
159. Renau-Morata, B.; Carrillo, L.; Dominguez-Figueroa, J.; Vicente-Carbajosa, J.; Molina, R.V.; Nebauer, S.G.; Medina, J. CDF transcription factors: Plant regulators to deal with extreme environmental conditions. *J. Exp. Bot.* **2020**, *71*, 3803–3815. [CrossRef]
160. Ye, Y.; Liu, Y.; Li, X.; Chen, Q.; Zhang, Y.; Luo, Y.; Liu, Z.; Wang, Y.; Lin, Y.; Zhang, Y. Transcriptome profile analysis of strawberry leaves reveals flowering regulation under blue light treatment. *Int. J. Genom.* **2021**, *2021*, 1–18. [CrossRef]
161. Goralogia, G.S.; Liu, T.K.; Zhao, L.; Panipinto, P.M.; Groover, E.D.; Bains, Y.S.; Imaizumi, T. CYCLING DOF FACTOR 1 represses transcription through the TOPLESS co-repressor to control photoperiodic flowering in Arabidopsis. *Plant J.* **2017**, *92*, 244–262. [CrossRef]
162. Liu, L.; Xie, Y.; Yahaya, B.S.; Wu, F. GIGANTEA Unveiled: Exploring Its Diverse Roles and Mechanisms. *Genes* **2024**, *15*, 94. [CrossRef] [PubMed]
163. Yang, M.; Lin, W.; Xu, Y.; Xie, B.; Yu, B.; Chen, L.; Huang, W. Flowering-time regulation by the circadian clock: From Arabidopsis to crops. *Crop J.* **2024**, *12*, 17–27. [CrossRef]
164. Jung, J.-H.; Seo, Y.-H.; Seo, P.J.; Reyes, J.L.; Yun, J.; Chua, N.-H.; Park, C.-M. The GIGANTEA-regulated microRNA172 mediates photoperiodic flowering independent of CONSTANS in Arabidopsis. *Plant Cell* **2007**, *19*, 2736–2748. [CrossRef] [PubMed]
165. Aukerman, M.J.; Sakai, H. Regulation of flowering time and floral organ identity by a microRNA and its APETALA2-like target genes. *Plant Cell* **2003**, *15*, 2730–2741. [CrossRef]
166. Hayama, R.; Sarid-Krebs, L.; Richter, R.; Fernández, V.; Jang, S.; Coupland, G. PSEUDO RESPONSE REGULATORs stabilize CONSTANS protein to promote flowering in response to day length. *EMBO J.* **2017**, *36*, 904–918. [CrossRef]
167. Toda, Y.; Kudo, T.; Kinoshita, T.; Nakamichi, N. Evolutionary insight into the clock-associated PRR5 transcriptional network of flowering plants. *Sci. Rep.* **2019**, *9*, 2983. [CrossRef]
168. Zhu, X.; Wang, H. Revisiting the role and mechanism of ELF3 in circadian clock modulation. *Gene* **2024**, *913*, 148378. [CrossRef] [PubMed]
169. Imaizumi, T.; Kay, S.A. Photoperiodic control of flowering: Not only by coincidence. *Trends Plant Sci.* **2006**, *11*, 550–558. [CrossRef]
170. Oakenfull, R.J.; Davis, S.J. Shining a light on the Arabidopsis circadian clock. *Plant Cell Environ.* **2017**, *40*, 2571–2585. [CrossRef]
171. Zhao, H.; Xu, D.; Tian, T.; Kong, F.; Lin, K.; Gan, S.; Zhang, H.; Li, G. Molecular and functional dissection of EARLY-FLOWERING 3 (ELF3) and ELF4 in Arabidopsis. *Plant Sci.* **2021**, *303*, 110786. [CrossRef]
172. Ponnu, J.; Hoecker, U. Illuminating the COP1/SPA ubiquitin ligase: Fresh insights into its structure and functions during plant photomorphogenesis. *Front. Plant Sci.* **2021**, *12*, 662793. [CrossRef]
173. Song, Y.H.; Estrada, D.A.; Johnson, R.S.; Kim, S.K.; Lee, S.Y.; MacCoss, M.J.; Imaizumi, T. Distinct roles of FKF1, GIGANTEA, and ZEITLUPE proteins in the regulation of CONSTANS stability in Arabidopsis photoperiodic flowering. *Proc. Natl. Acad. Sci. USA* **2014**, *111*, 17672–17677. [CrossRef]
174. Song, Y.H.; Smith, R.W.; To, B.J.; Millar, A.J.; Imaizumi, T. FKF1 conveys timing information for CONSTANS stabilization in photoperiodic flowering. *Science* **2012**, *336*, 1045–1049. [CrossRef] [PubMed]
175. Seaton, D.D.; Toledo-Ortiz, G.; Ganpudi, A.; Kubota, A.; Imaizumi, T.; Halliday, K.J. Dawn and photoperiod sensing by phytochrome A. *Proc. Natl. Acad. Sci. USA* **2018**, *115*, 10523–10528. [CrossRef] [PubMed]
176. Pedmale, U.V.; Huang, S.-s.C.; Zander, M.; Cole, B.J.; Hetzel, J.; Ljung, K.; Reis, P.A.; Sridevi, P.; Nito, K.; Nery, J.R. Cryptochromes interact directly with PIFs to control plant growth in limiting blue light. *Cell* **2016**, *164*, 233–245. [CrossRef]
177. Zhang, R.; Yang, C.; Jiang, Y.; Li, L. A PIF7-CONSTANS-centered molecular regulatory network underlying shade-accelerated flowering. *Mol. Plant* **2019**, *12*, 1587–1597. [CrossRef] [PubMed]
178. Kazan, K.; Manners, J.M. The interplay between light and jasmonate signalling during defence and development. *J. Exp. Bot.* **2011**, *62*, 4087–4100. [CrossRef]
179. Buti, S.; Hayes, S.; Pierik, R. The bHLH network underlying plant shade-avoidance. *Physiol. Plant.* **2020**, *169*, 312–324. [CrossRef]
180. Schwartz, C.; Lee, J.; Amasino, R. Variation in shade-induced flowering in Arabidopsis thaliana results from FLOWERING LOCUS T allelic variation. *PLoS ONE* **2017**, *12*, e0187768. [CrossRef]
181. Thomson, B.; Wellmer, F. Molecular regulation of flower development. *Curr. Top. Dev. Biol.* **2019**, *131*, 185–210.

182. Liu, Y.; Jafari, F.; Wang, H. Integration of light and hormone signaling pathways in the regulation of plant shade avoidance syndrome. *Abiotech* **2021**, *2*, 131–145. [CrossRef]
183. Freytes, S.N.; Canelo, M.; Cerdán, P.D. Regulation of flowering time: When and where? *Curr. Opin. Plant Biol.* **2021**, *63*, 102049. [CrossRef]
184. Jing, Y.; Guo, Q.; Zha, P.; Lin, R. The chromatin-remodelling factor PICKLE interacts with CONSTANS to promote flowering in Arabidopsis. *Plant Cell Environ.* **2019**, *42*, 2495–2507. [CrossRef] [PubMed]
185. Cerdán, P.D.; Chory, J. Regulation of flowering time by light quality. *Nature* **2003**, *423*, 881–885. [CrossRef] [PubMed]
186. Iñigo, S.; Alvarez, M.J.; Strasser, B.; Califano, A.; Cerdán, P.D. PFT1, the MED25 subunit of the plant Mediator complex, promotes flowering through CONSTANS dependent and independent mechanisms in Arabidopsis. *Plant J.* **2012**, *69*, 601–612. [CrossRef] [PubMed]
187. Siddiqui, H.; Khan, S.; Rhodes, B.M.; Devlin, P.F. FHY3 and FAR1 act downstream of light stable phytochromes. *Front. Plant Sci.* **2016**, *7*, 175. [CrossRef]
188. Xie, Y.; Zhou, Q.; Zhao, Y.; Li, Q.; Liu, Y.; Ma, M.; Wang, B.; Shen, R.; Zheng, Z.; Wang, H. FHY3 and FAR1 integrate light signals with the miR156-SPL module-mediated aging pathway to regulate Arabidopsis flowering. *Mol. Plant* **2020**, *13*, 483–498. [CrossRef]
189. Li, G.; Siddiqui, H.; Teng, Y.; Lin, R.; Wan, X.-y.; Li, J.; Lau, O.-S.; Ouyang, X.; Dai, M.; Wan, J. Coordinated transcriptional regulation underlying the circadian clock in Arabidopsis. *Nat. Cell Biol.* **2011**, *13*, 616–622. [CrossRef]
190. Qu, L.; Zhong, M.; Duan, F.; Li, X.; Yang, J.; Zhou, Q.; Tang, D.; He, R.; Liu, X.; Zhao, X. The PHYB–FOF2–VOZ2 module functions to fine-tune flowering in response to changes in light quality by modulating FLC expression in Arabidopsis. *Plant Commun.* **2024**, *5*, 100922. [CrossRef]
191. Wang, J.; Wang, Q.; Gao, J.; Lei, Y.; Zhang, J.; Zou, J.; Lu, Z.; Li, S.; Lei, N.; Dhungana, D. Genetic Regulatory Pathways of Plant Flowering Time Affected by Abiotic Stress. *Plant Stress* **2025**, *15*, 100747. [CrossRef]
192. Adams, S.; Pearson, S.; Hadley, P.; Patefield, W. The Effects of Temperature and Light Integral on the Phases of Photoperiod Sensitivity inPetunia× hybrida. *Ann. Bot.* **1999**, *83*, 263–269. [CrossRef]
193. Bernier, G.; Périlleux, C. A physiological overview of the genetics of flowering time control. *Plant Biotechnol. J.* **2005**, *3*, 3–16. [CrossRef] [PubMed]
194. Chen, J.; Zhou, G.; Dong, Y.; Qian, X.; Li, J.; Xu, X.; Huang, H.; Xu, L.; Li, L. Screening of key proteins affecting floral initiation of saffron under cold stress using iTRAQ-based proteomics. *Front. Plant Sci.* **2021**, *12*, 644934. [CrossRef] [PubMed]
195. Cho, L.H.; Yoon, J.; An, G. The control of flowering time by environmental factors. *Plant J.* **2017**, *90*, 708–719. [CrossRef]
196. Wingler, A. Transitioning to the next phase: The role of sugar signaling throughout the plant life cycle. *Plant Physiol.* **2018**, *176*, 1075–1084. [CrossRef]
197. Modarelli, G.C.; Arena, C.; Pesce, G.; Dell'Aversana, E.; Fusco, G.M.; Carillo, P.; De Pascale, S.; Paradiso, R. The role of light quality of photoperiodic lighting on photosynthesis, flowering and metabolic profiling in *Ranunculus asiaticus* L. *Physiol. Plant.* **2020**, *170*, 187–201. [CrossRef]
198. Lejeune, P.; Bernier, G.; Requier, M.-C.; Kinet, J.-M. Sucrose increase during floral induction in the phloem sap collected at the apical part of the shoot of the long-day plant *Sinapis alba* L. *Planta* **1993**, *190*, 71–74. [CrossRef]
199. Duplat-Bermúdez, L.; Ruiz-Medrano, R.; Landsman, D.; Mariño-Ramírez, L.; Xoconostle-Cázares, B. Transcriptomic analysis of Arabidopsis overexpressing flowering locus T driven by a meristem-specific promoter that induces early flowering. *Gene* **2016**, *587*, 120–131. [CrossRef]
200. Kolbe, A.; Tiessen, A.; Schluepmann, H.; Paul, M.; Ulrich, S.; Geigenberger, P. Trehalose 6-phosphate regulates starch synthesis via posttranslational redox activation of ADP-glucose pyrophosphorylase. *Proc. Natl. Acad. Sci. USA* **2005**, *102*, 11118–11123. [CrossRef]
201. Wahl, V.; Ponnu, J.; Schlereth, A.; Arrivault, S.; Langenecker, T.; Franke, A.; Feil, R.; Lunn, J.E.; Stitt, M.; Schmid, M. Regulation of flowering by trehalose-6-phosphate signaling in *Arabidopsis thaliana*. *Science* **2013**, *339*, 704–707. [CrossRef]
202. Ortiz-Marchena, M.I.; Albi, T.; Lucas-Reina, E.; Said, F.E.; Romero-Campero, F.J.; Cano, B.; Ruiz, M.T.; Romero, J.M.; Valverde, F. Photoperiodic control of carbon distribution during the floral transition in Arabidopsis. *Plant Cell* **2014**, *26*, 565–584. [CrossRef] [PubMed]
203. Ortiz-Marchena, M.I.; Romero, J.M.; Valverde, F. Photoperiodic control of sugar release during the floral transition: What is the role of sugars in the florigenic signal? *Plant Signal. Behav.* **2015**, *10*, e1017168. [CrossRef] [PubMed]
204. Yang, J.; Song, J.; Jeong, B.R. The flowering of SDP chrysanthemum in response to intensity of supplemental or night-interruptional blue light is modulated by both photosynthetic carbon assimilation and photoreceptor-mediated regulation. *Front. Plant Sci.* **2022**, *13*, 981143. [CrossRef] [PubMed]
205. Sun, J.; Wang, H.; Ren, L.; Chen, S.; Chen, F.; Jiang, J. CmFTL2 is involved in the photoperiod-and sucrose-mediated control of flowering time in chrysanthemum. *Hortic. Res.* **2017**, *4*, 17001. [CrossRef]

206. Luccioni, L.; Krzymuski, M.; Sánchez-Lamas, M.; Karayekov, E.; Cerdán, P.D.; Casal, J.J. CONSTANS delays Arabidopsis flowering under short days. *Plant J.* **2019**, *97*, 923–932. [CrossRef]
207. Wang, S.; Liu, X.; Liu, X.; Xue, J.; Ren, X.; Zhai, Y.; Zhang, X. The red/blue light ratios from light-emitting diodes affect growth and flower quality of hippeastrum hybridum 'red lion'. *Front. Plant Sci.* **2022**, *13*, 1048770. [CrossRef]
208. Lee, B.-D.; Kim, M.R.; Kang, M.-Y.; Cha, J.-Y.; Han, S.-H.; Nawkar, G.M.; Sakuraba, Y.; Lee, S.Y.; Imaizumi, T.; McClung, C.R. The F-box protein FKF1 inhibits dimerization of COP1 in the control of photoperiodic flowering. *Nat. Commun.* **2017**, *8*, 2259. [CrossRef]
209. Zhang, B.; Wang, L.; Zeng, L.; Zhang, C.; Ma, H. Arabidopsis TOE proteins convey a photoperiodic signal to antagonize CONSTANS and regulate flowering time. *Genes Dev.* **2015**, *29*, 975–987. [CrossRef]
210. Song, Y.H.; Shim, J.S.; Kinmonth-Schultz, H.A.; Imaizumi, T. Photoperiodic flowering: Time measurement mechanisms in leaves. *Annu. Rev. Plant Biol.* **2015**, *66*, 441–464. [CrossRef]
211. Hajdu, A.; Dobos, O.; Domijan, M.; Bálint, B.; Nagy, I.; Nagy, F.; Kozma-Bognár, L. ELONGATED HYPOCOTYL 5 mediates blue light signalling to the Arabidopsis circadian clock. *Plant J.* **2018**, *96*, 1242–1254. [CrossRef]
212. Bao, Y.; Liu, X.; Feng, C.-H.; Niu, M.-X.; Liu, C.; Wang, H.-L.; Yin, W.; Xia, X. Light and Light Signals Regulate Growth and Development in Woody Plants. *Forests* **2024**, *15*, 523. [CrossRef]
213. Dwivedi, S.L.; Quiroz, L.F.; Spillane, C.; Wu, R.; Mattoo, A.K.; Ortiz, R. Unlocking allelic variation in circadian clock genes to develop environmentally robust and productive crops. *Planta* **2024**, *259*, 72. [CrossRef] [PubMed]
214. He, Y.; Yu, Y.; Wang, X.; Qin, Y.; Su, C.; Wang, L. Aschoff's rule on circadian rhythms orchestrated by blue light sensor CRY2 and clock component PRR9. *Nat. Commun.* **2022**, *13*, 5869. [CrossRef]
215. Putterill, J. Flowering in time: Genes controlling photoperiodic flowering in Arabidopsis. *Philos. Trans. R. Soc. London Ser. B* **2001**, *356*, 1761. [CrossRef] [PubMed]
216. Li, X.; Ma, D.; Lu, S.X.; Hu, X.; Huang, R.; Liang, T.; Xu, T.; Tobin, E.M.; Liu, H. Blue light-and low temperature-regulated COR27 and COR28 play roles in the Arabidopsis circadian clock. *Plant Cell* **2016**, *28*, 2755–2769. [CrossRef]
217. Kim, W.-Y.; Fujiwara, S.; Suh, S.-S.; Kim, J.; Kim, Y.; Han, L.; David, K.; Putterill, J.; Nam, H.G.; Somers, D.E. ZEITLUPE is a circadian photoreceptor stabilized by GIGANTEA in blue light. *Nature* **2007**, *449*, 356–360. [CrossRef]
218. Roeber, V.M.; Schmülling, T.; Cortleven, A. The photoperiod: Handling and causing stress in plants. *Front. Plant Sci.* **2022**, *12*, 781988. [CrossRef]
219. Sawa, M.; Nusinow, D.A.; Kay, S.A.; Imaizumi, T. FKF1 and GIGANTEA complex formation is required for day-length measurement in Arabidopsis. *Science* **2007**, *318*, 261–265. [CrossRef]
220. Fujiwara, S.; Oda, A.; Yoshida, R.; Niinuma, K.; Miyata, K.; Tomozoe, Y.; Tajima, T.; Nakagawa, M.; Hayashi, K.; Coupland, G. Circadian clock proteins LHY and CCA1 regulate SVP protein accumulation to control flowering in Arabidopsis. *Plant Cell* **2008**, *20*, 2960–2971. [CrossRef]
221. Izawa, T. What is going on with the hormonal control of flowering in plants? *Plant J.* **2021**, *105*, 431–445. [CrossRef]
222. Farré, E.M.; Harmer, S.L.; Harmon, F.G.; Yanovsky, M.J.; Kay, S.A. Overlapping and distinct roles of PRR7 and PRR9 in the Arabidopsis circadian clock. *Curr. Biol.* **2005**, *15*, 47–54. [CrossRef]
223. Covington, M.F.; Panda, S.; Liu, X.L.; Strayer, C.A.; Wagner, D.R.; Kay, S.A. ELF3 modulates resetting of the circadian clock in Arabidopsis. *Plant Cell* **2001**, *13*, 1305–1316. [CrossRef]
224. Huang, H.; Alvarez, S.; Bindbeutel, R.; Shen, Z.; Naldrett, M.J.; Evans, B.S.; Briggs, S.P.; Hicks, L.M.; Kay, S.A.; Nusinow, D.A. Identification of evening complex associated proteins in Arabidopsis by affinity purification and mass spectrometry. *Mol. Cell. Proteom.* **2016**, *15*, 201–217. [CrossRef] [PubMed]
225. Ronald, J. Extrinsic and Intrinsic Factors Regulate the Spatio-Temporal Localisation of the Arabidopsis Circadian Component ELF3. Doctoral Thesis, University of York, York, UK, 2021.
226. Balcerowicz, M.; Kerner, K.; Schenkel, C.; Hoecker, U. SPA proteins affect the subcellular localization of COP1 in the COP1/SPA ubiquitin ligase complex during photomorphogenesis. *Plant Physiol.* **2017**, *174*, 1314–1321. [CrossRef]
227. Zhang, L.; Li, T.; Su, S.; Peng, H.; Li, S.; Li, K.; Ji, L.; Xing, Y.; Zhang, J.; Du, X. Functions of COP1/SPA E3 ubiquitin ligase mediated by MpCRY in the liverwort Marchantia polymorpha under blue light. *Int. J. Mol. Sci.* **2021**, *23*, 158. [CrossRef] [PubMed]
228. Liu, Y.; Li, X.; Ma, D.; Chen, Z.; Wang, J.W.; Liu, H. CIB 1 and CO interact to mediate CRY 2-dependent regulation of flowering. *EMBO Rep.* **2018**, *19*, e45762. [CrossRef]
229. Leivar, P.; Monte, E. PIFs: Systems integrators in plant development. *Plant Cell* **2014**, *26*, 56–78. [CrossRef]
230. Sharma, A.; Samtani, H.; Sahu, K.; Sharma, A.K.; Khurana, J.P.; Khurana, P. Functions of Phytochrome-Interacting Factors (PIFs) in the regulation of plant growth and development: A comprehensive review. *Int. J. Biol. Macromol.* **2023**, *244*, 125234. [CrossRef]
231. Sakuraba, Y.; Kim, E.-Y.; Han, S.-H.; Piao, W.; An, G.; Todaka, D.; Yamaguchi-Shinozaki, K.; Paek, N.-C. Rice Phytochrome-Interacting Factor-Like1 (OsPIL1) is involved in the promotion of chlorophyll biosynthesis through feed-forward regulatory loops. *J. Exp. Bot.* **2017**, *68*, 4103–4114. [CrossRef]

232. Ammari, M.; Maseh, K.; Zander, M. PIF transcription factors-versatile plant epigenome landscapers. *Front. Epigenet. Epigenom.* **2024**, *2*, 1404958. [CrossRef]
233. Wu, M.; Liu, D.; Abdul, W.; Upreti, S.; Liu, Y.; Song, G.; Wu, J.; Liu, B.; Gan, Y. PIL5 represses floral transition in Arabidopsis under long day conditions. *Biochem. Biophys. Res. Commun.* **2018**, *499*, 513–518. [CrossRef]
234. Castillon, A.; Shen, H.; Huq, E. Blue light induces degradation of the negative regulator phytochrome interacting factor 1 to promote photomorphogenic development of Arabidopsis seedlings. *Genetics* **2009**, *182*, 161–171. [CrossRef]
235. Leivar, P.; Quail, P.H. PIFs: Pivotal components in a cellular signaling hub. *Trends Plant Sci.* **2011**, *16*, 19–28. [CrossRef] [PubMed]
236. Bhatnagar, A.; Singh, S.; Khurana, J.P.; Burman, N. HY5-COP1: The central module of light signaling pathway. *J. Plant Biochem. Biotechnol.* **2020**, *29*, 590–610. [CrossRef]
237. Liu, S.; He, M.; Lin, X.; Kong, F. Epigenetic regulation of photoperiodic flowering in plants. *Plant Genome* **2023**, *16*, e20320. [CrossRef]
238. Chu, L.; Yang, C.; Zhuang, F.; Gao, Y.; Luo, M. The HDA9-HY5 module epigenetically regulates flowering time in Arabidopsis thaliana. *J. Cell. Physiol.* **2022**, *237*, 2961–2968. [CrossRef] [PubMed]
239. Kang, X.; Zhou, Y.; Sun, X.; Ni, M. Hypersensitive to red and blue 1 and its C-terminal regulatory function control flowering locus T expression. *Plant J.* **2007**, *52*, 937–948. [CrossRef]
240. Du, S.; Li, L.; Li, L.; Wei, X.; Xu, F.; Xu, P.; Wang, W.; Xu, P.; Cao, X.; Miao, L. Photoexcited cryptochrome2 interacts directly with TOE1 and TOE2 in flowering regulation. *Plant Physiol.* **2020**, *184*, 487–505. [CrossRef]
241. Song, Z.; Bian, Y.; Xiao, Y.; Xu, D. B-BOX proteins: Multi-layered roles of molecular cogs in light-mediated growth and development in plants. *J. Plant Physiol.* **2024**, *299*, 154265. [CrossRef]
242. Xu, X.; Xu, J.; Yuan, C.; Chen, Q.; Liu, Q.; Wang, X.; Qin, C. BBX17 interacts with CO and negatively regulates flowering time in Arabidopsis thaliana. *Plant Cell Physiol.* **2022**, *63*, 401–409. [CrossRef]
243. Graeff, M.; Straub, D.; Eguen, T.; Dolde, U.; Rodrigues, V.; Brandt, R.; Wenkel, S. MicroProtein-mediated recruitment of CONSTANS into a TOPLESS trimeric complex represses flowering in Arabidopsis. *PLoS Genet.* **2016**, *12*, e1005959. [CrossRef] [PubMed]
244. Li, Y.; Shi, Y.; Li, M.; Fu, D.; Wu, S.; Li, J.; Gong, Z.; Liu, H.; Yang, S. The CRY2–COP1–HY5–BBX7/8 module regulates blue light-dependent cold acclimation in Arabidopsis. *Plant Cell* **2021**, *33*, 3555–3573. [CrossRef]
245. Jung, C.; Müller, A.E. Flowering time control and applications in plant breeding. *Trends Plant Sci.* **2009**, *14*, 563–573. [CrossRef]
246. Yang, J.; Song, J.; Jeong, B.R. Blue light supplemented at intervals in long-day conditions intervenes in photoperiodic flowering, photosynthesis, and antioxidant properties in chrysanthemums. *Antioxidants* **2022**, *11*, 2310. [CrossRef]
247. Kohler, A.E.; Birtell, E.M.; Runkle, E.S.; Meng, Q. Day-extension Blue Light Inhibits Flowering of Chrysanthemum When the Short Main Photoperiod Includes Far-red Light. *J. Am. Soc. Hortic. Sci.* **2023**, *148*, 89–98. [CrossRef]
248. SharathKumar, M.; Luo, J.; Xi, Y.; van Ieperen, W.; Marcelis, L.F.; Heuvelink, E. Several short-day species can flower under blue-extended long days, but this response is not universal. *Sci. Hortic.* **2024**, *325*, 112657. [CrossRef]
249. Fukuda, N.; Yoshida, T.; Olsen, J.; Senaha, C.; Jikumaru, Y.; Kamiya, Y. Short main shoot length and inhibition of floral bud development under red light can be recovered by application of gibberellin and cytokinin. *Acta Hortic.* **2012**, *956*, 215–222. [CrossRef]
250. Spaninks, K.; Van Lieshout, J.; Van Ieperen, W.; Offringa, R. Regulation of early plant development by red and blue light: A comparative analysis between Arabidopsis thaliana and Solanum lycopersicum. *Front. Plant Sci.* **2020**, *11*, 599982. [CrossRef]

Disclaimer/Publisher's Note: The statements, opinions and data contained in all publications are solely those of the individual author(s) and contributor(s) and not of MDPI and/or the editor(s). MDPI and/or the editor(s) disclaim responsibility for any injury to people or property resulting from any ideas, methods, instructions or products referred to in the content.

plants

MDPI

Article

The Involvement of the *S2P2* Intramembrane Protease in the Response of *Arabidopsis thaliana* Chloroplasts to High Light Stress

Maria Ciesielska, Małgorzata Adamiec and Robert Luciński *

Department of Plant Physiology, Institute of Experimental Biology, Faculty of Biology, Adam Mickiewicz University in Poznań, ul Uniwersytetu Poznańskiego 6, 61-614 Poznań, Poland;
maria.ciesielska1604@gmail.com (M.C.); msolin@amu.edu.pl (M.A.)
* Correspondence: rtl@amu.edu.pl

Abstract: High light intensity constitutes a critical abiotic stress factor that profoundly affects the structural and functional integrity of the photosynthetic apparatus. Excessive irradiance triggers accelerated degradation of the PsbA polypeptide, increases susceptibility to photoinhibition, and promotes overproduction of reactive oxygen species (ROS), thereby inducing oxidative damage to proteins, lipids, and nucleic acids. Among the chloroplast-localized site-2 proteases of *Arabidopsis thaliana*, *S2P2* remains the least characterized. In this study, our analyses revealed a pronounced upregulation of the *S2P2* (AT1G05140) gene and a concomitant accumulation of the *S2P2* protein under high light conditions. Functional characterization using two independent *S2P2* insertional mutant lines lacking the protease demonstrated that loss of *S2P2* significantly exacerbates photoinhibition. Mutants exhibited reduced photosystem II (PSII) efficiency, accompanied by accelerated degradation of the PSII core proteins PsbA, PsbD, and PsbC, as well as elevated ROS generation. These findings provide the first direct evidence that *S2P2* plays a pivotal role in maintaining the stoichiometric balance of PSII core components and conferring resilience of the photosynthetic machinery to high light stress. This work expands the functional repertoire of chloroplast site-2 proteases and underscores *S2P2* as a potential target for improving stress tolerance in plants.

Keywords: high irradiance; intramembrane protease; photosystem II; photosynthesis; proteolysis; thylakoid

1. Introduction

The acclimation of plants to constantly changing environmental conditions requires the involvement of numerous precise regulatory mechanisms. One of the most fundamental among them is proteolysis. Proteases are involved, among other functions, in protein quality control and protein turnover processes. These mechanisms are relatively well understood and have been extensively described in the literature [1–5]. However, in recent years, a surprising novel process related to proteolytic activity has been discovered—regulated intramembrane proteolysis (RIP). This process is carried out by a highly specific group of proteolytic enzymes known as intramembrane proteases. These enzymes are transmembrane proteins that exhibit protease activity within the lipid bilayer of biological membranes. They are widely recognized for their role in the cleavage and release of membrane-anchored transcription factors from biological membranes [6–9]. To date, numerous enzymes belonging to various classes of intramembrane proteases have been identified (for details, see [9]).

In plant cells, the first identified intramembrane protease was the chloroplast-localized protein EGY1 (ethylene-dependent gravitropism deficient and yellow-green 1), which belongs to the site-2 protease (S2P) family [10]. The absence of this protease in *A. thaliana* cells results in numerous pleiotropic effects, the most characteristic of which are yellow-green leaf pigmentation and a deficiency in ethylene-dependent gravitropism. EGY1-deficient mutants exhibit a poorly developed internal membrane [10,11]. Moreover, EGY1 has been shown to participate in plant responses to ammonium and phosphate stresses [12,13].

In addition to EGY1, other S2Ps are also localized in the chloroplasts of *A. thaliana*, namely EGY2, AraSP, and *S2P2* [9]. EGY3, which is also present in the thylakoid membranes of chloroplasts, is closely related to EGY1 and EGY2; however, due to the absence of a key motif required for proteolytic activity, it is proteolytically inactive and is classified as a so-called pseudo-protease [9,14–16]. Within chloroplasts, all of the mentioned proteases—except AraSP—are localized in the thylakoid membranes [9,14,15,17]. AraSP is the only one found in the chloroplast envelope membranes [18].

The physiological roles and precise molecular mechanisms of action of S2Ps remain poorly understood. It has been shown that AraSP plays an essential role in chloroplast biogenesis and plant development. *A. thaliana* mutants lacking this protease are characterized by extremely small size, poorly developed root systems, reddish cotyledons, and a drastically shortened lifespan of less than 20 days [18]. However, the exact molecular mechanisms underlying these phenotypes have yet to be elucidated.

Similarly, *A. thaliana* mutants deficient in EGY2 display a number of phenotypic abnormalities, including shortened hypocotyls, reduced fatty acid content, and increased sensitivity to photoinhibition [14,19,20].

To date, virtually nothing is known about the protein substrates of chloroplast-localized S2Ps. Only our previous studies have indicated that the transcription factor pTAC16, which is also localized in the thylakoid membranes and is involved in interactions with the plastid-encoded RNA polymerase complex, may represent a natural substrate of EGY2 [20].

A substantial body of literature indicates the involvement of chloroplast-localized S2Ps—particularly EGY1 and EGY2—in the regulation of stoichiometric relationships between the polypeptides that constitute photosystem II (PSII) and its major light-harvesting antenna complex, LHCII [10,13,19–23]. The absence of either EGY1 or EGY2 in *A. thaliana* mutant cells is also associated with increased plant sensitivity to photoinhibition [19,20,23].

Among the chloroplast S2Ps, *S2P2* remains the least characterized. The *S2P2* (AT1G05140) gene exhibits a high level of expression in both cotyledons and mature leaves of *A. thaliana*, suggesting a potentially important role in chloroplast development and function [24]. *S2P2* has also been proposed to participate in the plant's response to cold stress [25]. Interestingly, until recently, the intrachloroplast localization of *S2P2* remained unknown. It was only through our recent study that *S2P2* was definitively localized to the thylakoid membranes, similarly to EGY1, EGY2, and the pseudo-protease EGY3 [16].

Moreover, we demonstrated that the loss of *S2P2* in *A. thaliana* leads to disruptions in chloroplast pigment content and reductions in the levels of core PSII polypeptides and LHCII trimers. *A. thaliana* mutants lacking *S2P2* showed decreased levels of PsbA, PsbC, and PsbD proteins, as well as the light-harvesting proteins Lhcb1 and Lhcb2. These changes were accompanied by a reduced abundance of PSII–LHCII supercomplexes under light-optimal conditions and a marked increase in sensitivity to photoinhibition [16].

Considering this information, we decided to investigate the involvement of the *S2P2* protease in the response of *A. thaliana* chloroplasts to high light (HL) stress. Specifically, we examined how the levels of key core PSII proteins—PsbA, PsbC, and PsbD—are affected during prolonged high light exposure, and how these changes influence PSII function. Our

results showed that *S2P2* gene expression is significantly induced in response to high light intensity, accompanied by an increase in the abundance of the *S2P2* protease.

Stress conditions are often associated with a marked increase in the accumulation of reactive oxygen species (ROS) within plant cells. According to the literature [26] and our previous work [19,22], *egy2* mutants exhibit significantly elevated ROS levels under stress conditions compared to wild-type (WT) plants. Based on the fact that *S2P2* also belongs to the chloroplast S2Ps, we decided to verify the hypothesis regarding the generation of increased amounts of ROS under high light stress conditions in *S2P2* mutants. This is the first report demonstrating that the absence of the *S2P2* protease leads to a substantial impairment of the photosynthetic apparatus in *A. thaliana* and causes excessive ROS production under high light conditions. These findings identify *S2P2* as an important additional component of the complex regulatory network responsible for chloroplast acclimation to fluctuating light environments.

2. Results

2.1. Changes in S2P2 Gene Expression and Protein Abundance in Response to High Light Stress in A. thaliana Leaves

Quantitative real-time PCR (qRT-PCR) was employed to assess the expression dynamics of the *S2P2* gene in response to high light stress. Four-week-old *A. thaliana* WT plants were exposed to high light intensity (1000 μmol m^{-2} s^{-1}) for 0, 3, 6, 12, and 24 h (Figure 1).

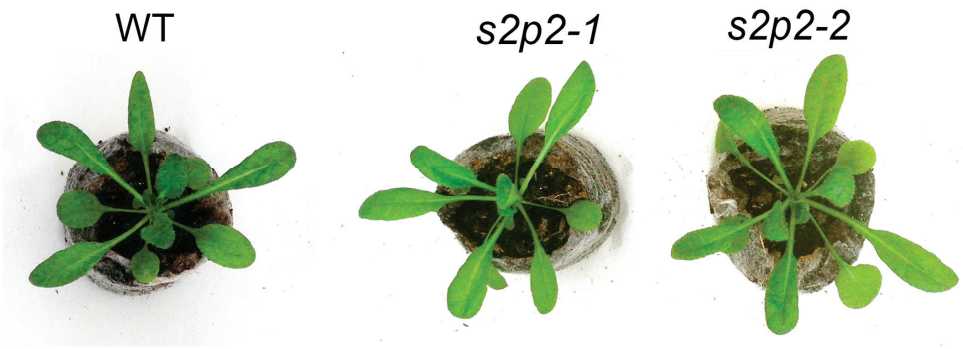


Figure 1. The 4-week old WT, *s2p2–1*, and *s2p2–2* mutant line plants.

A rapid and significant upregulation of *S2P2* transcript levels was observed as early as 3 h post-exposure, reaching approximately an 11-fold increase relative to the control (0 h). Between 3 and 6 h, *S2P2* expression increased by an additional ~30%. This elevated expression level remained relatively stable up to 12 h. After 24 h of high light exposure, *S2P2* transcript levels declined by approximately 50% compared to the peak level but remained above the baseline expression level observed under control light conditions (Figure 2).

The transcriptional activation of *S2P2* was accompanied by a corresponding increase in *S2P2* protein accumulation. Western blot analysis revealed that *S2P2* protein levels increased to over 180% of the initial level after 3 h of high light treatment. Continued exposure led to further accumulation, reaching approximately 275% of the control level at 6 h. Similar to transcript levels, *S2P2* protein abundance began to decline by 24 h, although it remained elevated compared to the control (Figure 3). These results indicate a strong correlation between *S2P2* gene expression and protein accumulation in response to high light stress.

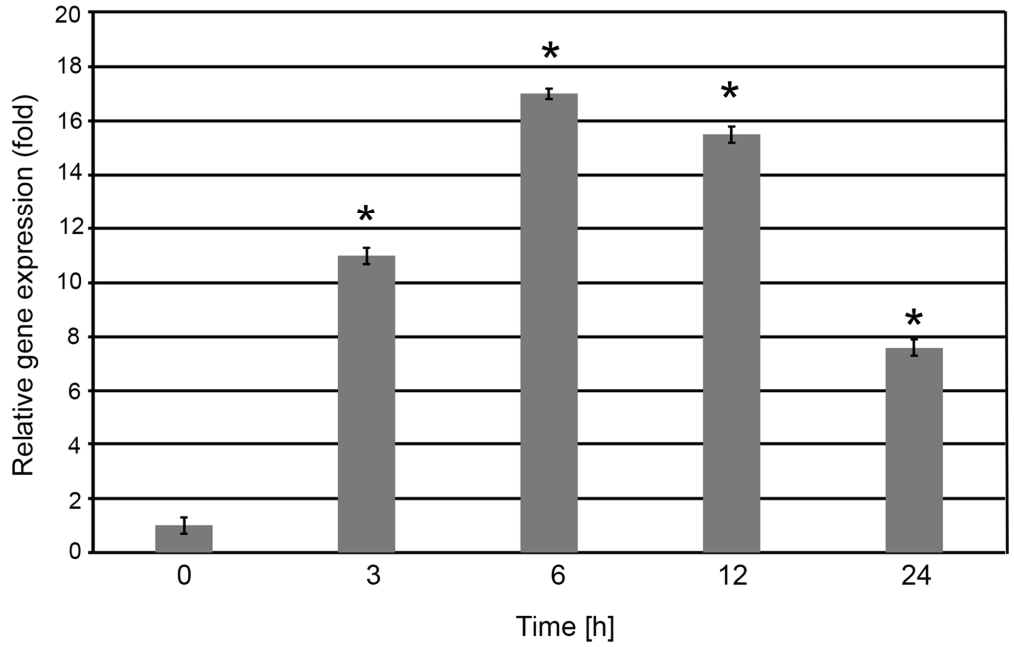


Figure 2. Relative expression of the *S2P2* gene in *A. thaliana* leaves exposed to high light conditions. Four-week-old wild-type *A. thaliana* plants were subjected to high light intensity (1000 μmol m^{-2} s^{-1}) for 0, 3, 6, 12, and 24 h. Following treatment, total RNA was extracted from leaf tissues and reverse-transcribed into complementary DNA (cDNA), which was subsequently used as a template for quantitative real-time PCR (qRT-PCR) analysis. Expression level of *S2P2* was normalized against the endogenous reference gene *CYP5*. Asterisks (*) indicate statistically significant changes compared to the 0 h base time value ($p < 0.05$).

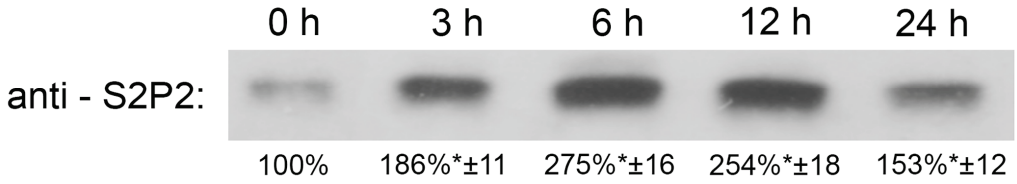


Figure 3. Immunoblot-based quantification of *S2P2* protein levels in wild-type *A. thaliana* exposed to high light. Wild-type *A. thaliana* plants were exposed to high light intensity (1000 μmol m^{-2} s^{-1}) for 0, 3, 6, 12, and 24 hours. Protein extracts from leaf tissues were subjected to immunoblot analysis to determine *S2P2* protein abundance. Protein concentration in extracts was determined according to the Lowry method. Before hybridization with antibodies, the membranes were transiently stained with Ponceu S to verify the transfer efficiency and control loading. The experiment was conducted using three independent biological replicates. Data are presented as mean ± standard deviation (s.d.). Asterisks (*) denote statistically significant differences related to the 0 h time point ($p < 0.05$).

2.2. Functional Status of Photosystem II in S2P2 Mutant Lines Under High Light Stress

To assess whether the loss of *S2P2* protease function affects PSII performance during the exposure of plants to excessive irradiance, we evaluated PSII activity in two independent *S2P2* mutant lines using pulse amplitude-modulated (PAM) chlorophyll fluorescence analysis. The parameters measured included minimum fluorescence yield (F_0), maximum quantum efficiency of PSII photochemistry (F_v/F_m), photochemical quenching (qP), and non-photochemical quenching (NPQ).

Given that the most pronounced upregulation of *S2P2* gene expression occurred within the first 6 h of high light exposure, functional measurements were conducted after 3 and 6 h of treatment at high irradiance (1000 μmol m^{-2} s^{-1}). Under control light conditions, both *S2P2* mutant lines exhibited elevated F_0 levels compared to WT plants. During high light

exposure, F_0 levels remained higher in the mutants, although the relative decline in F_0 appeared slightly more pronounced in *S2P2* mutant plants than in WT (Figure 4A).

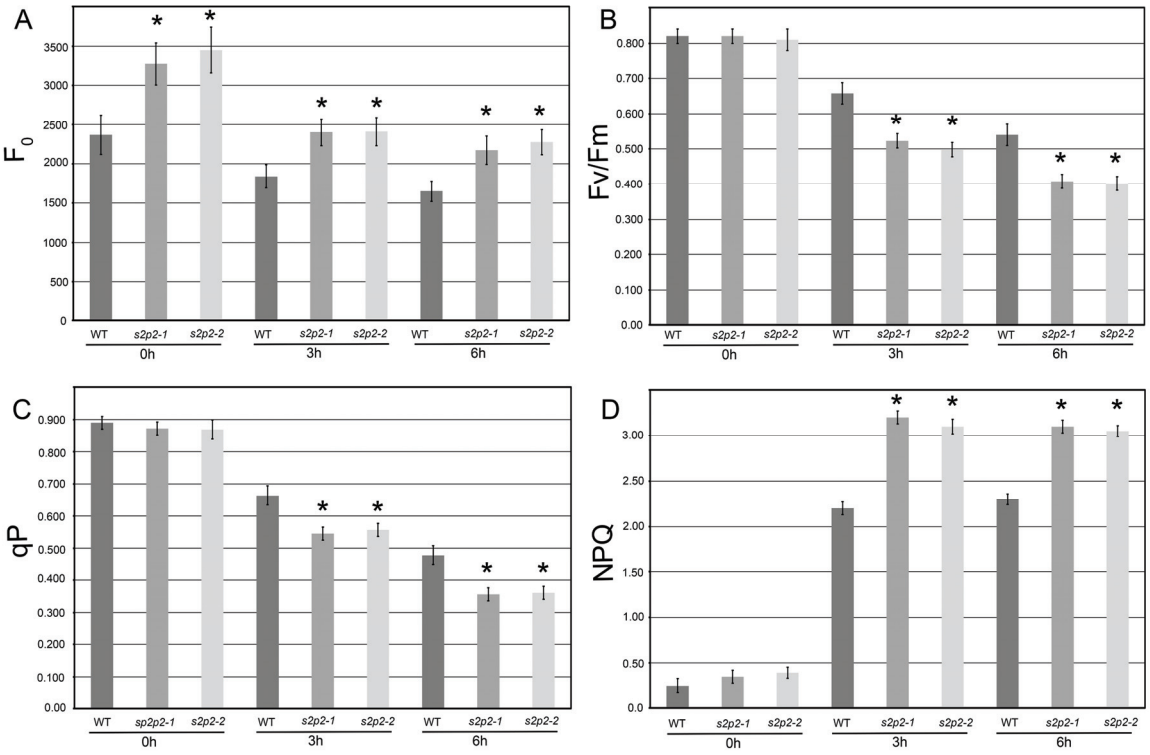


Figure 4. Chlorophyll *a* fluorescence parameters in wild-type and *S2P2* mutant lines under high light stress. Chlorophyll *a* fluorescence measurements were conducted in wild-type *A. thaliana* (WT) plants and *s2p2–1* and *s2p2–2* mutant lines following exposure to high light intensity (1000 μmol m^{-2} s^{-1}) for 0, 3, and 6 h. The following parameters were analyzed: (**A**) minimum fluorescence yield (F_0), (**B**) maximum quantum efficiency of PSII (F_v/F_m), (**C**) photochemical quenching (qP), and (**D**) non-photochemical quenching (NPQ). Actinic light intensity matched the pre-dark adaptation irradiance: 110 μmol m^{-2} s^{-1} for control conditions (0 h) and 1000 μmol m^{-2} s^{-1} for high light stress treatments (3 h and 6 h). Measurements were performed on 30 individual plants per genotype across three independent biological replicates. Data are presented as mean ± standard deviation (s.d.). Asterisks (*) indicate statistically significant differences between WT and mutant lines ($p \leq 0.05$).

Under standard light conditions, no significant differences were observed in qP, F_v/F_m, or NPQ between WT and mutant lines. However, following high light treatment, *S2P2* mutants showed a significantly greater reduction in both qP and F_v/F_m values compared to WT plants, indicating a higher susceptibility of PSII to photoinhibition in the absence of functional *S2P2* intramembrane protease (Figure 4B,C).

The NPQ parameter, indicative of thermal energy dissipation, increased markedly in all genotypes under high light. Notably, the *S2P2* mutant lines exhibited a stronger NPQ response, with an average increase of approximately 40% compared to WT after 3 h of high light exposure (Figure 4D).

2.3. Abundance of Selected PSII Core Proteins in S2P2 Mutant Lines Under High Light Stress

Given the functional impairments in PSII observed in *S2P2* mutant lines under high light stress (Figure 4), we hypothesized that these mutants would also exhibit altered accumulation of PSII core proteins in comparison to WT plants. Therefore, we assessed the levels of three essential PSII core polypeptides—PsbA (D1), PsbD (D2), and PsbC (CP43)—in *S2P2* mutants during high light stress.

As expected, exposure to high light conditions resulted in a significant decrease in PsbA protein levels in WT *A. thaliana* plants. Both *s2p2–1* and *s2p2–2* mutant lines also exhibited a pronounced reduction in PsbA levels after 3 and 6 h of high light treatment. However, the rate of decline was notably faster in the mutant lines compared to WT (Figure 5).

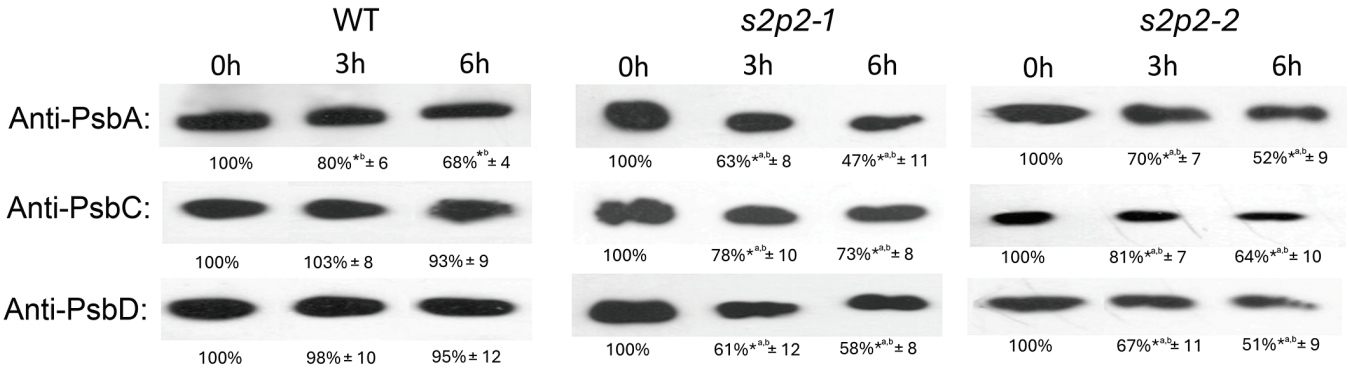


Figure 5. Immunoblot quantification of PsbA, PsbC, and PsbD proteins in wild-type and *S2P2* mutant lines under high light conditions. Protein levels of PsbA, PsbC, and PsbD were analyzed in wild-type *A. thaliana* (WT) plants and *s2p2–1* and *s2p2–2* mutant lines following exposure to high light intensity (1000 μmol m^{-2} s^{-1}). Thylakoid membrane proteins (2 μg), isolated from leaf tissues, were separated by SDS-PAGE and subjected to immunoblot analysis using protein-specific primary antibodies. Protein concentration in extracts was determined according to the Lowry method. Before hybridization with antibodies the membranes were transiently stained with Ponceu S to verify the transfer efficiency and control loading. Quantification of immunoblot signals was performed using GelixOne software. Signal intensities were normalized to the corresponding 0 h time point (set as 100%) for each genotype. The experiment included three independent biological replicates. Data are expressed as mean ± standard deviation (s.d.). ^{*a} denote statistically significant differences among treatments at identical time point; ^{*b} indicate statistically significant differences related to 0 h time point in each genotype ($p \leq 0.05$).

In contrast, a different pattern was observed for PsbD and PsbC polypeptides. While their levels remained relatively stable in WT plants during the high light exposure, both *S2P2* mutant lines showed a marked reduction in the abundance of these proteins. After 6 h of stress, PsbD levels in *S2P2* mutants had declined to approximately 50% of the initial value, while PsbC content was reduced to 65–70% (Figure 5).

2.4. Accumulation of Superoxide Anion Radical and Hydrogen Peroxide in S2P2 Mutants Under High Light Stress

It is well established that high irradiance induces enhanced production of ROS in chloroplasts. These ROS are major contributors to oxidative stress, rapidly leading to oxidative damage of proteins, including those constituting photosynthetic complexes within thylakoid membranes. This oxidative damage is associated with a decline in the efficiency of photosynthetic reactions and reduced performance of the photosystems. The changes observed in PSII functionality and the reduced abundance of PSII core proteins in *S2P2* mutants under high light stress prompted us to examine ROS accumulation in the leaves of these mutants.

To this end, we quantified the levels of both superoxide radical (Figure 6) and hydrogen peroxide (Figure 7) in response to high light exposure. Hydrogen peroxide content was measured using two independent approaches: a titanium-based assay and spectrophotometric quantification using 3,3′-diaminobenzidine (DAB). Both methods yielded consistent results.

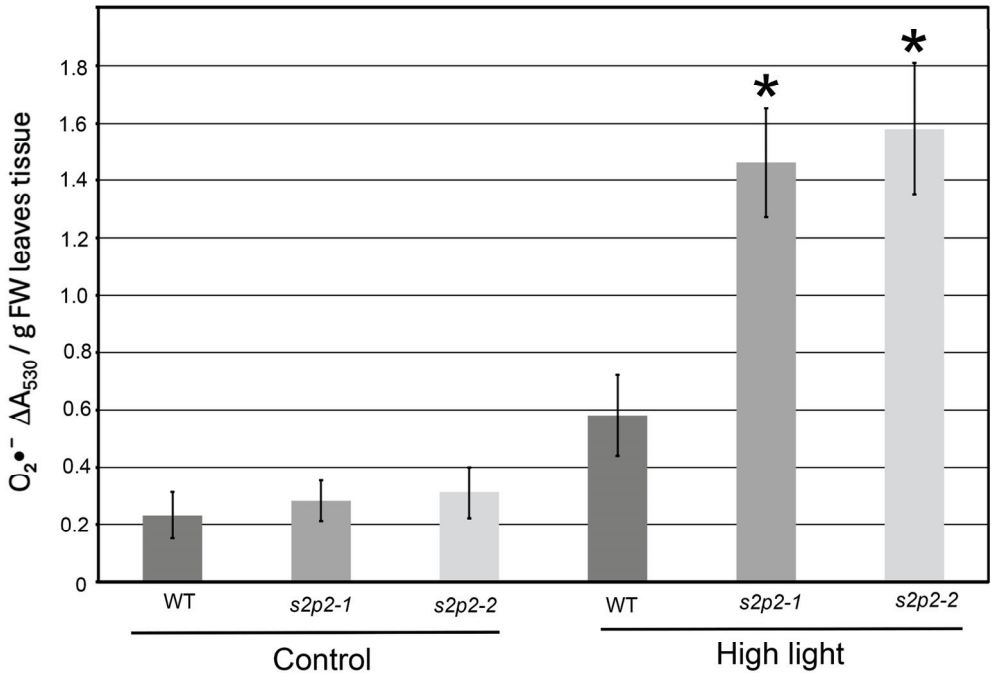


Figure 6. Superoxide radical accumulation in wild-type and *S2P2* mutant lines under high light stress. The accumulation of superoxide radicals ($O_2^{\bullet-}$) was evaluated in wild-type *A. thaliana* (WT) plants and *s2p2–1* and *s2p2–2* mutant lines following exposure to high light intensity (1000 µmol m^{-2} s^{-1}) based on the reduction in nitroblue tetrazolium (NBT). Quantitative data represent mean values from three independent biological replicates. Asterisks (*) indicate statistically significant differences between mutant lines and the wild-type plants ($p \leq 0.05$).

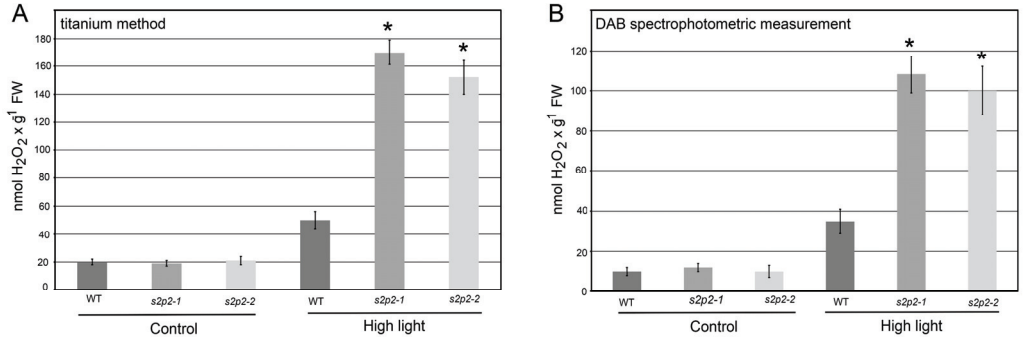


Figure 7. Hydrogen peroxide accumulation in wild-type and *S2P2* mutant lines following high light stress. Hydrogen peroxide (H_2O_2) accumulation was assessed in wild-type *A. thaliana* (WT) plants and *s2p2–1* and *s2p2–2* mutant lines after 3 h of exposure to high light conditions (1000 µmol m^{-2} s^{-1}). (**A**) Titanium (Ti^{4+}) staining method. (**B**) 3,3′-diaminobenzidine (DAB) staining spectrophotometric measurement. Results represent the mean values from three independent biological replicates, each comprising 30 plants. Asterisks (*) indicate statistically significant differences between mutant lines and the wild-type plants ($p \leq 0.05$).

Under non-stress conditions, ROS levels in both WT and *S2P2* mutant leaves were low and comparable. However, following a 3 h exposure to high light intensity, ROS accumulation in the *S2P2* mutants significantly exceeded that in WT plants. Specifically, the level of superoxide radical in *S2P2* mutant leaves was over 60% higher than in WT leaves (Figure 6), while hydrogen peroxide content was more than threefold higher in the mutants compared to WT (Figure 7).

2.5. Changes in the Abundance of Copper/Zinc Superoxide Dismutase 2 (CSD2) During High Light Stress

Given the markedly elevated levels of both superoxide radical and hydrogen peroxide observed in the leaves of *S2P2* mutants under high light stress, we investigated the accumulation of CSD2 in chloroplasts under these conditions, as it is a key enzyme scavenging the superoxide radical generated in chloroplasts.

After 3 h of exposure to high light intensity, the abundance of the CSD2 protein in the chloroplasts of both the *s2p2–1* and *s2p2–2* mutant lines was more than twofold higher than that observed in the chloroplasts of WT plants (Figure 8). This elevated CSD2 level in the mutants likely represents a compensatory response to increased oxidative stress and enhanced superoxide radical production under high irradiance.

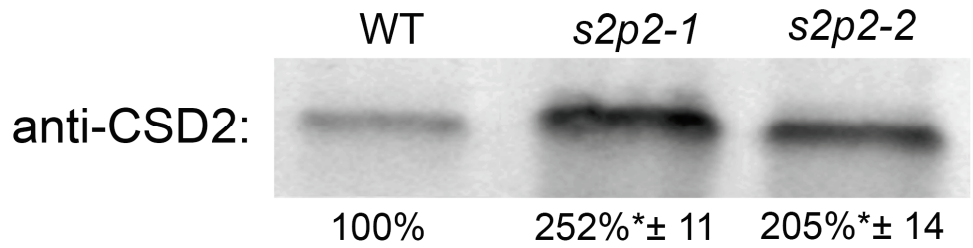


Figure 8. Immunoblot quantification of CSD2 protein in wild-type and *S2P2* mutant lines following high light exposure. CSD2 protein levels were analyzed in wild-type *A. thaliana* (WT) plants and *s2p2–1* and *s2p2–2* mutant lines after 3 h of exposure to high irradiance (1000 μmol m^{-2} s^{-1}). Protein extracts from leaf tissues were subjected to SDS-PAGE and immunoblotting using a CSD2-specific primary antibody. Protein concentration in extracts was determined according to the Lowry method. Before hybridization with antibodies, the membranes were transiently stained with Ponceu S to verify the transfer efficiency and control loading. Quantification was based on three independent biological replicates. Data are presented as mean ± standard deviation (s.d.). Asterisks (*) indicate statistically significant differences between mutant lines and the WT control ($p \leq 0.05$).

3. Discussion

S2P2 is a nuclear-encoded member of the zinc metalloprotease family, specifically classified within the site-2 protease (S2P) family [9]. It is believed that intramembrane proteases such as *S2P2* function in regulated intramembrane proteolysis (RIP), a mechanism by which membrane-bound, protein transcription factors are cleaved and released to mediate changes in gene expression [9]. In *A. thaliana*, six genes encoding S2P family proteases have been identified: EGY1, EGY2, EGY3, S2P2, ARASP, and the product of At4g20310 [10,14,18,27,28]. With the exception of At4g20310, all are localized to the chloroplast. Much is already known about the significance and possible functions of EGY1 [10,13,15,21–23] and EGY2 proteases [14,19,20], as well as EGY3, which, due to the lack of the characteristic zinc-binding motif (HExxH), lacks proteolytic activity and is classified as a so-called pseudo-protease [16,29]. However, knowledge about the physiological functions of *S2P2* is extremely limited.

In our previous work [16], using a large set of immunological methods, we established the thylakoid membrane localization of the *S2P2* protease and highlighted its contribution to maintaining photosynthetic apparatus integrity under non-stressful conditions. In the present study, we investigated the role of *S2P2* in *A. thaliana* exposed to short-term high light stress. For most chloroplast S2Ps studied to date, their importance in maintaining the correct stoichiometry of PSII polypeptides under light stress has been observed. *A. thaliana* mutants lacking both EGY1 and EGY2 were characterized by significant changes in the abundance of key PSII core polypeptides under high light exposure. This resulted in the increased sensitivity of these mutants to photoinhibition, significantly less efficient

PSII function, and reduced ability of the mutants to regenerate after light stress was removed [6,10–12,14,18,19,22].

However, no molecular mechanism leading to the effects observed in these mutants has been described to date. No endogenous substrates for S2P proteases in chloroplasts are known, with the exception of the transcription factor pTAC10, which we propose as a substrate for EGY2 [19].

We first examined the expression pattern of the *S2P2* gene and the corresponding protein abundance in WT plants subjected to high irradiance. A significant upregulation of *S2P2* transcripts was observed, which was strongly correlated with increased *S2P2* protein accumulation in chloroplasts. The relationship between protein accumulation and transcript levels depends, among other things, on the location and function of the protein [30,31]. Therefore, the observed increase in both *S2P2* transcript and protein levels strongly suggests that this protease plays a crucial role in modulating the chloroplast response to short-term high light stress.

It is well documented that high light intensity leads to the impairment of PSII function, which is associated with photoinhibition. The PSII core polypeptide PsbA, together with PsbD, forms the reaction center and is particularly vulnerable to photodamage [32–34]. Our previous studies have demonstrated that the absence of the *S2P2* intramembrane protease, as well as other chloroplast-localized S2Ps, can result in significant disruptions in the stoichiometry of core PSII proteins during non-stressful conditions [17,19,20,23]. Here, we investigated how the absence of the *S2P2* protease affects the behavior of *A. thaliana S2P2* mutants exposed to short-term light stress. Based on our previous studies [4,18] and the existing literature [22,35], it is well established that short-term exposure (3–6 h) to high light intensity (1000 μmol m^{-2} s^{-1}) is sufficient to induce measurable changes in the abundance of proteins constituting the PSII complex.

Western blot analyses revealed that the absence of *S2P2* resulted in a more pronounced degradation of PsbA, PsbD, and PsbC polypeptides under high light stress in both the *s2p2–1* and *s2p2–2* mutant lines compared to WT. The strong degradation of PsbA in both WT and *S2P2* mutants was expected, as PsbA is a protein highly sensitive to photodamage [33,34,36]. However, the rate of PsbA degradation in *S2P2* mutants was significantly higher than in WT. Furthermore, PsbD and PsbC remained relatively stable in WT plants but were significantly degraded in the mutants.

The marked reduction in the levels of PsbD and PsbC in *S2P2* mutants, but not in wild-type plants, under severe light stress, combined with the accelerated degradation of PsbA, clearly indicates an increased intensity of degradation of these polypeptides in *S2P2* mutants (compared to WT), despite the obvious fact that protein levels always reflect a dynamic balance between synthesis and degradation [32,37,38]. These three polypeptides are typically present in thylakoid membranes in equimolar amounts in functional, dimeric PSII particles [31,32,37]. Thus, it is not particularly surprising that the changes in the levels of individual polypeptides observed in *S2P2* mutants are correlated with each other, despite the fact that the genes coding these polypeptides are located in the chloroplast genome within two different operons [39]. However, it is worth noting that the pattern of PsbA, PsbD, and PsbC polypeptide degradation observed in the *S2P2* mutants and the resulting unchanged stoichiometric ratio between these proteins is different from that observed in other *A. thaliana* mutants lacking the EGY1 or EGY2 intramembrane proteases [15,18,20]. In the case of the EGY1 and EGY2 mutants, we observed a disturbance in the stoichiometric ratios between PsbA and PsbD; namely, there was a clear overrepresentation of PsbA in relation to PsbD, which in itself was an unusual situation that was difficult to explain. Here, in the case of *S2P2* mutants, we observe a more classic situation in which a reduced amount of PsbA also corresponds to a reduced amount of PsbD. Considering that all chloroplast

S2P mutants studied so far, namely EGY1, EGY2, and-now-*S2P2*, exhibit disturbances in the stoichiometry of PSII core proteins, one may suspect that there is some mechanism by which these proteases cooperate, ultimately maintaining normal levels of chloroplast-encoded PSII core polypeptides.

The altered stoichiometry of PSII core components under high light conditions can impair PSII function. Chlorophyll a fluorescence parameters confirmed that *S2P2* mutants exhibited increased sensitivity to photoinhibition. Specifically, a greater reduction in F_v/F_m indicated severe damage to the PSII reaction center, while elevated NPQ values suggested enhanced thermal dissipation [40]. The observed increase in the F_0 parameter in *S2P2* mutant lines likely reflects a decreased number of functional PSII centers, consistent with reduced levels of PSII core proteins. Consequently, these mutants displayed diminished electron transport efficiency (lower qP values) and heightened susceptibility to light-induced damage.

High irradiance also promotes the generation of reactive oxygen species (ROS), leading to oxidative stress and cellular damage. These highly reactive molecules are, in turn, the cause of oxidative stress and associated damage to many key proteins. ROS production is particularly prominent in chloroplasts and mitochondria [40–42]. The situation observed in the *S2P2* mutants, i.e., increased abnormalities in the content of key PSII core proteins and reduced PSII functionality, clearly seems to promote excessive ROS production in chloroplasts. The measurements of the content of superoxide radical and hydrogen peroxide confirm this assumption. ROS accumulation in *S2P2* chloroplasts was significantly higher than that recorded in WT plants. Simultaneously, we did not observe increased ROS production in *S2P2* mutants under non-stressful conditions. Once generated, the superoxide radical is quickly metabolized in chloroplasts to hydrogen peroxide. This is an extremely important element in the protection of the photosynthetic apparatus and, more broadly, chloroplasts and the entire cell in conditions such as light stress. The superoxide radical, if not scavenged, as an extremely reactive one, has a very large potential to destroy cellular components such as lipids, proteins, and DNA [43]. The enzyme playing a vital role in detoxifying superoxide radicals in chloroplasts is Cu/Zn superoxide dismutase 2 (CSD2), which is responsible for the dismutation of superoxide radicals into molecular oxygen and hydrogen peroxide [44,45]. CSD2 is crucial for plant survival and health, particularly under conditions that promote oxidative stress, such as high light intensity, drought, and nutrient deficiencies [45]. According to the literature information, CSD2 expression and activity are regulated by light and redox signals. In response to high irradiance and ROS production, the expression of CSD2 is upregulated to enhance its protective role [44]. In our study, CSD2 protein levels were more than twofold higher in *S2P2* mutants under high light compared to WT. As the product of CSD2 activity is hydrogen peroxide, its significantly higher level in *S2P2* mutants seems to be a consequence of the increased CSD2 content. The elevated level of CSD2 in mutant lines is an obvious response of *S2P2* mutants to the increased production of ROS under high light stress conditions.

The absence of chloroplast-localized *S2P2* protease results in the impaired accumulation of key PSII core proteins, compromised PSII efficiency, and increased vulnerability to high light-induced photoinhibition. This is accompanied by heightened ROS production and a robust induction of the antioxidant enzyme CSD2.

4. Materials and Methods

4.1. Plant Material, Growth, and Stress Conditions

Arabidopsis thaliana (L.) Heynh (ecotype Columbia) wild-type (WT) and two commercially available T-DNA insertion mutants, *s2p2–1* (SALK_046599C) and *s2p2–2* (SALK_071288), were used. Mutant lines were obtained from NASC (Nottingham Ara-

bidopsis Stock Centre, Nottingham, United Kingdom). The homozygosity of both lines was previously confirmed with the PCR technique, and the lack of the *S2P2* protein was confirmed with the use of an anti-*S2P2* antibody [16].

All plants were grown on sphagnum peat moss and wood pulp in 42 mm Jiffy peat pellets (AgroWit, Przylep, Poland) under a 16 h light/8 h darkness photoperiod at an irradiance of 110 μmol m^{-2} s^{-1}, relative humidity of 70%, and constant temperature of 22 °C for 4 weeks. For the light stress, the 4-week-old plants were exposed to continuous light at an intensity of 1000 mmol m^{-2} s^{-1} for 1, 3, 6., and 24 h. The light source was a white fluorescent light lamp, the Philips Master T-E-D 58 W/840 REFLEX Eco (Eindhoven, Holland).

4.2. S2P2 Gene Expression Analysis

Total RNA was extracted from *A. thaliana* WT leaves using the GeneMATRIX Universal RNA Purification Kit (EURX®, Gdańsk, Poland), following the manufacturer's instructions. To remove genomic DNA contamination, the isolated RNA was treated with RNase-free DNase (Thermo Fisher Scientific, Waltham, MA, USA) according to the provided protocol. Complementary DNA (cDNA) synthesis was performed using 5 μg of total RNA with the RevertAid H Minus First Strand cDNA Synthesis Kit (Thermo Fisher Scientific, Waltham, MA, USA), employing random hexamer primers. cDNA synthesis was carried out for 60 min at 42 °C and was preceded by a 5 min incubation at 25 °C.

Quantitative real-time PCR (qRT-PCR) was conducted as described previously [16,19], utilizing the CFX96 Real-Time PCR Detection System (Bio-Rad, Hercules, CA, USA) and iTaq Universal SYBR Green Supermix (Bio-Rad, Hercules, CA, USA). Reactions were prepared in a final volume of 20 μL, including 1 μL of synthesized cDNA. The applied cycling conditions were as follows: 94 °C for 20 s, 55 °C for 30 s, and 68 °C for 30 s (40 cycles).

Relative expression of the *S2P2* gene under high light stress conditions was determined using the comparative CT ($2^{-\Delta\Delta CT}$) method [46]. For normalization, *CYP5* (At2g29960) was used as the endogenous control.

The primers used in this study were as follows:
S2P2 (AT1G05140):
Forward: 5′-AGAACACAAGCTCTCGGTCG-3′
Reverse: 5′-ATCGGACCAAACCCTATCGC-3′
CYP5 (AT2G29960):
Forward: 5′-GAGAAAGGTGTAGGGAAGAGTGG-3′
Reverse: 5′-CAAACTTCTGACCATAGATTGATTC-3′

All primers were designed and validated by melting curve analysis to confirm specificity and the absence of primer-dimer formation using Primer3Input software (https://primer3.ut.ee/ accessed on 15 February 2023). Each sample was analyzed in three biological replicates, with three technical replicates per biological sample.

4.3. SDS-PAGE and Immunoblotting

SDS-PAGE was performed following the method of Laemmli [47], with minor modifications. Proteins were separated on 12% (*w*/*v*) polyacrylamide gels containing 6 M urea (Sigma-Aldrich, Loius, MO, USA). Gel running conditions were as follows: 25 mA per gel 90 min. Following electrophoresis, proteins were electrotransferred onto polyvinylidene fluoride (PVDF) membranes (Bio-Rad), and Western blotting was carried out as previously described by Adamiec et al. [19]. Before hybridization with antibodies, the membranes were transiently stained with Ponceu S to verify the transfer efficiency and control loading.

The PVDF membranes were blocked for 1 h with 4% BSA (BioShop, Burlington, Canada) and then incubated with primary antibodies for 90 min. This was followed

by a 1 h incubation with secondary antibodies (Agrisera, Vännäs, Sweden), and signal development was achieved with a 5 min incubation using Clarity Western ECL Substrate (Bio-Rad). Protein bands were visualized with the ChemiDoc Imaging System (Bio-Rad).

Densitometric analysis of the immunostained bands was conducted using GelixOne software (Biostep GmbH, Burkhardtsdorf, Germany). Only blots demonstrating a linear relationship between signal intensity and the amount of protein loaded were included in the analysis. The linearity of signal detection was previously validated and reported by Adamiec et al. [19].

4.4. Antibodies

Custom polyclonal anti-*S2P2* antibodies were generated in rabbits by Davids Biotechnologie GmbH (Regensburg, Germany) using a highly specific synthetic peptide antigen (amino acid sequence: DNDPDSDIPVDDRNLLKNR). Commercial antibodies against PsbA, PsbD, PsbC, and CSD2, as well as the corresponding secondary antibodies, were obtained from Agrisera (Vännäs, Sweden).

4.5. Chlorophyll a Fluorescence Measurement

Chlorophyll *a* fluorescence measurements were performed using the FMS1 fluorometer (Photon System Instruments, Brno, Czech Republic), operated with Modfluor software. Prior to each measurement, leaves were dark-adapted for 30 min. The procedure followed the protocol established by Genty et al. [48].

The minimum fluorescence yield (F_0) was recorded at the start of the measurement. The maximum quantum yield of PSII (F_v/F_m) were calculated according to Genty et al. [48]. Actinic light intensity matched the pre-dark adaptation irradiance: 110 μmol m^{-2} s^{-1} for control conditions and 1000 μmol m^{-2} s^{-1} for high light stress treatments.

Photochemical quenching (qP), and non-photochemical quenching (NPQ) were calculated following the formulas described by Maxwell and Johnson [49]. For each treatment variant, 30 individual plants were measured per replicate, with three biological replicates conducted in total.

4.6. Hydrogen Peroxide Detection

Hydrogen peroxide (H_2O_2) detection was carried out using two different methods, as described in our previous work [15].

DAB-Based Quantification: Quantitative determination of H_2O_2 levels in DAB-stained tissues was performed with modifications to the method of Boyidi et al. [50]. DAB-stained leaves were weighed, homogenized, and extracted in 2 mL of perchloric acid per 1 mg of fresh tissue. The homogenates were centrifuged at 10,000× *g* for 10 min, and absorbance was measured at 450 nm. H_2O_2 concentration was expressed in nmol per gram of fresh weight (FW).

Titanium-Based Spectrophotometric Assay: Spectrophotometric measurement of H_2O_2 was performed using the titanium (Ti^{4+}) complex method, following Becana et al. [51]. *A. thaliana* leaves (0.25 g) were homogenized in 3 mL of 100 mM phosphate buffer (pH 7.8) with activated charcoal (1:5 ratio). The homogenate was centrifuged at 15,000× *g* for 30 min at 4 °C. For analysis, the supernatant was mixed in a cuvette with the titanium reagent (0.3 mM 4-(2-pyridylazo) resorcinol and 0.3 mM titanium potassium tartrate, mixed 1:1) and 100 mM phosphate buffer (pH 7.8). Absorbance was read at 508 nm and compared against a standard curve generated with known H_2O_2 concentrations (0–100 nmol). H_2O_2 levels were expressed as nmol per gram of fresh weight. The measurement was performed in 3 biological replicates and 3 technical replicates for each.

4.7. Detection of Superoxide Anion Radical

Superoxide radical ($O_2^{\bullet -}$) accumulation was quantified based on the reduction in nitroblue tetrazolium (NBT), following the methodology described by Ratajczak et al. [52] and Doke [53]. A total of 0.5 g of leaf samples was incubated in 3 mL of 0.05 M potassium phosphate buffer (pH 7.8) containing 0.05% (*w*/*v*) NBT and 10 mM sodium azide. Incubation was carried out at room temperature in the dark for 30 min. Subsequently, the reaction mixture was subjected to heat treatment at 85 °C for 15 min, followed by immediate cooling on ice. The absorbance of the resulting solution was measured at 530 nm using a spectrophotometer. Superoxide radical generation was expressed as DA_{530}/g FW leaves tissue. The measurement was performed in 3 biological replicates and 3 technical replicates for each.

4.8. Isolation of Leaf Proteins and Determination of Protein Concentration

Total soluble proteins were extracted from 100 mg of *A. thaliana* leaf tissue using a commercial protein extraction buffer (PEB; Vannas, Agrisera), following the manufacturer's protocol. Protein concentration was quantified using a modified Lowry assay [54] with the DC Protein Assay kit (Bio-Rad, Hercules, CA, USA), according to the manufacturer's instructions. Protein isolation was performed in 3 biological replicates and 3 technical replicates for each.

4.9. Statistical Analysis

Differences in the measured parameters were analyzed for statistical significance using one-way ANOVA. Means were regarded as significantly different at $p \leq 0.05$.

5. Conclusions

Our results demonstrate that *S2P2* plays a critical role in maintaining the appropriate levels of three essential polypeptides within the PSII core complex—PsbA, PsbC, and PsbD. In *S2P2* mutant plants, the absence of *S2P2* resulted in a more pronounced decline in the abundance of these polypeptides under high light stress compared to wild-type controls. This disruption in PSII core stoichiometry was associated with a significant reduction in the maximum quantum efficiency of PSII (F_v/F_m) and an increase in the NPQ, indicating elevated photoinhibition and enhanced thermal energy dissipation in the mutants.

Furthermore, impaired PSII function in the *S2P2* mutants under high irradiance led to increased ROS accumulation, accompanied by a marked upregulation of CSD2, a key enzyme involved in the detoxification of superoxide radicals. Collectively, these findings suggest that *S2P2*, alongside other intramembrane S2P-type chloroplast proteases, contributes to the regulation of PSII core protein stoichiometry and efficiency, thereby modulating the plant's sensitivity to photoinhibitory stress.

Author Contributions: Conceptualization, R.L.; methodology, M.C., M.A. and R.L.; validation, M.A. and R.L.; investigation, M.C. and R.L.; data curation, M.A. and R.L.; writing—original draft preparation, R.L.; writing—review and editing–R.L. All authors have read and agreed to the published version of the manuscript.

Funding: This research received no external funding.

Data Availability Statement: All original contributions presented in this study are included within the article. For additional information or specific inquiries, readers are encouraged to contact the corresponding author.

Conflicts of Interest: The authors declare no conflicts of interest.

References

1. Eckhard, N.A.; Avin-Wittenberg, T.; Bassham, D.C.; Chen, P.; Chen, Q.; Fang, J.; Genschik, P.; Ghifari, A.S.; Guercio, A.M.; Gibbs, D.J.; et al. The lowdown on breakdown: Open questions in plant proteolysis. *Plant Cell* **2024**, *36*, 2931–2975. [CrossRef]
2. Adam, Z.; Rudella, A.; van Wijk, K. Recent advances in the study of Clp, FtsH and other proteases located in chloroplasts. *Curr. Opin. Plant Biol.* **2006**, *9*, 234–240. [CrossRef]
3. Van der Hoorn, R.A.L.; Klemencic, M. Plant proteases: From molecular mechanisms to functions in development and immunity. *J. Exp. Bot.* **2021**, *72*, 3337–3339. [CrossRef] [PubMed]
4. Lucinski, R.; Adamiec, M. The role of plant proteases in the response of plants to abiotic factors. *Front. Plant Physiol.* **2023**, *1*, 1330216. [CrossRef]
5. Liu, Y.; Jackson, E.; Liu, X.; Huang, X.; van der Hoorn, R.A.L.; Zhang, Y.; Li, X. Proteolysis in plant immunity. *Plant Cell* **2024**, *36*, 3099–3115. [CrossRef] [PubMed]
6. Adam, Z. Emerging roles for diverse intramembrane proteases in plant biology. *Biochim. Biophys. Acta (BBA)-Biomembr.* **2013**, *1828*, 2933–2936. [CrossRef]
7. Schneider, J.S.; Glickman, M.S. Function of site-2 proteases in bacteria and bacterial pathogens. *Bioch. Biophys. Acta Biomembr.* **2013**, *1828*, 2808–2814. [CrossRef]
8. Knopf, R.R.L.; Feder, A.; Mayer, K.; Lin, A.; Rozenberg, L.A.M.; Schaller, A.; Adam, Z. Rhomboid proteins in the chloroplast envelope affect the level of allene oxide synthase in *Arabidopsis thaliana*. *Plant J.* **2012**, *72*, 559–571. [CrossRef]
9. Adamiec, M.; Ciesielska, M.; Zalaś, P.; Lucinski, R. *Arabidopsis thaliana* intramembrane proteases. *Acta Physiol. Plant.* **2017**, *39*, 146. [CrossRef]
10. Chen, G.; Bi, Y.R.; Li, N. EGY1 encodes a membrane-associated and ATP-independent metalloprotease that is required for chloroplast development. *Plant J.* **2005**, *41*, 364–375. [CrossRef]
11. Guo, D.; Gao, X.; Li, H.; Zhang, T.; Chen, G.; Huang, P.; An, L.; Li, N. EGY1 plays a role in regulation of endodermal plastid size and number that are involved in ethylenedependent gravitropism of light-grown *Arabidopsis* hypocotyls. *Plant Mol. Biol.* **2008**, *66*, 345–360. [CrossRef]
12. Li, B.; Li, Q.; Xiong, L.; Kronzucker, H.J.; Kramer, U.; Shi, W. *Arabidopsis* plastid AMOS1/EGY1 integrates abscisic acid signaling to regulate global gene expression response to ammonium stress. *Plant Physiol.* **2012**, *160*, 2040–2051. [CrossRef]
13. Yu, F.; Zhu, X.; Li, G.; Kronzucker, H.J.; Shi, W. The chloroplast protease AMOS1/EGY1 affects phosphate homeostasis under phosphate stress. *Plant Physiol.* **2016**, *172*, 1200–1208. [CrossRef]
14. Chen, G.; Law, K.; Ho, P.; Zhang, X.; Li, N. EGY2, a chloroplast membrane metalloprotease, plays a role in hypocotyl elongation in *Arabidopsis*. *Mol. Biol. Rep.* **2012**, *39*, 2147–2155. [CrossRef]
15. Adamiec, M.; Misztal, L.; Kasprowicz-Maluśki, A.; Lucinski, R. EGY3: Homologue of S2P protease located in chloroplasts. *Plant Biol.* **2020**, *22*, 735–743. [CrossRef]
16. Ciesielska, M.; Adamiec, M.; Lucinski, R. S2P2—The chloroplast-located intramembrane protease and its impact on the stoichiometry and functioning of the photosynthetic apparatus of A. thaliana. *Front. Plant. Sci.* **2024**, *15*, 1372318. [CrossRef] [PubMed]
17. Bötler, B.; Nada, A.; Fulgosi, H.; Soll, J. A chloroplastic inner envelope membrane protease is essential for plant development. *FEBS Lett.* **2006**, *580*, 789–794. [CrossRef] [PubMed]
18. Adamiec, M.; Misztal, L.; Kosicka, E.; Paluch-Lubawa, E.; Lucinski, R. *Arabidopsis thaliana egy2* mutants display altered expression level of genes encoding crucial photosystem II proteins. *J. Plant Physiol.* **2018**, *231*, 155–167. [CrossRef]
19. Luciński, R.; Dobrogojski, J.; Ishikawa, T.; Adamiec, M. The role of EGY2 protease in response to high light stress. *Funct. Plant Biol.* **2024**, *51*, FP23243. [CrossRef]
20. Chen, Y.E.; Yuan, S.; Schroder, W.P. Comparison of methods for extracting thylakoid membranes of *Arabidopsis* plants. *Physiol. Plant.* **2016**, *156*, 3–12. [CrossRef]
21. Qi, Y.; Wang, X.; Lei, P.; Li, H.; Yan, L.; Zhao, J.; Meng, J.; Shao, J.; An, L.; Yu, F.; et al. The chloroplast metalloproteases VAR2 and EGY1 act synergistically to regulate chloroplast development in *Arabidopsis*. *J. Biol. Chem.* **2020**, *295*, 1036–1046. [CrossRef]
22. Adamiec, M.; Misztal, L.; Ciesielska, M.; Lucinski, R. The changes of PSII supercompelex stoichiometry in *egy1* mutants are related to chlorophyll b deficiency. *Photosynthetica* **2021**, *59*, 294–302. [CrossRef]
23. Winter, D.; Vinegar, B.; Nahal, H.; Ammar, R.; Wilson, G.V.; Provart, N.J. An "Electronic Fluorescent Pictograph" browser for exploring and analyzing large-scale biological data sets. *PLoS ONE* **2007**, *2*, e718. [CrossRef]
24. Wang, S.; Bai, G.; Wang, S.; Yang, L.; Yang, F.; Wang, Y.; Zhu, J.-K.; Hua, J.; Qu, L.-J. Chloroplast RNA-Binding Protein RBD1 Promotes Chilling Tolerance Through 23S rRNA Processing in *Arabidopsis*. *PloS Genet.* **2016**, *12*, e1006027. [CrossRef]
25. Zhang, S.; Chen, C.; Dai, S.; Yang, M.; Meng, Q.; Lv, W.; Ma, N. A tomato putative metalloprotease SlEGY2 plays a positive role in thermotolerance. *Agriculture* **2022**, *12*, 940. [CrossRef]
26. Yamamoto, Y. Quality control of photosystem II: The mechanisms for avoidance and tolerance of light and heat stresses are closely linked to membrane fluidity of the thylakoids. *Front. Plant Sci.* **2016**, *7*, 1136. [CrossRef]

27. Che, P.; Bussell, J.D.; Zhou, W.; Estavillo, G.M.; Pogson, B.J.; Smith, S.M. Signaling from the endoplasmic reticulum activates brassinosteroid signaling and promotes acclimation to stress in *Arabidopsis*. *Sci. Signal.* **2010**, *3*, ra69. [CrossRef]
28. Adamiec, M.; Szomek, M.; Gabała, E.; Dobrogojski, J.; Misztal, L.; Luciński, R. Fatty acid composition and cpDNA content in *Arabidopsis thaliana* mutants deprived of EGY1 protease. *Photosynthetica* **2021**, *59*, 633–639. [CrossRef]
29. Adamiec, M.; Dobrogojski, J.; Wojtyla, Ł.; Luciński, R. Stress-related expression of the chloroplast EGY3 pseudoprotease and its possible impact on chloroplasts' proteome composition. *Front. Plant Sci.* **2022**, *13*, 965143. [CrossRef] [PubMed]
30. Baerenfaller, K.; Massonnet, C.; Walsh, S.; Baginsky, S.; Bühlmann, P.; Hennig, L.; Hirsch-Hoffmann, M.; A Howell, K.; Kahlau, S.; Radziejwoski, A.; et al. Systems-based analysis of *Arabidopsis* leaf growth reveals adaptation to water deficit. *Mol. Syst. Biol.* **2012**, *8*, 606. [CrossRef]
31. Liu, Y.; Beyer, A.; Aebersold, R. On the dependency of cellular protein levels on mRNA abundance. *Cell* **2016**, *165*, 535–550. [CrossRef]
32. Luciński, R.; Jackowski, G. The structure, functions and degradation of pigment-binding proteins of photosystem II. *Acta Biochim. Pol.* **2006**, *53*, 693–708. [CrossRef]
33. Chotewutmontri, P.; Barkan, A. Light-induced *psbA* translation in plants is triggered by photosystem II damage via assembly-linked autoregulatory circuit. *Proc. Natl. Acad. Sci. USA* **2020**, *117*, 21775–21784. [CrossRef]
34. Zybailov, B.; Rutschow, H.; Friso, G.; Rudella, A.; Emanuelsson, O.; Sun, Q.; van Wijk, K.J.; Koch, K.-W. Sorting signals, N-terminal modifications and abundance of the chloroplast proteome. *PLoS ONE* **2008**, *3*, e1994. [CrossRef]
35. Telfer, A.; Bishop, S.M.; Philips, D.; Barber, J. Isolated photosynthetic reaction center of photosystem II as a sensitizer for the formation of singlet oxygen. Detection and quantum yield determination using a chemical trapping technique. *J. Biol. Chem.* **1994**, *269*, 13244–13253. [CrossRef]
36. Vass, I. Molecular mechanism of photodamage in the photosystem II complex. *Biochim. Biophys. Acta (BBA)-Bioenerg.* **2012**, *1817*, 209–217. [CrossRef] [PubMed]
37. Shen, J.R. The structure of photosystem II and the mechanism of water oxidation in photosynthesis. *Annu. Rev. Plant Biol.* **2015**, *66*, 23–48. [CrossRef]
38. Umena, Y.; Kawakami, K.; Shen, J.R.; Kamiya, N. Crystal structure of oxygen-evolving photosystem II at a resolution of 1.9 Å. *Nature* **2011**, *473*, 55–60. [CrossRef] [PubMed]
39. Hruz, T.; Laule, O.; Szabo, G.; Wessendorp, F.; Bleuler, S.; Oertle, L.; Widmayer, P.; Gruissem, W.; Zimmermann, P.; Van de Peer, Y. Genevestigator v3: A reference expression database for the meta-analysis of transcriptomes. *Adv. Bioinform.* **2008**, *2008*, 420747. [CrossRef] [PubMed]
40. Xiong, H.; Hua, L.; Reyna-Llorens, I.; Shi, Y.; Chen, K.M.; Smirnoff, N.; Kromdjik, J.; Hibberd, J.M. Photosynthesis-independent production of reactive oxygen species in the rice bundle sheath during high light is mediated by NADPH oxidase. *Proc. Natl. Acad. Sci. USA* **2021**, *118*, e2022702118. [CrossRef]
41. Borbély, P.; Gasperl, A.; Palmai, T.; Ahres, M.; Asghar, M.A.; Galiba, G.; Muller, M.; Kocsy, G. Light Intensity- and Spectrum-Dependent Redox Regulation of Plant Metabolism. *Antioxidants* **2022**, *11*, 1311. [CrossRef] [PubMed]
42. Panda, S.K.; Gupta, D.; Patel, M.; Van Der Vyver, C.; Koyama, H. Functionality of Reactive Oxygen Species (ROS) in Plants: Toxicity and Control in Poaceae Crops Exposed to Abiotic Stress. *Plants* **2024**, *13*, 2071. [CrossRef]
43. Tripathy, B.C.; Oelmuller, R. Reactive oxygen species generation and signaling in plants. *Plant Signal. Behav.* **2012**, *7*, 1621–1633. [CrossRef]
44. Aguirre, G.; Pilon, M. Copper Delivery to Chloroplast Proteins and its Regulation. *Front. Plant Sci.* **2015**, *6*, 1250. [CrossRef]
45. Pilon, M.; Ravet, K.; Tapken, W. The biogenesis and physiological function of chloroplast superoxide dismutases. *Biochim. Biophys. Acta-Bioenerg.* **2011**, *1807*, 989–998. [CrossRef]
46. Schmittgen, T.D.; Livak, K.J. Analyzing real-time PCR data by the comparative C_T method. *Nat. Protoc.* **2008**, *3*, 1101–1108. [CrossRef]
47. Laemmli, U.K. Cleavage of structural proteins during the assembly of the head of bacteriophage T4. *Nature* **1970**, *227*, 680–685. [CrossRef]
48. Genty, B.; Briantais, J.M.; Baker, N.R. The relationship between the quantum yield of photosynthetic electron transport and quenching of chlorophyll fluorescence. *Biochim. Biophys. Acta (BBA)-Gen. Subj.* **1989**, *990*, 87–92. [CrossRef]
49. Maxwell, K.; Johnson, G.N. Chlorophyll fluorescence—A practical guide. *J. Exp. Bot.* **2000**, *51*, 659–668. [CrossRef]
50. Boyidi, P.; Trishla, V.S.; Botta, H.K.; Yadav, D.; Kirti, P.B. Heterologous expression of rice annexin OsANN5 potentiates abiotic stress tolerance in transgenic tobacco through ROS amelioration. *Plant Stress* **2021**, *2*, 100022. [CrossRef]
51. Becana, M.; Aparicio-Tejo, P.; Irigoyen, J.J.; Sanchez-Diaz, M. Some enzymes of hydrogen peroxide metabolism in leaves and root nodules of *Medicago* sativa. *Plant Physiol.* **1986**, *82*, 1169–1171. [CrossRef]
52. Ratajczak, E.; Małecka, A.; Bagniewska-Zadworna, A.; Kalemba, E.M. The production, localization and spreading of reactive oxygen species contributes to low vitality of long-term stored common beech (*Fagus sylvatica* L.) seeds. *J. Plant Physiol.* **2015**, *174*, 147–156. [CrossRef] [PubMed]

53. Doke, N. Generation of superoxide anion by potato tuber protoplasts during the hyper-sensitive response to hyphal wall components of *Phytophtora infestans* and specific inhibition of the reaction by suppressors of hypersensitivity. *Physiol. Plant Pathol.* **1983**, *23*, 359–367. [CrossRef]
54. Lowry, O.H.; Rosenbrough, N.J.; Farr, A.L.; Randall, R.J. Protein measurement with the Folin phenol reagent. *J. Biol. Chem.* **1951**, *193*, 265–275. [CrossRef] [PubMed]

Disclaimer/Publisher's Note: The statements, opinions and data contained in all publications are solely those of the individual author(s) and contributor(s) and not of MDPI and/or the editor(s). MDPI and/or the editor(s) disclaim responsibility for any injury to people or property resulting from any ideas, methods, instructions or products referred to in the content.

MDPI AG
Grosspeteranlage 5
4052 Basel
Switzerland
Tel.: +41 61 683 77 34

Plants Editorial Office
E-mail: plants@mdpi.com
www.mdpi.com/journal/plants



Disclaimer/Publisher's Note: The title and front matter of this reprint are at the discretion of the Guest Editor. The publisher is not responsible for their content or any associated concerns. The statements, opinions and data contained in all individual articles are solely those of the individual Editor and contributors and not of MDPI. MDPI disclaims responsibility for any injury to people or property resulting from any ideas, methods, instructions or products referred to in the content.





Academic Open
Access Publishing

mdpi.com

ISBN 978-3-7258-8120-8